Design of the Communication, Power Management and Interchangeable Sensor Payload System for an Inspection-class Robotic Platform

Greig Knox
KNXGRE001
M.Sc. Mechanical Engineering Dissertation
8/28/2015

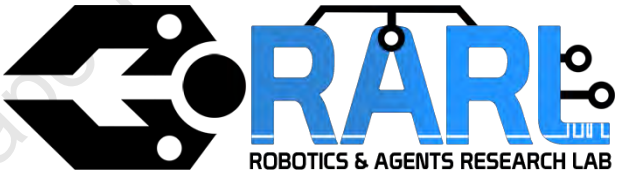

Supervisors:
Samuel Ginsberg and Tracy Booysen

Design and Implementation of Lithium-Ion battery management,
Wireless Communication and Sensor Fusion

Summary

Introduction

With the "golden day" being the first 24 hours after an urban disaster, after which the survival rate of victims decreases dramatically, there is a requirement for a low-cost first-response robotic platform. UCT robotics is developing a platform to fulfil this requirement, with the Scarab (Figure 0-1) — a low-cost, man-packable, throwable inspection-class robotic platform with interchangeable payloads. The system was designed to create a 1:1 human-to-robot ratio which improves the efficiency of rescue operations. Once the operator has reached the inspection void, the Scarab is thrown in where the sensor stimulus from the inspection environment is communicated, via wireless communications, from the payload back to the operator station. The interchangeable payload allows the sensor configuration to be tailored to the needs of the disaster, while reducing the cost of the platform. The design of the battery and battery management system, communications and interchangeable sensor payload for this platform are described in this report.

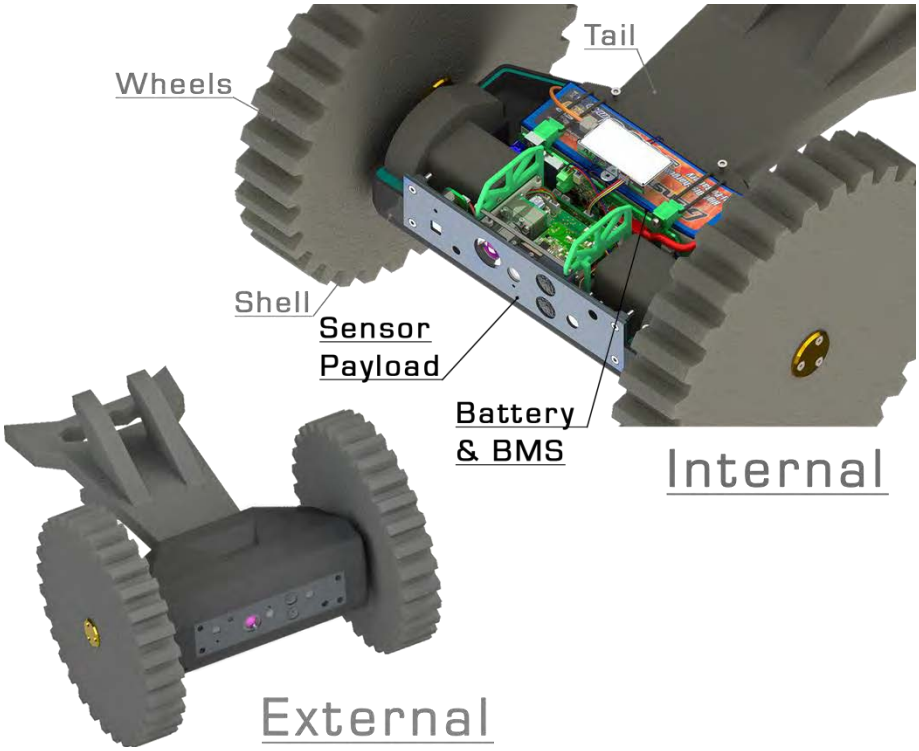

Figure 0-1: The Scarab

Battery Selection and BMS Design

Background research suggested that a Lithium-Ion battery be used. This, however, should be coupled with a battery management system for safe operation. The BQ20z45-R1 IC was selected as a primary battery protection and gas gauge, which uses an **ImpedanceTrack™** algorithm to correct for integration drift, providing an accurate estimation of the operational time remaining. A requirement of the system was the ability for in-field charging and hence a BQ24753A battery charger IC was selected. As the system is to be charged while being carried by the operator during operations, a secondary analog battery protection IC was selected as an additional safety measure. The three modules of the BMS are mounted to the battery with a flexible coupling to allow for the swelling of the battery during operation.

Communication

The communications for the system are split across two separate frequencies to reduce the bandwidth requirement on a single frequency. The data and commands are communicated using a pair of 433 MHz RF1101SE transceivers and video using a 1.3 GHz Range Video FPV video transmitter and receiver pair. An analog video switch is used to select between the sources on the platform.

To ensure valid data communication, a communication protocol using a combination of timer-based events, packet stretching and a CRC checksum was used. The packet stretching was used to ensure that the packet contains unique header and terminator characters, while the CRC checksum is employed to detect data corruption. The state of the received data is then communicated back to the transmitter via a packet confirmation. Should the transmitter not receive the confirmation packet before a 30 ms timer expires, the communication is considered lost and is resent. The protocol enables all of the communication errors to be detected.

Sensor Payload Design

A pair of sensor payloads were developed to demonstrate the interchangeability of the payloads. The first payload was developed as a low-cost payload which limited the sensor configuration to a camera, microphone and environmental temperature sensor. The second extended payload has the addition of a thermal camera and additional processing power. A board edge connector is used to create an electro-mechanical connection upon insertion of the payload.

The platform is symmetrical about the plane splitting the two halves of the shell; therefore, the platform can operate in the orientation in which it lands after a fall or being thrown. Therefore, the image signal and the motor commands are modified so as not to disorientate the operator. This is achieved using an accelerometer for the low-cost payload and an IMU in the case of the extended payload. The image produced by the camera and the motor commands received are modified according to the orientation of the platform.

As this is the first prototype for the platform, gathering data for analysis is critical for future design. Therefore, system diagnostics were added to monitor the system temperatures, current and voltages throughout the operation.

Concluding Remarks

The primary battery protection system functioned as expected; there was a maximum error of -12.5 % in the estimation of the time remaining, the error being due to an underestimation that decreased throughout the discharge cycle of the battery. Without active cooling, which is impractical in a system such as this, the maximum charge rate is limited to 6 A which corresponds to a minimum charge time of 51 minutes which is equivalent to 18 % of the maximum operational time.

The communication range exceeds the specification by 50 %, and the maximum communication frequency is 300 % of the maximum specification. However, the combination of the sensor payload data packet structure and the communication protocol leads to a data loss of 0.114 %. Recommendations to correct this data loss have been made.

Due to the layout of the systems, the processing of the communication and BMS data is embedded on the microcontroller in the payload. This renders the platform inoperable once the payload is removed and hence should be revised.

The cost of the system, when the low-cost payload is used, exceeds the specification; however, many of the recommended alterations to the system would lead to increased expenditure. Therefore, either the cost should be reconsidered or the functional requirements of the system reduced.

Acknowledgements

Many people have helped, guided and supported me to the point of completion of this thesis. The following people have made a significant contribution and will be acknowledged accordingly.

- My parents: for their unwavering love, support and motivation, which has guided me to the point at which I could begin and complete my masters.
- Tracy Booysen and Samuel Ginsberg (my supervisors): for the guidance throughout project, ensuring my focus remained on the specific goal of the project.
- Catherine Knox: for the help with editing. Her inspirational, genuine, joyful, enthusiasm for knowledge in all areas has inspired and motivated a quest for knowledge.
- The Senders (Brent and Janet): for the caring guidance and support throughout the last few years.
- Collin for winter discussions and debates.
- Shrimp: for ensuring that there is enough enjoyment in between the work and helping me keep an eye on the big picture (the grand plan).
- My fellow lab inmates (Tim, Victor, Thomas and Max): for being a thought-wall for bouncing ideas off — which, in general, lead to solutions.

The financial assistance of the National Research Foundation (NRF) towards this research is hereby acknowledged. Opinions expressed and conclusions arrived at, are those of the author and are not necessarily to be attributed to the NRF.

Plagiarism Declaration

This thesis is submitted in complete fulfilment of a Master of Science degree (Mechanical Engineering) at the University of Cape Town. I know the meaning of plagiarism and declare that all of the work in the document, save for that which is properly acknowledged, is my own. Each contribution to, and quotation in, this document from the work(s) of other people has been attributed, and has been cited and referenced according to the style for IEEE Transactions.

I have not allowed, and will not allow anyone to copy my work with the intention of passing it off as their own.

Signed by candidate

Greig Knox (Friday, 26 June 2015)

Contents

List of Figures

List of Tables

List of Acronyms

AFE	-	Analogy Front End
BMS	-	Battery Management System
CRC	-	Cyclic Redundancy Checksum
DMA	-	Direct Memory Access
DOF	-	Degrees of Freedom
DSP	-	Digital Signal Processor
EEPROM	-	Electrically Erasable Programmable Read-Only Memory
ESD	-	Electrostatic Discharge
FIFO	-	First-In-First-Out
FOV	-	Field of View
FPU	-	Floating Point Unit
GPIO	-	General Purpose Input Output
GUI	-	Graphical User Interface
HAZMAT	-	Hazardous Materials
I^2C	-	Inter-Integrated Circuit
IC	-	Integrated Circuit
IMU	-	Inertial Measurement Unit
IP (rating)	-	Ingress Protection rating
IR	-	Infrared
LDO	-	Linear Drop Out
LED	-	Light Emitting Diode
LSB	-	Least Significant Bit
MOSFET	-	Metal-Oxide-Semiconductor Field-Effect Transistor
MSB	-	Most Significant Bit
PCB	-	Printed Circuit Board
PWM	-	Pulse Width Modulation
RF	-	Radio Frequency
SMD	-	Surface-mount Device
SMPS	-	Switch Mode Power Supply
SOC	-	State of Charge
SOH	-	State of Health

SPI	-	Serial Peripheral Interface
STM	-	STMicroelectronics
TI	-	Texas Instruments
UCT	-	University of Cape Town
UGV	-	Unmanned Ground Vehicle
USAR	-	Urban Search and Rescue
µC	-	Microcontroller

Introduction

This chapter describes the intended field of use for the inspection-class robotic platform, the history of the UCT RARL (Robotics and Agents Research Laboratory) and USAR and the basis on which the project was conceived. Finally, the chapter will introduce the scope and limitations of the project.

1.1: Urban Search and Rescue Robotics (USAR)

Chapter 1 : Introduction

"The attractiveness of robots for man-made disasters stems from their potential to extend the senses of the responders into the interior of the rubble or through hazardous material." [1] This enables rescuers to search the rubble more efficiently. This is critical as the number of live victims rescued drops dramatically 24 hours after the initial disaster, a period known as the "golden day" [2]. This fact is well illustrated by Figure 1-1, which shows the number of alive and dead victims recovered over a period of days following the initial incident.

Secondly; "many first responders state that they can rescue a victim, if the victim's position is known. Often, search is beyond the human ability." [3] This is solved by the ability of a robot to enter voids and search areas which would have otherwise been impossible to enter without excavation, thus improving the efficiency of victim location.

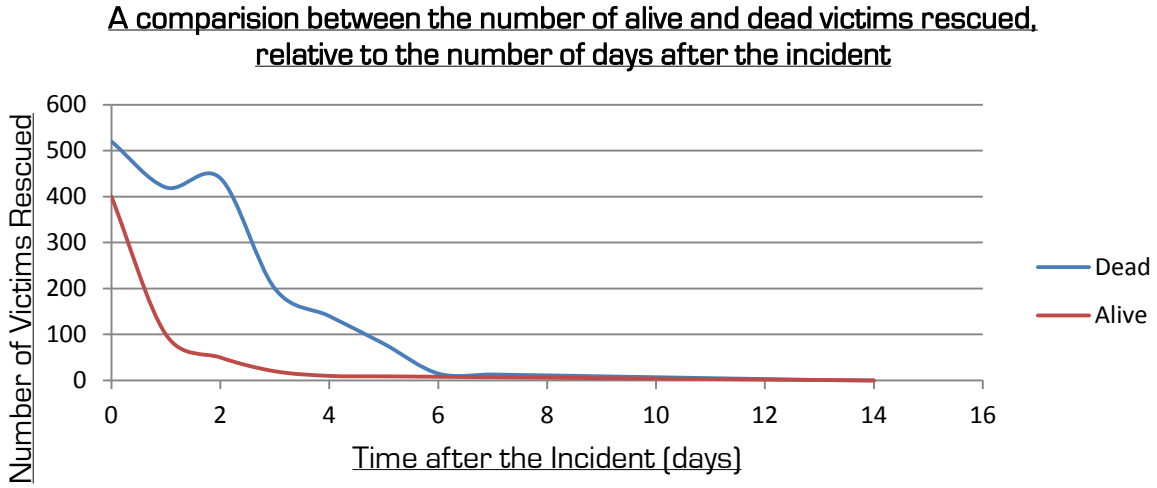

Figure 1-1: Number of victims rescued by the Kobe Fire Department in Hanshin Awaji earthquake [4]

The purpose of the introduction of a robotic system into an urban search and rescue is to improve the efficiency of the rescue operation, by performing tasks that are either too dangerous or impossible for human rescue workers. The robotic system reduces the potential of secondary fatalities to rescue teams while improving the efficiency of victim location, thus improving the survival rate of both victims and the rescue team alike.

In order to achieve this, some of the following capabilities are required of an urban search and rescue (USAR) robot [3];

1) Gather overview information of the disaster
2) Gather information about dangerous materials and environmental conditions
3) Search for and diagnose survivors
4) Investigate and quantify the damage
5) Support recovery actions

These actions are performed through the use of sensors and manipulators incorporated into the robotic system (be it an aerial or ground system). For the purpose of this project, the focus will be on an inspection-class **U**nmanned **G**round **V**ehicle system (UGV).

Some of the UGV inspection-class robotic systems used during the USAR operation carried out on the World Trade Centre can be seen in Figure 1-2. During the use of the robotic systems, it was found that the deployment time, complexity and size of the system limited their use. Operators carried the systems to small voids for inspection. The inspections took on average six minutes and 44 seconds [5] to complete. Due to the complexity of the systems, a skilled operator is required, extending the deployment times of the systems.

Figure 1-2: A number of the inspection-class robotic systems used during the USAR operation at the World Trade Centres [5]

A USAR robotic system similar to the platforms used at the World Trade Centres was developed over a number of years at the UCT **R**obotics and **A**gents **R**esearch **L**ab (RARL). The Ratel, seen in Figure 1-3, is a tracked robotic platform with a specialized sensor payload mounted on a six DOF arm. The system provided many valuable insights into the challenges of USAR.

The fifth generation Ratel was taken to RoboCup Rescue in Mexico, which was a challenging but valuable experience for the students at the time. The specialization of the Ratel requires extensive setup time and a skilled operator that extends the response time of the system, and limits the usability of the system as a rapid response system. It was proposed that a smaller simpler first-response system would be more effective, a sentiment that was echoed by the rescue workers at the 2012 IEEE/RAS conference in Turkey. Thus, the need for a general-purpose first-response robotic system was highlighted.

Figure 1-3: The Ratel

1.2: General-purpose first-response, throwable, man-packable inspection-class robotic system

A general first-response system should be small, reconfigurable and functional with an operator who has little or no training. The purpose of the first-response system is to search and identify survivors and determine the requirements of a dedicated robotic platform should one be required. Thus, the platform can be classed as an inspection-class robotic system.

An inspection-class man-packable, throwable robotic system is both quick to deploy and compact in design. The robotic system is designed to communicate sensory stimulus to the operator providing an awareness of the environment, allowing the operator to make informed decisions about hazards and subsequent protection requirements, prior to entering the environment. One of the major defining aspects of any robotic system is the method of deployment. A requirement for this system is that a single operator should be able to carry it and throw it into the deployment environment. Therefore, the robotic system should be both man-packable and throwable.

In order for a robotic system to be defined as man-packable "the entire robotic system, including the control unit, batteries, and tools, must fit into one or two back-packs" [1]. A 1:1 human-to-robot ratio is a requirement for this system and therefore a single operator should be able to transport the entire system. This will enable the robotic system to be carried into an environment and deployed from a position of relative safety. The mass of the system will also be a deciding factor in the distance that the operator can throw it.

A throwable robot or "ThrowBot" is defined by Recon Robotics as a "sub-kilogram class of robot that provides short range remote eyes and ears" [6]. However the mass of the robot is not limited to sub-kilogram as can be noted by the fact the iRobot FirstLook, is throwable at a mass of 2.45 kg [7]. The Recon Scout XT (Figure 1-4) is an example of a throwable, man-packable inspection-class robot which is designed for military applications. The purpose of this robot is to allow military personal to throw the robot into a zone and inspect the area for explosives and armed enemies.

Figure 1-4: The Recon Scout XT an example of a throwable, man-packable inspection-class robot. [4]

The final consideration for a first-response system is the cost. A low-cost system will allow a system to be based with every rescue team, reducing the response time. The currently available systems cannot be considered as low-cost — the Recon Scout is priced at US$ 7500. The cost of the system reduces the feasibility as a first-response system, as it is not affordable for every disaster management team to own one. Thus, the need for low-cost was proposed.

1.3: The Scarab

The Scarab is a two-wheeled tail-dragger designed to be a general-purpose first-response system with a target cost of US$ 300 for the platform. As seen in Figure 1-5, a single operator carries the Scarab to the point of deployment. An operator station and transportation harness, seen in Figure 1-6, was developed and attached to a MOLLE vest, to carry the entire system. The system is tetherless and is, therefore, battery-operated and communications are enabled via wireless.

Figure 1-5: The Scarab

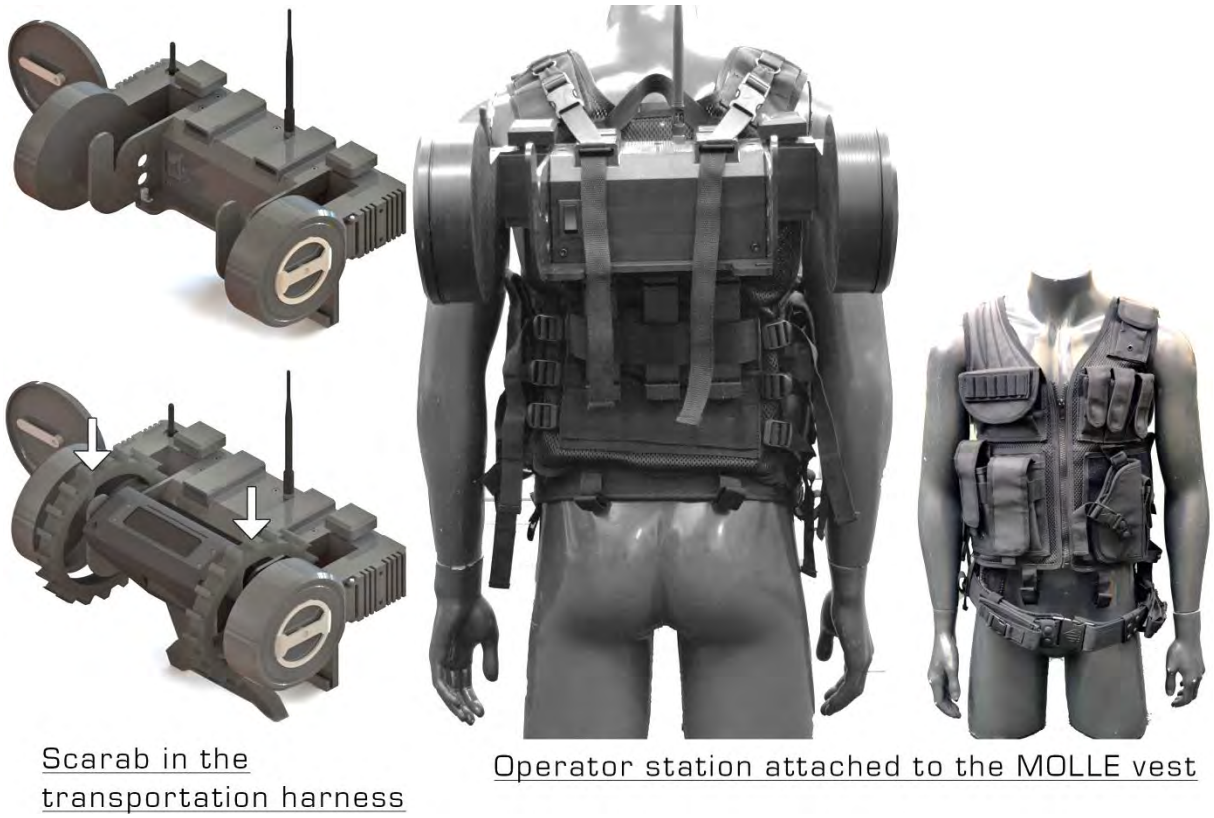

Figure 1-6: The Scarab in the transportation harness on the left and the operator station attached to the operator and MOLLE vest on the left [Credit: Wai Fong]

The operation of the system is illustrated by Figure 1-7. The platform is carried to the point of deployment from whence it is thrown; the symmetrical design allowing for operation in the orientation in which the platform lands. A single operator can perform the entire operation with the system. To reduce the cost and allow the single platform design to be used in multiple disasters, the payload is interchangeable allowing the sensor configuration to be tailored to the needs of the disaster. The cost and 1:1 human-to-robot ratio is ideal for rescue applications.

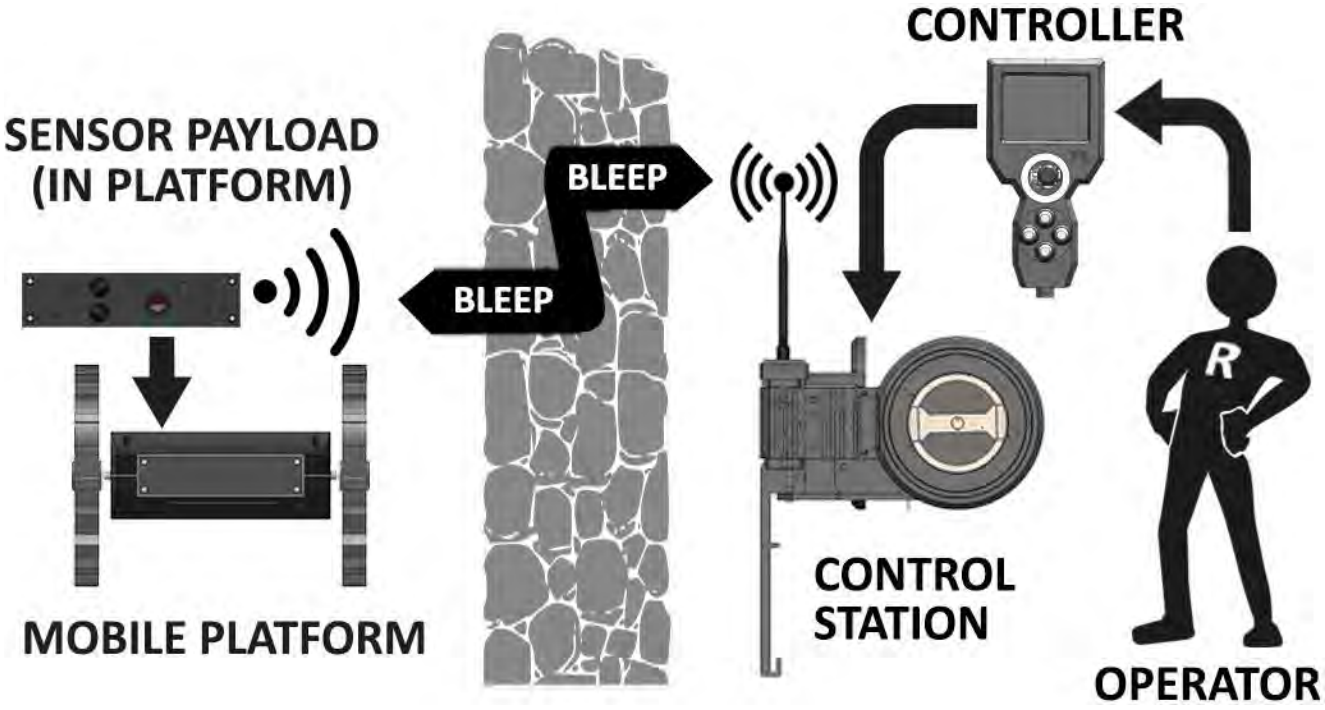

Figure 1-7: Illustration of the operation of the Scarab [Credit: Wai Fong]

The interchangeable sensor payloads, battery management and communication systems which are the subject of this report were developed for the Scarab robotic platform.

1.4: Scope and limitations of the project

The intention of the project is to design an interchangeable sensor payload, communication and power management system for low-cost, throwable USAR robotic system. Thomas Mathew and Wai Kit Fong have designed the remainder of the robotic system: the platform and motor control and the control station and controller in tandem.

Features required in the system are outlined below;

- Man-Packable: A single operator should be able to transport and deploy the platform.
- Throwable: The robotic platform should be able to survive a 3 m vertical drop.
- The system will be tetherless, therefore the communications will be wireless and the system will be battery powered.
- Additionally, the system will be required to perform multiple drops before returning to the base of operations, and hence should be capable of field charging.
- Two sensor payloads will be designed: one that will fill the minimum requirements of an inspection-class robotic system and the second will support a FLIR Quark thermal camera.
- Finally, the transmitter for the video communication has been pre-selected: the Range Video FPV 1.3 GHz video transmitter.

The report begins by exploring the sensor composition of currently available systems and the sensory needs of a USAR inspection-class robotic platform. This knowledge was used to explore sensors relevant as determined by the requirement of an inspection-class robotic platform. The information gained from the research, along with the design brief, was then used to formulate a quantifiable set of specifications for the system. According to these specifications, the sensor configuration of the sensor payload was then determined and the supporting circuitry and software was developed for the sensors. A data communication protocol was developed to ensure that data corruption could be detected. This was followed by the selection and design of a battery and BMS, after which the entire system was tested, conclusions drawn and recommendations made.

Background Research

As the basis for the project has been outlined, this chapter will summarize the background research carried out as a basis for many of the design decisions. This began with research into the similar systems that are currently commercially available. This was followed by research into wireless communications and battery chemistry selection and management systems.

2.1. Sensor payloads of currently available systems

In the course of this section the sensor payloads of currently available throwable inspection-class robotics systems will be investigated: namely, the iRobot Firstlook and the Recon Robotics Throwbots.

The iRobot Firstlook, seen in Figure 2-1, is a tracked robotic platform designed to carry multiple sensor configurations. However, some of the sensors are mounted externally, thus limiting the mobility of the platform. For this reason only the internally mounted sensors will be considered. The Throwbot offers no sensory expansions but it is considerably lighter and less costly than the iRobot — at US$ 7500 compared to the US$ 20,000 for the iRobot. A specification comparison between the two systems can be seen in Table 2-1.

Figure 2-1: iRobot Firstlook [7] (left) and the Recon Scout Throwbot XT [8]**(right)**

The Firstlook is considered as throwable, however, at 2.45 kg, the range of the throw will be limited. Both systems are designed for military applications and therefore both use IR camera systems so as not to alert combatants of the presence of the system. However, in a rescue situation this is not preferred. The optimal sensor configuration for the Scarab platform will be determined for a rescue situation; therefore victim identification and HAZMAT (**Haz**ardous **Mat**erials) sensors will be required.

Table 2-1: Specification comparison between the iRobot Firstlook and the Recon Scout Throwbot XT

	Firstlook	Recon Scout Thowbot XT
Camera	4 x encased sensitive to IR and Near IR Light, pan, tilt and 8 x digital zoom	Black and white camera
Illumination	Near IR	Near IR
Range line of sight	200 m	91 m
Range non line of Sight	n/a	30 m
Run time	>6 hrs	60 min
Mass	2.45 kg	0.54 kg
Water resistance	IP67	300 mm
Audio	Bidirectional	Listening only
Sensory expansion	Port facility for externally mounted sensors	none

While this makes it ideal for many military and rescue applications there are other commercial applications of an inspection-class robotic system.

2.2: Commercial application of a throwable, man-packable inspection-class robotic system

The possible commercial application of the system will be explored in future revisions of the robotic system. A brief summary of a number of the possible commercial applications of the system are summarized in Table 2-2.

In order to perform the tasks summarized in Table 2-2, the sensory requirements vary from x-ray imaging for weld and crack inspection in tanks, bridges and pipes to thermal imaging and environmental sensors for human detection and leak detection. Due to the widely varied sensor requirements, a system with an interchangeable payload is ideal for fulfilling many of the requirements of the commercial applications. As USAR is one of the most challenging environments in terms both mobility and durability, a platform designed for USAR will be able to overcome many of the challenges in the commercial applications mentioned.

USAR robotics has been described as challenging by Blitch because "the robot is, by definition, operating in a harsh, mobility-challenging environment. The presence of abrasive dust and water, the corrosive effects of wet cement, and the wide range of obstacles in the environment serve to accelerate the wear and tear on a robot" [1]. Therefore, it can be concluded that once the challenges of urban search and rescue have been met, the modification, which will allow the robotic system to meet the requirements of the remaining applications, will be minimal. The modifications would be in the form of changes in the sensor configuration of the sensor payload rather than the mechanical structure of the robot. These modifications could be achieved with plug-in modules or interchangeable sensor payloads.

Table 2-2: Possible usage fields for a low-cost, man-packable, throwable robot [9]

Field	Task
Nuclear waste inspection	Waste tank inspection
Civil engineering	Bridge and pipe inspections
Civil engineering & urban search and rescue	Inspection/ Surveying damaged buildings that are unsafe to enter
Urban search and rescue: victim recovery	Searching collapsed rubble to find survivors
Industrial maintenance	Inspection/ Sweeping out of building air duct lines
Shipping/ Maritime	Inspection of hull interior
Mining industry	Remote visual inspection of unstable shafts/ newly opened areas and sealed mines
Construction industry	Remote visual inspection
Law enforcement	Remote surveillance

As USAR was the most challenging environment the Scarab will be designed as a USAR robotic platform and future designs of sensor configurations will consider the sensory requirements of the remaining commercial applications.

2.3: Sensors and urban search and rescue

There are three classes of sensors: control, victim identification [10] and HAZMAT sensors [3]. Many of these sensors, however, lie at the union of the classes and, therefore, have multiple functions. A potential configuration of sensors for control would be the following:

- Video cameras
- Digital compass
- Accelerometer
- Inclinometer
- Laser range finder or another method for determining distance/ size of an object
- LED lights

Similarly, the likely victim identification and HAZMAT sensor configurations would be as follows;

- Video cameras
- Infrared camera/ Heat sensors, cost dependent
- Gas detection sensors (oxygen, hydrogen sulphide, methane, carbon dioxide)
- Microphone/ speakers for communication with victims
- Radiation detection

2.3.1 It is of extreme importance that the robot provides adequate situational awareness for the operator [11]. Therefore, one of the most important sensors for an inspection-class robot is the camera as it communicates visual information to the operator.

Video cameras

Video cameras are critical for both control and victim identification, as stated by Blackburn "video is the primary source of information for tele-operated navigation and surveillance" [5]. When selecting a camera the following factors should be considered;

- Due to the nature of a disaster zone the dust coating all surfaces provides an even grey tone when viewing with a black and white camera [10]. Therefore colour images are essential in order to be effective.
- The second constraint would be the Field Of View (FOV) of the camera as "it is only a fraction of the FOV normally available to a human" [5]. Therefore, most of, if not all of the information provided by the human peripheral vision is lost; as a result, in order to improve the operator's awareness, the FOV should mimic that of a human eye [10], which is "by regular field of view 120-180 degrees" [12] . Alternatively, a system using multiple cameras could be considered.

The FOV of the selected camera lens can be calculated using equation (2-1).

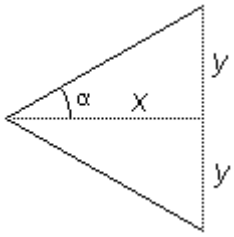

Figure 2-2: Sketch representing the calculation of FOV [13]

$$FOV = 2 \times \tan^{-1}\left(\frac{y}{x}\right) \quad (2\text{-}1)$$

When analysing the operations of USAR robots at the 2001 World Trade Centre USAR operations, Robin Murphy stated the video feedback did "not provide adequate depth and size information to the operators" [5]. One potential solution to the problem of depth perception is the concept of stereo vision proposed by Burion [14] whereby two cameras are used and the difference between the two images is used to determine distances. This could be used as an effective method of range finding and provide adequate information for the operator to determine depths. However, the cost of a second camera should be considered as it will also increase the bandwidth requirement for the communication system.

A final consideration for camera selection is the fact that many USAR operations are conducted in low light environments. Therefore, low light camera modules with an alternative illumination source should be considered. As the intended use of the platform is for rescue, stealth is not a requirement. Near IR will be not be considered, as LED illumination will alert survivors to the presence of the platform, increasing the chances of identifying survivors.

Finally, as the system is required to operate in all orientations, a digital camera will allow the image to be mirrored about the horizontal or vertical plane, reducing the requirement for processing at the operator station. However, the point at which a mirroring is required, and about which plane, does need to be determined. While the mirror about the horizontal plane can easily be determined with the use of a simple mercury switch, the detection of a mirror about the vertical plane requires a more inclusive measurement system such as an IMU.

2.3.2.

Inertial measurement unit

An Inertial Measurement Unit (IMU) is used to determine the orientation of a system referenced to the earth. A true 9 Degree of Freedom (DOF) IMU consists of a three-axis accelerometer,

gyroscope and magnetometer. Individually the sensors cannot reliably estimate the orientation of the body, however, when the data outputs from the three devices are combined, it allows an accurate estimation of the orientation to be calculated.

The attitude of a static object can be calculated from an accelerometer by determining the attitude of the accelerometer relative to gravity. However, as the body begins to accelerate, differentiating between the acceleration and acceleration due to gravity becomes impossible. Similarly, correcting for integration drift using the gyroscopic data is not possible without a point of reference for correction. The solution is, therefore, to use a fusion of the data from both devices to determine the attitude of the body. Three such methods are the Madgwick, Kalman and Mahony filters. The Mahony is an extension of the Madgwick filter. The advantage of the Madgwick filter is the low processing power requirement as the filter uses the quaternion representation against the Euler representation used by the Kalman filter. Therefore, an attitude is stored using four variables against the nine of the Euler matrix. However, as seen in Table 2-3, the Kalman filter provides a more accurate calculated attitude.

Table 2-3: Error comparison between the Kalman, Madgwick and Mahony filters [15]

Angular Speed (deg/s)	Euler angle	Kalman Filter (% error)	Madgwick Filter (% error)	Mahony Filter (% error)
0	Roll	0.04	0.03	0.02
	Pitch	0.01	0.05	0.05
	Yaw	0.30	1.92	1.85
18	Roll	4.71	4.85	5.07
	Pitch	1.91	2.65	2.89
	Yaw	5.19	5.13	5.67
45	Roll	6.55	6.51	6.69
	Pitch	2.83	3.34	2.85
	Yaw	6.71	7.07	6.92

2.4: Wireless communication

The communication is critical to the success of the robotic system and particular care should be taken when considering the impact of the environment on wireless communications [1]. "Wireless communication in the interior of the rubble is unpredictable and generally non-existent." [1] The factors to consider when selecting a wireless frequency are the signal penetration, bandwidth and power requirements. The final consideration when selecting the frequency is the frequency licence regulations, which should be adhered too. This, however, varies with location as seen in Figure 2-3. 433 MHz is one of the most widely available of the licence-free frequencies; however, it lacks the bandwidth to transmit video signals. Therefore, a higher frequency will be required for the video transmission. One such frequency (which is licence-free) not listed in Figure 2-3 is the 1.3 GHz frequency [16].

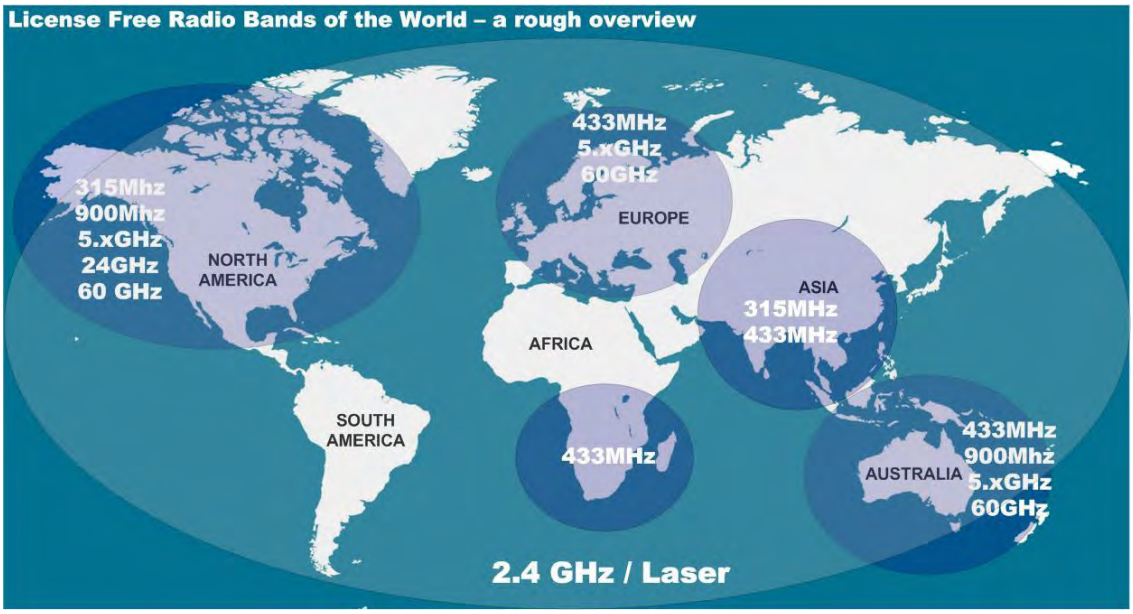

Figure 2-3: Illustration of the licence-free frequencies across the world [17]

2.5: Data processing

A microcontroller is required to process, integrate the data and direct the commands between the operator and the robot, with the wireless communication being the medium via which the communications occur. The microcontroller acts as an anchor for communications throughout the system, therefore the processing ability of the microcontroller can have dramatic effects to the latency of communication and overall the performance of the system.

The first consideration is communication between the controller and the devices, which will likely be in the form of UART, SPI and I^2C communication. The second consideration is the method of implementation of the microcontrollers to perform the data manipulation efficiently. There are two different methods to consider. The first is the use of a network of low-cost microcontrollers of which each processor controls a few sensors. Efficiency is achieved by clustering the sensors to microcontrollers to process the data and only transferring the minimum required data to a central microcontroller for wireless transmission. The second option is to perform all the control and data manipulation from a single controller. This would require a higher processing ability in order to achieve the same efficiency.

2.5.1: UART communication

A FLIR Quark thermal camera had been pre-selected for use in the extended sensor payload and, therefore, Universal Asynchronous Receiver Transmitter communication is required for communication with the thermal camera. As the communications are asynchronous, both the transmitter and the receiver are required to be communicating at the same baud rate. A start bit synchronizes the receiver clock with the transmitter clock as seen in Figure 2-4. After the start bit the eight data bits are transmitted which can be followed be a parity bit to enable error checking. A stop bit or bits then terminate the data byte.

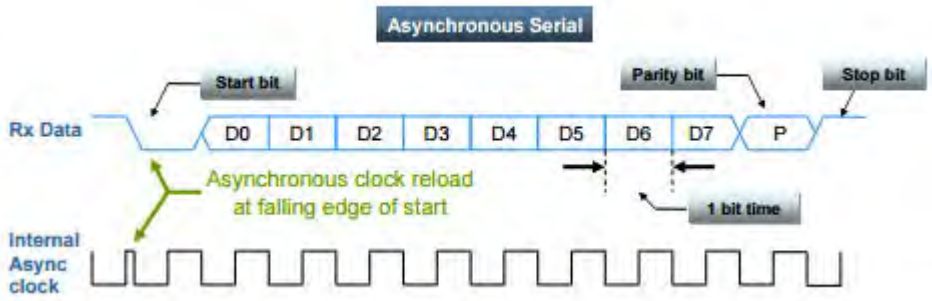

Figure 2-4: Asynchronous serial communication [18]

SPI communication

Serial Peripheral interface (SPI) is a bus communication system established by Motorola [19]. It provides a synchronous, full duplex data link with data transferred from the master controller to the slave device along the MOSI (master-output-slave-input) line (seen in Figure 2-5) and received on the MISO (master-input-slave-output) line.

2.5.2

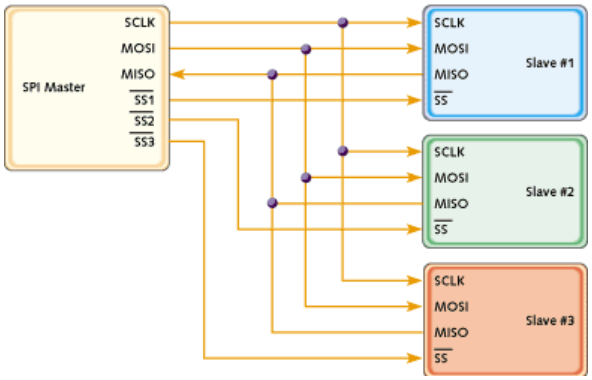

Figure 2-5: Block diagram of SPI communication protocol [20]

As seen in Figure 2-5, there are four signal lines required:

- The SS (slave select) line which indicates which device (slave) should be listening
- The SCLK line, which provides the clock signal, generated by the master, indicating the timing for the reading and writing of each data bit. The clock polarity (CPOL) and the clock phase (CPHA) setting determine the edge of the clock pulse on which the data is transmitted and received.
- Lastly, the two data lines — the MISO and MOSI lines.

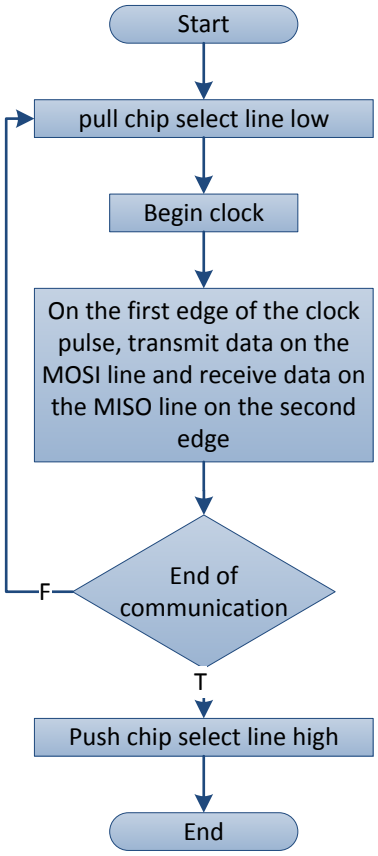

Figure 2-6: Basic SPI communications

The advantage of the SPI system is that it supports higher clock frequencies and therefore higher transfer rates than those of I^2C and UART. This allows for an improved communication rate. However, the disadvantage of the SPI system is that is requires additional GPIO pins on the microcontroller in order to select the device.

SPI protocol

The SPI protocol is a method of communication over an SPI system whereby all communication contains an address byte. Table 2-4 shows the format of the address byte. Setting the R/W bit indicates that the master is requesting a read from the register identified by the bits $A_{[5:0]}$. If the device supports burst communications, setting the burst bit indicates that the master is requesting multiple communication starting at the register identified by the bits $A_{[5:0]}$.

Table 2-4: SPI protocol address byte

Bit	7	6	5	4	3	2	1	0
Data	R/W	Burst	A_5	A_4	A_3	A_2	A_1	A_0

2.5.3:

I^2C communication

"The I^2C bus was designed by Philips in the early 1980s to allow easy communication between components which reside on the same circuit board." [21] The communication system uses two bus lines, one clock line (SCL) generated by the master and bidirectional data line (SDA). As seen in Figure 2-7, both lines are pulled up to V_{CC} and the bits are communicated by pulling the line low and releasing it, to produce a high.

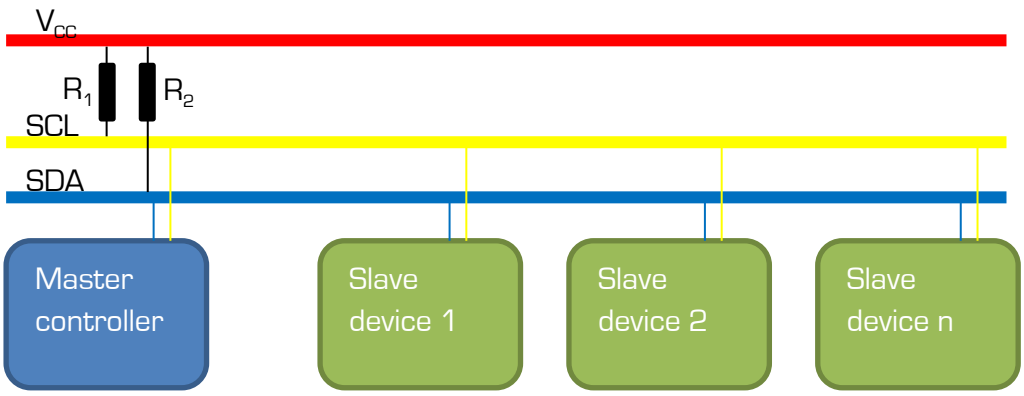

Figure 2-7: I²C communication bus

I²C protocol

The beginning of each data byte is indicated by a start condition whereby the SDA line is pulled low while the SCL line is high. The receiver indicates the receipt of the byte by pulling the SDA line low in the ninth clock pulse. The byte is terminated by a stop condition, releasing the SDA line while the SCL line is high as seen in Figure 2-8.

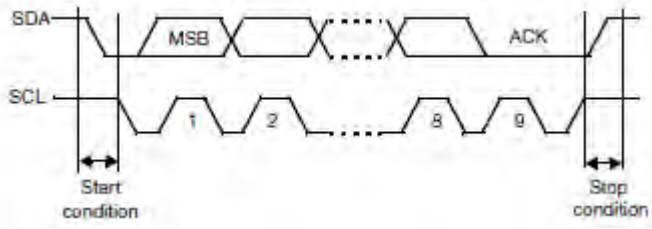

Figure 2-8: I²C bus protocol [22]

Each slave device on the bus has a unique address; therefore, the device is selected by beginning the communication with the address of the slave device, the zeroth bit of the address indicating the direction of the communications.

2.6: Power management

The power management can be broken down into three subsections: the power source, power monitoring and, lastly, power regulation. As described on page 6, the robotic system is tetherless, therefore power will be sourced from a battery.

2.6.1:

Battery chemistry selection

As the battery is the sole source of power, it is of utmost importance. However, it will potentially be a major contributor to the overall mass of the entire system. As the system is to be man-packable and throwable, the cell chemistry of the battery should be carefully selected for both the power-to-weight ratio and for the stability of the battery chemistry. Additionally, cell chemistries can be categorized into two forms: primary and secondary – the latter being rechargeable. As multiple drops are required, to reduce the need for multiple cells to be carried by the operator, a rechargeable chemistry will be selected. The optimal battery chemistry will be determined by

considering the following characteristics: energy density, charging and storage requirements, cost and (importantly) the stability of the chemistry.

Figure 2-9 shows the energy density against the power-to-volume ratio of a number of common secondary cells. Based purely on the specification of energy density, the Lithium Polymer would be the optimal cell chemistry. However, as the robotic system will be charged while attached to operator, the stability of the battery should be considered in the cell chemistry selection.

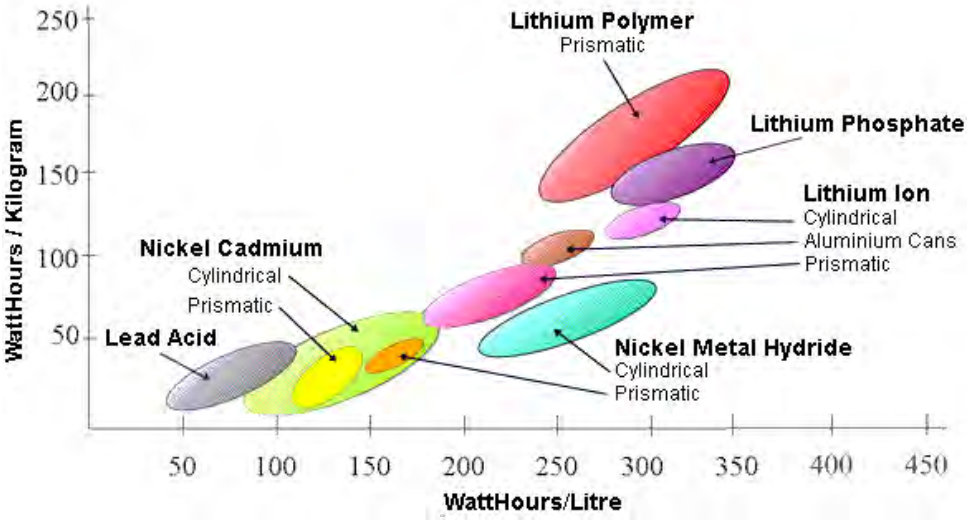

Figure 2-9: Relative energy density of common secondary cells [23]

What can be concluded from Figure 2-9, is that the stability of lithium batteries should be investigated for the use in this application, on the basis of energy density. Many of the lithium polymer chemistries have been described as unstable [23]. However, the Li-phosphate chemistry has been described as having an "Extremely safe/stable chemistry: no explosions and will not catch fire under collision, over charging or when short circuited" [24]. However, the Li-phosphate chemistry is not readily commercially available as of yet. However, "Lithium-Ion batteries were designed to overcome the safety problems associated with the highly reactive properties of Lithium metal" [23]. In order to ensure the safety of the cells, battery monitoring is required for all Lithium-Ion based battery packs. Additionally, Lithium-Ion cells have "no memory effect and excellent discharge performance" [23], meaning that the battery can be recharged before it is fully discharged, which is optimal for an in-field multiple-use charging system. In Lithium-Ion batteries, each cell has a nominal voltage of 3.6 V compared to the standard of 1.2 V per cell for lead acid and Nickel Cadmium cells — therefore requiring fewer cells for higher battery voltages [25].

2.6.2. As the Lithium-Ion chemistry is the preferred choice of cell chemistry optimising for both energy density, stability, further research into Lithium-Ion battery management systems is required to ensure the health, and stability of the battery is maintained.

Lithium-Ion battery management systems

The functions of the battery management system (BMS) can be described as follows: to prevent damage to the cells and battery, in order to maintain and prolong the life of the battery ensuring that it is able to fulfil the requirements of the application [26]. This is achieved with multiple modules as seen in Figure 2-10. The BMS is comprised of a primary battery protection, cell balancing, a fuel gauge and optional secondary battery protection.

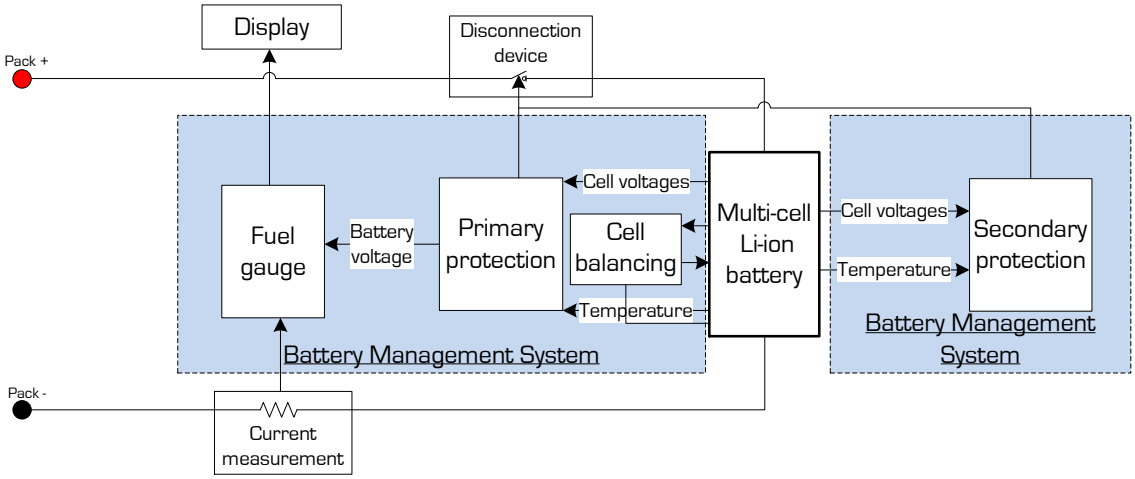

Figure 2-10: Diagram of a simplified battery management system

Lithium-Ion battery protection

There are a number of states, which if entered into, will lead to a reduction in the State-Of-Health (SOH) and therefore stability and capacity of the battery. While the battery manufacturer outlines the specific values, the values stated below are nominal for the Lithium-Ion chemistry:

- **Cell over voltage:** Cell voltages of above 4.3V per Cell. Exceeding the maximum voltage of the cell can lead to catastrophic failure of the battery.
- **Cell Under voltage:** Cell voltages below 2.9V per Cell.
- **Cell over discharge\ charge rate**: Discharging and charging the battery at a rate higher than specified by the manufacturer will lead to higher rates of degradation of the battery capacity reducing the lifespan of the battery.
- **Cell over temperature:** A combination of both the environmental temperature and the internally generated heat, as a product of the internal resistance, can lead to the battery being exposed to temperatures that negatively affect the batteries SOH.
- **Cell imbalance:** Cell imbalance can only occur in multi-cell configurations. It is a result of the differences in internal resistances of the cells causing a difference in the potential across each cell. If left uncorrected, this will reduce the usable capacity of the battery as an individual cell may enter a cell under or over voltage state causing a loss of usable capacity in the remaining cells.

Fuel gauging

One of the primary sections of the BMS that allows the system to maintain the battery is the fuel gauge. This allows for estimations of the usable charge remaining to ensure the relevant buffers are in place so as to allow for soft shutdowns and memory maintenance. This is achieved by determining the State Of Charge (SOC) of the battery. The state of charge can be defined as the remaining charge relative to the maximum possible, as seen in equation (2-2), where Q is described as the energy.

$$SOC(\%) = \frac{Q_{max} - Q_{released}}{Q_{max}} \times 100\ \% \qquad (2\text{-}2)$$

There are a number of methods of determining the state of charge. The simplest method is that of voltage translation. However, while voltage measurements are used in the battery protection systems, there are a number of factors which result in voltage translation being an ineffective method of determining the SOC of the battery. The non-linearity of the discharge profile of Lithium-Ion cells as seen in Figure 2-11 reduces the effectiveness of a voltage measurement when being used to determine the SOC. What can be seen in Figure 2-11 is the difference between the **O**pen **C**ircuit **V**oltage (OCV) and the **C**losed **C**ircuit **V**oltage (CCV) that is a result of the internal resistance of the battery. This results in the discharge profile being dependent on the rate of discharge (Figure 2-12) and the internal resistance of each cell; which varies between cells and increase as the SOH of the cell decreases [27]. This, in turn, affects the SOC calculation as the $Q_{use} < Q_{max}$ and should be included, to accurately predict the remaining capacity. Therefore, it can be seen that while voltage measurements can be used to determine the points of both fully charged and discharged states, an alternate method is required for determining the SOC at any given point along the discharge profile.

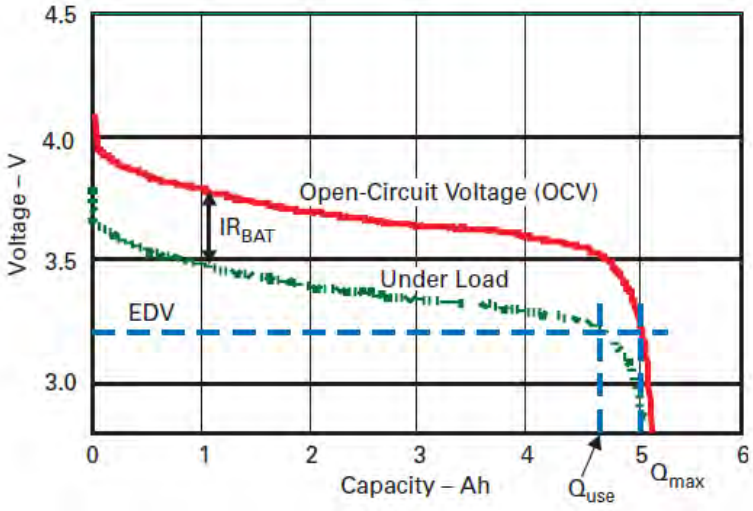

Figure 2-11: SOC definition for an arbitrary rate of discharge [28]

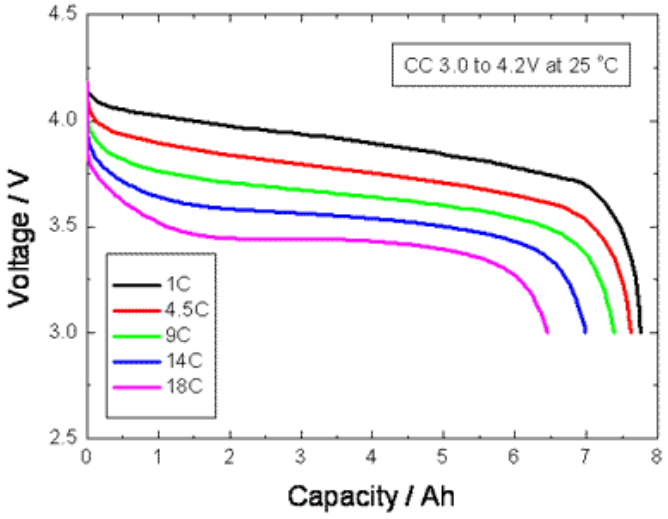

Figure 2-12: Discharge curve of a Lithium-Ion battery at different discharge rates [29]

The second possible method of determining the SOC is that of current integration or coulomb counting. The charge entering and leaving the battery is determined by integrating the measured current with respect to time, hence determining the remaining charge relative to an initial charge

at a given time. Current integration cannot be used alone to determine SOC though, as firstly it neglects the following losses:

- Cell self-discharge: Charge "leakage" causes a small factor of the charge to be lost over a period of time without passing through the current measurement.
- Cell efficiency: During the charge process not all current entering the battery is absorbed by the battery.

Furthermore, current integration relies on an accurate current reading, which can be costly; and a known initial SOC. While some of the losses can be accounted for, over time, errors introduced by integration drift require a recalibration point. Therefore, a fusion of both voltage translation and current integration becomes the preferred method of determining SOC.

While this could be implemented via the main system controller, the timing, data storage and data processing requirements for current integration make implementation impractical. However, there are dedicated ICs developed for this function. While many manufactures offer stackable solutions for batteries, Texas Instruments offer single IC fuel gauges for batteries.

Texas Instruments offer a number of battery monitoring IC's which calculate the SOC using coulomb counting, compensated using a one of three different method: **E**nd-**O**f-**D**ischarge-**V**oltage (EDV), **C**ompensated **E**nd-**O**f-**D**ischarge-voltage (CEDV) or **ImpedanceTrack™.** The three methods of fuel gauging are summarized in Table 2-5. The fact that the robotic platform should not deplete the capacity of the cells on every deployment, but will require the full charge for every deployment, means that **ImpedanceTrack™** is the preferred method of determining SOC, as both CEDV and EDV require the cell be to discharged in order to recalibrate.

Table 2-5: Summary of the methods of fuel gauging offered by Texas Instruments

Fuel Gauging Method	Implementation	Advantages	Disadvantages
EDV End-of-Discharge-Voltage	Current integration calibrated at fixed voltage references near the termination voltage of the discharge cycle Figure 2-13	Simple to implement. Effective at low discharge rates	Effective only at low discharge rates where the IR drop corresponds to a low voltage drop. Cells should be discharged full to allow for the calibration
CEDV Compensated End-of-Discharge-Voltage	Uses similar principle to EDV. However the calibrations point is adjusted according to the rate of discharge. Therefore compensating for the internal resistance Figure 2-14	Simple to implement	Cells should be discharged full to allow for the calibration. Internal resistance of the cell increases with the decline of the SOH of the battery
ImpedanceTrack™	Uses the correlation between OCV and the SOC. Therefore, during zero discharge charging periods the OCV can be measured allowing for a SOC to be determined and used as a calibration point for the current integration as seen in Figure 2-15	Cells don't need to be discharged fully to account for integration drift. The stored OCV values can be used to determine the internal resistance of the cells as they age, improving the SOC estimation	Increased data storage requirement as the OCV and corresponding SOC are stored and updated as the cells age

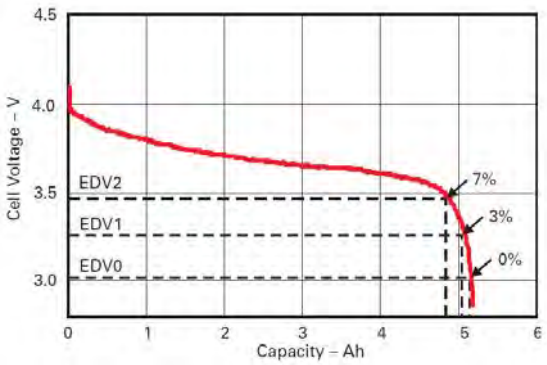

Figure 2-13: Graphic description of EDV [28]

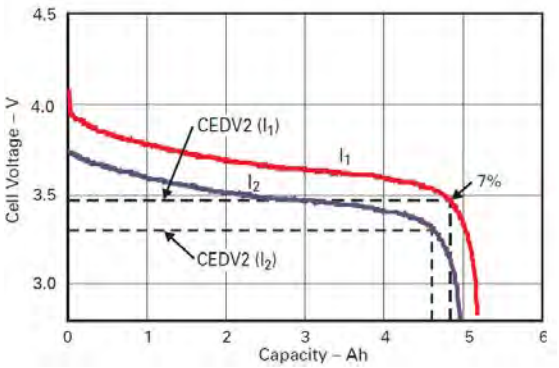

Figure 2-14: Graphic description of CEDV [28]

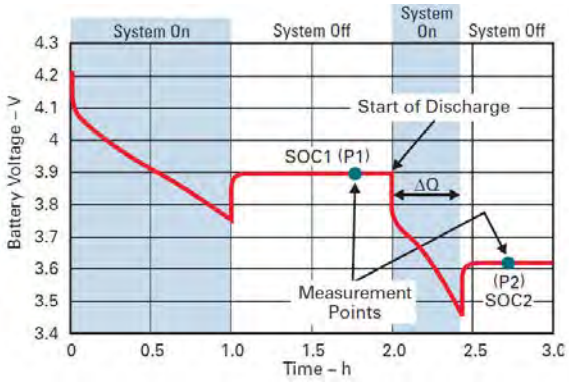

Figure 2-15: Determining the total chemical capacity during discharge [28]

2.6.3: Lithium-Ion battery charging

Lithium-Ion battery charging requires a two-stage charge process. The charge profile consists of a constant current phase followed by a constant voltage phase leading up to the charge termination [30]. This can be seen in Figure 2-16. As the battery charging is not perfectly efficient due the internal resistance of the cell, the rate of charge does not directly relate to the charge time. Due to the internal resistance of the cells, higher charge rates will be less efficient, and the relative time spent during the saturation charge will increase [30]. The loss of efficiency will result in an increase in the battery temperature and therefore the battery temperature should be monitored during charging to ensure the temperature of the battery does not reach a catastrophic level.

As with the fuel gauging, there are a number of ICs that are designed for the specific function of charging Lithium-Ion batteries. This system will use a dedicated battery charging IC, which will be described later.

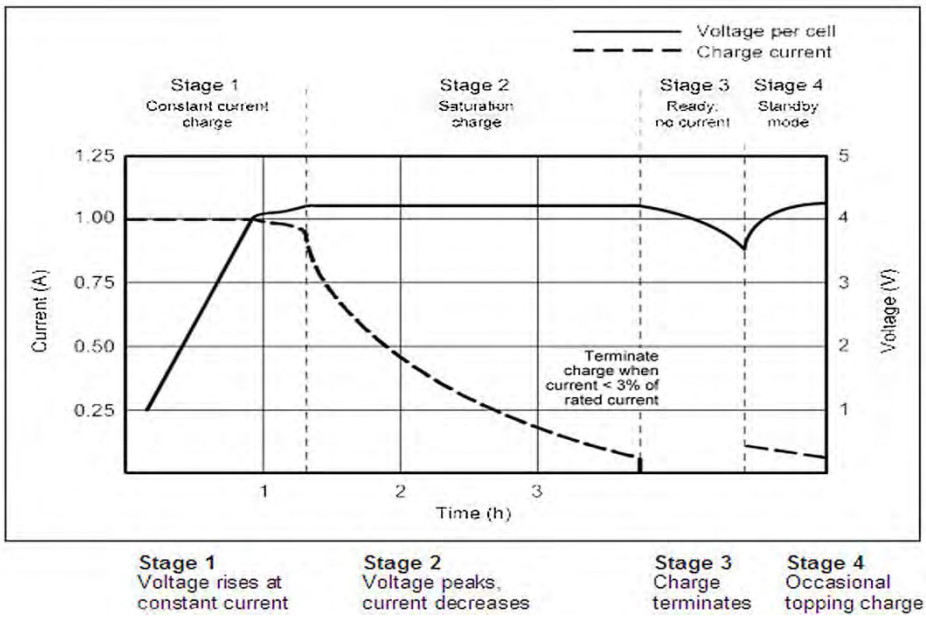

Figure 2-16: The graph indicating the charging profile of a Lithium-Ion cell [30]

Voltage regulation methods

2.6.4. The system will require the power to be supplied at a number of voltage levels. This is a result of the fact the motor will require 12 V and any microcontroller selected will require 5 V or lower. Therefore, voltage regulation will be required. There are two main forms of step-down voltage regulation: a **S**witch **M**ode **P**ower **S**upply (SMPS) or a **L**inear **D**rop **O**ut regulator (LDO).

In the majority of cases, a SWPS is more efficient than a LDO and is, therefore, used where a large voltage drop is required. The drawback of such a system is the output noise and the dropout voltage. The dropout voltage is defined as the minimum potential difference between the input and output of the regulator. The disadvantage of the LDO is the fact that the efficiency is linearly dependent on the voltage drop required. As a result, of this the use of a LDO should be limited to smaller voltage drops for higher current draws. The advantage of an LDO is a reduced output noise in comparison to the SMPS and dropout voltages of as low as 150 mV. Should a large voltage drop and a low noise power supply be required, the optimal solution is that of two-stage regulation system. A SMPS is used to provide an efficient regulation of a large voltage drop and the LDO is used for the final regulation, to provide a low noise output.

2.7: Printed circuit board layout considerations

The layout of any PCB can have a considerable effect on the operation of the system. As a result, of this a number of PCB layout methods were researched in order to improve the performance of the system.

Track widths

The width of the trace affects the operational temperature of the system. This is a result of the internal resistance of the system; recommended trace width for a 10 °C rise in temperature for a given current can be seen in Table 2-6. This table should be used as a guideline on which PCB track widths should be selected.

Table 2-6: PCB current ratings and track widths [31]

Copper Thickness	Track Width (mm)	Current Rating (A)
35 µm	0.25	0.5
	0.50	1.0
	1.00	2.2
70 µm	0.50	2.0
	1.50	4.5
	2.00	6.0
	4.00	9.0

Kelvin contact

One of the common methods of determining the current flow along a path is to determine the potential across a shunt resistor, which is the method used by the BMS. The accuracy of the potential reading across the sense resistor has a direct relationship to the SOC estimation. In order to reduce the loss of potential and power dissipation, a low value resistor is used in the range of 1 to 10 m Ω. This, however, presents a problem: the potential difference being measured is nominally in the range of 0 to 200 mV, which is small compared to the battery voltage, and therefore the parasitic circuit resistance can have an effect on the measurement.

"A Kelvin connection is a means of making electrical potential contact with a current carrying component in such a way that eliminates or greatly reduces the effects of contact resistance." [32] A Kelvin connection is achieved by laying a trace from the neutral point of the SMD footprint as seen in Figure 2-17, this reduces the connection resistance and noise induced in the sensing lines as a result of the current flow along the high current path. As the measurement device will typically draw a current in the magnitude of µA, the potential drop across the sensing traces will add no significant error to the measurement. [32]

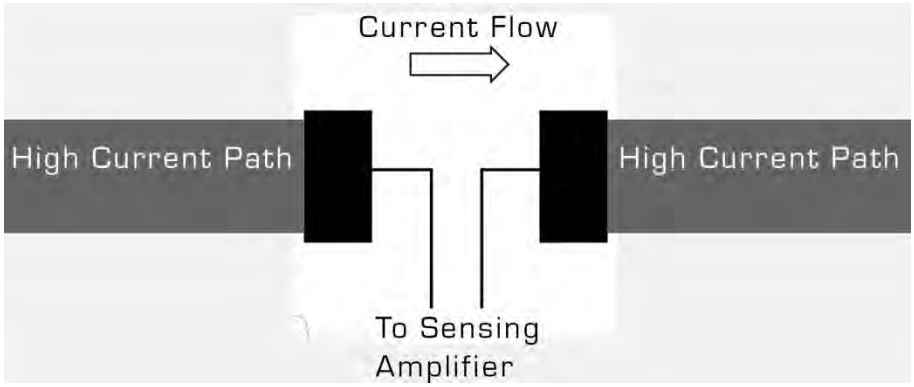

Figure 2-17: Kelvin contact for a SMD component [33]

2.8: Concluding remarks

While there are at least two potential solutions which are currently commercially available – Recon Scout and the iRobot Firstlook – both systems are too costly to be considered as low-cost and hence expendable. The Firstlook is capable of supporting multiple sensor payloads, but they are externally mounted and thus reduce the mobility of the platform. There is a need for a low-cost throwable urban search and rescue robotic platform. Due to the variable nature of an urban disaster environment, selecting a sensor payload that has sensing capabilities for every disaster is

impractical, therefore the ability to change the sensor payload is critical, as this will allow first responders to select the sensor configuration most suitable to the specific disaster environment.

Sensor payloads

With the three possible classes of sensors being control, victim identification and HAZMAT, the first prototype will focus on the control and victim identification sensors. Two sensor payloads will be developed to illustrate the ability of the system to support multiple sensor payloads. One of which will include a FLIR Quark thermal camera and the focus of the other will be to provide an awareness of the environment at the lowest possible cost.

Communication

It is a requirement that the system is tetherless and therefore the communication will be wireless. In order to reduce the bandwidth requirement, the communication should be on separate, license-free frequencies. For this system, the optimal frequencies are 433 MHz for the data and 1.3 GHz for the video and audio communications.

Battery management

As the system is tetherless, the power source will be a battery. The optimal battery chemistry for the application would be Lithium-Ion. In order for the power to be reliably supplied, the system will require a BMS to prevent battery failure. The BMS will also provide an estimation of the remaining time through "coulomb counting" and the optimal method of combating integration drift is that of **ImpedanceTrack™**. A dedicated IC will execute the estimation and primary battery protection. The system will be designed for in-field charging, which will be controlled by a dedicated IC. As the system will be charged while attached to an operator, a secondary battery protection system should be implemented, should the primary battery protection fail.

Design Requirements

In this chapter, the design brief is expanded into a quantifiable set of requirements shown in Table 3-1. This is followed by a justification of the selected requirements, which will be used to develop a list of specifications for each subsystem. The design brief was as follows: "The design of communication, power management and interchangeable sensor payload subsystems for a low-cost throwable urban search and rescue robotics platform."

Table 3-1: Table of system requirements

Explanation Location	System requirement	Desired Value
3.1: Physical requirement		
3.1.1:	System mass	600 g
3.1.2:	Dimensions	145 x 122 x 80 mm
3.1.3:	Cost	US$ 150 [1]
3.2: Functional requirement		
3.2.1:	Colour camera	Yes
3.2.2:	Microphone	Yes
3.2.3:	Temperature sensor	Yes
3.2.4:	Swappable sensor payload	Yes
3.2.5:	Multi orientation operation	Yes
3.2.6:	Output supply voltage	12 V, 3.3 V
3.2.7:	Output supply power	6 W (12 V), 0.33 W (3.3 V)
3.2.8:	Wireless communication	Yes
3.2.9:	Video transmitter	Range Video FPV
3.2.10:	System diagnostics	Yes
3.3: Extended payload functional requirement		
3.3.1:	Thermal camera	FLIR Quark
3.4: Performance requirement		
3.4.1:	Operational range(Indoor)	30 m
3.4.2:	Operational time	20 min
3.4.3:	Standby time	5 hrs

[1] The cost specification applies to the low-cost sensor payload only

3.1.1:

3.1: Physical requirement

System mass

3.1.2: In order to meet the platform specification of 1400 g, assuming that the battery will be one of the major contributors to the overall system mass, the entire system should be no more than half the mass of the entire platform.

Dimensions

As the system is intended to be integrated into the Scarab platform, it will have to be designed to fit into the allocated area shown in Figure 3-1.

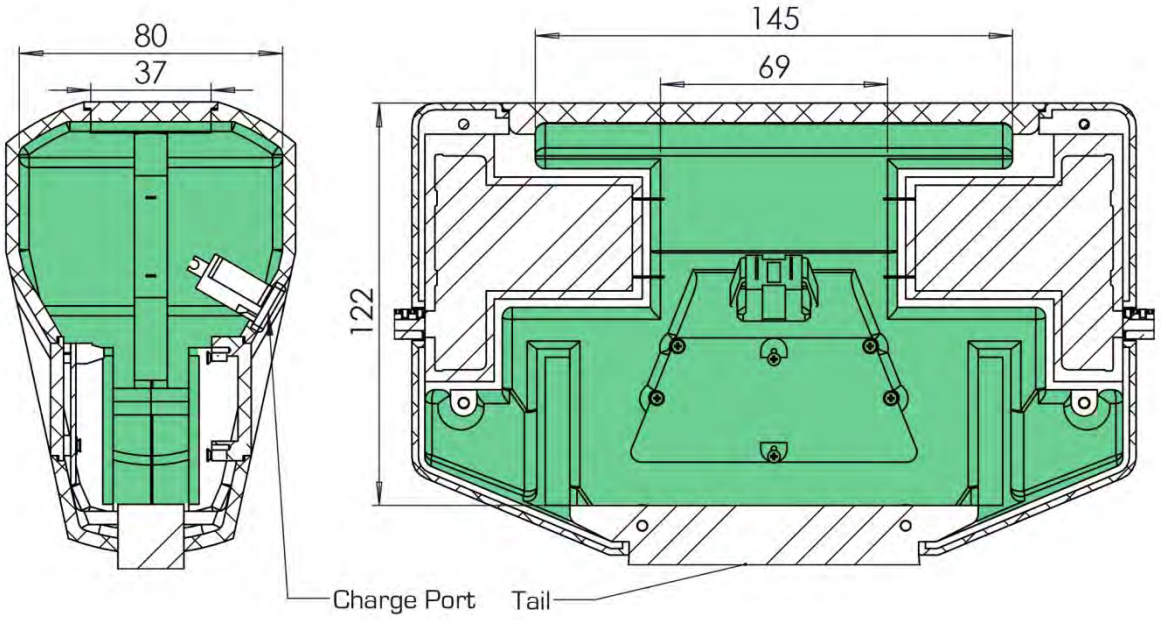

Figure 3-1: Drawing showing the dimensional boundaries of the system

Cost

3.1.1: It was assumed that the two major costs of the platform are expected to be the battery and the motors. In order to achieve the target of US$ 300, the system should cost no more than US$ 150.

3.2: Functional requirement

3.2.1: Colour camera

As explained on page 10, an urban disaster environment is generally covered with a layer of dust. This causes the entire environment to become an even tone of grey on a greyscale image, making a colour camera essential to allow details to be identified [10].

3.2.2: Microphone

3.2.3: A microphone will allow rescuers to listen for the voice of a survivor, allowing for a survivor to be identified when outside the FOV.

Temperature sensor

3.2.4: An environmental temperature sensor will allow the operator to make informed decisions on the potential of identifying a survivor in the environment, based on the temperature related habitability of the area into which the robot travels.

Interchangeable sensor payload

Allowing for the sensor payload to be changed in the field will allow for multiple sensor payloads to be developed. This will allow the operator to select the optimal sensor configuration for the deployment.

Multi orientation operation

As the platform design is that of a two wheel tail-dragger without any method self-righting. The platform should be able to operate in all orientations.

Output supply voltages

3.2.5: The motors require a 12 V input and the motor driver requires 3.3 V supply voltage

Output supply power

3.2.6: A pair of 3 W motors has been selected and 100 mA is required for the motor driver circuitry

Wireless communication

3.2.7: The system is required to be tetherless and therefore, wireless communication is a requirement.

3.2.8: Video transmitter

The Range Video FPV 1.3 GHz video transmitter and receiver pair have been provided.

3.2.9:

System diagnostics

3.2.10: As the system is a first prototype system, diagnostics are crucial to provide insight to the internal operation of the system during testing. The system diagnostics should provide the relevant information to improve the efficiency of future designs.

3.3: Extended payload functional requirements

3.3.1: Thermal camera

A requirement of the project is that the second sensor payload can support a thermal camera.

3.4: Performance requirements

3.4.1:

Indoor range

3.4.2: 30 m is the indoor range of the Recon Scout Throwbot [8], the aim is therefore to meet or improve on this range.

Operational time

3.4.3: The operational time is the time for which the system can be fully functional with the motors running at an average of 75 % power. As was described in the background research the average time of an operation during the operations at the World Trade Centres was 6 minutes and 44 seconds [5]. Therefore an operation time of 20 minutes greater than 3 times the average will be sufficient, when coupled with the ability for field charging.

Standby time

As described in [5] the average time for extraction of a victim once identified is 4.5 hours. During this period the robotic system is the interface between the victim and the rescue operation and therefore the communications should remain functional. During this period the system is assumed to be stationary and therefore no power will be drawn by the motors.

The system is designed to be integrated into the Scarab robotic platform as seen in Figure 4-1, the shell to provide the structural support for the system. The system comprised three subsystems: the BMS and battery, communications and, finally, the sensor payload as seen in Figure 4-2.

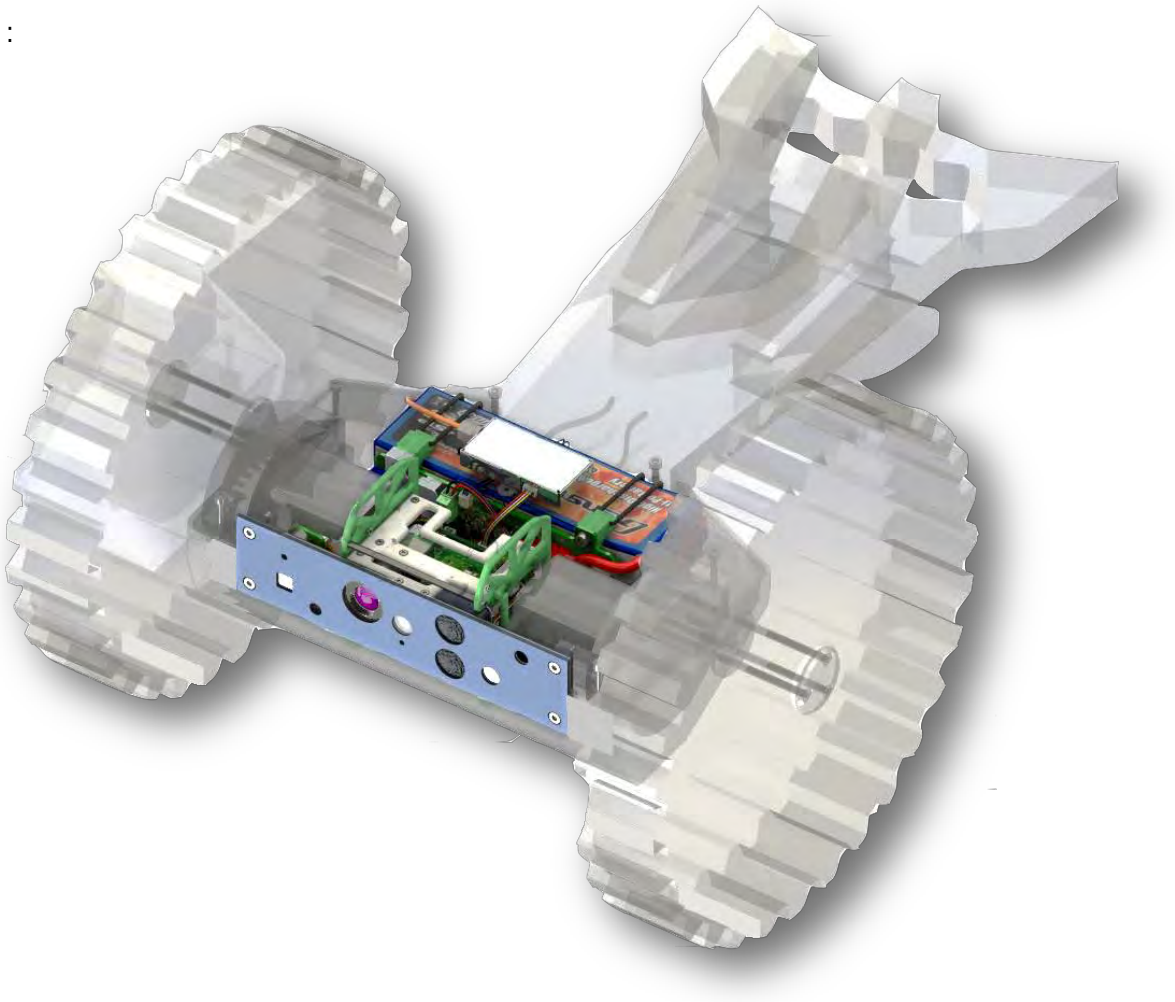

Figure 4-1: Rendering of the sensor payload, communication system and BMS mounted inside the Scarab

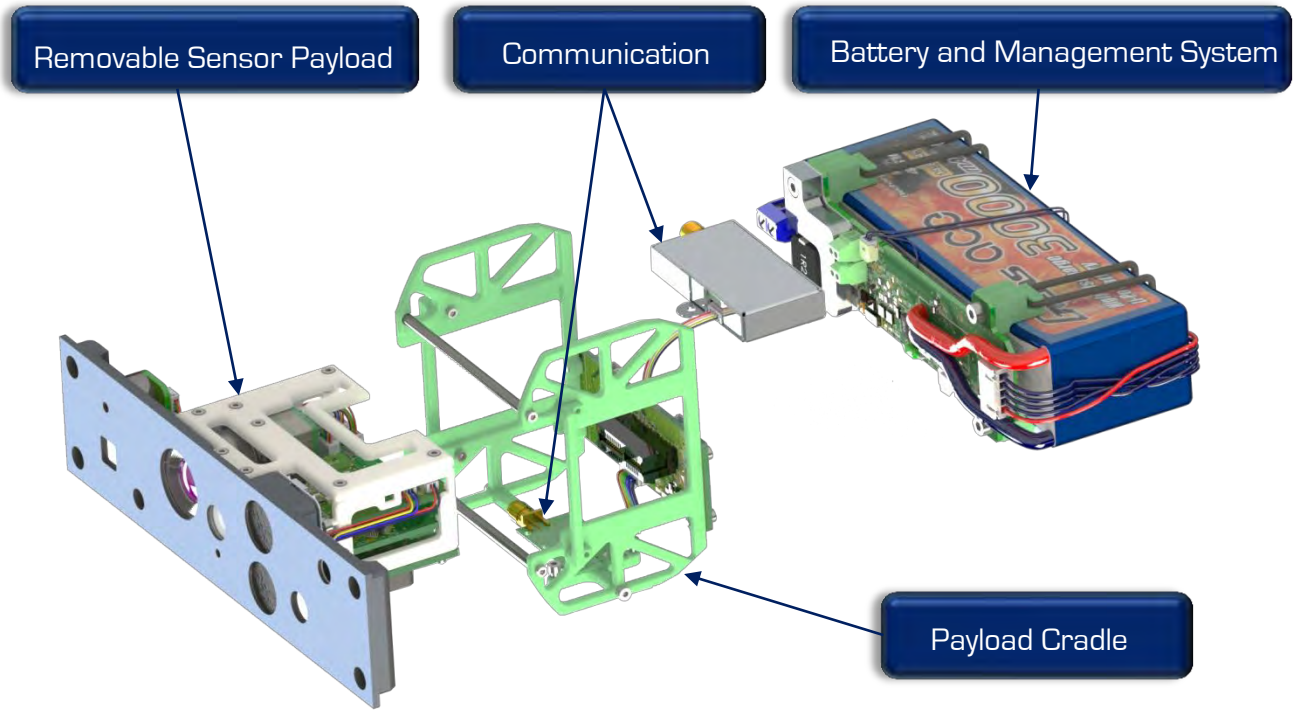

Figure 4-2: Subsystem breakdown

The first iteration of the system included the design of two interchangeable sensor payloads. The aim of the interchangeable sensor payload is such that the payloads will be field swappable and hence will share a similar mechanical structure. As the payload is removable, the subsections to be fixed to the shell will be the BMS and communications subsystems. For the purpose of this prototype, the payload support was not included as part of the shell and thus a sensor payload cradle was designed to provide internal support to the payload. The use of a PCB board edge connector for the power and signals between sensor payloads and the remaining systems allows an electrical connection to be made simultaneously with the insertion of the payload. A simplified version of the connection diagram, shown in Figure 4-3, shows this connection along with the addition of a motor controller which Thomas Mathew developed.

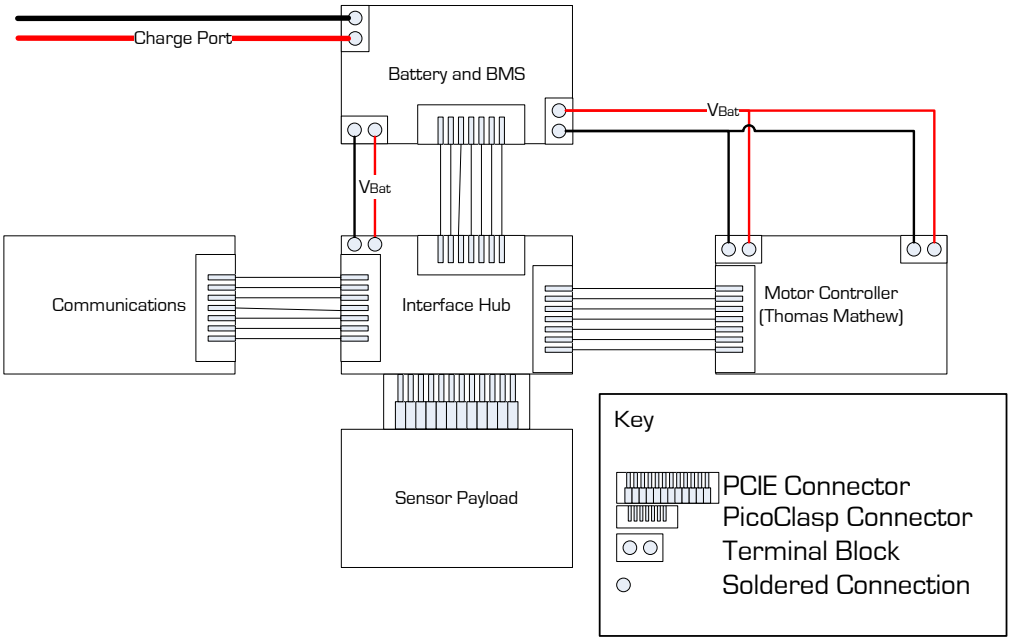

Figure 4-3: Basic overview of the subsystem connections

4.1: Sensor payload

The function of the sensor payload in an inspection-class urban search and rescue robotic platform is to provide the operator with an awareness of the environment in which the robot is located. For this project, two sensor payloads have been designed: a low-cost and an extended version. The primary objective of the low-cost sensor payload is to provide an awareness of the environment and to enable inspection at a minimal cost. The extended sensor payload includes a thermal camera and demonstrates the interchangeability of the payloads. Both where achieved with the following sensors shown in Table 4-1. The location of the sensors is shown in Figure 4-4.

Table 4-1: Sensor payload sensor compositions

Feature	Low-cost Payload	Extended Payload
Video Camera	•	•
Micro Phone	•	•
LED Lighting	•	•
Temperature Sensor	•	•
Thermal Camera		•
STM32F0 µC	•	
STM32F4 µC		•
Accelerometer	•	•
6DOF IMU		•

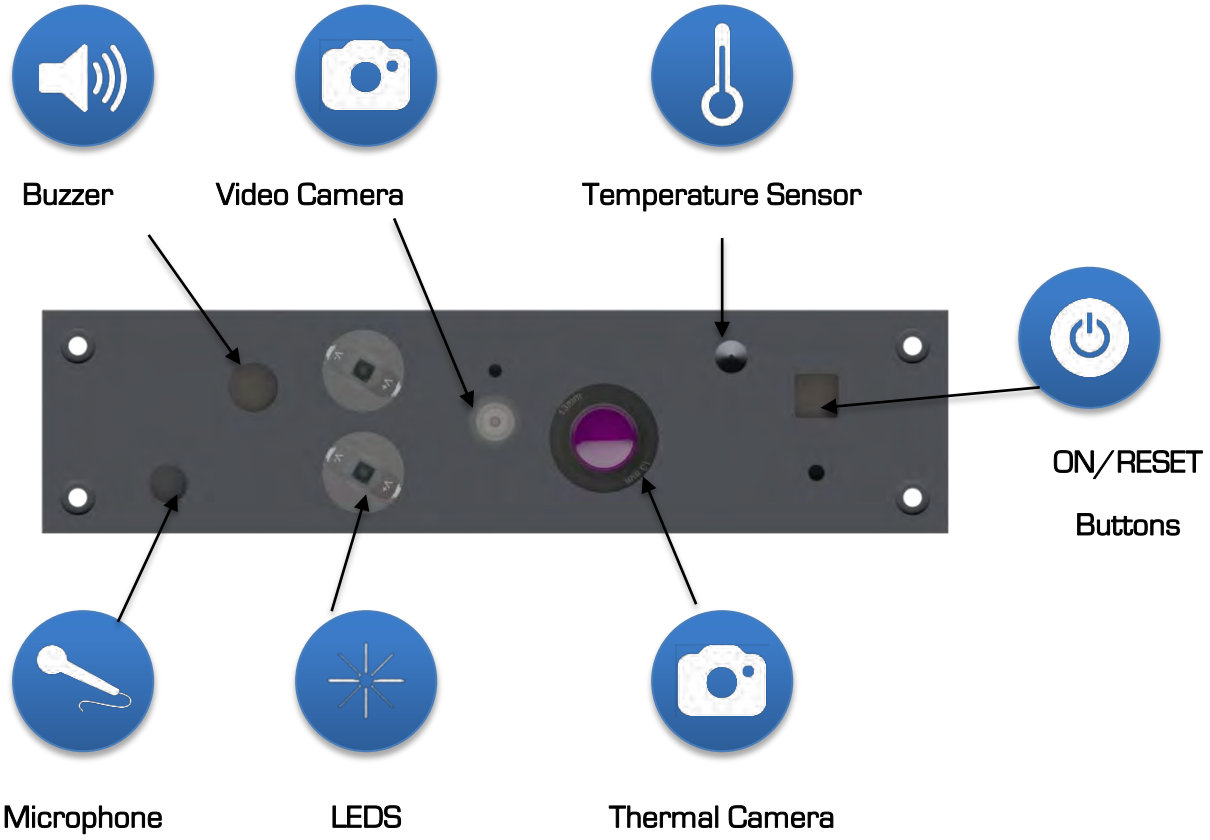

Figure 4-4: Configuration of the front panel of the sensor payload

The location of the camera is of significance, as the platform is symmetrical, with the ability to operate in all orientations. The fact that the camera is located in the centre of the face allows for a simple manipulation of the camera feed to allow the image to be rotated or flipped when necessary. These same rotations are applied to the received motor commands to simplify the operation of the platform.

While the focus of the sensor payload is one of collection and processing of sensory data, there are two additional functions performed by the sensor payload. The software for monitoring the BMS and communication systems is embedded in the payload microcontroller, responsible for the processing of the sensor data. The final function of the sensor payload is voltage regulation for the 3.3 V line. This allows the aluminium front panel to be used as a heat sink.

4.2: Communication

The platform is designed to be tetherless so the communications are transferred via Radio Frequency (RF). In order to improve the efficiency of the communication system, the communication subsystems have been separated onto two different frequencies. This leads to a reduction in the bandwidth requirement per frequency. Therefore the analog data, the video and the audio are communicated using a Range Video FPV 1.3GHz transmitter and receiver pair. The commands to the platform and the data from the sensor payload are transmitted using a pair of CC110L 433MHz transceivers. Packet handling software was developed in order to detect data corruption and reduce the volume of data to be communicated between the command station and the platform.

4.3: BMS

With the selection of a Lithium-Ion battery and the requirement for in-field charging, a battery management system was required. The BMS incorporates battery charging, fuel gauging and battery protection. This is all placed on single PCB which was attached to the battery using a flexible mounting to allow for battery expansion during usage.

4.4: Mechanical overview

Besides the mechanical challenge of the interchangeable sensor payloads, the mechanical design is focused on the positioning of the sensors and the heat sinking of the voltage regulation module. One of the key features of the system is the field-swappable sensor payload. Significant to this feature is the PCB board edge connector. It allows the electrical connection to be made without the potential for damaging the pins. The dimensions of the system can be seen in Figure 4-5.

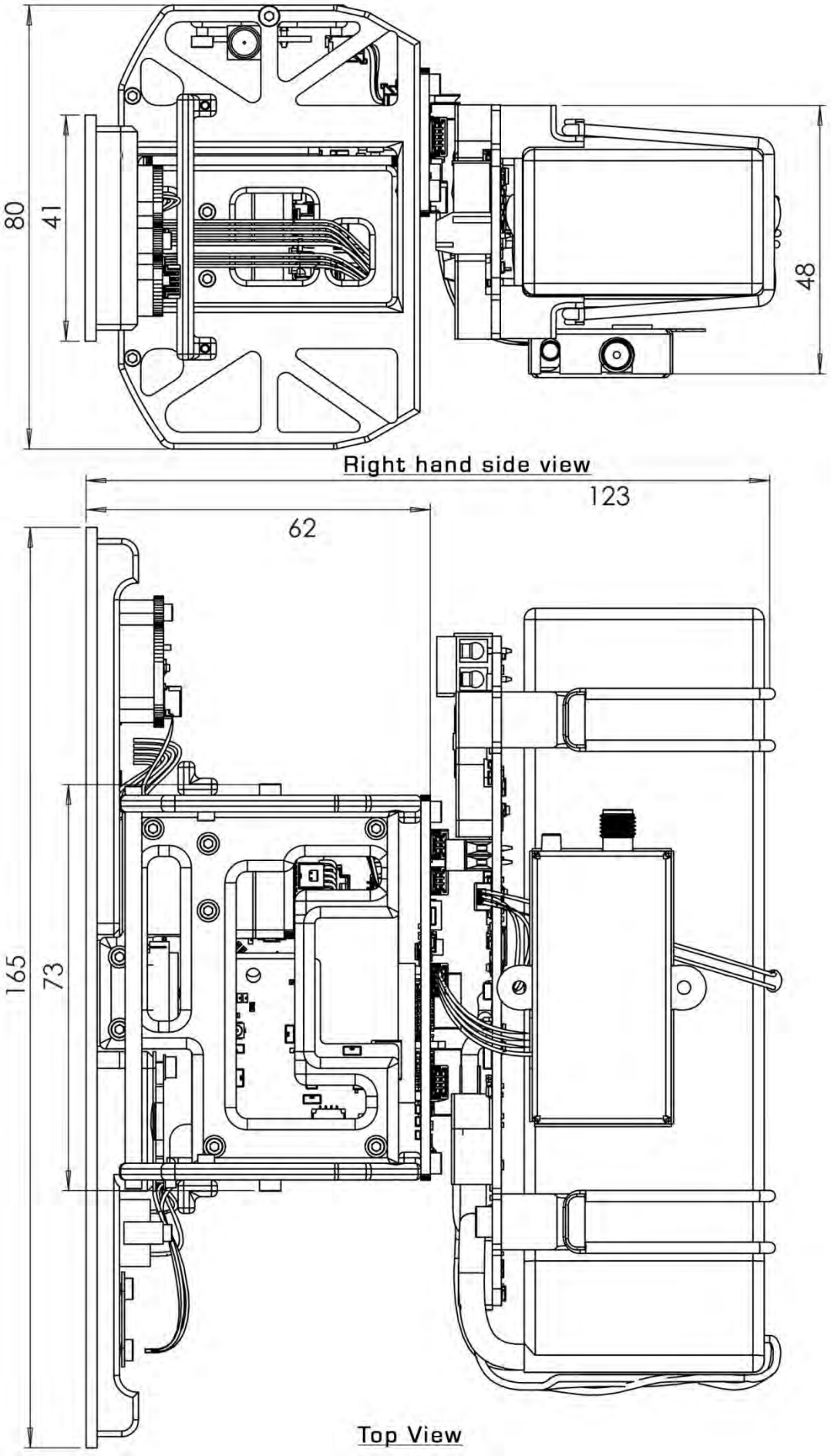

Figure 4-5: Dimensions of the system

Sensor Payload Design

Chapter 5 :

This chapter introduces the sensor selection, PCB design and mechanical layout of the two sensor payloads. As noted in the design specification, two sensor payloads were required. The first was a low-cost design with the minimum sensor requirement; the second was an extended version of the minimum sensor payload. The extended capabilities will include a thermal camera and increased processing power. As noted in the background research, the minimum sensor requirements are visual, temperature and audio sensors; hence a combination of these sensors is used.

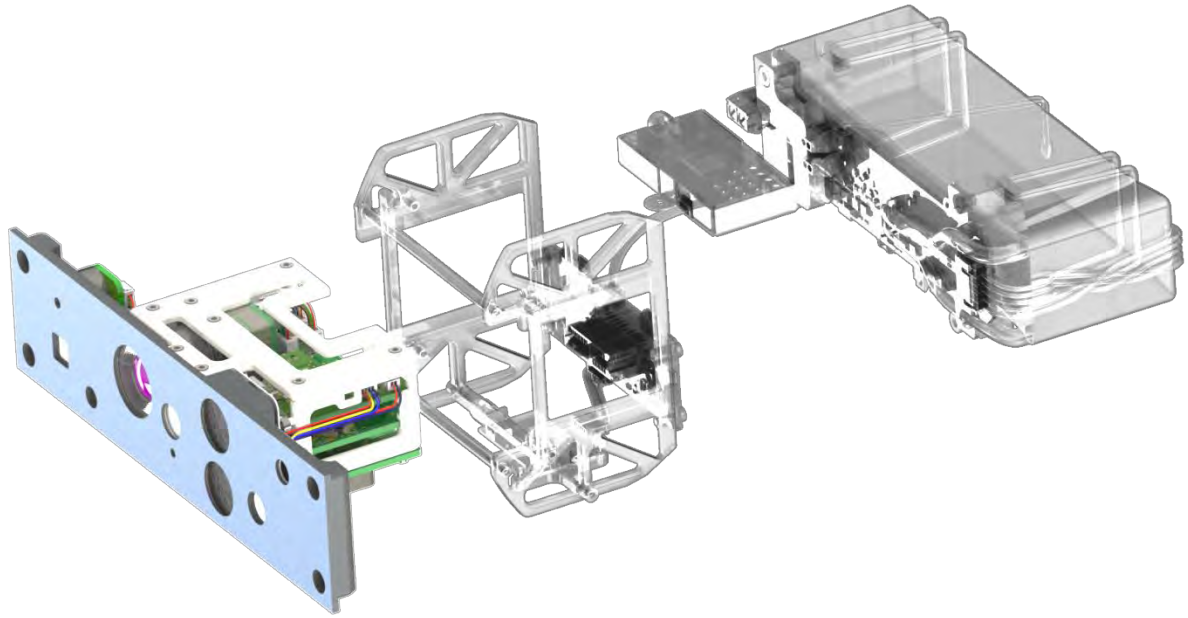

Figure 5-1: Sensor payload location in the system

The purpose of the extended sensor payload is to demonstrate the interchangeability of the payloads. As the low-cost and the extended sensor payloads share dimensional constraints and a number of sensors, for the ease of manufacturing, the power management system of the low-cost sensor payload was designed to fill requirements of the extended sensor payload. A result is that the electrical hardware design for the extended payload is limited to the PCB that houses the microcontroller and the interface for the thermal camera.

For these reasons, the extended payload will contain all the basic features of the low-cost sensor payload with the addition of features to demonstrate the flexibility of the payload. The addition of a thermal camera improves the ability of the operator to detect a survivor in a rescue situation. The increased capability of the microcontroller will allow for further data processing in future work.

5.1: Sensor payload specifications

The purpose of the sensor payload specifications is to expand and further quantify the requirements laid out in Table 3-1. The expansion of the requirements (Table 5-1) is followed by an explanation of the specification.

Table 5-1: Sensor payload specifications

Explanation Location	Subsystem Specification	Desired Value
5.1.1: Physical specifications		
5.1.1.1:	Subsystem mass	200 g
5.1.1.2:	Dimensions	72 x 65 x 41 mm
5.1.1.3:	Cost	US$ 50
5.1.2: Functional specifications		
5.1.2.1:	Camera output	PAL
5.1.2.1:	Microphone audio output	Analog
5.1.2.2:	Multi orientation operation	Yes
5.1.2.3:	Output supply voltage	10 V, 3.3 V
5.1.2.3:	Output supply power	2.6 W (10 V), 0.33 W (3.3 V)
5.1.2.4:	Illumination type	LED
5.1.2.5:	System diagnostics	Temperature, Current, Voltage
5.1.3: Extended payload specifications		
5.1.3.1:	Thermal camera	Yes

5.1.1: Physical specifications

5.1.1.1: Subsystem mass

To achieve the total system mass of the 600 g, with battery estimated at 250 g, the sensor payloads and cradle should be 200 g.

5.1.1.2: Dimensions

As the subsystem is required to be interchangeable, the sensor payloads will a have to be removed through the void surrounding the front panel. Hence, the front panel and the area directly behind define the dimensional constraints of the subsystem.

5.1.1.3: Cost

If the system is to cost US$ 150 with a preselected component, the video transmitter costing US$ 32.63 and the battery being estimated at US$ 45; the target cost of the sensor payload should be US$ 50, to achieve the system cost.

5.1.2: Function specifications

5.1.2.1: Camera output and microphone output

The video transmitter transmits both an analog video and audio signal. PAL video and analog audio signals are required for wireless transfer.

5.1.2.2: Multi orientation operation

The platform is symmetrical and, because of this, does not require a re-orientation mechanism. Therefore the motor commands and images produced should be transformed, so not to disorientate the operator.

5.1.2.3: Output voltage supply

As the voltage regulation module is located in the sensor payload, the regulated power for the motor controller and communication system is supplied from the sensor payload.

5.1.2.4: Illumination

Illumination is required for low light operations and as the system is a rescue platform and therefore stealth is not a concern (as in military applications). LEDs will provide the illumination.

5.1.2.5: System diagnostics

As the subsystem is the first working prototype and the system should operate as a sealed platform, incorporated system diagnostics will provide valuable insight into the operation of the system. This information can be used to guide improvements in future work. The two main areas of concern in the system are the temperature inside the sealed system and the power draw as it is a battery-operated system. Therefore, temperature sensors should be located at all major heat sources with an additional sensor to monitor the ambient temperature inside the shell. The power supplied by the regulators should be monitored.

5.1.3: Extended payload specifications

The extended sensor payload will meet the specification of the low-cost sensor payload with the addition of increased processing power and the following specification:

5.1.3.1: Thermal camera

The extended sensor payload will include a thermal camera to improve the operator's ability to identify victims.

5.2: Component selection

As the cost of the sensor payload is a major consideration, the sensor configuration is required to be minimalistic. Following the recommendation of the background research, the selected sensor configuration consists of a camera, environmental temperature sensor and a microphone.

The most important sensor (as outlined in the background research) is the camera. The requirement for multi orientation capabilities suggests the selection of a camera which has the functionality to both mirror and flip an image. This is due to the complexity of the process of mirroring a PAL image signal.

5.2.1: Camera selection

The camera is used for both control and victim identification. Therefore selecting a camera that will optimise the potential to fill both roles is critical. The camera should be both low-cost and lightweight. In Table 5-2 a summary of the specifications of two of the possible camera modules can be seen.

Toshiba camera has a higher resolution, but also a higher cost. The OV7670 has a higher frame, smaller dimensions and costs less, so this will be selected in order to reduce the cost of the sensor payload.

Table 5-2: Specifications of two of the possible camera modules

Specifications	OmniVision OV7670	Toshiba TCM8240MD
Output	YUV 422, RGB565/555, GRB 422	YUV 422, RGB565 8 bit parallel
Image Communications	8 bit parallel	8 bit parallel
Frame Rate	30 fps	15 fps
Resolution	VGA	1.3 MP
Power Supply	3.0 V, 1.8 V	2.8 V, 1.6 V
Dimensions	6 x6 x 5 mm	10 x 10 x 7 mm
Cost	US$ 3.22 [34]	US$ 9.95 [35]

Temperature sensor selection

5.2.2: The environmental temperature can provide information on the survivability of an environment. However, obtaining an accurate temperature measurement without exposing the electronic circuitry to the environment, limits the choice of sensor. One of the methods of attaining a temperature measurement while maintaining an environmental seal, is through the use of an IR temperature sensor, as the sensor is sealed behind an IR transparent film. One such temperature sensor is the TMP006 from TI. The size and cost of the component coupled with the low supporting component count makes it ideal for the application.

The TMP006 returns the difference between the IR emitted and absorbed as a voltage. The sensor voltage along with the temperature of the TMP006 die is communicated via I^2C. These two measurements make it possible to calculate the temperature of the object emitting the IR.

5.2.3: Processor selection

The microcontroller is the centre of the performance and efficiency of the system. It is responsible for the tasks of implementing the communication and distributing the commands to the relevant modules, while receiving and processing the data from the sensors for transmission to the operator. To enable communications with the BMS, motor driver and CC110L communication IC, the selected processor should have at least one I^2C and SPI peripheral.

Low-cost microcontroller

Initially an MSP430G2995 was considered, however, in order to implement the system diagnostics, a second micro would be required due to the package limitations of the processor. The second option was the STM32F030R8 microcontroller, which has many advantages over the MSP430 — including a reduced cost, increase package size, allowing a single processor to be used, and increased processing power. Additionally, UCT has now adopted the STM32F0xx range of microcontrollers as the educational processor, therefore securing knowledge of the processor for further development. Therefore, the STM32F030R8 was selected as it met the requirements of the system and is sustainable.

Extended sensor payload microcontroller

While the full extent of the processing capability of the STM32F030 was not been exhausted by the low-cost sensor payload, greater processing power will allow for future work to include more computationally expensive processes such as image processing. The STM32F4 family offers a DSP

with hardware FPU, clocked at 168 MHz. As the STMF4 and F0 are both based on ARM architecture, the F4 is a theoretical extension of the F0 allowing for a level of compatibility between the processors. As the microcontroller will be implementing data fusion for an IMU, the hardware FPU will allow an estimate orientation to be calculated accurately and efficiently.

Inertia measurement sensor selection

A result of the symmetrical design of the platform is that the payload should have a multi-orientation design. In order to estimate the orientation of the platform, an accelerometer was used in the case of the low-cost sensor payload and an 9 DOF measurement IC was used on the extended sensor payload.

5.2.4.

In the case of the low-cost sensor payload, the readings from the accelerometer will only be useful when the platform is either stationary or experiencing low accelerations. Therefore, a tri-axis accelerometer with a high full-scale acceleration reading was not required. A cost effective I^2C based accelerometer is the MMA8653, with a selectable full-scale range of up to $\pm$ 78 $m.s^{-2}$, for the purpose of this application a range of $\pm$ 18 $m.s^{-2}$ was selected.

At the time at when the components were selected, there were only two ICs incorporating 9 DOF sensing; these were the Invesense MPU9150 and the STMicroelectronics LSM9DS0. While both devices are similar in cost and communicate via I^2C, the LSM9DS0 offers the option to communicate via either SPI or I2C. Communication via SPI allows for higher communication and sampling rates. The LSM9DS0 was selected for this reason.

Remaining primary component selections

5.2.5:

The remainder of the primary components for the sensor payload and the deciding feature can be seen in Table 5-3.

Table 5-3: Summary of the remaining primary component selection

Component	Selected Device	Feature
Microphone	CMA-4544PF	Cost, analog output
LED	Cree XPG	250 Lumen
LED Driver	LM3401	Cost and Output Current
Buzzer	PKB9-2A0	Large Voltage Range ([3:20] V),

Extended sensor payload

Other than the two component changes already discussed, the microcontroller and the accelerometer, the remaining addition to the system was the thermal camera. As the system is thrown into the disaster environment, it is important to minimise the mass of any component added. Additionally the shock load rating of the device is important. For this reason, the FLIR Quark 336 was selected with a shock rating of 250 g (2450 $m.s^{-2}$) and a mass of 23 grams.

5.3: Electro-mechanical design

Both the platform and the shell were designed in parallel; therefore a volumetric estimation of the system was performed for the platform designer, Thomas Mathew. Based on these constraints, coupled with mechanical requirements of the system, the shell was designed as shown in Figure 5-2.

In order to ensure that the sensor payloads are field-swappable, the entire payload is removable via the void in the shell created by the front panel. Therefore the green area assigned in Figure 5-2, is reserved for the sensor payload. The blue battery bay was designed in conjunction with Thomas Mathew to support the battery with the areas above and below the battery assigned to the motor driver and video transmitter. The remaining red areas in Figure 5-2 are for the components that are not interchangeable: the communications and sensor payload interface.

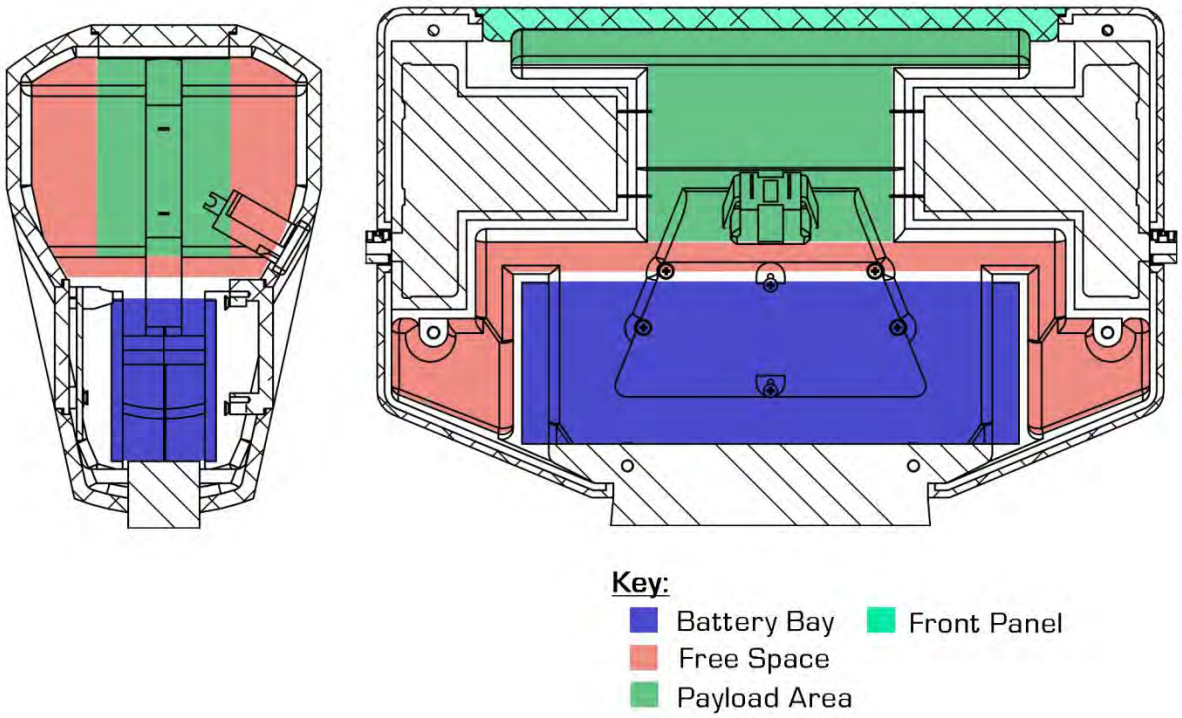

Figure 5-2: Diagram showing the areas, inside the shell, allocated to the system

5.3.1:

Sensor payload outline

The template for the front panel of the sensor payload was designed with the shell by Thomas Mathew to ensure the system face would seal. The template seen in Figure 5-3 was modified to support the environmental sensor.

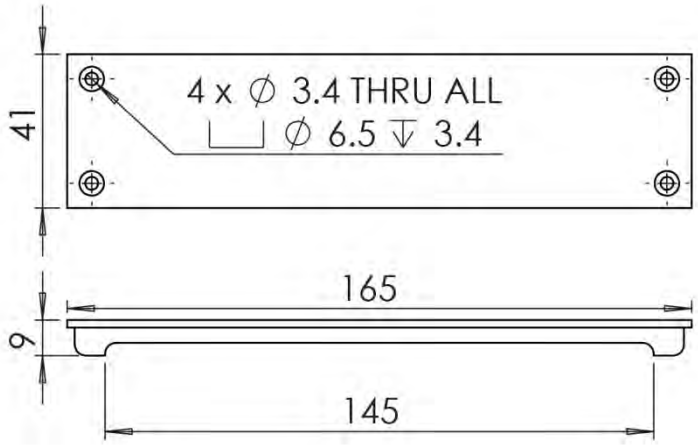

Figure 5-3: Template of the front panel designed by Thomas Mathew

The voltage regulation system designed required a heat sink. As the front panel of the shell had been machined out of aluminium, it provided a large surface area for heat sinking components, therefore an additional piece of aluminium was machined to provide mounting points for the electrical components that required heat sinking. Figure 5-4 shows an exploded view of the mechanical structure. The power distribution PCB forms the base of the PCB stack, which will be explained later in further detail. This is mounted to the heat sink and the 3D printed frame. A heat-conducting pad is located between the heat sink and the PCB, electrically isolating the PCB.

The purpose of the 3D printed frame is to further support the PCBs, and provide cable management. Additionally, the power distribution PCB supports the PCB edge connector, which is the interface between the sensor payload and the remainder of the system. The edge connector allows for both a mechanical and an electrical connection to be created upon insertion of the sensor payload into the cradle.

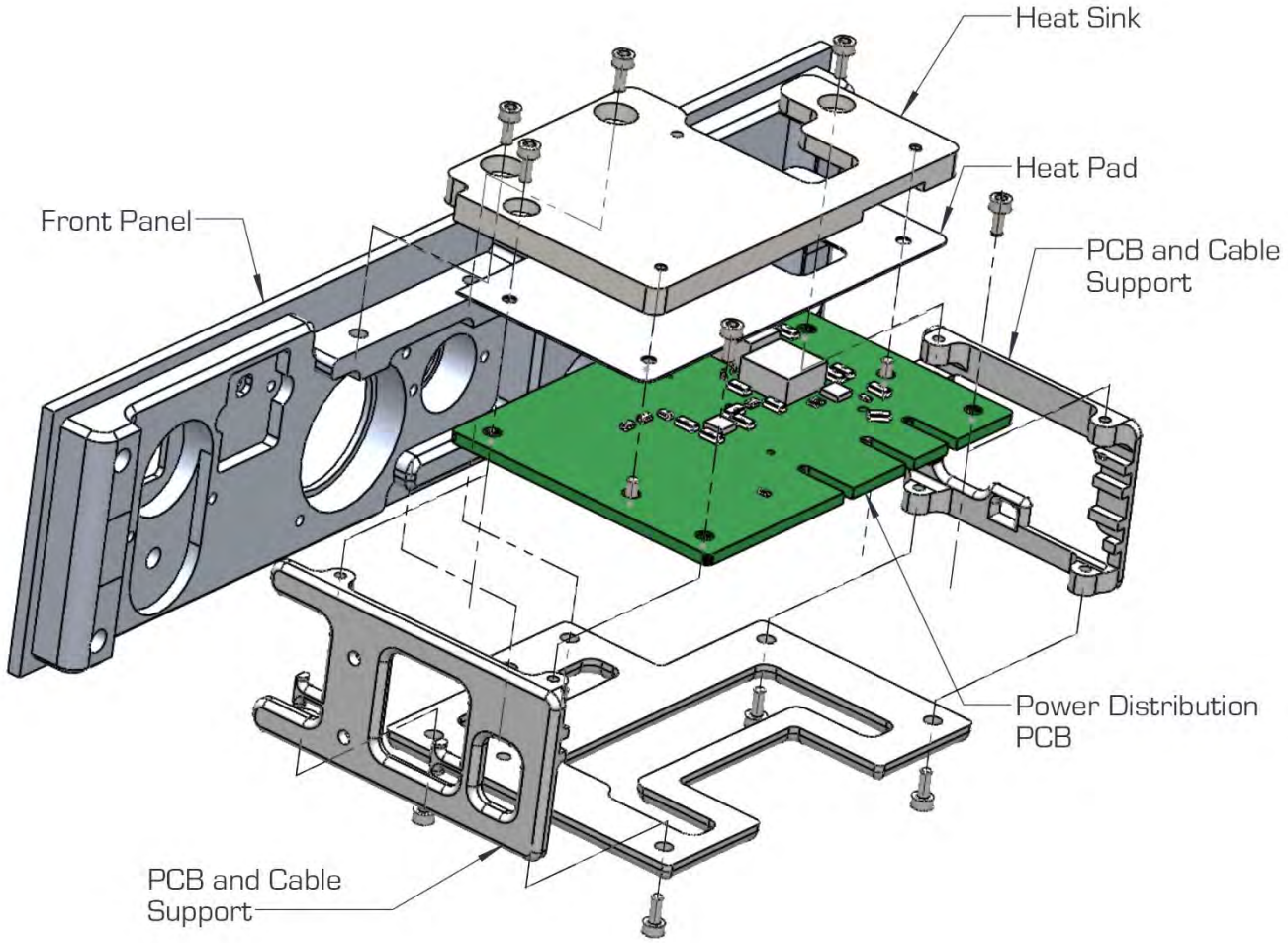

Figure 5-4: Mechanical structure of the sensor payload

5.3. Sensor payload cradle design

The sensor payload cradle was designed to ease integration of the systems due to the parallel nature of the design process. For future iterations of the platform, the cradle will be integrated into the shell. For this iteration, the cradle was designed and 3D printed to provide a guide for the sensor payload to mate with the board edge connector. The guide rail seen in Figure 5-5 guides the heat sink of the sensor payload towards the Hub PCB, which supports the female board edge connector. The Hub PCB mounts to the cradle using four M2 screws. The rail supports, noted in

Figure 5-5, maintain the separation between the two rails and provide an anchor point for the cradle, as they mount against the motor housing.

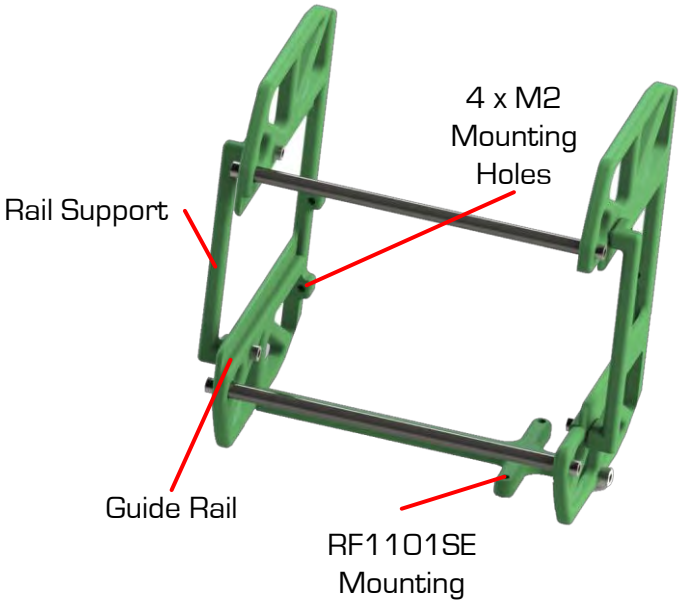

Figure 5-5: Sensor payload cradle

5.3.3. Sealing the front panel

While Thomas Mathew considered the seal between the front panel and the shell, the final mechanical consideration was the seal between the sensors and the front panel. A silicon elastomer seal is compressed between the sensors and the front panel. In the case of the OV7670, as shown in Figure 5-6, a lens and an additional spacer prevents the focusing of the camera, prior to placement, from affecting the seal.

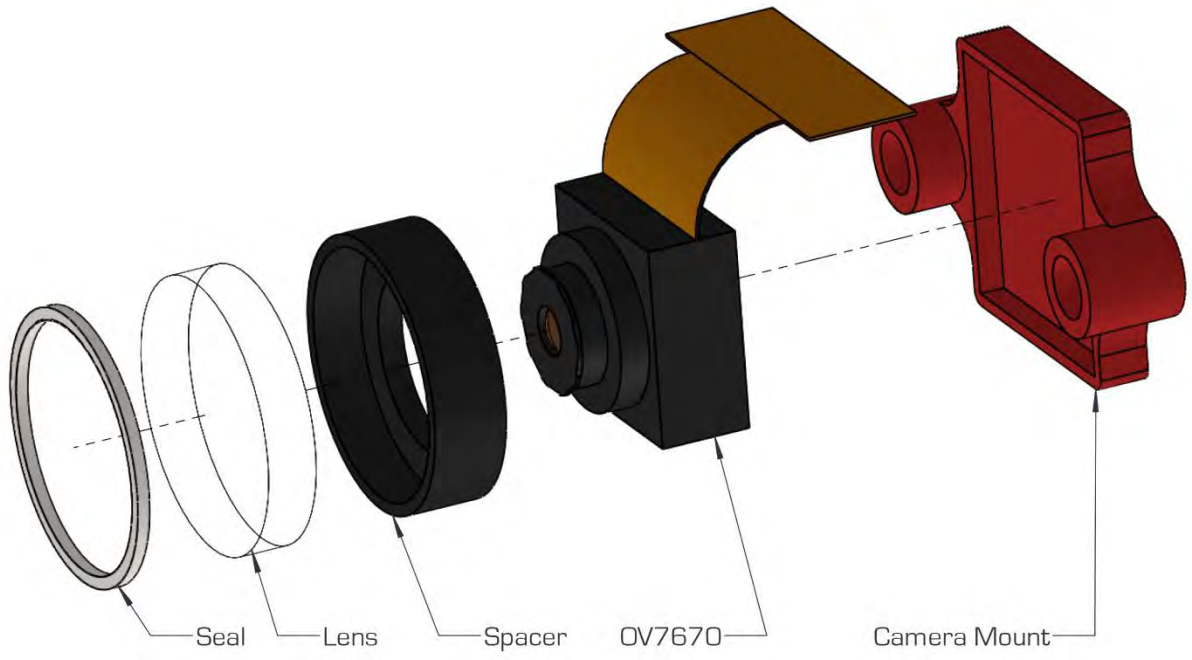

Figure 5-6: Sealing between the front panel and the OV7670 camera

5.4: Sensor placement

The two major considerations for the mechanical design of the sensor payload were, firstly, the integration into the platform and, secondly, the placement of the camera so the system will maintain symmetry. Locating the sensor in the centre of the front panel (Figure 5-7) ensures that the perspective of the operator is preserved when the orientation of the platform changes. This ensures that the image correction is limited to either a mirror or flip, when the system rotates about an axis. As both sensor payloads share a similar environmental sensor configuration, to reduce manufacturing costs, a single front panel was manufactured. The FLIR Quark was placed as close to the OV7670 camera as possible to limit the offset of the image when the orientation of the platform changes.

Located on the front panel is an On button. Pressing the button for two seconds enables the power supply from the battery to the platform. The Off button was recessed to ensure that the button is protected during operation as it is only intended for use during a communication failure. Under normal conditions, an Off command communicated from the operator disables the system programmatically.

To aid in the removal of the payload, an M3 hole placed in the front panel provides an anchor point where one of the four screws used to secure the sensor payload, can be inserted (Figure 5-8). This allows the sensor payload removal using a single 3 mm Allen Key.

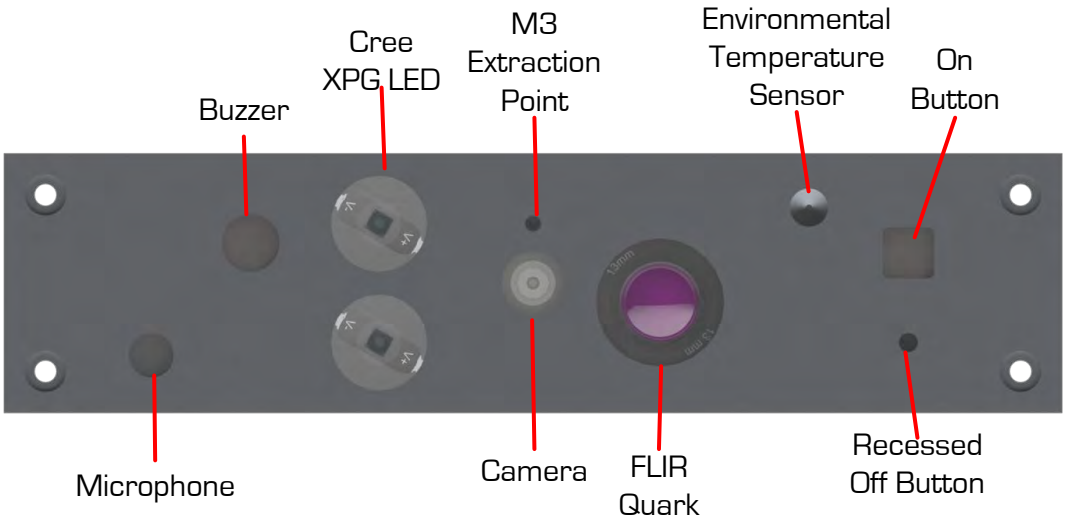

Figure 5-7: Front panel sensor configuration

Figure 5-8: Illustration of the removal process

5.5: System diagnostics

The purpose of the system diagnostics was to provide information on the power supplies and temperatures throughout the system during testing operations. As the diagnostics will not be included in the final design, the cost is not of major concern. However, the dimensions, mass and data format will govern the selection.

The INA220 is an IC that provides all the necessary power data via an I^2C communication interface. As a result, no additional GPIOs will be required; therefore, the presence of the INA220 will have little to no effect on the requirements of the microcontroller. The INA220 circuitry will be placed on all supply lines.

The temperature sensors selected were the LM60, because of their range and accuracy. The temperature is output as an analog signal. As the signal will be transmitted down a length of track and potentially through a number of connectors, it should be filtered prior to being connected to the ADC of the microcontroller. The LM60 will be placed in order to measure the temperature of all major power dissipaters. These would include the following:

- Voltage regulators
- Video DAC
- Battery charger
- LEDs

The final sensor will be located in the free space seen in Figure 5-2. This will allow measurement of the ambient temperature measurement inside the platform.

5.6: Electrical hardware design

Electrically the sensor payload can be broken down into environmental sensors, which are all located on the front panel and supporting components, which are located in the PCB stack seen in Figure 5-9. The final component is the Hub PCB, which is the interface between the sensor payload and the remainder of the system.

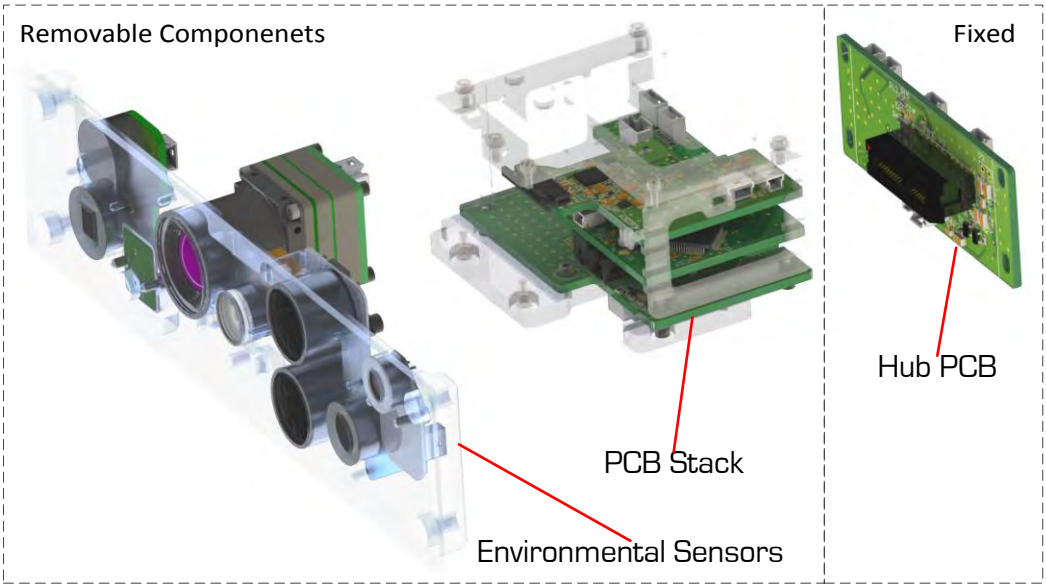

Figure 5-9: Breakdown of the sensor payload

The PCB stack is comprised of three boards, which are the camera, microcontroller and power distribution boards. The three boards are stacked as seen in Figure 5-10.

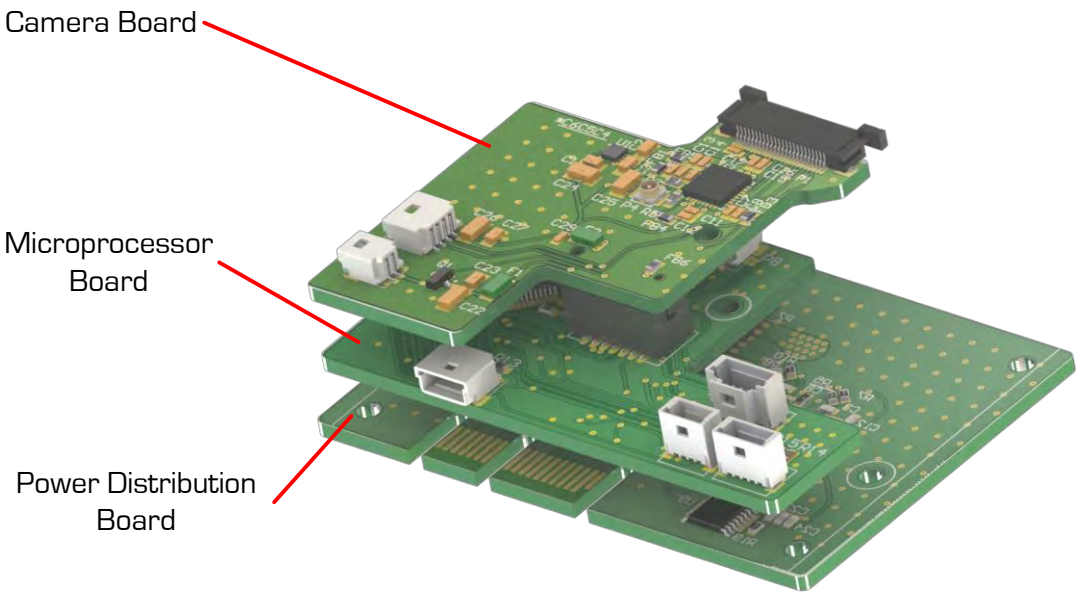

Figure 5-10: Electrical hardware of the sensor payload

5.6.1: Camera PCB

The function of the Camera PCB is to convert the digital image, produced by the OV7670, to an analog PAL signal for transmission via the Range Video FPV video transmitter. Additionally the PCB is responsible for regulating 3.3 V to 1.8 V and 2.8 V, required by the camera, and providing power to the microphone and buzzer when required.

The layout of the PCB and connector designation can be seen in Figure 5-11.

ADV7390

The ADV7390 Video DAC performs the main function of the PCB. The IC is versatile accepting a number of 8-bit parallel digital video formats, with four DAC outputs, outputting either PAL or NTSC. The analog video signal is communicated to the power distribution PCB via a UMC connector and a coaxial cable reducing the electrical noise. For this system, a CCIR656 digital video format was selected as the input from the camera and a PAL signal was selected as the DAC output. The CCIR656 8 bit parallel video signal is received via the FPC connector from the OV7670.

OV7670

The supporting circuitry for the OV7670 is located on the Camera PCB; these include the power supplies, pull up resistors and clock source. While the OV7670 uses the Omni Vision SCCBus to communicate, it uses the same hardware as I^2C (used by the ADV7390) for the communication of the configuration setting. Therefore, the pair of devices are connected to the same I^2C bus controlled by the microcontroller on the microcontroller PCB.

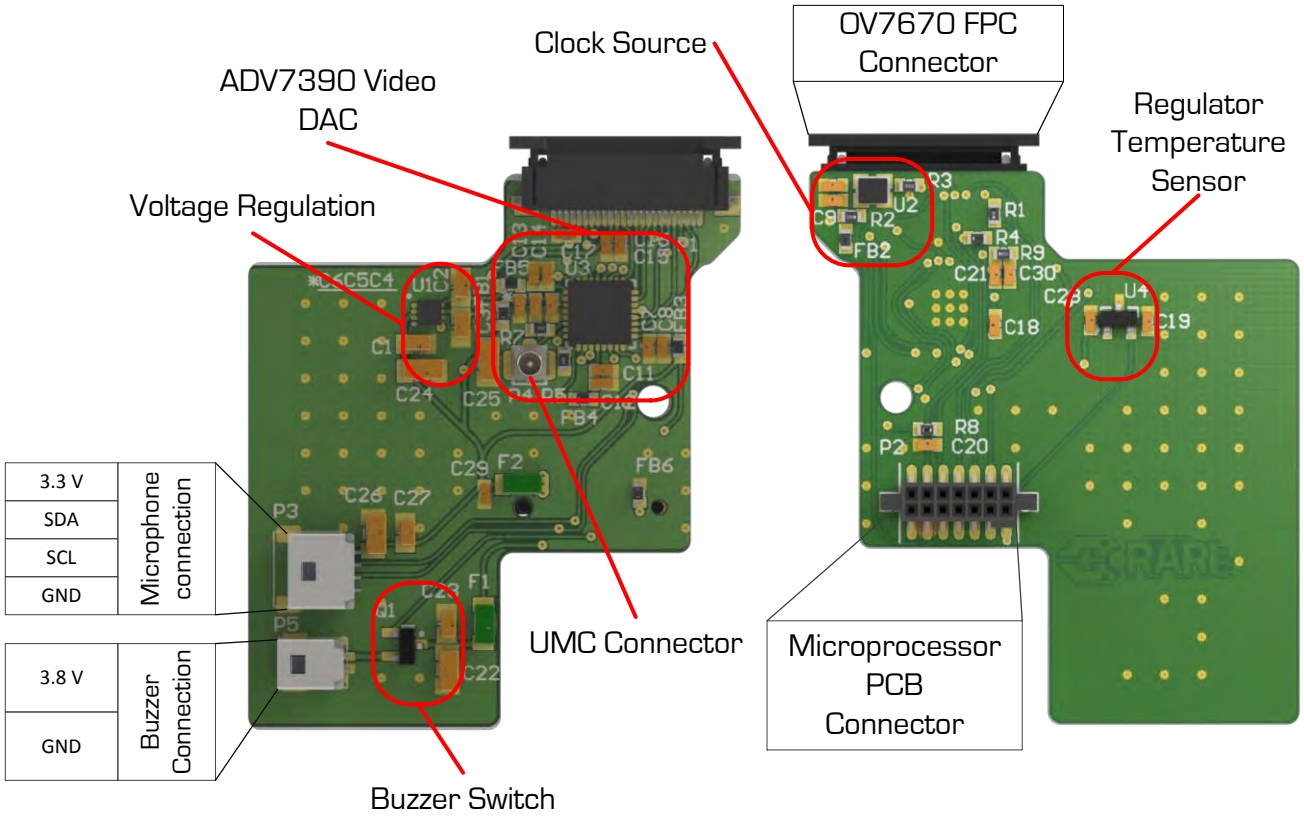

Figure 5-11: Diagram showing the PCB layout of the Camera PCB and connector designation

5.6.2: Microcontroller PCB

The Microcontroller PCB is the only PCB in the stack that differs between the low-cost and the extended sensor payload. As the orientation detection system also differs between payloads, it is placed on the same PCB.

Low-cost Microcontroller PCB

The microcontroller selected was the STM32F30R8, because it can be used without an external crystal, and the additional processing ability outweighs the added cost, as the system clock frequency can be increased from 16 to 48 MHz. Additionally, the MMA8653 tri-axis accelerometer and MAG3110 magnetometer can be seen on the bottom of the PCB in Figure 5-12. However, during system integration, the proximity of the magnetometer to the motors meant made it impractical to implement and it should be removed or improved for future design.

The microcontroller is the central node of all communication throughout the system and hence is connected to all devices throughout the system. For a detailed description of the microcontroller pinout see the schematic on the accompanying CD or Appendix E, on page E-8. As the mechanical structure of the payload allows for the thermal camera on both sensor payloads and the only limitation of the camera is the cost, the connection has been included.

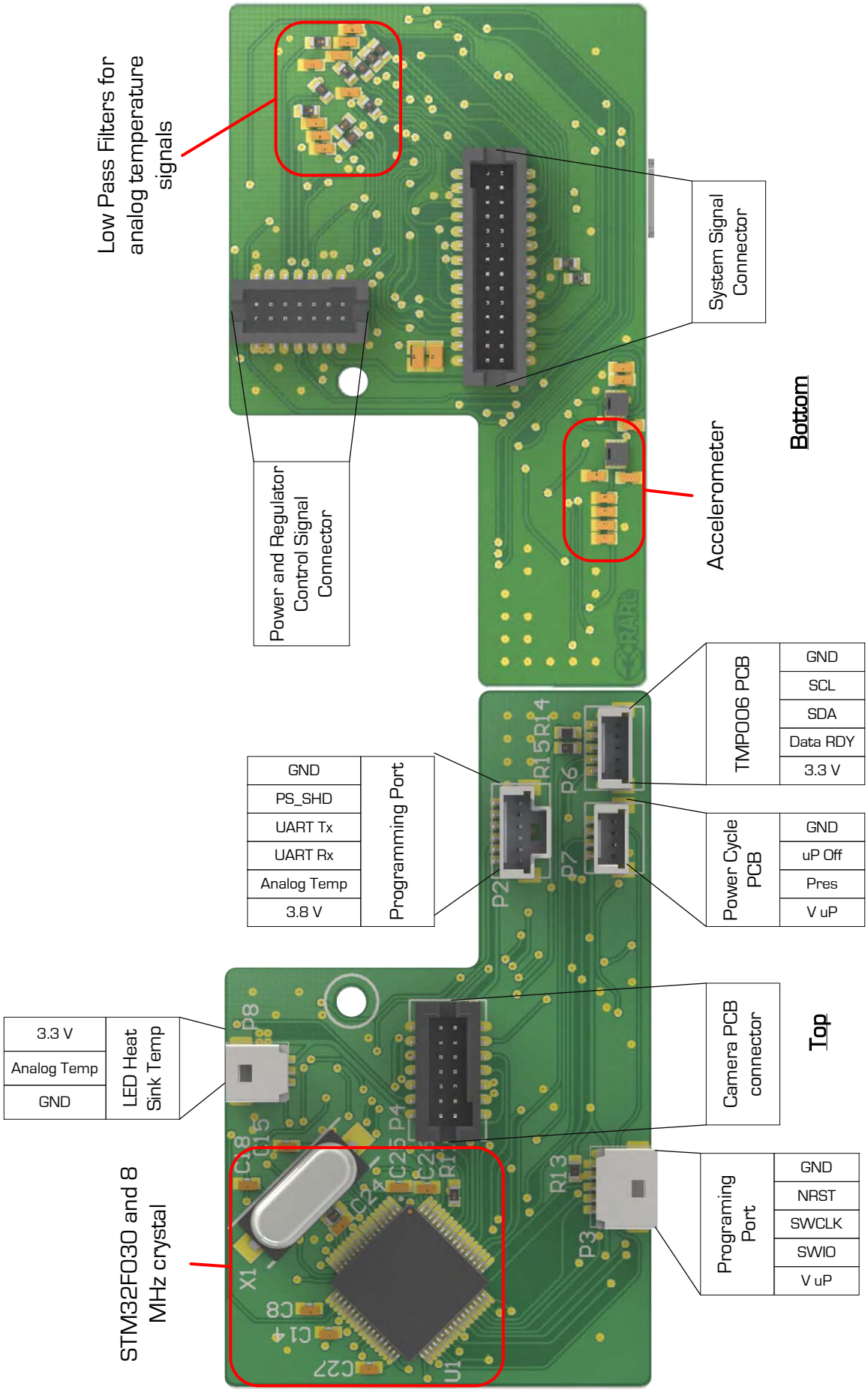

Figure 5-12: The layout of the Microcontroller PCB

Extend sensor payload Microcontroller PCB

As the extended and low-cost microcontroller PCBs are interchangeable, the profile and pinout of both PCB's is identical. Therefore, only the microcontroller and the accelerometer change to a STM32F407VGT6 and an LSM9DS0 IMU respectively. The increased processing power and hardware FPU on the microcontroller allows for the fusion of the accelerometer and gyroscopic data, to provide accurate orientation estimation.

Power Distribution PCB

The Power Distribution PCB forms the base of the PCB stack and is mounted to the heat sink; because of this the PCB supports the modules that require heat sinking. These modules are the voltage regulation and the LED driver. As the PCB is also the male board edge connector, the PAL source select is located on the PCB close to the edge connector, minimising length of the unshielded signal path. This layout can be seen in Figure 5-13.

5.6.3:

A brief description of all the Power Distribution PCB modules will now be provided.

Voltage regulation

The voltage regulation is achieved through a two-stage process. Firstly, an SMPS drops the battery voltage to 3.8 V, followed by a LDO to drop the voltage to 3.3 V. This combination of regulators reduces the power dissipated by the LDO. As a result of the selected sensors and devices, a 5 V source is not required.

LED driver

The LEDs selected were a pair of cool white Cree Xlamp-XPG LEDs, allowing both a spot lens and a diffused lens to be used. The result is a wide beam of light in the short range, with a spot to illuminate at distance. The LED driver will be required to provide up to 1.5 A at 7 V, as the pair were connected in series. A driver meeting these requirements is the LM3401 from Texas Instruments. Using the equations provided in the data sheet, the values for the supporting components were selected.

PAL source select

The sensor payload was designed to support both a thermal camera and a CMOS camera. To enable the signal transmission without increasing the number of video transmitters, only one camera can operate at a time. The operator will be required to select the image signal source. This is achieved using a TS3V330 analog video switch.

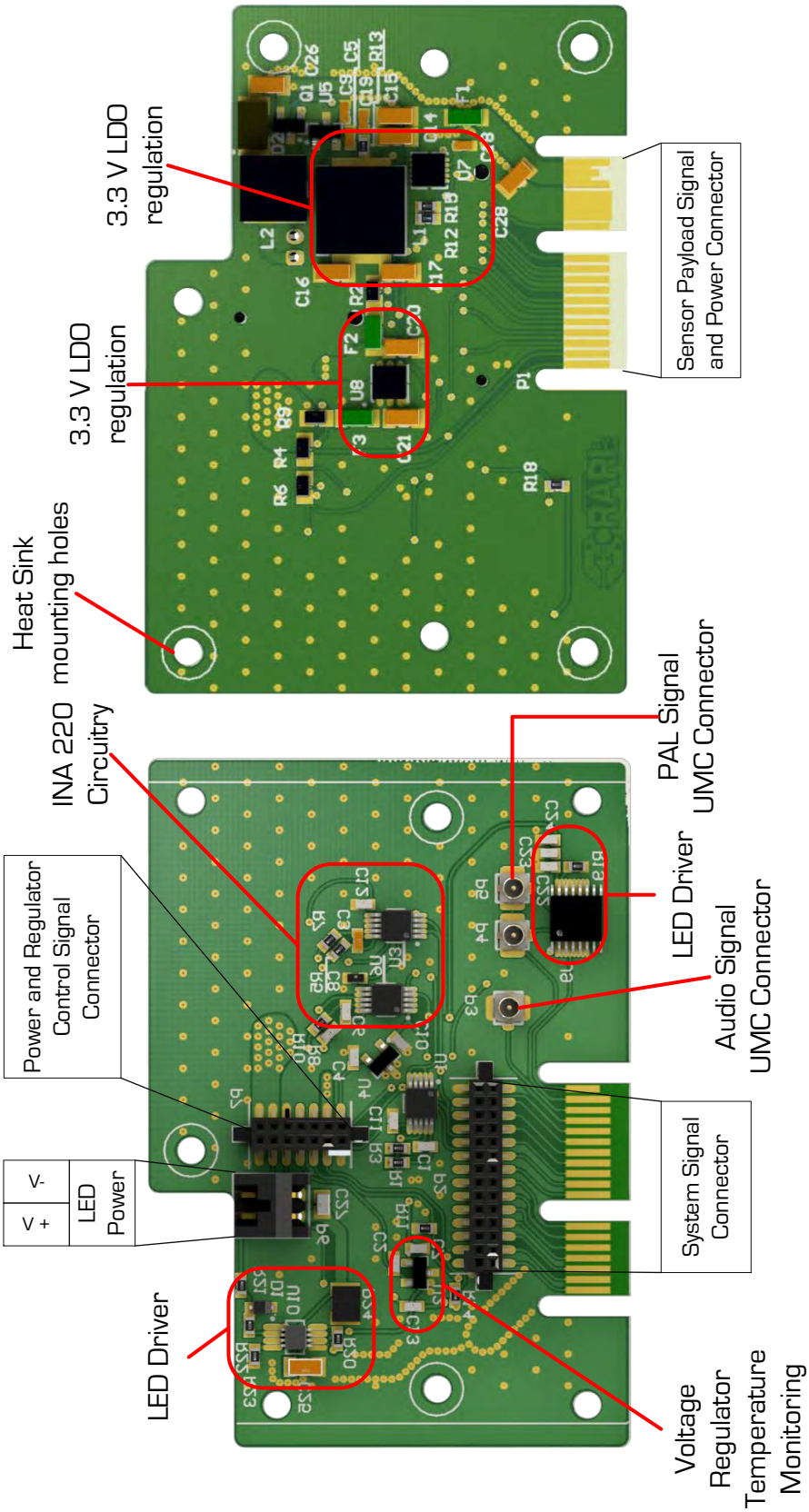

Figure 5-13: Layout of the Power Distribution PCB

Hub PCB

The Hub PCB is the electrical interface between the sensor payload and the system. Additionally, the Hub PCB supports the componentry that is common to multiple sensor payloads.

To allow the sensor payload to be truly interchangeable in the field, the method of inserting the payload should provide both the electrical and mechanical connection. This could be achieved through a standard DIN PCB header strip. However, the chances of deforming a pin are relatively high. A favourable alternative is a PCB board edge connector, as the PCB edge forms the male connector, removing the potential for deformed pins during the insertion procedure. The PCB is therefore tasked with distribution of the signals and power supplies between the payloads and the system. The Hub PCB is mounted to the sensor payload cradle using M2 screws through the slotted holes, seen in Figure 5-14, to enable the vertical position of the PCB to be adjusted for alignment of the board edge connector.

5.6.4.

The componentry that is common to multiple sensor payloads is the 10 V regulator for the video transmitter and the power supply source select for the microcontroller. The video transmitter is the only device that required a 10 V supply. Therefore, a SMPS located on the Hub PCB is used.

The BMS provided a linearly regulated 3.3 V output which can be used to power the microcontroller to allow for a controlled start up procedure of the regulators. Once the 3.3 V regulated supply is present, the supply is switched from the BMS supply, as the regulated supply is theoretically more efficient.

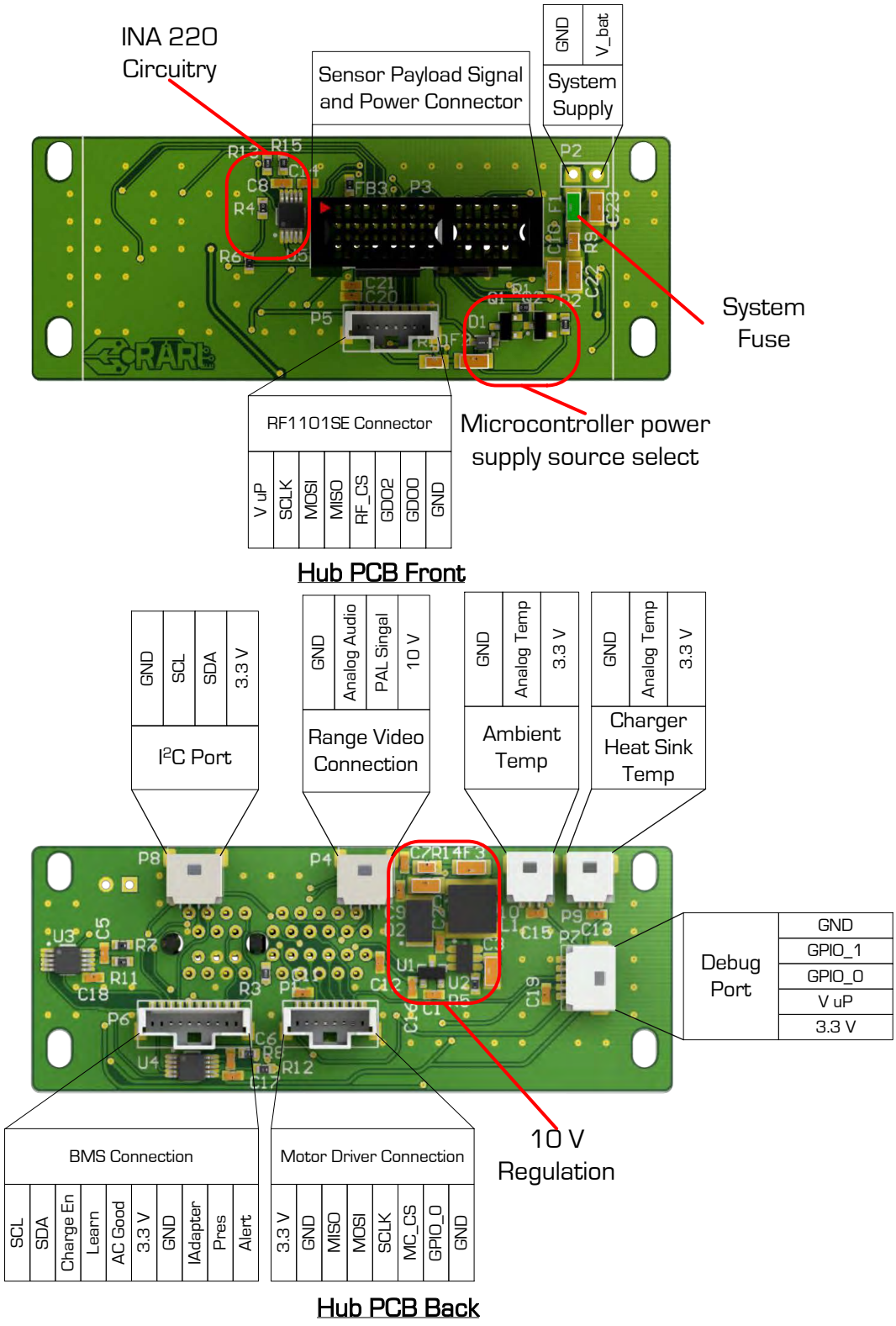

Figure 5-14: Layout and connection diagram for the Hub PCB

5.7: Sensor payload cost

While the cost of the extended sensor payload is of no concern, as the cost of the FLIR Quark (US$ 4500) far outweighs the cost of the remainder of the system. Table 5-4 illustrates a breakdown of the cost of the low-cost sensor payload on a production run of 250 units, the unit cost was estimated to be US$ 63.29, excluding the cost of the system diagnostics and assembly. The electrical component cost was calculated based on the prices from DigiKey.

Table 5-4: Component cost of the low-cost sensor payload

Item	Cost (US$)(per 250)
Electrical Components	12947.84
Materials	1500.00
Fasteners	375.00
Total	14822.84
Unit Cost	63.29

5.8: Sensor payload software design

The primary task of the software embedded on the microcontroller is to read, scale and collate the data from the sensors and to enable simple communication to the operator. In order to achieve this, the microcontroller is configured for the application, followed by the configuration of the sensors, before accurate and relevant data can be read. Therefore, the basic outline of the software can be seen in Figure 5-15.

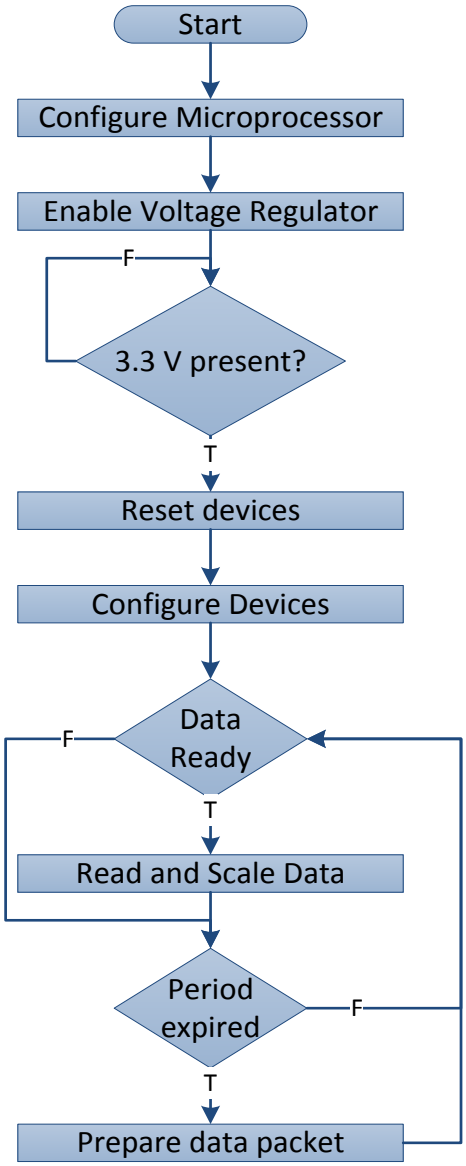

Figure 5-15: Basic software outline

The software is designed so that throughout the operation, there are no periods of waiting for one process to be completed, when a second process could be completed in parallel. This is achieved using interrupts, flags and time-based events. A structure containing a status byte and a data byte or array of bytes was designed for each device connected to the microcontroller and for the communication peripherals of the microcontroller. The status byte comprised of a number of bits which represent status flags. An example of a status byte can be seen in Table 5-5, which shows the flag definitions of the bits of the byte.

Table 5-5: The bit definitions of the status byte for the STM32F0 SPI peripheral

Bit	7	6	5	4	3	2	1	0
Data	0	0	0	0	Time Out	Software Busy	New Data	Overrun error

Communication peripheral software

5.8.1: Foremost to the success of the design was the packet handling software of the SPI and I^2C peripherals. This was achieved using packet-length headers and pointers to indicate the address of the end of the data packet and the next byte to be transmitted. When the address of the next byte to be transmitted is equal to that of the end of the packet, communication of the packet is complete and indicated by setting a bit of the status byte. This is executed in the peripheral interrupt handler seen in Figure 5-16 and for SPI and in Figure 5-17 for I^2C; therefore once the pointers have been initiated the microcontroller is free to process further code in between loading the next byte into the shift register.

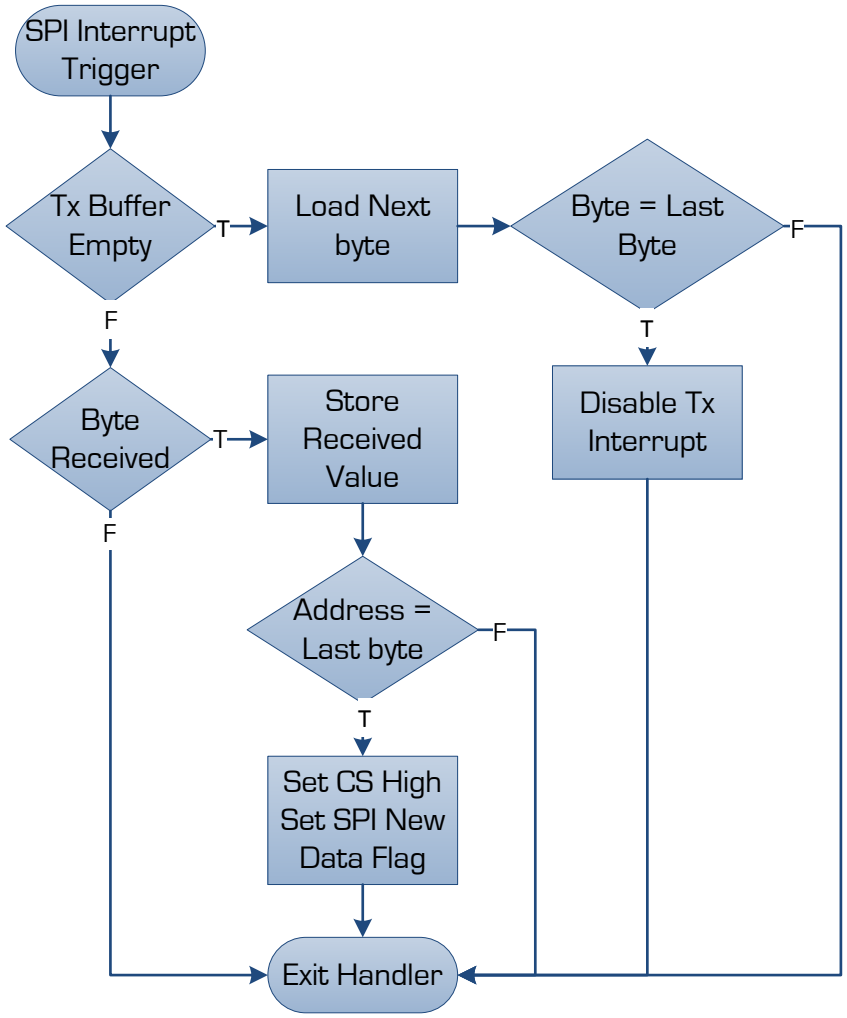

Figure 5-16: SPI communication interrupt handler

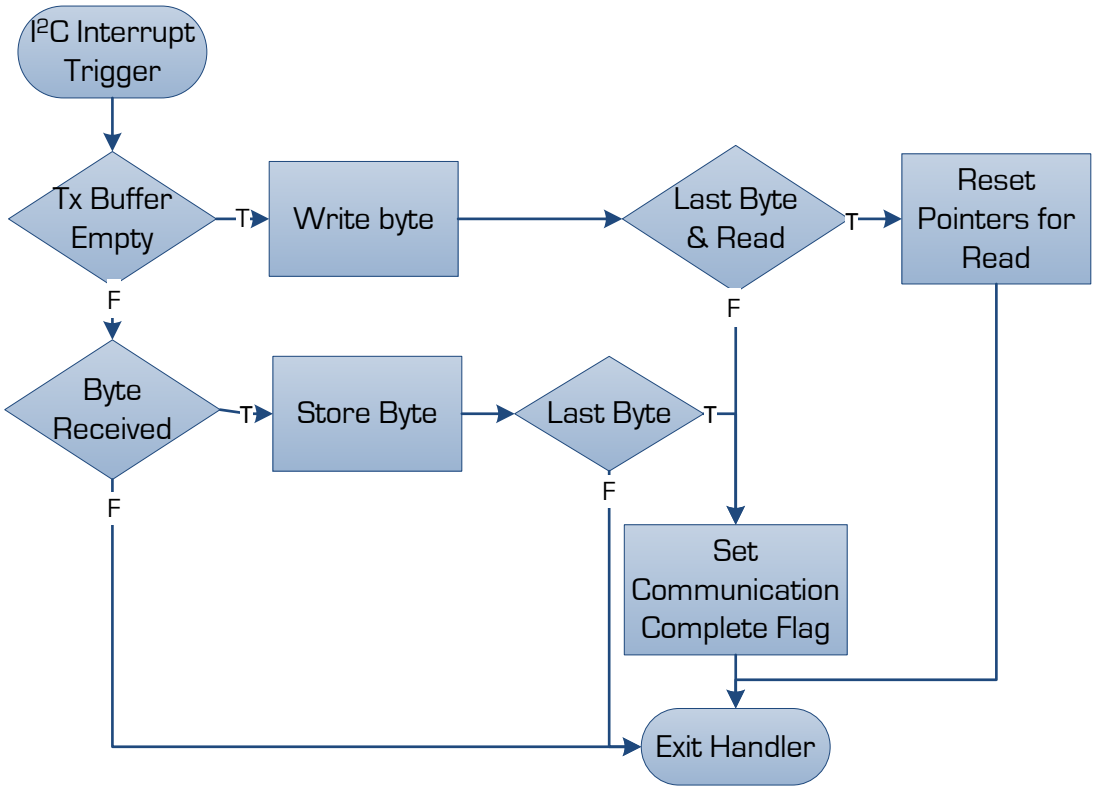

Figure 5-17: I2C communication interrupt handler

Once the *communication completion* flag has been set, polling the peripheral status flag will initiate the processing of the data. The device with which the last communication occurred, is determined by the slave address in the case of I^2C or the selected chip select line in the case of SPI, which is stored in the peripheral structure.

Therefore, the objective of the communication peripheral software is to prepare the data pack and pointers, so that the peripheral interrupt handler can execute the communication. This allows further processes to execute in the period during which the byte is being shifted into or out of the shift register. This design approach is continued to the device handling software.

Device handling software

The device handling software was designed so that if a device requires a peripheral that is currently busy, the software will continue processing data from other devices until the peripheral has completed its task and is free to begin the task. This is achieved using flags set in the status byte of the device.

5.8.2.

The process is illustrated using the communication with the MMA8653 accelerometer. Figure 5-18 illustrates the process in the data ready interrupt. While many of the devices have an interrupt pin that is connected to a microcontroller GPIO, configured for interrupts triggered on an edge, some of the devices do not have this feature and are, therefore, polled on a time-based interrupt. Such devices are the BMS and the INA220 network.

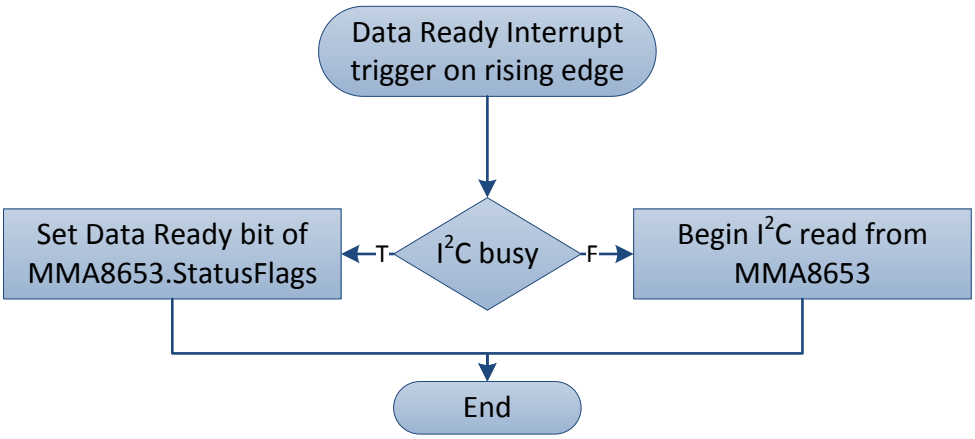

Figure 5-18: Data ready interrupt routine for the MMA8653

In the case where the I^2C is not busy, the end of the communication and subsequent scaling of the data is detected in the main loop of the software as shown in Figure 5-19. The alternative case (where the I^2C peripheral is busy) the flag is set indicating that data should be read and this is initiated once the peripheral has completed the current communication process, illustrated in Figure 5-19.

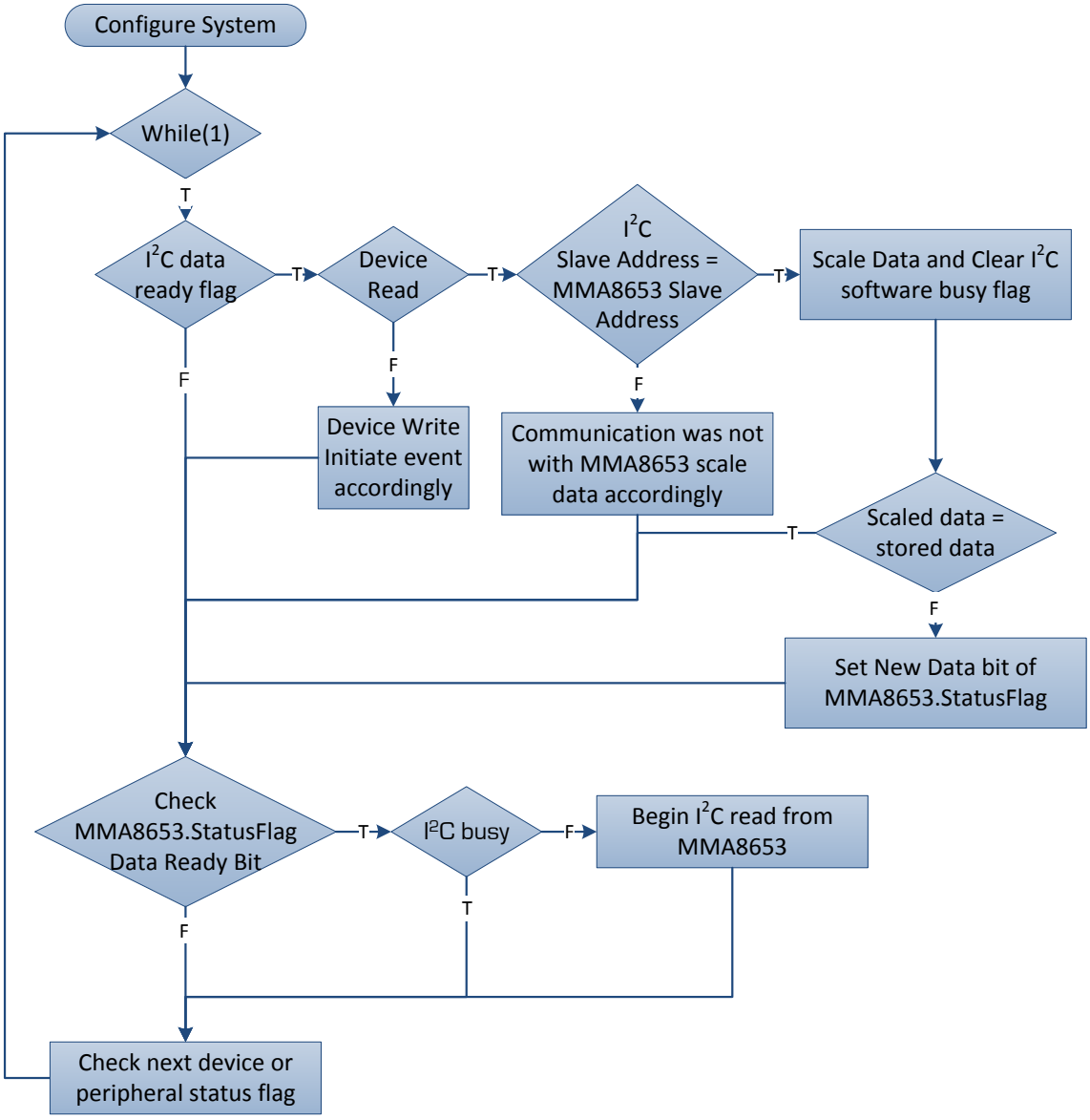

Figure 5-19: Flowchart showing the process of reading data from the MMA8653 accelerometer

This process is duplicated for all the devices connected to the microcontroller. The priority of devices is set by the order that the device or peripheral status flag is read. As multiple devices use the communication peripherals, their priorities are the highest, with the SPI higher than the I²C due to the wireless communication.

5.8.3. In order to reduce the amount of data communicated and processed, the *new data* flag is set only if the latest reading is not equal to the currently stored value for the device. Hence, further processing or communication to the operator is executed when the *new data* flag is set.

Data processing

With the exception of the temperature and accelerometer/IMU, the processing of the device data consists of scaling and collating the data for communication. The temperature data is used to limit functionally during high temperature events (above 75 ℃). The two areas where over temperature events are most likely to occur are the LEDs and the battery charger. These events cause the LED output power to be limited to 20 % and the charging rate limited to 0.5 C (1.5 A).

In order for the platform to operate in all orientations, both the image transmitted to the operator and the motor commands received from the operator are manipulated according to the orientation changes. The point at which the manipulation should occur was determined from the accelerometer data in the case of the low-cost sensor payload and the IMU data in the case of the extend sensor payload.

Orientation detection with an accelerometer

In order to initiate a flip about the horizontal or vertical axis the exact orientation is not required, but rather the point where the platform crosses the boundary of an octant. As a result of the positioning of the accelerometer, the axis of the platform can be considered to be oriented as seen below in Figure 5-20.

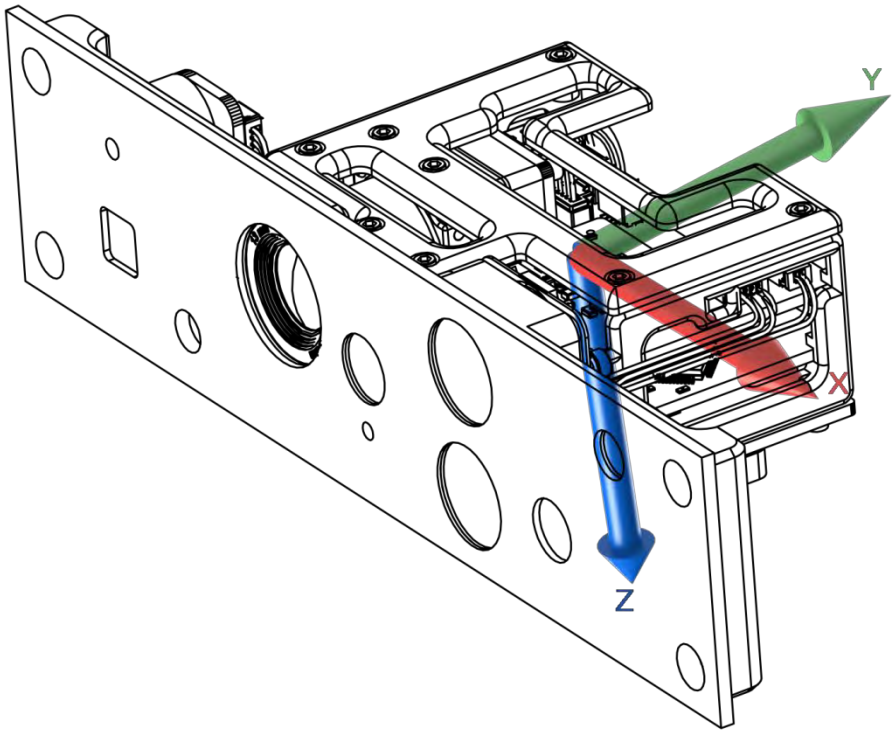

Figure 5-20: Figure showing the orientation of the axis of the low-cost sensor payload

It can be noted that a 180˚ rotation about either the X-axis or the Y-axis will result in a change in the direction of the Z-axis. Therefore, in order to reduce unnecessary processing of the data, the orientation of the platform is only processed when the direction of the Z-axis changes.

Accelerometer and gyroscopic data fusion

Due the increased processing power of the microcontroller and the lack of a cost consideration, the extended sensor payload has both an accelerometer and a gyroscope. This allows the orientation to be accurately calculated during acceleration events. As noted during the background research, three of the possible methods for fusing the data are the Kalman, Madgwick and Mahony filters. As can be seen in Table 2-3, the Kalman is the most accurate at higher rates, however it has a much greater processing requirement. As the system is not designed to move at a high rate, the reduced computational power required for the Madgwick filter outweighs the loss of accuracy and hence was used.

Therefore, when a flip about the X-axis was detected, the directions of the motor commands are flipped and the image is flipped about the horizontal plane. A rotation about the Y-axis results in an image mirror about the vertical plane and a flip about the horizontal plane; the motor commands are mirrored between left and right.

While the orientation calculation is a computationally intensive process, the final function of the *new data* flag is to indicate when the scaled sensor data should be transmitted to the operator. This is done to reduce the packet length, as only the new data will be transmitted.

Data packet structure

A method of achieving a variable packet length is to assign a data header that indicates the contents of the packet. In this case, the data header is a bit mask. This allows for communication of multiple combinations of data and commands. The bit assignment for a sensor payload data packet transmitted from the system can be seen in Table 5-6, and the command packet header received by the system can be seen in Table 5-7. The process of building a packet can be seen in Figure 5-21. The code is implemented with the use of a pointer that is used to store the address at which the next data byte should be added. When the *new data* flag is set for a specific device, the data is added and the pointer address is incremented accordingly.

5.8.4:

Table 5-6: Header of a sensor data packet

Bit	7	6	5	4	3	2	1	0
Data	0	BMS Data	Environmental Temperature	Voltage and Current Data	Temperature Data	Charge Adapted Current	X (don't care)	Accelerometer Data

Table 5-7: Header of a command packet

Bit	7	6	5	4	3	2	1	0
Data	0	X (don't care)	Shut Down	Enable Charging	Set Charge Rate	Buzzer Enable	LED Command	Motor Command

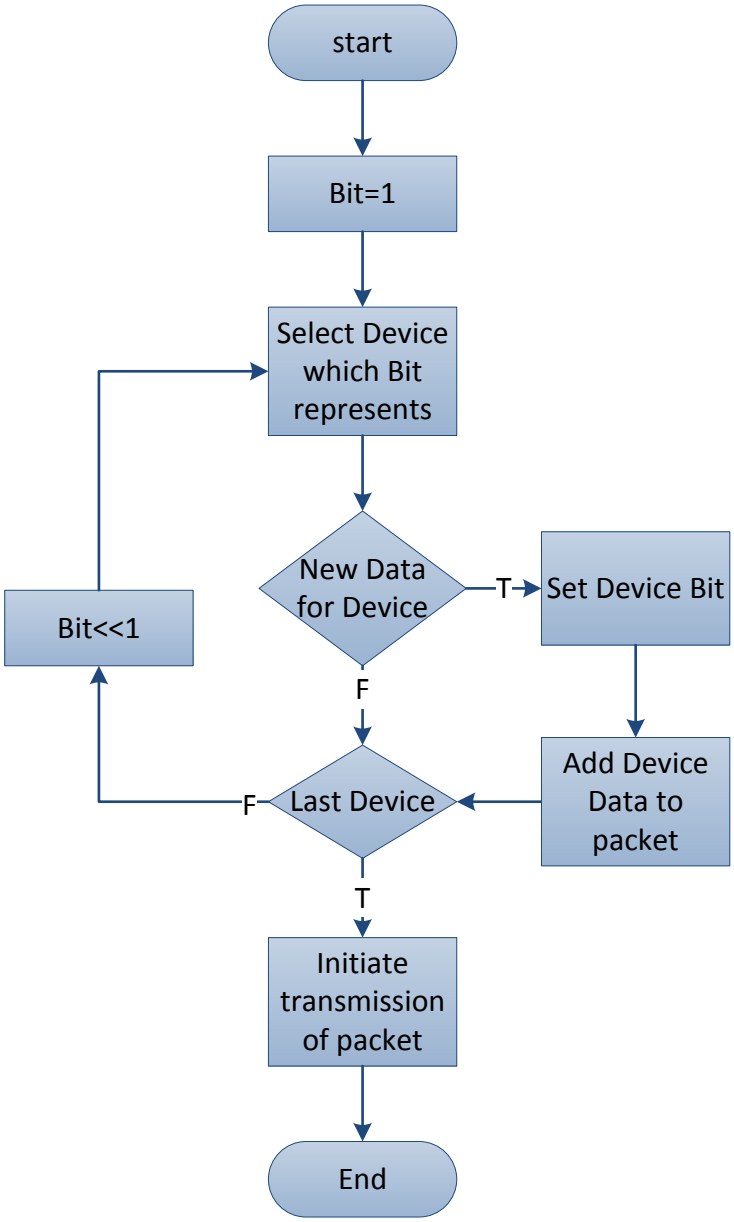

Figure 5-21: Flowchart representing the packet preparation function

The order of the data is indicated by the order of the bits in the bit mask, with the data represented by the LSB that is set being positioned first after the bit mask. This is shown in Figure 5-22: the first example of a data packet where the *motor command* bit is set and therefore the motor command follows the header byte. The flexibility of the packet structure is illustrated in Figure 5-23, a second example: here the *LED Command* and *Set Charge Rate* bits are set indicating the presence of the data. In this case the LED command data byte follows the header byte. The next byte will be the charge rate as the *Buzzer Enable* bit is not set. The packet header allows for multiple combinations of data to be selected, ensuring that the entire packet is not transferred unnecessarily (which would reduce the efficiency of the system).

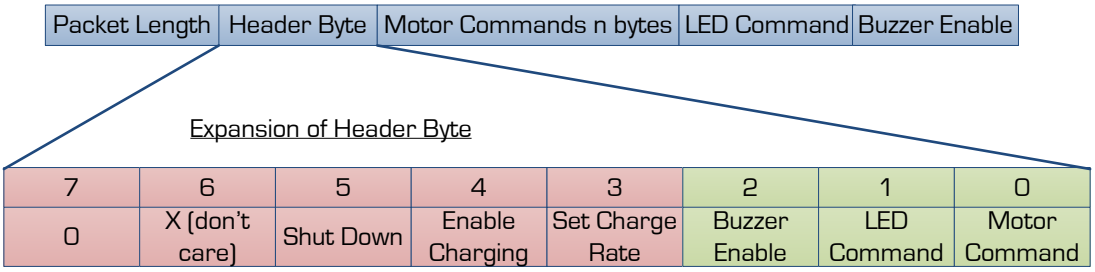

Figure 5-22: Example of a command packet

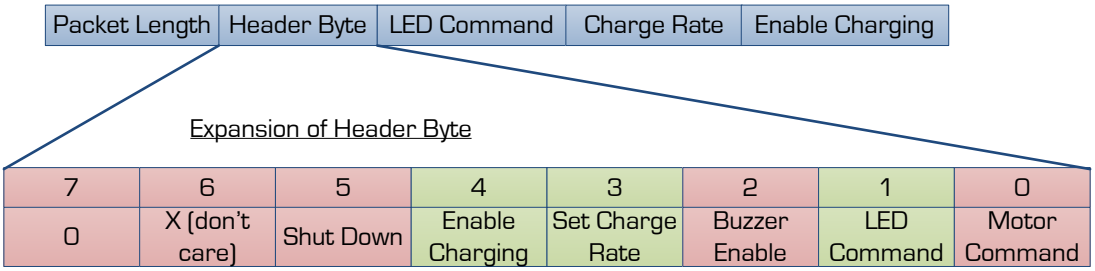

Figure 5-23: Second example of a command packet

5.9: Concluding remarks

The purpose of the sensor payload was to collect and process data from the system and the environment, with the primary aim of achieving this at the least possible cost. The target of US$ 50 was not met. However, any further reduction in cost will only be achieved through a reduction in functionality. A second sensor payload illustrates the interchangeability of the subsystem, thus enabling diversification of the platform's features, through the development of sensor payloads.

A method of orientation detection allowed for the transformation of both the returned images and the received commands so as not to disorientate the operator during operations. This was a requirement because of the platform's symmetrical design.

Finally, a data packet structure was designed to inform the data receiver of the contents of the data packet. This will allow for a variable packet to be sent which contains only the latest data and commands.

Key to the operation of any tele-operated platform is the communication system, as it provides the link between the operator station and the platform. To improve the efficiency and effectiveness of the system, the video and audio communication and the data communication are placed on separate frequencies according to their bandwidth requirements.

Chapter 6 :

6.1: Communications specifications

This section provides an extension of the communication specifications of the primary system requirements and justifications as laid out in Table 3-1.

Table 6-1: Detailed communication specifications

Explanation Location	Subsystem Specification	Desired Value
6.1.1:Physical specification		
6.1.1.1:	Dimensions	40 x 30 x 10 mm
6.1.1.2:	Cost	US$ 35
6.1.2:Functional specifications		
6.1.2.1:	Colour image transmission	Yes
6.1.2.2:	Bidirectional data communications	Yes
6.1.2.3:	Error detection	Yes
Performance specifications		
6.1.3.1:	Operational range(indoor)	30 m
6.1.3.2:	Minimum communication rate	10 Hz
6.1.3.3:	Maximum communication rate	20 Hz

6.1.1:

Physical specification

6.1.1.1: Dimensions

For the data transceiver to be located in the allocated free space in Figure 5-2, the transceiver should not exceed the bound of the above dimensions.

6.1.1.2: Cost

To achieve a total cost of US$ 150 for the entire system, the cost of the communication system should not exceed US$ 35. The cost of the battery, BMS and sensor payloads were estimated at US$ 115.

6.1.2:

Functional specifications

6.1.2.1: Colour image transmission

As explained in the background research, a colour image is required as the dust in a disaster environment causes an even tone of grey on a greyscale image. The bandwidth requirement for a colour image is, however, higher.

6.1.2.2: Bidirectional data communications

The data communication system will be used to both transmit data from the payload and receive commands from the operator, therefore requiring bidirectional communication.

6.1.2.3: Error detection

A disaster zone is a highly challenging environment for wireless communications; as a result, packet loss and corruption is expected.

Performance specifications

6.1.3.1: Operational range (indoor)

30m is the indoor range of the Recon Scout Throwbot [8]. The aim is to meet or improve on this range.

6.1.3:

6.1.3.2: Minimum communication rate

A minimum communication rate of 10 Hz is required to operate the platform. Frequencies below this will limit the ability of the operator to command the platform.

6.1.3.3: Maximum communication rate

A communication rate of 20 Hz will enable commands and the data to be communicated without impeding the operation of the platform.

6.2: Device selection

The random nature of a collapsed structure, coupled with the materials used in urban building, create a challenging environment for tetherless devices. For this reason two devices have been selected, one with a bandwidth for video and the second will be a narrow band transceiver for data and commands. Background research suggested that the data transceiver should be on a 433 MHz frequency. A device that fills that requirement and can be considered as low-cost is a CC110L from TI. The IC was purchased on a RF1101SE break out board for this design.

6.3: Software for data transmission

The CC110L has a 64 byte transmit and receive FIFO buffer that is used to implement the communications. The basic implementation of the software is shown in Figure 6-1. The device is first reset to ensure the contents of all the registers are of a known value, this is followed by the configuration of the device — a summary of the configuration settings is seen in Table 6-2. This process was implemented on the software embedded on the microcontroller of the sensor payload. During operation, when the device is not transmitting, it is in a "ready to receive state", listening for a preamble and sync word.

Table 6-2: Summary of the CC110L settings

Setting	Value
Frequency	433 MHz
Baud Rate	19200 bps
Modulation Format	GFSK
Receiver Filter Bandwidth	101 kHz
Deviation	20 kHz

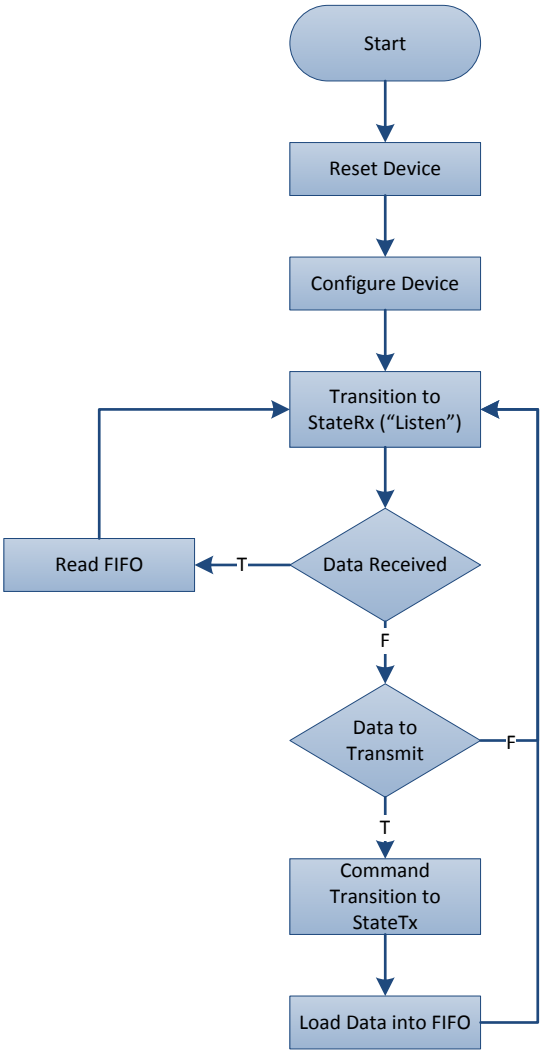

Figure 6-1: Flowchart showing an overview of the implementation of the embedded communication software

6.4: Packet structure

Due to the nature of a disaster environment, high data corruption rates and losses are expected. Therefore, the ability to detect when there has been data corruption or loss and to enable a resend is required. Therefore the basic overview of the data communications was expanded to include a data check and confirmation as seen in Figure 6-2. The transmitter sends the data packet, the receiver receives the packet, checks and then confirms reception of the packet. Should the transmitter not receive a packet confirmation, the packet would be deemed to be lost and resent. Alternatively, a corrupted data packet would fail the check and the receiver would send confirmation of a packet error, causing the transmitter to resend the data. The transmitter could resend the data multiple times until the data has been successfully transferred.

This method of communication relies on two abilities: detection of a complete packet and the ability to detect corrupt data. To achieve this, two methods have been implemented. Firstly, a unique packet header and terminator have been added to the data packet and, secondly, a CRC is calculated across the data payload. Therefore, Table 6-3 is a representation of a complete data packet.

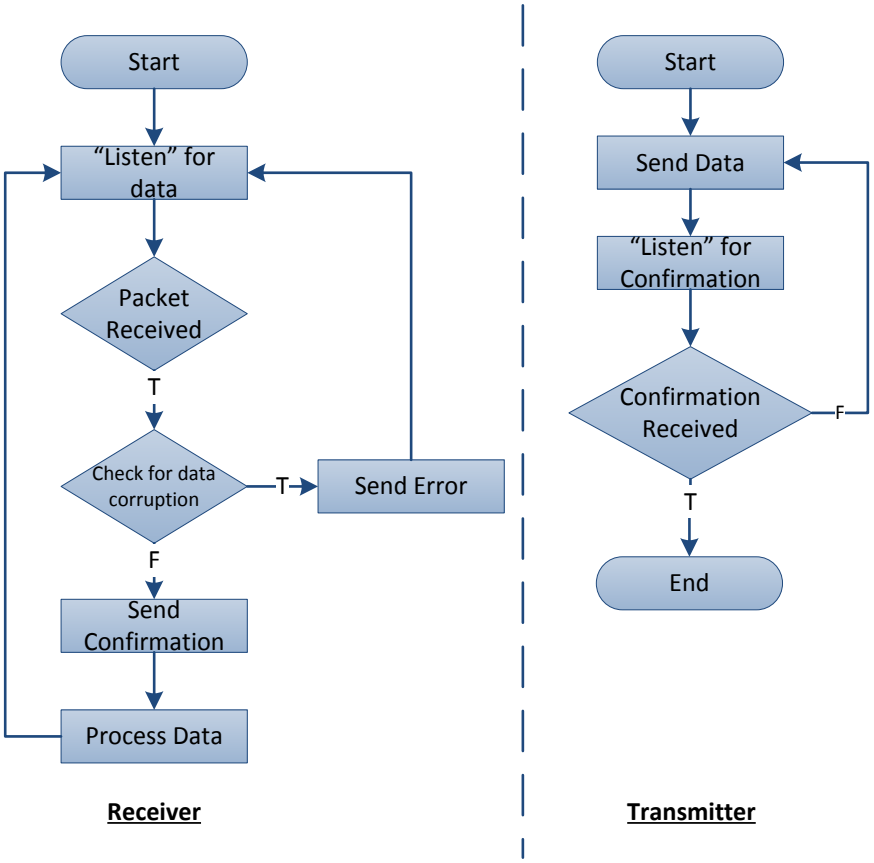

Figure 6-2: Basic data communication protocol

Table 6-3: Representation of a complete data packet

Byte	0	1	2 ... n-3	n-2	n-1	n
Function	Packet Header	Data Payload Length	Data Payload	CRC MS_{nibble}	CRC LS_{nibble}	Packet Terminator

6.4.1:

Data manipulation

The aim of the packet header and terminator bytes is primarily to determine when a complete command has been received. This can be achieved through the use of a fixed packet length or alternatively a unique packet header and packet terminator byte. To ensure that the packet header and terminator are detected, both designated values should to be unique. Reserving data values for packet header and terminator will lead to restrictions on further sensor payload designs. Therefore, the data transmitted should be manipulated in order to create unique header and terminator bytes.

A method of ensuring that there will be unique values for use as packet headers and terminators is to stretch every 7 bytes into 8 bytes of data. This was achieved by removing a single bit from each of the 7 bytes to form an eighth "carrier byte". The new structure of the data bytes can be seen in Table 6-4. It can be noted that the 7^{th} bit is cleared and placed into the "carrier byte", the placement of these bits can be seen in Table 6-5. The process of removing the 7^{th} bit from each of the data bytes and recombining them into an 8^{th} byte can be seen in Figure 6-3. Therefore, any byte which has the 7^{th} bit set is either a packet header or terminator byte, ensuring a possible 127 different values to be selected from.

Table 6-4: Structure of a stretched data byte

Bit	7	6	5	4	3	2	1	0
Data	0	D_6	D_5	D_4	D_3	D_2	D_1	D_0

Table 6-5: Structure of a carrier byte

Bit	7	6	5	4	3	2	1	0
Data	0	$Byte_1$:D_7	$Byte_2$:D_7	$Byte_3$:D_7	$Byte_4$:D_7	$Byte_5$:D_7	$Byte_6$:D_7	$Byte_7$:D_7

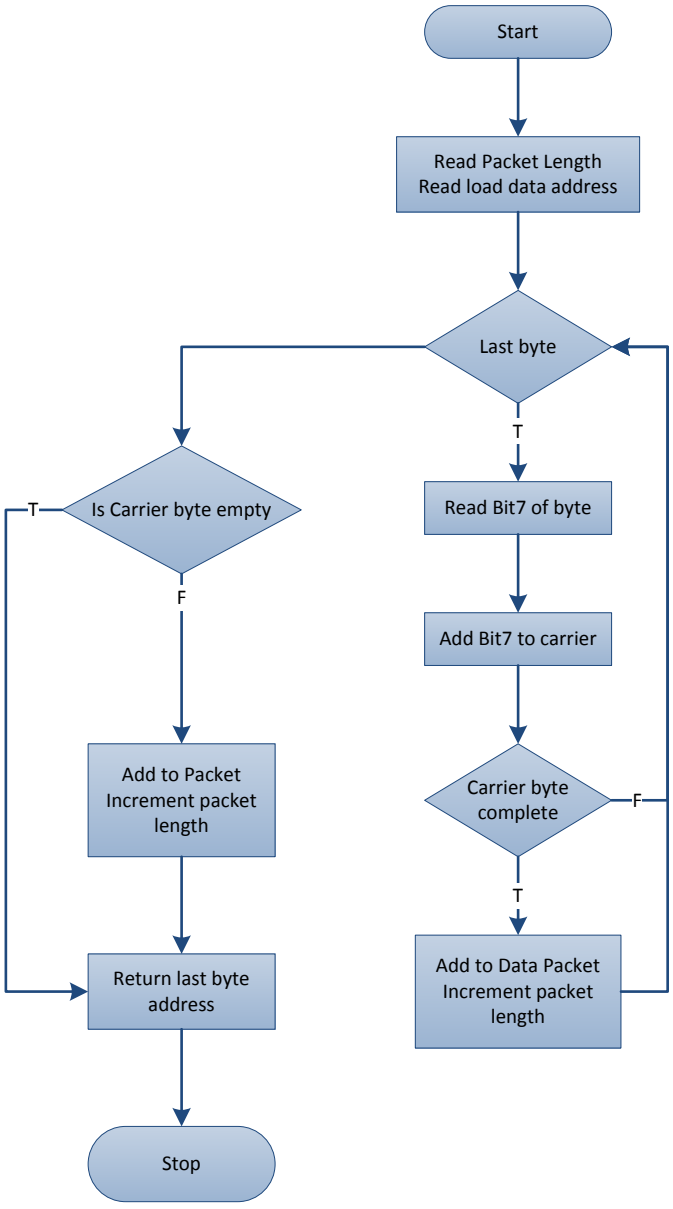

Figure 6-3: Flowchart of the 7 to 8 byte stretch

One of the drawbacks of this method was that it required the data to be in multiples of 7 bytes, this was circumvented by adding a packet length byte. In this case the packet length byte is added after the header byte and performs a dual role;

- Check the location of the terminator byte; the packet length indicates the position of where the terminator byte should be located in the data array. In the unlikely case the data could be corrupted in such a manner that a data byte is received as a packet terminator the

terminator would not be located correctly. Therefore the packet can be determined as corrupted and all further processing of the packet stopped.

- Secondly, the packet length allows for the number of carrier bytes to be calculated. This enables the protocol to handle packets of data that are not a multiple of 7 bytes. Reducing the number of bytes sent as padding of the packet is not required to ensure the packet length is a multiple of seven.

In the case where the packet length is not a multiple of seven, the carrier byte is calculate across the remaining bytes and added to the end of the data packet. Upon receipt of the data packet, the original packet length is calculated using method shown in Figure 6-4. If the packet length is a multiple of eight, then the original packet length was a multiple of seven and the number of carrier bytes are equal to the quotient of the packet length and eight, else it is equal to the quotient incremented.

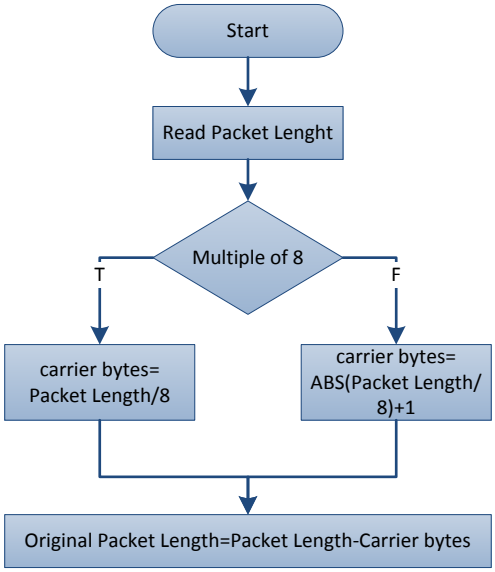

Figure 6-4: Flowchart depicting the method used to determine the original packet length

The original packet length and the carrier byte can then be used to compress the data.

While the packet length byte and the pack header and terminator bytes are to determine when data has been lost from the packet, the more likely event is that a number of bits in the data payload are corrupted. In order to detect this data corruption, a CRC is calculated across the data payload.

6.4.3

Cyclic redundancy checksum

A **C**yclic **R**edundancy **C**hecksum (CRC) is generated by treating the entire packet as a single binary number and dividing (XOR) by a CRC polynomial. The remainder is then attached the tail of the data packet. In order to determine data corruption the packet is divided by the same CRC polynomial. If there is a remainder, data corruption has occurred.

For the purposes of this system, an 8 bit CRC polynomial was selected (**6-1**).

$$CRC_{polynimial} = x^8 + x^2 + x^1 + x^0 \qquad (6\text{-}1)$$

Table 6-6: CRC byte data

Byte	$CRC\ Byte_1$		$CRC\ Byte_2$	
Bit	7:4	3:0	7:4	3:0
Data	0	CRC [7:4]	0	CRC [3:0]

The CRC remainder is calculated first, then the low nibble and high nibble are split across two bytes (Table 6-6) in order to ensure unique packet header and terminator bytes.

6.5: Communication software

As a packet structure has been established, the basic communication structure shown in Figure 6-2, can be expanded to include the packet preparation for the transmitter and the processing of the packet for the receiver. This is seen in Figure 6-5.

While the packet structure enables the detection of data loss or corruption it is possible for a complete packet to be lost. This case is handled by the transceiver software, through the use of a timeout. After a transmission, if the period of time passes without the receipt of a confirmation, the data packet is assumed to be lost and the data is resent.

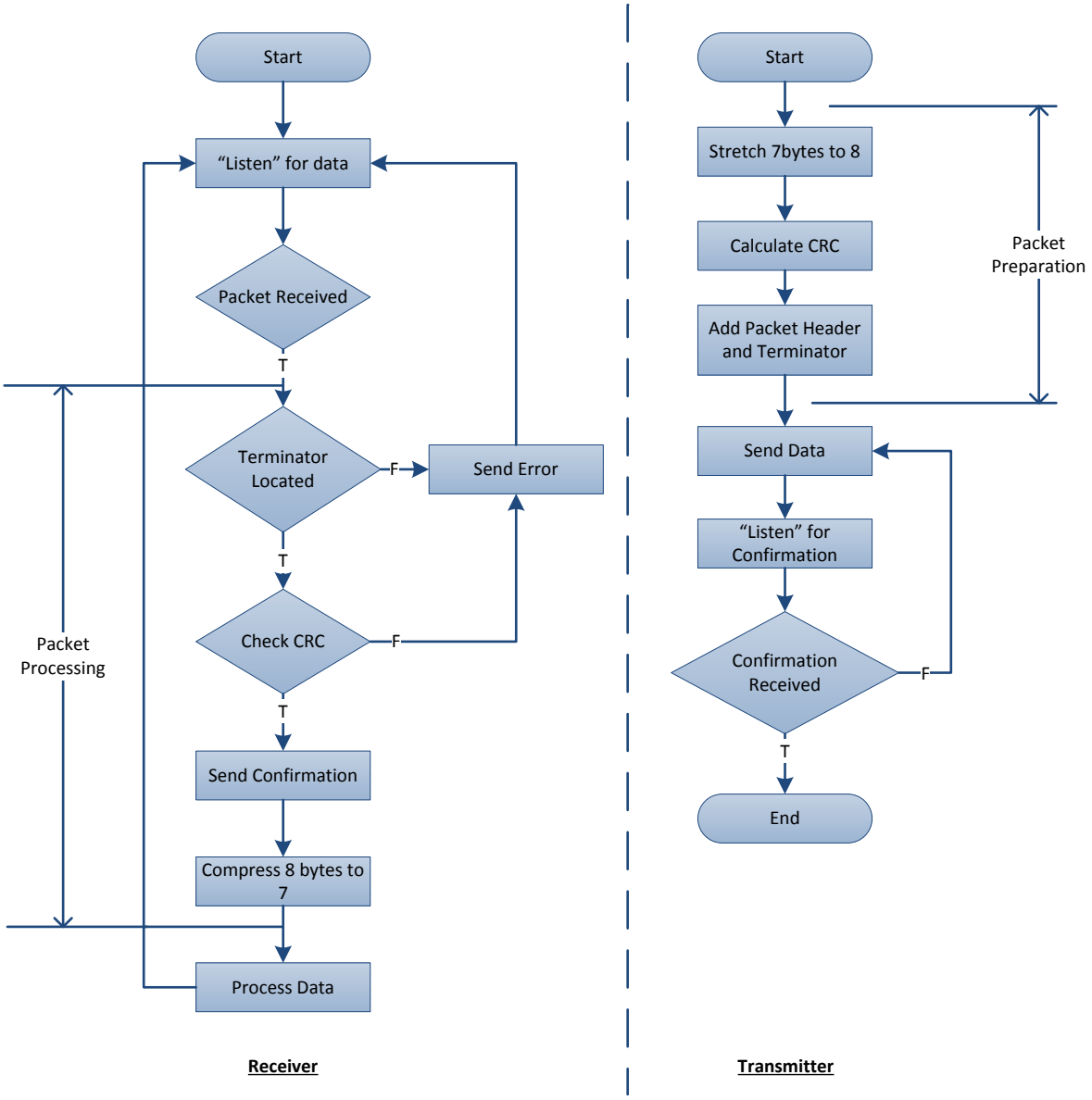

Figure 6-5: Flowchart showing communication structure including the packet handling process

6.6: Video and audio transmission system

The images and audio are transmitted from the platform using a Range Video transmitter/receiver pair. The images are provided to the transmitter as a PAL analog signal, from the camera PCB. As there are currently two image sources on the sensor payload, with potentially more in the future, a switch is required to allow the operator to select the preferred image source. This is achieved through a TS3V330 IC.

As the operational temperature of the transmitter is in the range of 50˚C to 60˚C, the transmitter is mounted on a heat sink to the rear of the shell. This is to minimise the effect of this temperature on the remainder of the system.

6.7: Communication subsystem cost

The cost of the system is US$ 36.13. This excludes the Range Video FPV receiver which is included in the cost of the operator station. The breakdown of the cost can be seen in Table 6-7.

Table 6-7: Cost breakdown of the communication subsystem

Item	Cost (US$)
Range Video FPV Transmitter	32. 63
RF1101SE transceiver	3.50
Total	36.13

6.8: Concluding remarks

Wireless communications have been established. The bidirectional data communications, with error checking, operate at a baud rate of 19200 bps, using a pair of RF1101SE transceiver modules. A CRC byte is calculated to enable data corruption detection across the data packet and data manipulated to produce unique header and terminator bytes to indicate the presence of a complete packet. Of some concern, however, is the operational temperature of the video transmitter and the effects that is will have on the system.

As the platform is a tetherless platform, the power source is a battery. This section describes the selection of a battery and design of the battery management system, seen in Figure 7-1. Background research suggested that a Lithium-Ion battery should be used, because of its high energy density and relative stability. In order to maximise the potential of the Lithium-Ion battery, a battery management system is required, to protect the battery and estimate the remaining operational time. Additionally, in-field charging is a requirement of the system and a charging module will be included in the battery management system.

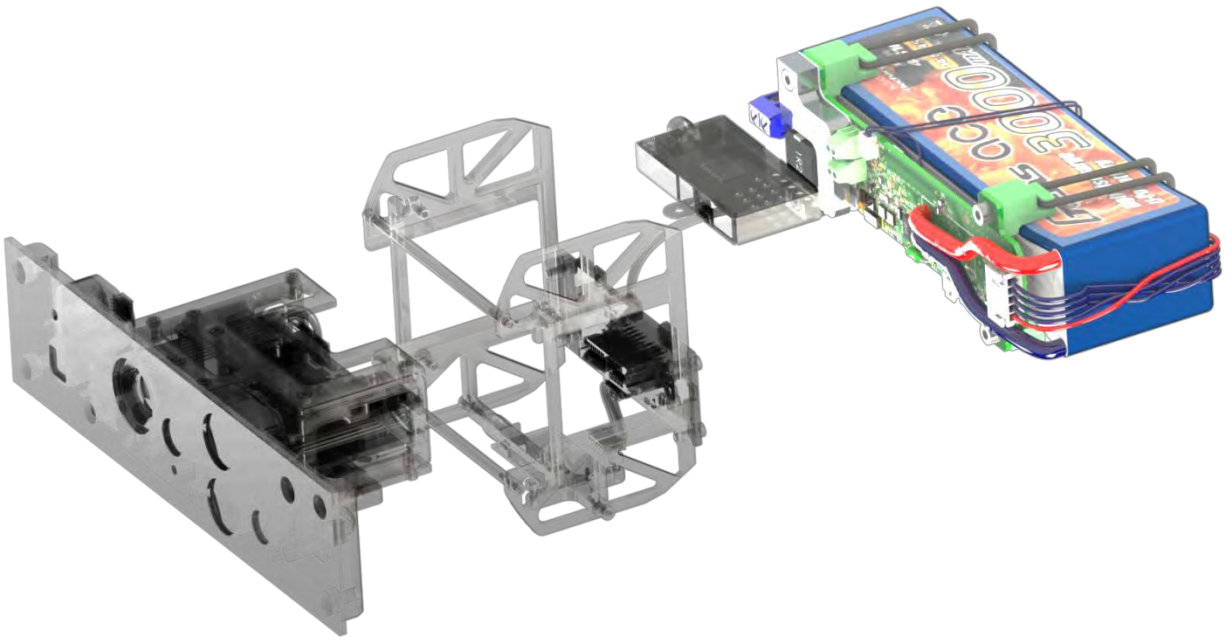

Figure 7-1: The battery and battery management system

7.1: System specifications

The subsystem specifications are an expansion and quantisation of the primary system requirements, Table 3-1 for the battery and its management system.

Table 7-1: BMS and battery specification

Explanation Location	Subsystem Specification	Desired Value		
7.1.1:Physical specifications				
7.1.1:	Overall mass	350 g		
7.1.1.2:	Dimensions	137 x 41 x 60 mm		
7.1.1.3:	BMS mounting	Attached to battery		
7.1.1.4:	Cost	US$ 60		
7.1.2:Functional				
7.1.2.1:	Over voltage protection	Yes		
7.1.2.2:	Short circuit protection	Yes		
7.1.2.3:	Thermal protections	Yes		
7.1.2.4:	Permanent failure safety	Yes		
7.1.2.5:	Gas gauge	Yes		
7.1.2.6:	Integration drift compensation	ImpedanceTrack™ / CEDV		
7.1.3:Charger specifications				
7.1.3.1:	Charging time	Min	Nominal	Max
		60 min	90 min	120 min
7.1.3.2:	Adjustable charge rate	Yes		
7.1.3.3:	System supply during charging	Yes		
7.1.4:Power supply specifications				
7.1.4.1:	Operational time	20 min		
7.1.4.2:	Standby time	5 hours		
7.1.4.3:	Minimum voltage	12 V		
7.1.4.4:	Discharge current	Min	Nominal	Max
		n/a	2 A	6 A
7.1.4.5:	Discharge ports	2		

Physical specifications

7.1.1.1: Overall mass:

The mass of the battery was estimated to be 60 % of the total system mass, which is specified at 700 g.

7.1.1 ### 7.1.1.2: Dimensions:

The dimensional specification is to ensure that the battery and BMS can be integrated into the system in the space allocated for the BMS. This location can be seen in Figure 5-2 on page 40.

7.1.1.3: BMS mounting:

The BMS should be mounted to the battery as, once the BMS has been calibrated to the battery, it should not be removed from the battery.

7.1.1.4: Cost:

In order to achieve the US$ 150 cost specification, the battery and management system should not exceed a cost of US$ 60.

Battery protection specifications

7.1.2 ### 7.1.2.1: Over voltage protection:

Aside from puncturing the cell, one of the most dangerous states for a Lithium-Ion to be in is an over voltage state. This can lead to explosive combustion.

7.1.2.2: Short circuit protection:

A short circuit will cause the discharge rate to exceed the recommended discharge of the battery, damaging the battery and reducing the operational life cycle of the battery.

7.1.2.3: Thermal protection:

Suspension of charging or discharging (if the temperature of the battery rises above 75 ℃) will prevent failure due to overheating that could result it catastrophic failure of the system.

7.1.2.4: Permanent failure protection:

Creation of an open circuit between the system and the battery to provide an additional safeguard, should the battery protection fail to prevent an event.

7.1.2.5: Gas gauge:

Provide an estimation of the remaining battery capacity and the time remaining. This will allow the operator to retrieve the system prior to expending the capacity of the battery.

7.1.3 ### 7.1.2.6: Integration drift compensation:

The method of gas gauging requires integration of the current flow during charging and discharging, as explained on page 18 — the methods of **ImpedanceTrack™**.

Charger specifications

7.1.3.1: Charging time:

The charging time is determined as 25 % of the maximum operational time of the system. This provides an adequate charging-to-operational-time ratio.

7.1.3.2: Adjustable charge rates:

Adjustable charge rates will allow charging according to the capabilities of the power source. Additionally, it will allow the system to adjust the charge rate according to the internal temperature of the system to prevent the thermal protection from suspending charging.

7.1.3.3: System supply during charging:

The sensor payload will control the charging allowing the system to charge from any suitable source during operations. In order to achieve this, the microcontroller and communication require power during charging.

Power supply specifications

7.1.4:

7.1.4.1: Operational time:

During research into urban search and rescue operations, it was noted that the average time of an operation was 6 minutes and 44 seconds [5]. Therefore, an operational time of greater than three times the average was selected for extended operations.

7.1.4.2: Standby time:

While the average operational time is relatively short, it was also noted that upon identifying a survivor the average excavation time was 4.5 hours [5]. During this time, the platform should remain with the victim to provide information on the survivor and the environment. Standby operation was defined as maintaining communications and images while stationary.

7.1.4.3: Minimum voltage:

The minimum voltage was determined from the fact that the motors are rated by 12 V and the video transmitter has an operational voltage range of 10 V to 12 V. Therefore, a 2 V dropout would be required for a switch mode regulator to provide 10 V.

7.1.4.4: Discharge current:

Initial calculations showed the motors would require 3 A. The sensor payload designed was estimated to sink 1.5 A, Therefore a maximum of 6 A would allow for future sensor payloads with a higher current requirement to be designed, as the system is designed for multiple sensor payloads without modifications to the power and communication systems.

7.1.4.5: Discharge ports:

Two discharge ports are required, one for the motor driver and a second for the sensor payload and communication systems.

7.2: Battery selection

The battery is the power source in a tetherless system and therefore critical to the success of the robotic system. From the background research it was determined that, if implemented correctly, the Lithium-Ion cell chemistry would be optimal for this system for both energy density and chemistry stability when coupled with a battery management system. From the voltage requirements, seen Table 7-1, 12 V is required; at a minimum of 3.0 V per cell the selected battery will have at least 4 cells in series. Therefore, the capacity can be calculated using 12 V as the minimum system voltage.

Table 7-2: System power requirements for battery selection

Item	Value
Sensor Payload Requirement	6W
Motor Power Requirement	36 W

As the battery was selected prior to the completion of the sensor payload, the power requirements where estimated, as seen in Table 7-2. The power requirements where estimated using the specified power requirements of the primary components of the sensor payload, with the addition of a 10 % buffer. From the power requirements, the required battery capacity can be calculated.

$$Capacity = I \times t \quad (7\text{-}1)$$

$$P_x = V_{BAT\_min} \times I \quad (7\text{-}2)$$

$$I = \frac{P_x}{V_{BAT\_min}} \quad (7\text{-}3)$$

$$\therefore Capacity = \frac{P_x \times t}{V_{BAT\_min}} \quad (7\text{-}4)$$

Using equation (7-4) the capacity requirement for a standby operation was estimated to be a minimum of 2200 mAh. Considering these requirements, cost and availability, a Gens Ace 4S1P 3000 mAh battery was selected. The specification of the battery can be seen in Table 7-3 below.

Table 7-3: Properties of the Gens Ace 4S1P battery

Property	Value		
Net Mass	365 g		
Capacity	3000 mAh		
Discharge Rate	35 C		
Max Continuous Current	105 A		
Max Burst Current	210 A		
Max Burst discharge Rate	70 C		
Cells in Parallel	1		
Cells in Series	4		
Voltage	Min	Nominal	Max
	12 V	14.8 V	16.8 V
Length (mm)	139 mm		
Width (mm)	43 mm		
Thickness(mm)	31 mm		
Wire Gauge	12 AWG		
Connector Type	T-XHR		
Balancer Connector Type	JST-XH		

As stated in the background research, the Lithium-Ion battery, while volatile, can be used safely when paired with a battery management system.

7.3: Battery management system

The role of the battery management system is to allow for the safe operation of the battery throughout the operational cycle of the battery. This is achieved by a battery management system comprised of the following modules: primary battery protection and gas gauging, a secondary

analog battery protection and a battery charging system. An additional feature is an inrush current limiting circuit to protect the battery management system.

BMS prototype design

There are two areas of focus for the prototype design of the BMS.

- The method of implementing the gas gauging and primary battery protection. Two methods were proposed, one being the use on an AFE with a microcontroller to implement the coulomb counting algorithm, or alternatively the use of a dedicated IC.
- The second point was the charge rate selection for the battery charger. The possible methods were to use a number of selectable fixed charging rates or a varied charging rate that would be implemented with a DAC.

7.3.1:

Three gas gauge prototypes where developed and evaluated on the following criteria:

- Cost: The hardware and the software development costs were considered. The main object of the project was to produce a working system therefore cost saving had to be weighed against what is achievable in the period.
- Functionality: The current profile of the system was assumed as a constant low current with short high current spikes during operation of the motor.

Gas gauge prototype 1

The first prototype was the implementation of the gas gauge and cell balancing using an AFE, the TI BQ267925 with a MSP430G2332 microcontroller. The simplified schematic of the implementation circuit can be seen in Figure 7-2. The I^2C communication interface allows the following actions:

- Enabling of internal cell balancing
- Access to the measured cell voltages
- Setting the shunt voltage gain
- Setting the voltage and current thresholds

The shunt voltage, multiplied by the selected gain, is read by the ADC on the microcontroller and converted to a current. This current is then used to implement a coulomb counting algorithm embedded on the microcontroller. The battery capacity is then stored on the microcontroller flash to prevent loss of data during resets. The prototype can be seen in Figure 7-3.

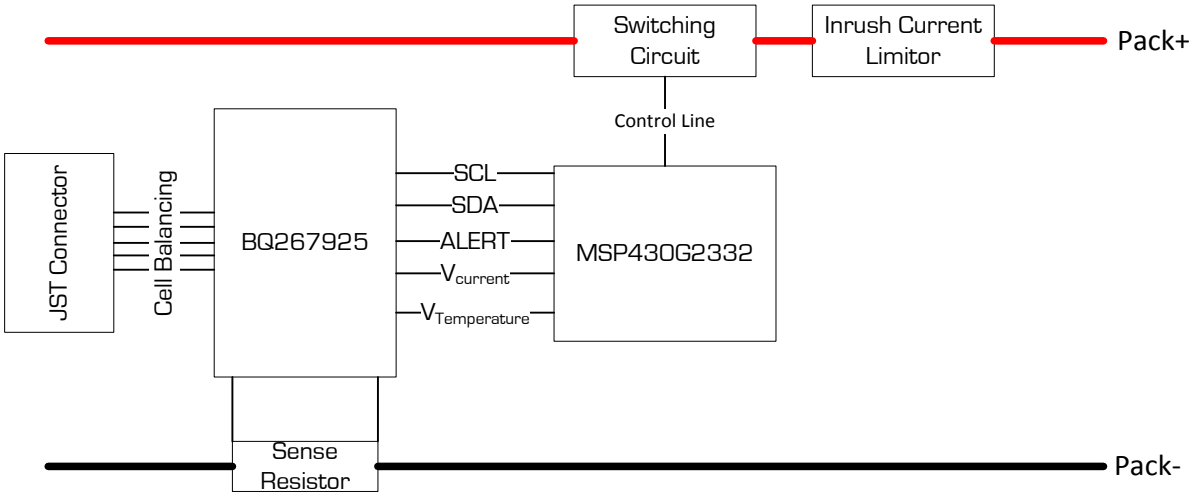

Figure 7-2: Simplified schematic of the implementation using the BQ267925 AFE and an MSP430G2332 microcontroller

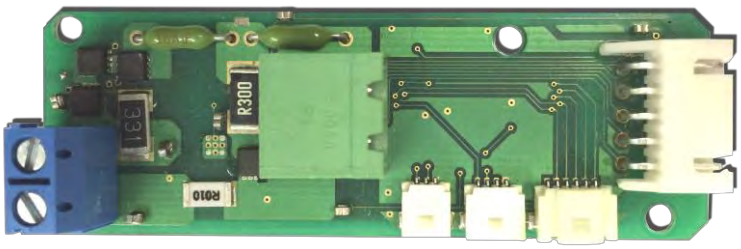

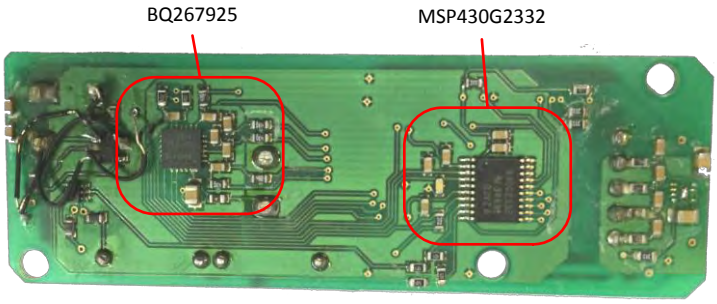

Figure 7-3: Diagram showing the PCB implementation of concept 1

With the cost of the ICs seen in Table 7-4 and the low additional component count, the cost was an advantage.

Table 7-4: Cost breakdown of the primary components

Primary Component	Unit Cost[1] (US$) [36]
BQ267925	1.91
MSP430G2332	1.21
Total	3.11

[1] at a quantity of 250 units

The second prototype was a dedicated gas gauge and primary battery protection IC, which will reduce the software development cost.

Gas gauge prototype 2

The second gas gauging prototype implemented the gas gauging through the use of a dedicated IC. The task was set as an Electrical Engineering undergraduate project and completed by Antony Wilson. The proposed solution uses a BQ3060 primary battery protection and gas gauge IC, the cost of which can be seen in Table 7-5. For the purpose of testing the IC and developing the software, an evaluation board was bought and software was developed to read the battery information from the BQ3060 IC. This successfully implemented the battery protection and gas gauging. The disadvantage of the system is that the BQ3060 requires external cell balancing and thus increases the additional component count.

Table 7-5: BQ3060 cost per unit

Gas Gauge IC	Unit Cost[1] (US$) [36]
BQ3060	5.12

[1] at a quantity of 250 units

Gas gauge prototype 3

The third and final gas gauge prototype used a BQ20z45 IC. While the primary purpose of the prototype was to test the gas gauge IC, it filled a secondary role, which was to investigate the integration of a complete battery management system. This prototype served as a basis on which the final BMS was developed. The main point of improvement between the prototype and the final design is the PCB layout. The error was selecting 35 µm copper layer PCB, the required track width resulted in impossible trace routing within the given dimension using a two layer board. The only solution was to route the charger return current path via an external wire as seen in Figure 7-4.

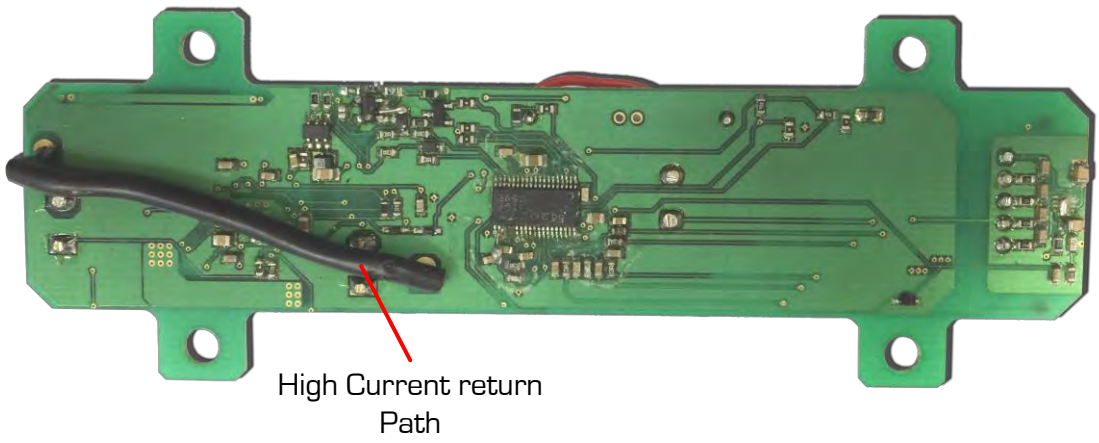

Figure 7-4: Picture showing the high current charging return path on the third prototype

Table 7-6: BQ20z45 cost per unit

Gas Gauge IC	Unit Cost[1] (US$) [36]
BQ20z45	5.43

[1] at a quantity of 250 units

Prototype selection

Three prototypes were developed. The software development cost required for safe implementation of the BMS, outweighed the US$ 2 saving on the primary components, when compared to the remaining prototypes. While the BQ3060 (prototype 2) proved to be an adequate solution, background research indicated that, for this application, **ImpedanceTrack™** was the optimal

method of compensating for integration drift. The BQ3060 uses CEDV. The cost of the BQ20z45 (used in the prototype 3) was greater than the BQ3060, however the fact that the BQ20z45 supports internal cell balancing means that the additional components required for the BQ3060 to perform cell balancing negates the minor cost saving. Therefore, the BQ20z45 was selected primarily because the method of calculating the SOC is better suited to the application and the difference in cost can be negated by the supporting component count. However, the PCB used in prototype 3 should change to a 70 µm thick to reduce the track width. This should enable the return path trace to be included.

Primary component selection

7.3.2: Texas instruments is one of the only manufacturers which produces a multi-cell gas gauge and primary battery protection system, incorporated in to a single IC. Therefore, in order to reduce the complexity of the battery management system, a BQ20z45-R1 battery protection and gas gauge IC was selected. The IC includes internal cell balancing, reducing the external component count leading to additional cost savings. The secondary analog protection system was selected from the TI range to limit potential interfacing issues and is selected according to the cell count and a maximum cell voltage of 4250mV. While this is within the maximum operational range of the battery, the event is most likely to occur during charging, when the platform is attached to the operator, therefore, a safety factor was added.

TI offers a BQ24753A battery charging IC with a system source select function, enabling the platform to be powered from the charge adapter, when present, or from the battery when the adapter power source is not present.

7.3.3: Hardware design

Both the primary battery protection and the battery charging IC's are provided with recommend circuits, which were configured for this application. In the case of the primary battery protection, two modifications were made. These were:

- The introduction of an inrush current limiter: any capacitive load will result in a large current inrush immediately after closing the circuit. This is a result of the capacitor charging at a rate limited only by the ESR of the capacitor. The ESR of the capacitor is typically low which results in large current spikes. This inrush of current damages the battery, inline fuses and switching components, gradually reducing the lifespan.
- The availability of a chemical fuse that was recommended proved to be a limiting factor due to cost and availability. The chemical fuse is used to open the circuit in the event of a permanent failure. Therefore it is critical to the safe implementation of the BMS and an alternative solution has been designed and tested.

As the majority of the circuitry accompanying the primary BMS ICs uses the recommended circuitry, the hardware design will be focused on the modification and the integration of modules of the battery management system.

An alternative to a chemical fuse

Firstly, the recommended circuit specifies a chemical fuse as a method of permanently disconnecting the battery from the rest of the system in the case of a critical failure. Due to the cost and availability of the chemical fuse, a cheaper alternative circuit was designed. The system

uses a current limited circuit to trigger a fuse, permanently opening the circuit between the battery and the system. The schematic of the circuitry can be seen in Figure 7-5.

Once the battery voltage reaches an unsafe level, the secondary battery protection system sets the gate of the N Channel MOSFET (Q10 Figure 7-5) high, closing the circuit. As this will occur at 17 V, this causes a 57 Amp current to flow through the fuse (F1 Figure 7-5) which will lead to the fuse opening the circuit in 8 milliseconds. To reduce costs, all the components for this circuit were designed for a single use. This is justified by the fact that, if a permanent failure was to occur, the battery and BMS should be rendered inoperable and returned to the manufacture to assess the cause of the failure. During this process the BMS should be replaced.

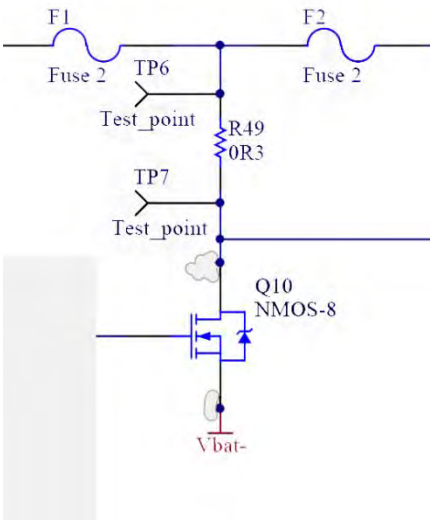

Figure 7-5: Schematic of the circuit used by the secondary battery protection to permanently open the circuit

Inrush current limiting

As an inline fuse has been introduced into the system, an inrush current limiting circuit is required in order to prevent the fuse from triggering due to repetitive loading. The inrush current limiting circuit is located on the output of the battery protection system, curbing the effect of capacitive charging. This system could be achieved using a NTC thermistor. The resistance of a thermistor varies with temperature of the device. This leads to two major disadvantages:

- Once the system is disabled, a delay period is required during cycling of the system. This is to allow for the thermistor temperature to decrease.
- The suitable thermistor for this application has an operational temperature of 185˚C. This could be potentially catastrophic, with the proximity of the BMS to the battery.

Alternatively, a high impedance path can be used during a soft start period, with a low impedance path being closed once the capacitors are suitably charged. The soft start can be achieved using the circuit seen in Figure 7-6.

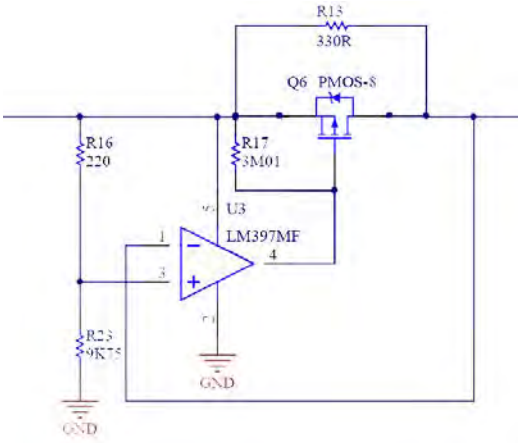

Figure 7-6: Schematic of the inrush current limiter

The current is limited to a maximum of 51mA during capacitive charging. Once the output voltage reaches 98 % of the input voltage, the comparator pulls the gate of the MOSFET (Q6) low, closing the circuit. This allows the flow of current along a low impedance path during normal operation, successfully limiting the maximum inrush current to a safe level.

Battery charging circuitry

The BQ24753A battery charger can be used for charging at rates of up to 10 A. As the Gens ACE battery has a maximum charging rate 9 A, the battery charging circuitry for this application was selected, following the procedure laid out in the IC's data sheet [37]. A DAC was used to provide the reference voltage input to the IC for selecting the charge rate. This will allow a charge rate of up to 8 Amps to be selected, which is safely within the limits of the battery.

7.3.4: BMS PCB design

The BMS PCB is mounted to the battery and thus the profile of the main body of the PCB is similar to that of the battery. The layout of the modules of the BMS, seen in Figure 7-7, was designed to reduce the length of the high current paths. The connection diagram and pinout descriptions can be seen in Figure 7-8, Table 7-7 and Table 7-8 respectively.

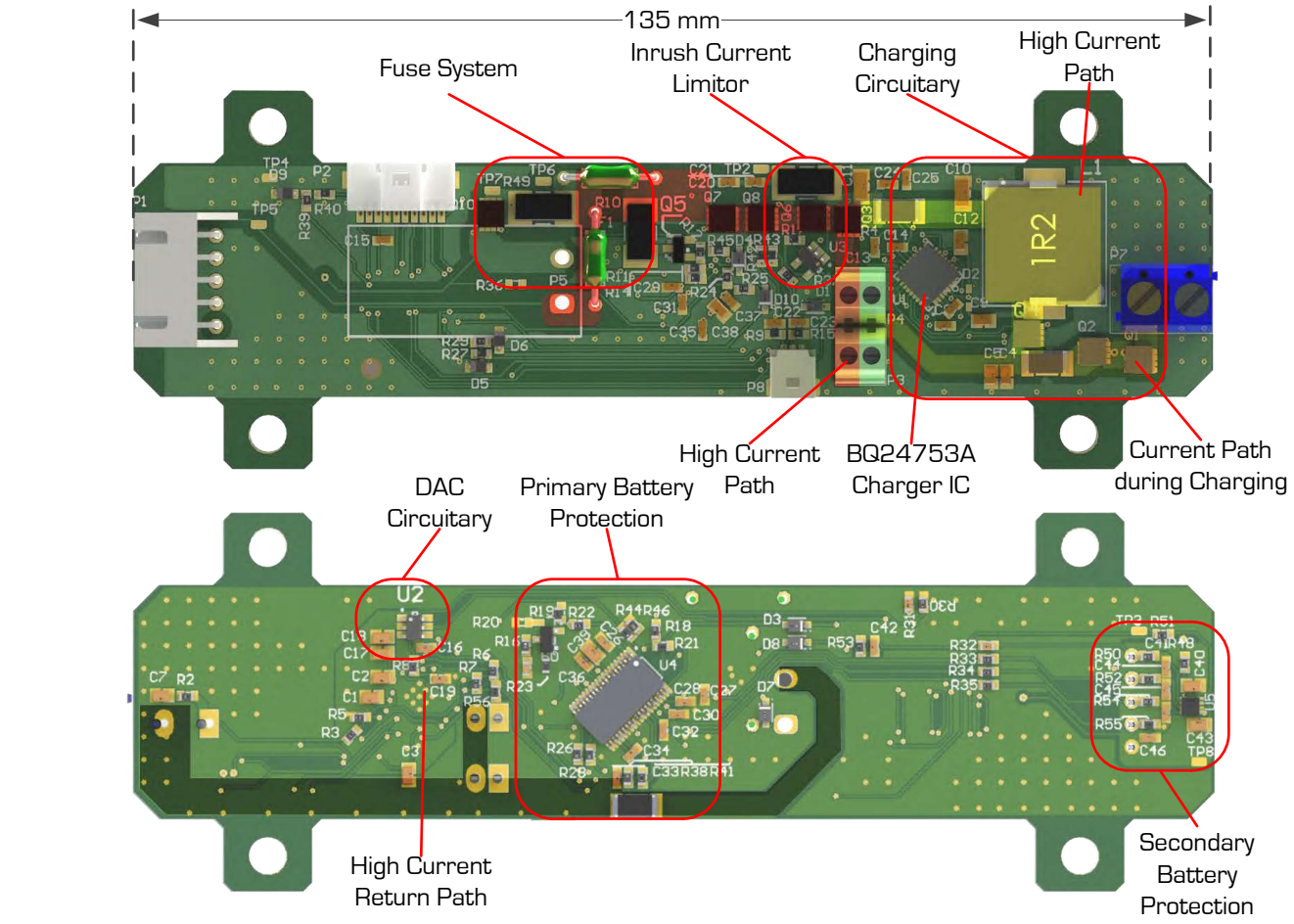

Figure 7-7: Diagram of the BMS PCB indicating the component locations

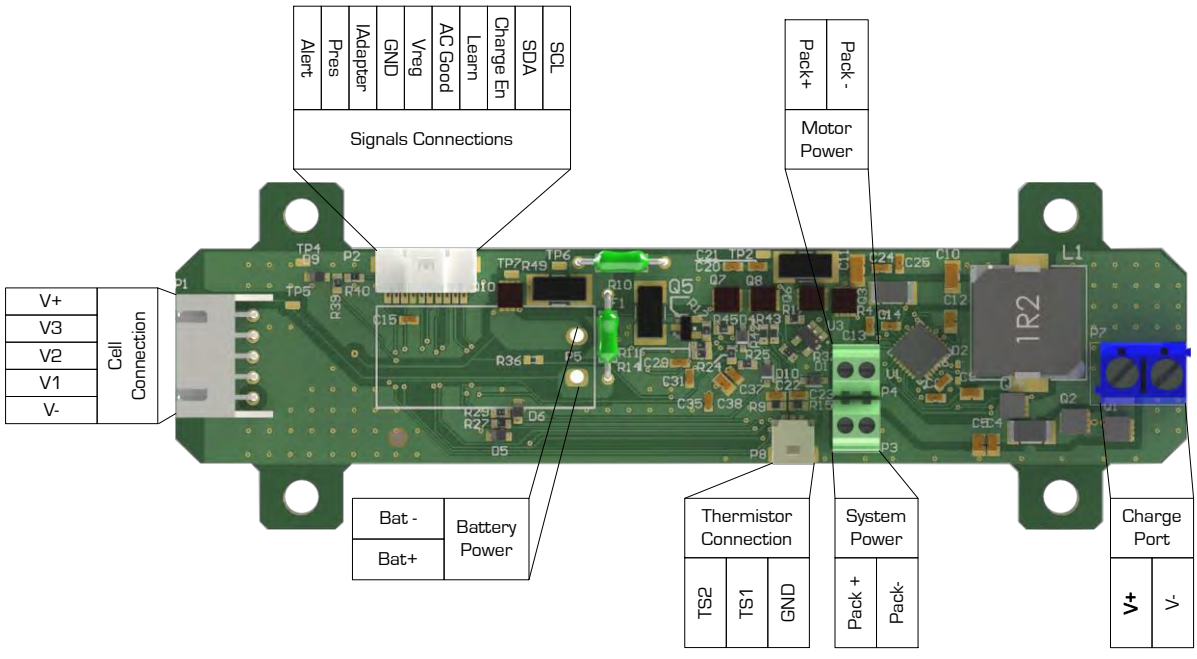

Figure 7-8: Render BMS indicating the assignments of the connectors

Table 7-7: BMS power connection description

Power Connections					
Connector	Pin	Direction	Min	Nominal	Max
System Power	Pack +	Output	13V	14.8V	24V
Motor Power	Pack +	Output	13V	14.8V	24V
Charge Port	V+	Input	17V	20V	24V
Signal Connection	V_{reg}	Output		3V	

Table 7-8: BMS signal pin descriptions

Signal Connections			
Connector	Pin	Direction	Description
Signal Connection	Alert	Output	SMBus alert pin. Signals battery fault has occurred. Active Low
	Pres	Input	System Present Pin. When held low it enables the system and motor power outputs
	I Adapter	Analog Output	Analog voltage representing the current draw by the system through the charging port
	AC Good	Output	Adapter supply good pin, which is pulled low to indicate the presence of a charging power supply. Active Low
	Learn	Input	When enabled allow the BMS to cycle, charging will only begin if charging is enabled, AC Good is low and the cell voltage is 2.9V
	Charge Enable	Input	Enables charging, active Low
	SDA	I/O	I^2C Data Line
	SCL	input	I^2C Clock Line
Thermistor Connection	TS1	Output	Thermistor 1 connection
	TS2	output	Thermistor 2 connection

7.3.5:

BMS mounting

The BMS should not be removed from the battery; hence, the battery is directly connected to the BMS. To prevent strain on the connections during maintenance and assembly, the BMS is mounted to the battery. It is important to note, however, that during usage, the temperature of the battery will rise, causing the battery to swell. Therefore the mounting should be flexible to prevent any possible puncturing of the battery.

A flexible mounting is achieved with a pair of dog bone shaped mounts to provide the support for the PCB to mount onto while maintaining a gap between the PCB and the battery to allow airflow reducing the effect of temperature caused by the charging circuitry on the battery. A pair of O-rings is used to secure the dog bone to the PCB, as seen in Figure 7-9. A heat sink is placed over the charging circuitry with a silicon elastomer heat pad — electrically, but not thermodynamically isolating the heat sink.

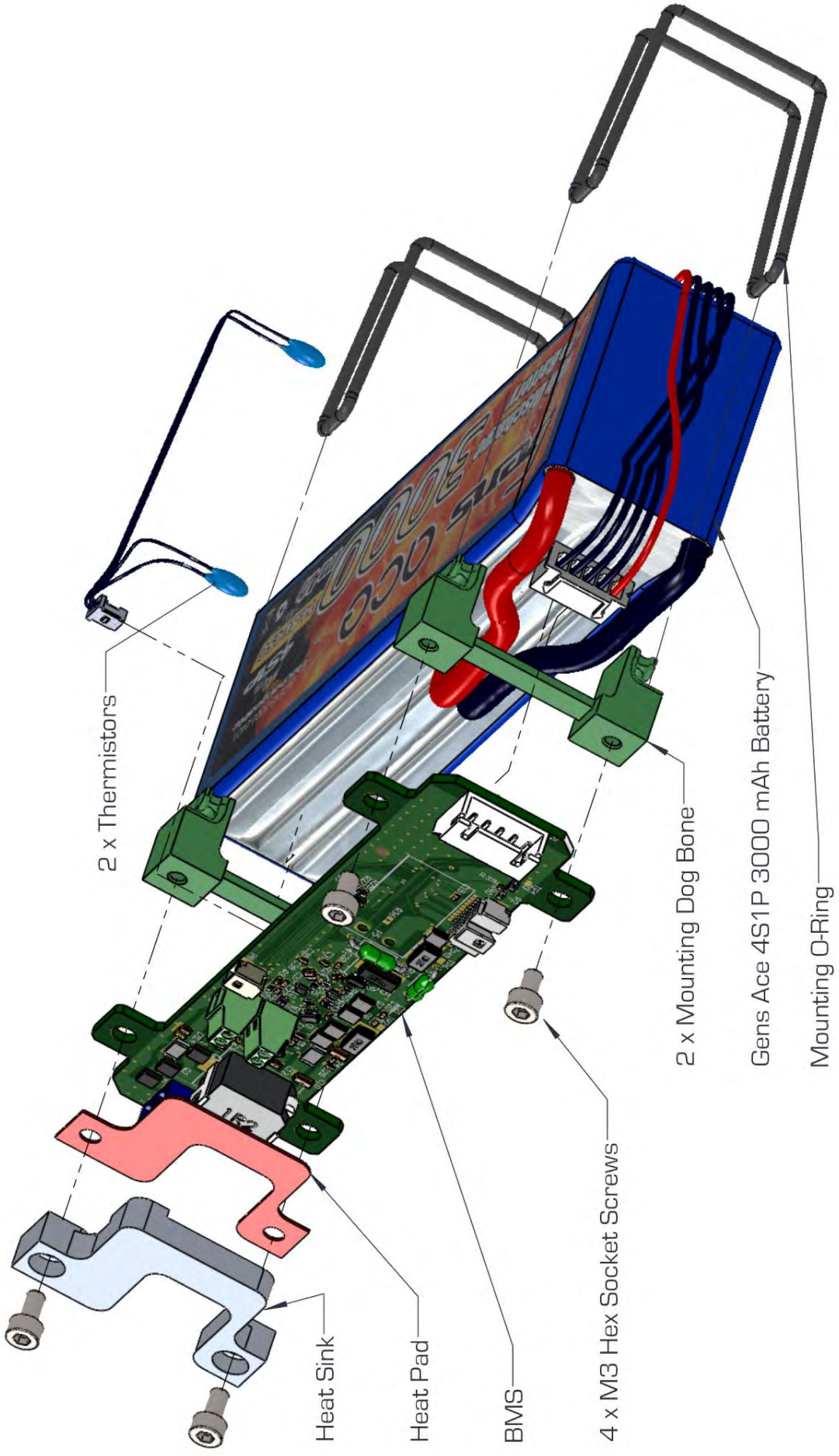

Figure 7-9: Exploded view of the BMS mounting system

7.4: Software design

The BQ20z45-R1 has an internal EEPROM and flash memory on which the BMS setting and battery states are stored. These settings were set during the configuration and calibration of the system. For this, the TI BQ evaluation software was used, as instructed in the BQ20zxx **ImpedanceTrack™** setup manual provided [38] by TI. Therefore, the software designed for the system is limited to reading the relevant data from the device, enabling charging and setting the charge rate.

While the BQ20z45-R1 supports SMBus, which is based on I^2C, the original selected microcontroller selected for the low-cost sensor payload, the MSP430G2995, does not support SMBus. Therefore I^2C was selected as the communication protocol for communication with the BMS device. Therefore, the software embedded on the microcontroller in the sensor payload was tasked with reading the following list of information from the BQ20z45-R1;

- SOC: defined as the remaining capacity as a percentage of the maximum capacity.
- Battery Current: This is represented as a negative current during discharging and a positive current during charging.
- Time Remaining: defined as the time remaining until empty during discharge and full during charging.
- Temperature: This represents the maximum temperature of the two thermistors and the internal temperature sensor on the BQ20z45-R1.

As the alert output from the BMS system shown in Figure 7-8 is used to indicate an error, the BMS data is polled at a 1 Hz. The new data is compared with the currently stored value of the reading, if there is a difference a flag is set to indicate the presence of new data to be transmitted, to the operator station.

7.5: BMS cost

The greatest cost was that of the battery. While a fuse system was developed to reduce the cost of the BMS, the cost of the system exceeded the requirements by US$ 3, as seen in Table 7-9.

Table 7-9: Cost breakdown of the battery and BMS

Item	Cost (US$)
Gens Ace 3000 mAh 4S1P Li-ion battery	45.00
Electronic Components	15.00
Materials	3.00
Total	63.00

7.6: Concluding remarks

The battery and management system were successfully implemented using dedicated ICs. While a system with lower component and material costs was purposed, the time required to implement a reliable and safe BMS outweighed the financial gain. The BMS PCB is mounted to the battery providing the capabilities for charging, charge estimation and battery protection.

The purpose of the testing is to validate the system against the specifications for the system (Table 3-1) and subsystems (Table 5-1, Table 6-1, Table 7-1). Therefore, the tests conducted were designed to verify the capabilities and limitations of the system. The results of these tests will be used to draw conclusions on the system and base recommendations for future work.

Chapter 8 :

8.1: System tests

The following tests pertain to the overall interaction between the subsystems.

Mass breakdown

As the system was designed to be throwable, the mass of the system is a limitation on this specification. It was therefore important to know the breakdown of the subsystem masses and identify the largest contribution to the mass, in order to specify which subsystem should be targeted for mass reduction techniques.

8.1.1

8.1.1.1: Procedure

Each subsystem was broken down into its major component groups and the mass recorded. For this test, the frame of the sensor payload cradle was considered as a subsystem, as it will be integrated into the shell in future designs (as previously discussed).

8.1.1.2: Results

The breakdown of the low-cost and extended payloads can be seen in Figure 8-1 and Figure 8-2 respectively. In both subsystems, the heat sink and the front panel contribute more than 50 % of the mass. In Figure 8-2, the increase in the electronic component contribution for the extended payload is because of the additional 23 grams of the thermal camera.

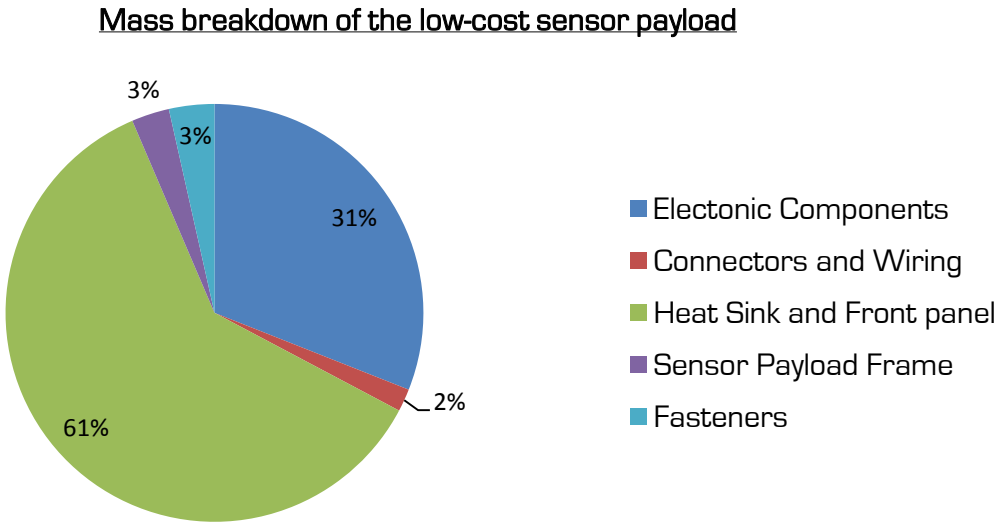

Figure 8-1: Low-cost sensor payload mass breakdown

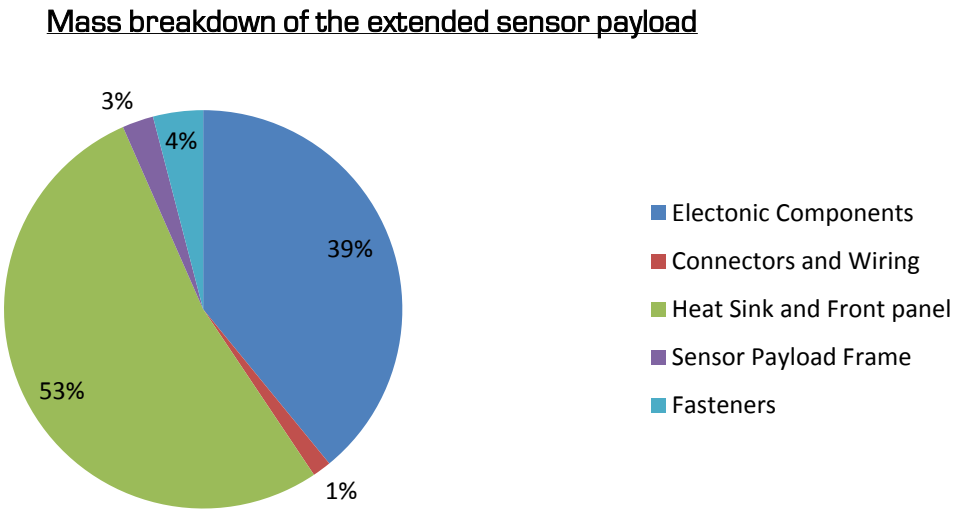

Figure 8-2: Extended sensor payload mass breakdown

As expected, the battery is responsible for the majority (89 %) of the BMS and battery subsystem's total mass as seen in Figure 8-3.

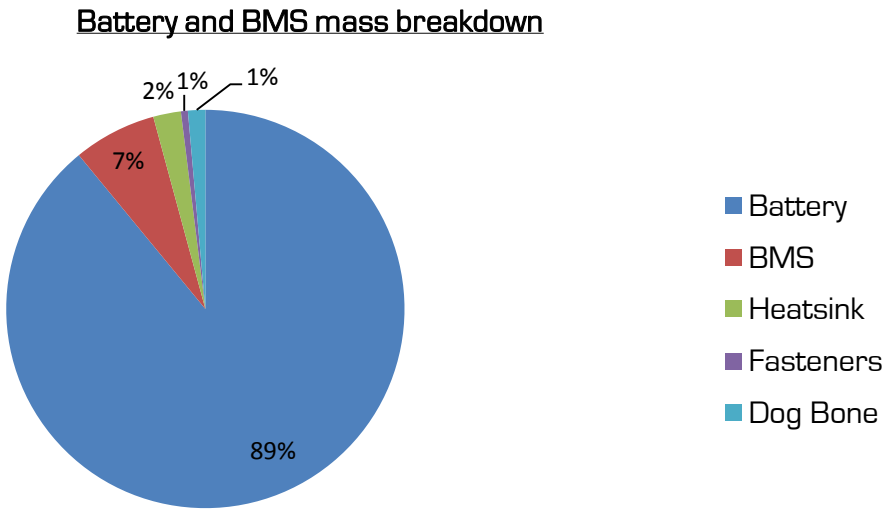

Figure 8-3: Mass breakdown of the battery and BMS

The final subsystem is the communications subsystem. It makes the smallest contribution, at only 6 % of the total mass (621 grams) of the entire system, as seen in the mass breakdown of the entire system (Table 8-1).

Table 8-1: Masses of the subsystems

Subsystem	mass (g)
Low-cost Sensor Payload	171
Extended Sensor Payload	197
Battery and BMS	356
Communications Subsystem	41
Sensor Payload Cradle	53
Total with Low-cost payload	621
Total Extended payload	647

Thermal test

8.1.2 To maintain an IP rating, the system would operate inside a sealed shell. Therefore it was important to verify that adequate heat sinking had been included, to ensure safe operation during normal operations. The test was therefore designed to verify that the system will not overheat during normal operations.

8.1.2.1: Procedure

The extended sensor payload was used, as the power requirement is greater than that of the low-cost sensor payload. The extra power required coupled with the inefficiencies will generate the greatest amount of heat. As the motors for the system were not operational at the time of testing, and given the efficiency of the motors, it was calculated that 2 W of power would be dissipated when the motors were operating at 70 % power. A pair of 10 W 2.2 Ω resistors were used as a substitute power dissipation source. The test was executed with the LEDs at 80 % power and the system operational; the temperature was logged every second for an hour, using the calibrated temperature sensors that were added to the system as a diagnostic tool.

8.1.2.2: Results

The maximum temperature over the period (68 °C) can be seen in Figure 8-4. While this test was conducted at room temperature of 20 °C and temperatures experienced during a rescue operation would be in excess of this, the system remained at a safe operating temperature throughout a period of an hour. Normal operation would last for a period of no more than 20 minutes with the full system operational.

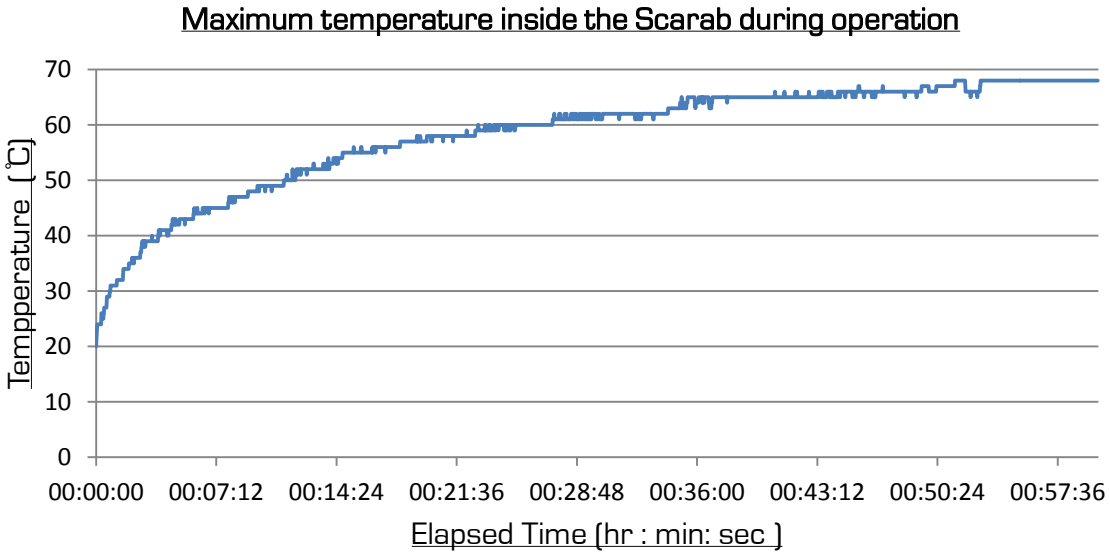

Figure 8-4: Graph showing the maximum temperature inside the Scarab during one hour of operation

8.2: Battery management subsystem testing

As the power is supplied from a Lithium-Ion battery, the ability of the BMS to maintain and prolong the life of the battery, will be verified. Five tests were designed to test the battery protection, gas gauge, charging, secondary battery protection and inrush current limiting modules.

8.2.1: Battery protection testing

The system uses a Lithium-Ion battery, which is be to charged from the operator station while being carried by the operator. The battery protection is critical for the safe operation of the system. Therefore, the ability of the BMS to protect the battery, allowing for safe operation and prolonging the life of the battery, was verified.

8.2.1.1: Procedure

Prior to connecting the BMS to the battery, the feature of the battery protection system was tested using a power supply and four resistors in series to create the cell voltages. The power supply was used to adjust the voltage levels, and a variable resistor was used to adjust the current draw. The over temperature event was created by exposing the thermistors to a temperature greater than the over temperature limit (75°C), with the use of a heat gun.

The state of the two MOSFETs used to open and close the path between the battery and the system were monitored, to check that the necessary protection was implemented.

8.2.1.2: Results

In all cases, the battery protection was successful. Table 8-2 shows state of the MOSFETs during the events. In the case of an under-voltage event, the discharge MOSFET is opened and the charge MOSFET is closed. This allows for charging of the battery, which would correct the event. This state of the MOSFETs is again used in the case of an over current event, when the discharge MOSFET is closed again after the prescribed 2 seconds. In the event of an over voltage level the primary battery protection system opens the charge MOSFET to allow current to be drawn from the

system, which will reduce the voltage. All current flow was prevented in the case of an over temperature event which can be seen by the fact that both MOSFETs opened.

Table 8-2: MOSFET behaviour during battery protection events

Event	Discharge MOSFET	Charge MOSFET
Under Voltage	Open	Closed
Over Voltage	Closed	Open
Over Current	Open	Closed
Over Temperature	Open	Open

Gas gauging and discharge current

8.2.2 The estimation of the operational time remaining is used to ensure that the operator has enough time to retrieve the platform. Additionally, the test was used to test the battery and the BMS's capability to safely provide the required current. Due to the internal resistance of the battery, the flow of current from the battery causes an increase in the cell temperature. As the temperature of the battery should not exceed 75 °C during operations, the purpose of the test was to show that the required power can be provided without entering into an over temperature state.

8.2.2.1: Procedure

The gas gauging test was performed by discharging the battery through a constant load at three different rates, 1.5 A, 3 A and 6 A. The estimated remaining time, calculated remaining capacity, battery voltage, cell voltages and the temperatures were logged. The tests were performed at room temperature. The purpose of this test was to illustrate the subsystem's ability to provide the required power and to accurately estimate the operational time remaining. The estimated time remaining, calculated by the BMS, was logged and compared to the actual elapsed time.

8.2.2.2: Results

The percentage error in the estimation can be seen in Table 8-3. The fact that the error is negative indicates that the BMS estimated time was less than the actual remaining time. What could be seen from the test results is that the error decreases throughout the discharge cycle as seen in Figure 8-5.

Table 8-3: Remaining time estimation error

Discharge Rate (A)	Difference between Elapsed and Estimated		
	min	mean	max
1.5	0.00 %	-3.20 %	-10.06 %
3.0	-0.03 %	-4.19 %	-10.47 %
6.0	-0.05 %	-8.52 %	-12.52 %

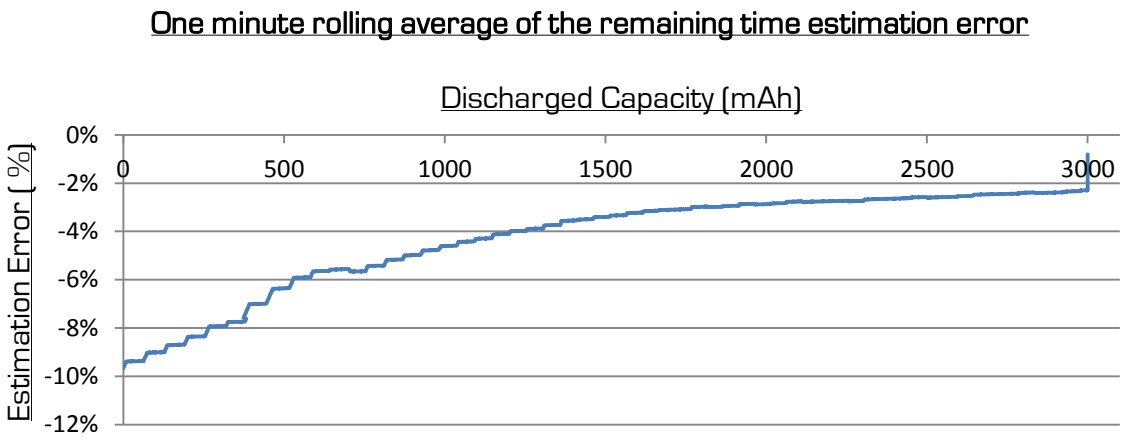

Figure 8-5: Remaining time estimation error over a 3 A discharge cycle

The temperature of the battery was logged throughout the discharge cycles and plotted as seen in Figure 8-6. The maximum temperature logged during the 6 A discharge cycle was less than 55 °C, well within the limit of the battery and the system.

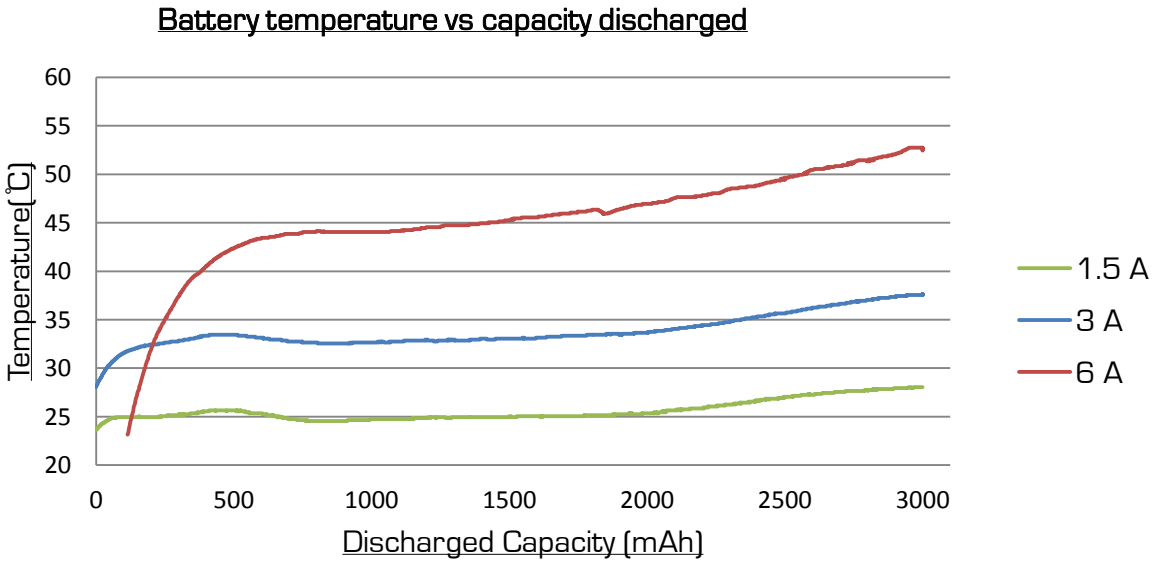

Figure 8-6: Graph showing the battery temperature during discharge

A second consideration was the ability of the battery to provide the required power. The discharge profile and times will be used to generate accurate predictions for future designs and to adjust the values of the battery protection. The total elapsed time during the discharge of the battery can be seen in Table 8-4. The profile of the battery can be seen in Figure 8-7 and the characteristics of the cell discharge provide for a 3 A discharge in Figure 8-8. It can be seen that cell 3 has a higher internal resistance than the remaining cells as the CCV drops rapidly towards the end of the discharge cycle.

Table 8-4: Battery discharge Time

Discharge Rate (A)	Elapsed Time (hour: min: sec)
1.5	02:08:59
3.0	01:03:42
6.0	00:32:50

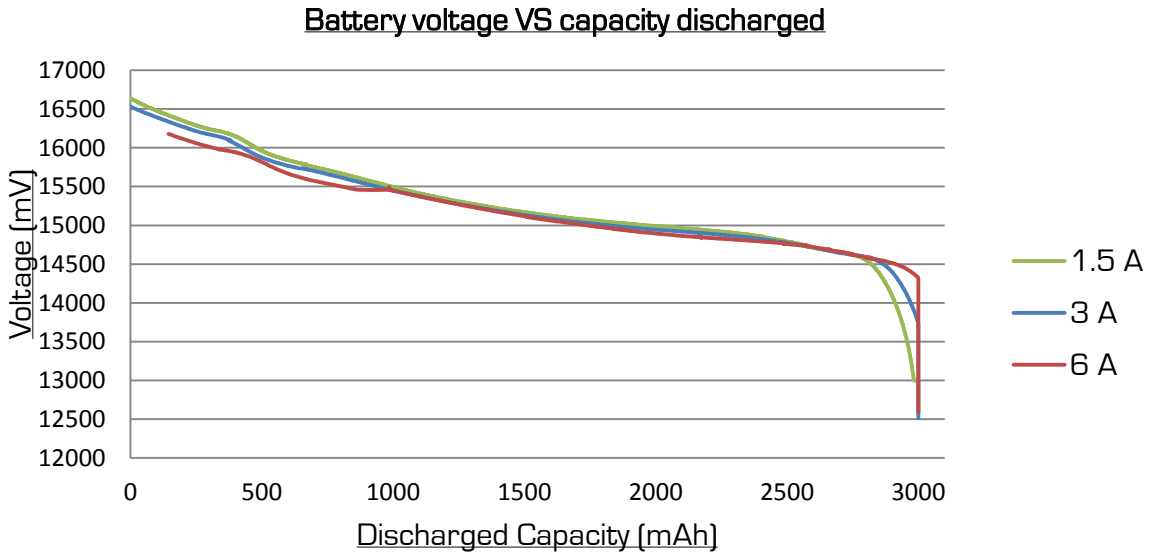

Figure 8-7: Graph showing the battery voltage during discharge

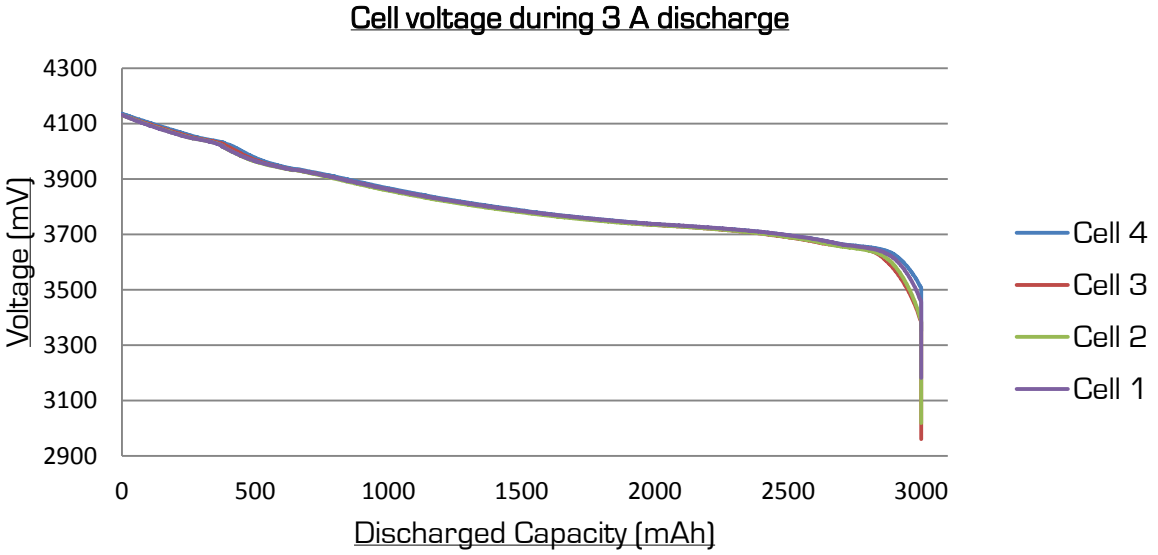

8.2.3:

Figure 8-8: Comparison between the cell voltages of the battery during a 3 A discharge

Charging testing

The charging test was designed to illustrate the BMS's ability to charge the battery when supplied with the correct 20 V power supply. Of significance is the time required to charge the system (which is dependent on the maximum charge rate) and, finally, the ability of the system to safely terminate the charge.

8.2.3.1: Procedure

The 20 V charging source was supplied by a power supply. The battery was then charged at three different rates illustrating the ability for a selectable charging rate. The temperature, battery voltage and elapsed time were logged during the charge cycles at a rate of 2 A, 3 A, 6 A and finally an 8 A charge was attempted. The termination of the charge was determined as the point at which the system entered into charge maintenance.

8.2.3.2: Results

The 8 A charge was abandoned due to multiple over temperature events, which can be seen in Figure 8-9. The temperature during the charge cycles, at the three remaining charge rates, remained within the temperature limit of 75 °C. With a maximum voltage of 16807 mV during the charging cycles (Table 8-5), the charging terminated within the maximum voltage rating of the battery.

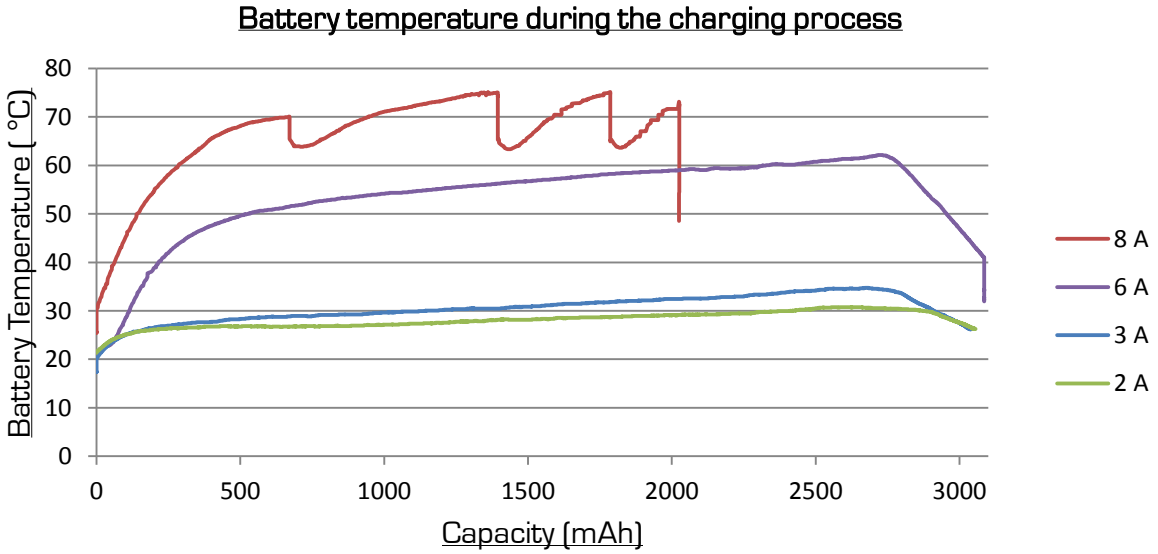

Figure 8-9: Battery temperature during the charging tests

Table 8-5: Charging results

Charge Current (A)	Maxim Voltage (mV)	Full Charge Capacity (mAh)	Charge Time (hour: min: sec)
2	16801	3071	01:47:50
3	16807	3077	01:20:39
6	16800	3086	00:50:51
8	n/a	n/a	n/a

8.2.4:

Fuse system

Should the primary battery protection fail, the secondary battery protection system should permanently disconnect the battery and the system. The recommended component to achieve this is a chemical fuse. However, due to costs and availability an alternative was designed. This test is, therefore, to verify the operation of the alternate circuit that was designed to trigger an inline fuse between the system and the battery.

8.2.4.1: Procedure

In order to test the fuse system without placing the battery in a potentially harmful over voltage state, a microcontroller was used to trigger the process, after a delay. The high current draw was a safety concern; because of this, the battery was placed in a charging pouch during the test. The test was then conducted in a safe open area. For a full outline of the safety procedure followed, please see the risk assessment form in Appendix D: Risk Assessment.

An oscilloscope was connected to the system to capture the response time of the fuse. Figure 8-10 shows the oscilloscope channel connection diagram.

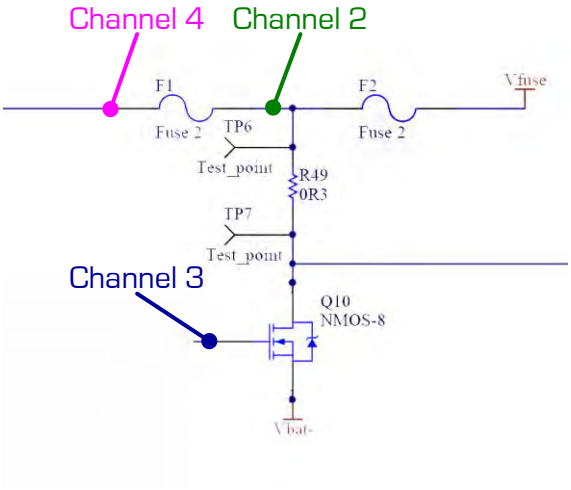

Figure 8-10: Scope probe connection diagram

8.2.4.2: Results

The test revealed that the MOSFET (Q10) used to close the high current path failed. The path was closed and current began to flow for a period of 2.5 ms before the MOSFET failed in an open state. This can be seen in Figure 8-11. The fuse did not blow as the failed MOSFET first. The test was repeated three times.

Voltage drop as a result of the current flow through the limiting resistor

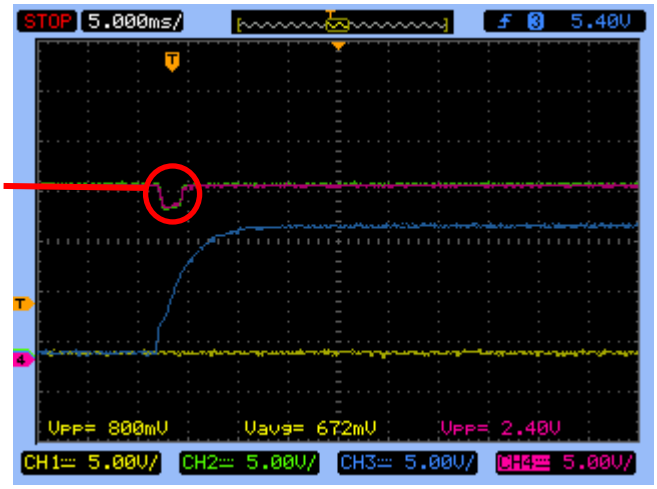

Figure 8-11: Oscilloscope trace from the fuse test

8.2.5:

Inrush current limiter testing

To protect the system during charging of capacitive loads, an inrush current limiting circuit was implemented. The purpose of the test was to illustrate the operation of the circuit and to ensure the maximum inrush current has been limited to below the 10 A rating of the fuse.

8.2.5.1: Procedure

A oscilloscope was used to measure the voltage levels at the three points of interest shown in Figure 8-12. These points are the input to the system, the output and the MOSFET gate control signal. Additional probes were also connected across the sense resistor and the difference used to calculate the current, once the path through the MOSFET was closed.

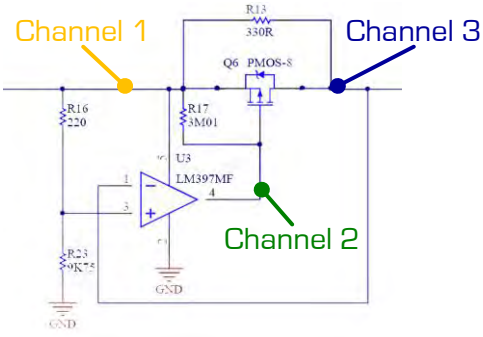

Figure 8-12: Diagram showing the oscilloscope probe connections during the test

8.2.5.2: Results

It can be seen from Figure 8-13 that the oscilloscope trace captured once the battery power is enabled, limits the current flow to the output. This can be noted from the controlled capacitive charging on the output (channel 3). Once the output reaches 97 % of the input voltage the gate of the P channel MOSFET is pulled low (channel 2) closing a low impedance path. While there is still an inrush current, it is for a reduced period of time and over 3 % of the potential difference. The induced inrush current is, therefore, limited to a maximum of 2.5 A which can be seen in Figure 8-14.

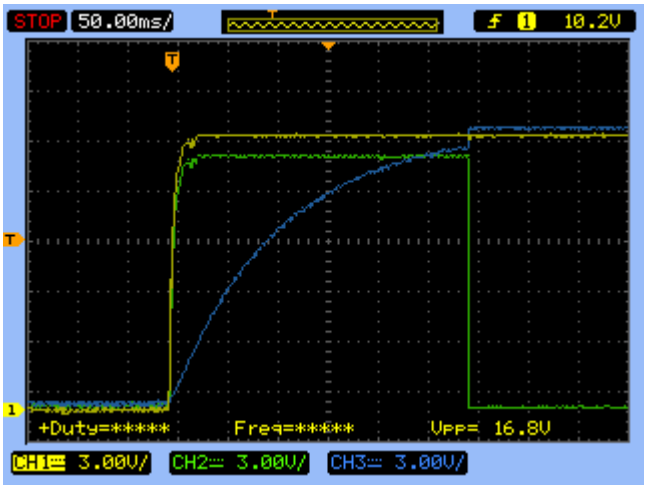

Figure 8-13: Oscilloscope trace captured during the inrush current limiter testing. Channel 1 is attached to the supply line, Channel 2 to the gate of the MOSFET and Channel 3 is attached to the output.

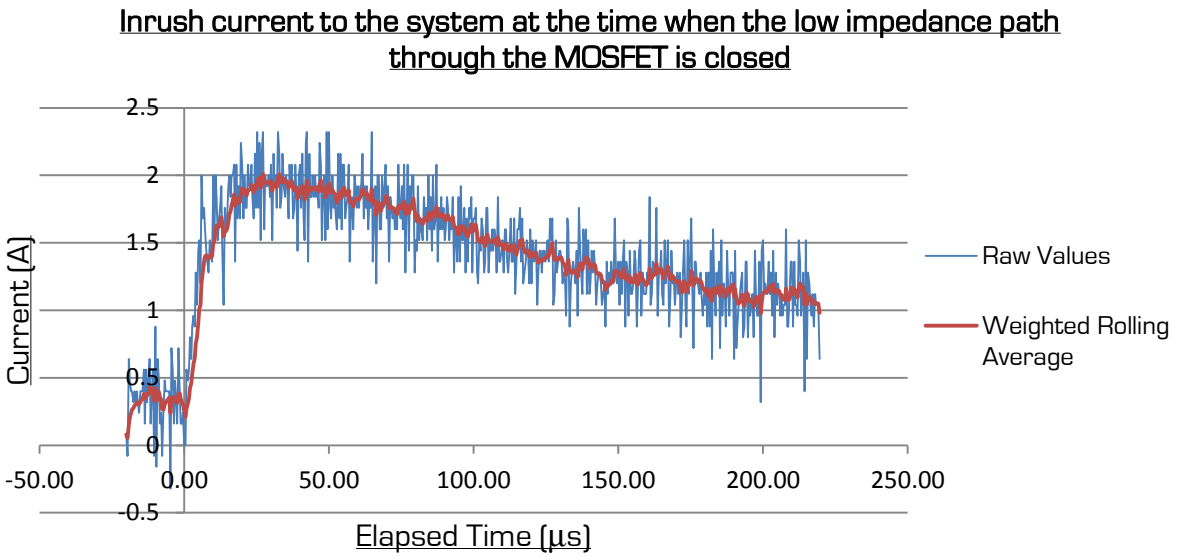

Figure 8-14: Inrush current experienced once the low impedance path through the MOSFET is closed

8.3: Communication testing

The communications of a tele-operated system have a significant effect on the performance of the system. The following tests will quantify the performance of the communications system, demonstrating the ability to meet the required specifications.

8.3.1: Communication range and latency test

The communication range affects the operational range of the platform; the latency affects the performance of the system, as it determines the time between the generation and execution of a command. Therefore, the test was designed to quantify the maximum range and latency of communications over the range. Additionally, the test was designed gather the data on the characteristics (listed and defined in Table 8-6) which are used to illustrate the operation of the communication software.

Table 8-6: Communication characteristics

Characteristics	Definition
Percentage Packet Loss	A packet is deemed to be lost if the transmitter does not receive a packet confirmation within 30 ms of transmission
Percentage of Corrupted Packets	The percentage of packets that fail a CRC checksum
Percentage of Complete failures	The percentage of packets that failed to be communicated after 10 attempts

8.3.1.1: Procedure

A Serial to RF1101SE adapter (described in Appendix B.1) was developed for use during both testing of the communication system and to create an interface, so that payload data could be logged using a LabVIEW GUI. The GUI generates a random payload packet of known length, varied between 2 and 10 bytes, to be sent via a Serial VCP to the RF1101SE adapter. A second adapter was configured to receive the data, add the data relevant to the test and then to resend the data back to the transmitter. The packet loss and corruption counts from the transmitter are added to the packet and sent back to the GUI, where the additional data was logged and the payload is

compared with the original to check for data corruption that the CRC check failed to detect. The flowchart of the LabVIEW GUI implementation can be seen in Figure 8-16. In order to negate the effect of the Serial VCP communication time which would not be present in the system, prior to the testing, a loop back was implemented to determine the average time of communication between the LabVIEW GUI and the adapter. This time was determined to be, on average, 9 ms and this was removed from the communication time.

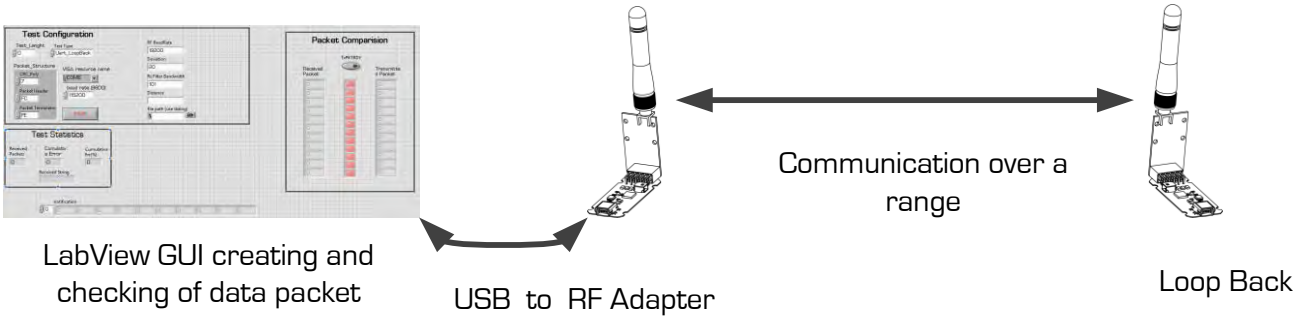

Figure 8-15: Pictorial diagram of the communication test

During the test, 2000 randomly generated packets were transmitted at 3 m intervals ranging over a distance ranging between 3 m and 54 m inside the Duncan McMillan building in UCT's Department of Mechanical Engineering. As soon as the GUI received a packet, a new packet was transmitted to determine the maximum communication frequency.

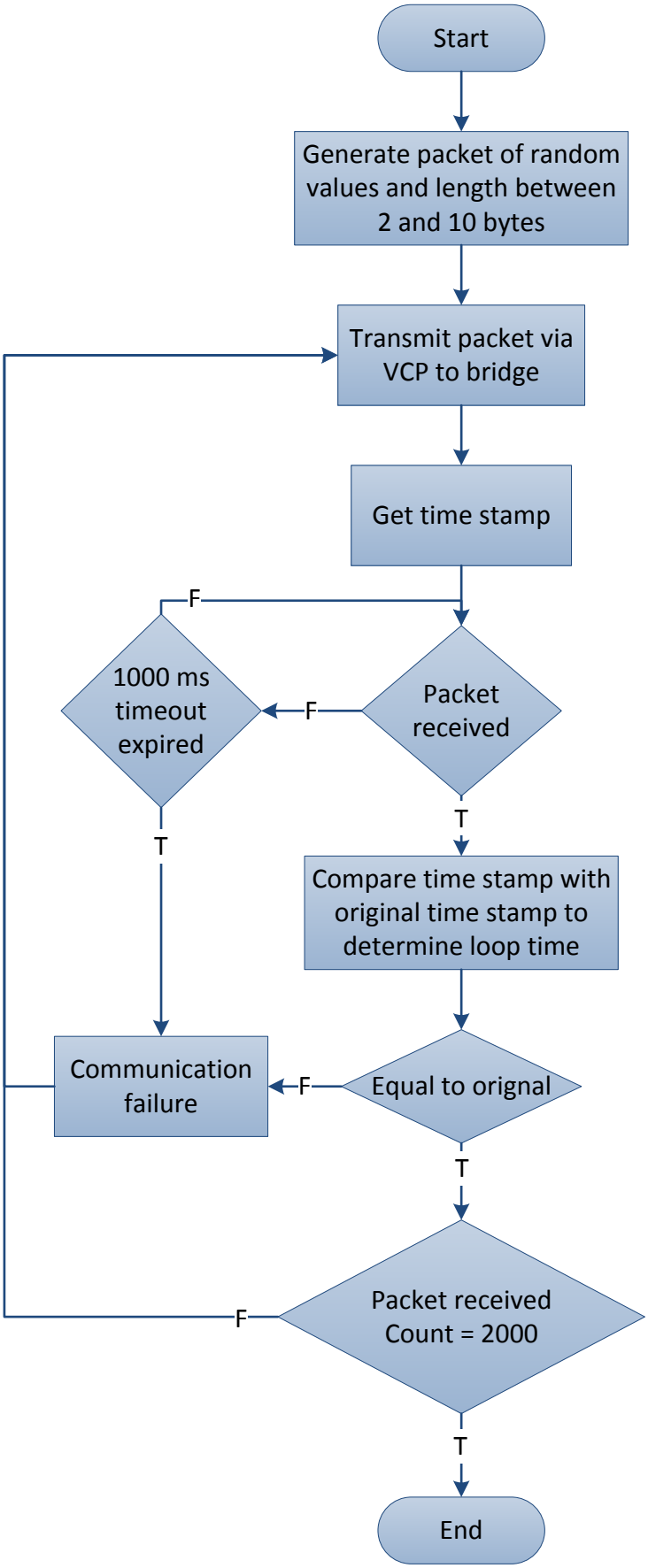

Figure 8-16: Flowchart of the implementation of the wireless data communication tests implemented in LabVIEW

8.3.1.2: Results

Over the specified range of 30 m, the communication latency remained stable, as can be seen by the consistency of the average communication time of ± 14.8 ms. As can be seen in Table 8-7, the maximum latency increased and become erratic at ranges over 30 m. However, within the specified range, the maximum latency was 218.5 ms and with a majority of the communications executed within 15 ms, an average rate of communications of 66 Hz was achieved.

Table 8-7: Communication latency over the range

Distance (m)	Max Time (ms)	Median Time (ms)	Average Time (ms)
3	32.0	15.0	14.6
6	27.0	14.5	14.6
9	34.0	14.5	14.6
12	32.0	14.5	14.7
15	29.5	14.5	14.6
18	30.0	14.5	14.6
21	31.5	15.0	14.7
24	29.5	14.5	14.6
27	30.5	14.5	14.7
30	218.5	14.5	14.8
33	29.5	14.5	14.7
36	107.0	14.5	14.8
39	61.0	14.5	14.6
42	230.5	15.0	15.0
45	37.0	14.5	14.6
48	31.0	15.0	14.7
51	106.0	14.5	14.9
54	291.5	33.5	35.7

The characteristics of the communication, as they affect the latency, follow a similar trend as shown in Figure 8-17 and Figure 8-18, with the maximum data corruption rate at 2.5 %. No packets that were returned to the GUI failed the packet comparison test.

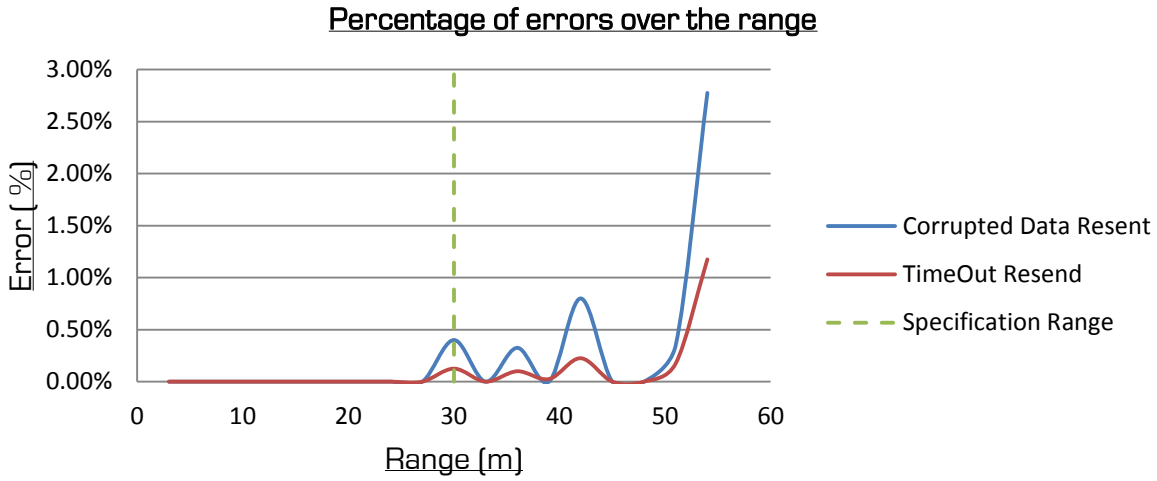

Figure 8-17: Graph showing the errors at communication ranges

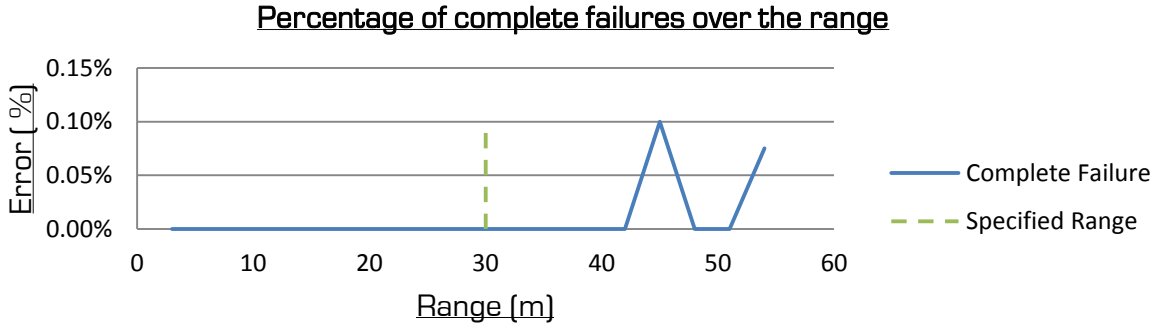

Figure 8-18: Complete communication failure

8.3.2:

Data loss

As the data and commands are transmitted when a parameter value changes and the communication software is configured to transmit the most recently prepared packet, there is a concern that data may be lost. The data loss will occur if the packet was not successfully transmitted, before the transmission interval expires and a new packet is prepared.

8.3.2.1: Procedure

The same communication equipment was used; however, the GUI was reconfigured to generate and transmit a packet at a rate of 20 Hz. The second RF1101SE adapter was reprogrammed not to loop back, instead it confirmed the data as per normal. The number of packet confirmations which the transmitting RF1101SE received were logged. The number of packets that failed to communicate within the 50 ms interval were calculated by comparing the number of packets received to the number of packet confirmations received. The test was repeated at 3 m increments, over a range from 3 m to 48 m.

8.3.2.2: Results

A summary of the test results can be seen in Table 8-8. On average, only 0.114 % of the packets failed to transmit within 50 ms. Therefore, data loss as a result of data being " overwritten" is only a concern for data or commands with infrequent value changes. These would be temperature measurements and on / off commands.

Table 8-8: Packet losses, over the test range, when communicating at a rate of 20 Hz

	Packet Losses
average	0.114 %
max	0.375 %
min	0.000 %

8.4: Sensor payload subsystem test

To display and log the data from the sensor payload subsystem testing, a LabVIEW GUI was developed (Figure 8-19). The controls can be manipulated using either a mouse or an Xbox controller. The Serial to RF1101SE adapter used during the communication testing was used to receive the data from the payload, which was displayed using the GUI. A Video2Go PAL to USB converter was used to import the image signal from the Range Video FPV receiver.

8.4.1:

Figure 8-19: Testing GUI

Current requirements of the system

A battery supplies the power to the system, therefore an understanding of the exact power requirements of the system is required for improvements in future designs and battery capacity selections.

8.4.1.1: Procedure

As explained during the design description, system diagnostics (which include voltage and current monitoring) were incorporated into the design. The calibrated data from these sensors was communicated using the wireless communication system to a LabVIEW GUI, where the data was logged. The system was connected to a 14.8 V power supply and the system consumption was taken as the current input to the Hub PCB. The current consumption of the LEDs was taken at three power levels, 10 %, 50 % and 90 %. The efficiency of the voltage regulators can be calculated

using equation 8-1 and the information gained from the current drawn on the voltage supply lines. This is important to quantify as the power lost during regulation is lost as heat energy.

$$\eta_{th} = \frac{Output\ Power}{Input\ Power} = \frac{V_{out} \times I_{out}}{V_{in} \times I_{in}} \quad (8\text{-}1)$$

8.4.1.2: Results

The current consumptions of the two systems can be seen in Table 8-9; the calculated efficiencies of the voltage regulation system can be seen in Table 8-10. The significant increase in the power requirement of the extended payload is due to the requirements of the thermal camera and microcontroller. Both devices require 3.3 V which is drawn from the 3.8 V line (the thermal camera adapter supplies the conversion from the 3.8 V down to 3.3 V for the thermal camera).

Table 8-9: Sensor payload current consumptions

Component	Current from the Battery (mA)			
	3.3 V	3.8 V	14.8 V	
Low-cost Payload	196	239	93	
Extended Payload	240	663	178	
	10 V	14.8 V		
Range Video FPV Transmitter	266	202		
LEDs	10 %	50 %	80 %	90 %
	50	244	372	419

Table 8-10: Voltage regulation efficiencies

Regulation	Low-cost payload efficiency (%)	Extended payload efficiency (%)
3.8 V SMPS	79.7	94.7
3.3 V LDO	61.1	61.1
10 V SMPS	92.8	92.8

8.4.2:

LED power

The LEDs provide ability to operate in low illumination conditions. The outputs of the LEDs in relation to the power requirements should be established.

8.4.2.1: Procedure

The LEDs were set to 80 % of the maximum power, an LM-8000 Lux metre was then used to measure the luminance at a range of distances from 1 m to 5 m. Additionally, measurements were taken at varied angular offsets from the centre of the face of the front panel. A second test was conducted to identify the relationship between the percentage brightness, current draw and distance from the LEDs. For this test the LM-8000 lux metre was used to measure the brightness of the LEDs, along a line perpendicular to the centre of the front panel.

8.4.2.2: Results

The distribution of the light intensity over the area can be seen in Figure 8-20. As the LEDs are not centred in the face of the front panel, it can be seen that the drop off in the luminance readings is far greater for the range of positive angles.

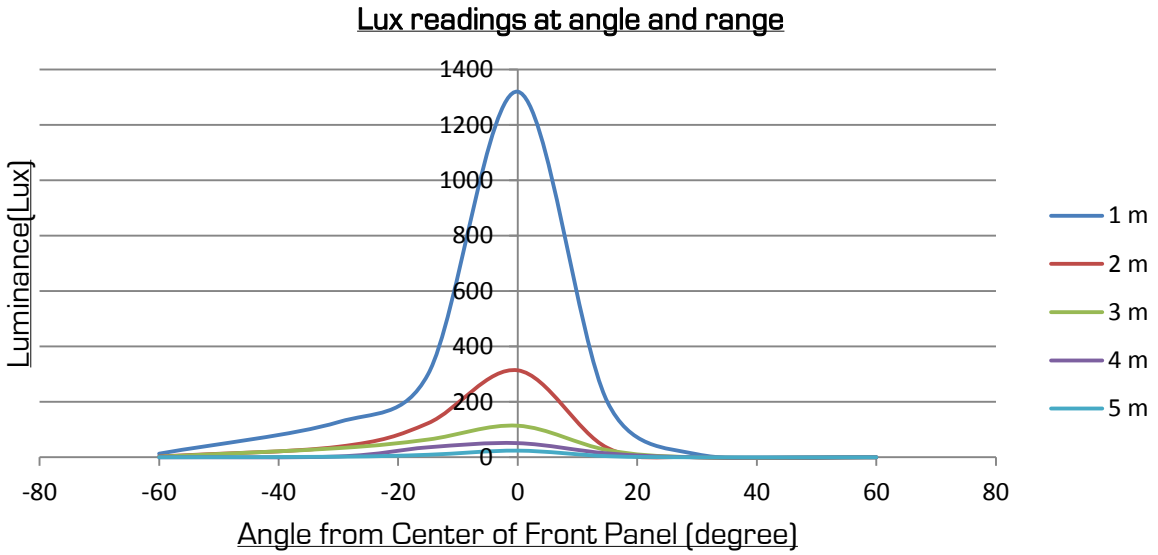

Figure 8-20: LED Lux measurements

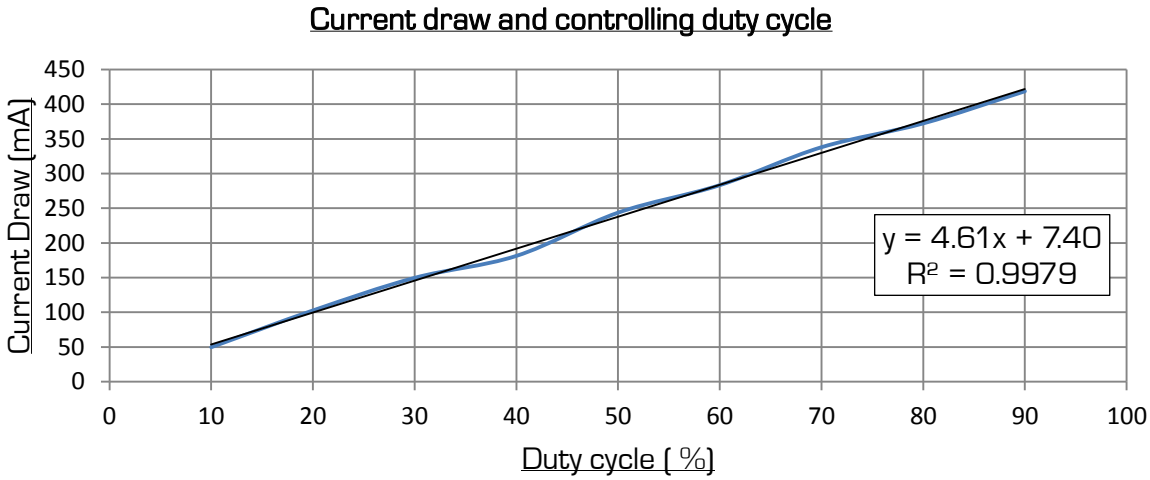

Figure 8-21: Graph representing the current draw against the duty cycle controlling the brightness of the LEDs

From Figure 8-21, it can be seen that the relationship can be represented by the equations y=4.61x+7.40, where x represents the duty cycle of the controlling PWM wave and y represents the current in milliamps. The offset of 7.40 mA, represents the current required by the LED driver.

In both Figure 8-22 and Figure 8-23, the 75 % reduction in the luminance reading between the range of 1 m and 2 m, is most likely due to the reduced luminance supplied by the wide beam LED lens. The luminance at a range of 3 m to 5 m will be entirely due to the effects of the spot lens.

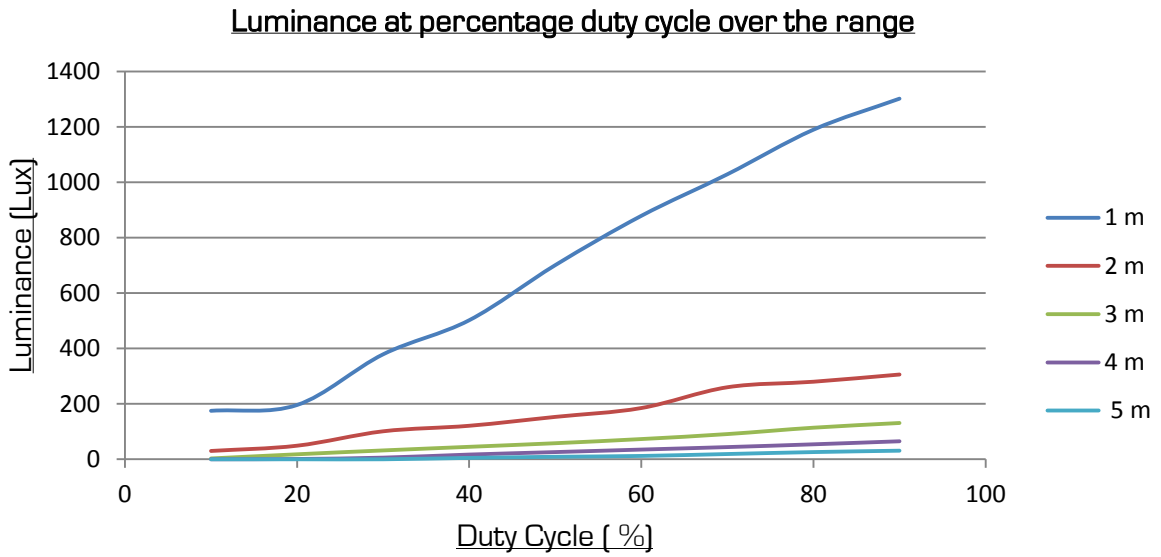

Figure 8-22: Luminance at percentage duty cycle over the range

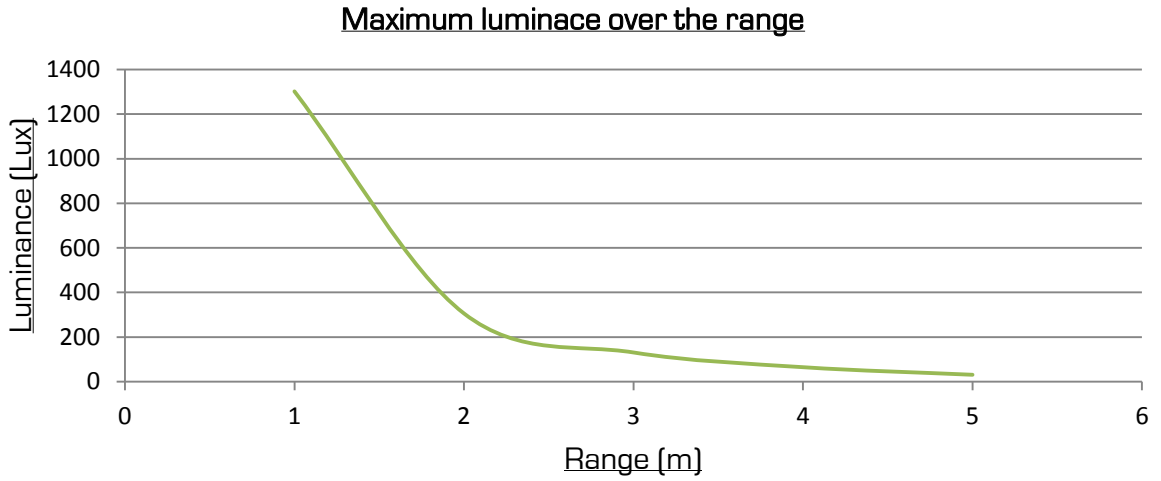

Figure 8-23: Maximum Luminance over the range

8.4.3:

Camera image quality

The camera is the primary sensor for victim identification and control. The camera sensor, the digital to analog converter and, finally, the communication platform used to transmit the signal, affect the quality of the image produced. The methods used to quantify the quality of the image were the Snellen chart and the EIA resolution chart as suggested by J Evans [39], in the *Standards for Visual Acuity*. Additionally, an image distortion test was performed. Finally, the image produced by the camera was used to identify HAZMAT warnings and hence the distance at which HAZMAT signs can be identified was tested.

8.4.3.1: Procedure

During all the test procedures, the LabVIEW test GUI developed for the testing of the sensor payload was used to capture the images produced.

Snellen chart

The Snellen chart shown in Figure 8-24 was scaled onto an A4 sheet. Because of this, the distance that chart was placed at was reduced from 6 m to 2.8 m. This was to maintain the relationship between the dimensions of the letters and the viewing distance [40].

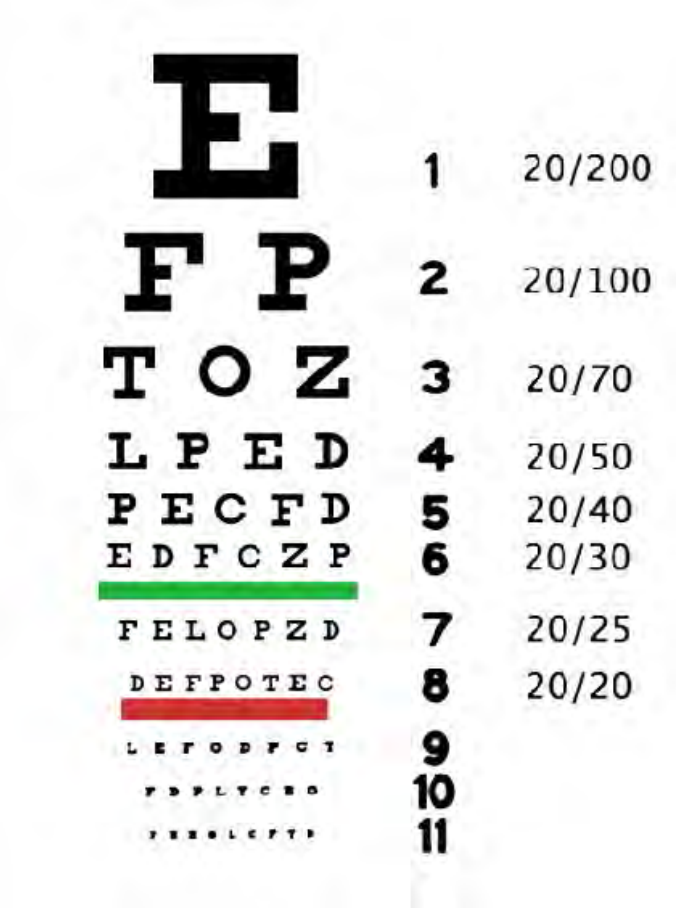

Figure 8-24: Snellen chart [39]

EIA resolution chart

The EIA resolution chart seen in Figure 8-25 was used to determine the limiting resolution of the camera image received. The chart was placed as to fill the image area and the limiting resolution can be read from the point where the wedges surrounding the central striped section begin to blur.

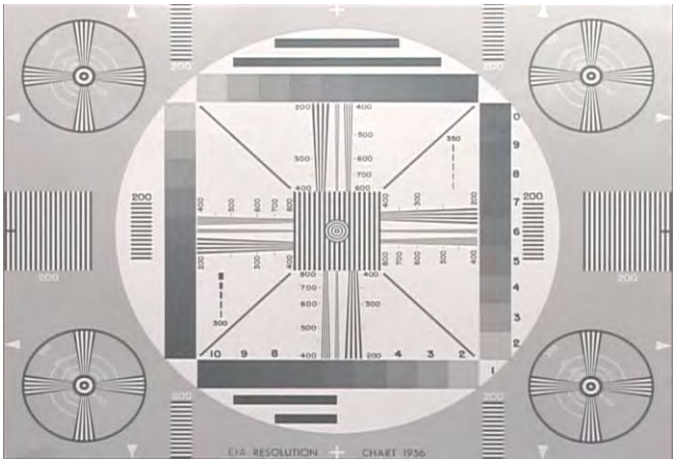

Figure 8-25: EIA resolution chart [39]

Image distortion

The distortion test was implemented to determine whether the image generated had been distorted. Image distortion can occur because of manufacturing defects in the lens or the image processor. A 20 x 20 mm grid was placed to fill the image.

HAZMAT warning identification

The camera will be used to identify HAZMAT warning signs. This will allow the operator to assess the HAZMAT safety requirements. To test the range at which HAZMAT warning signs can be identified, a number of HAZMAT signs with dimensions seen in Figure 8-26 were used. The distance between the camera and sign was increased at 1 m increments until the warning was no longer identifiable.

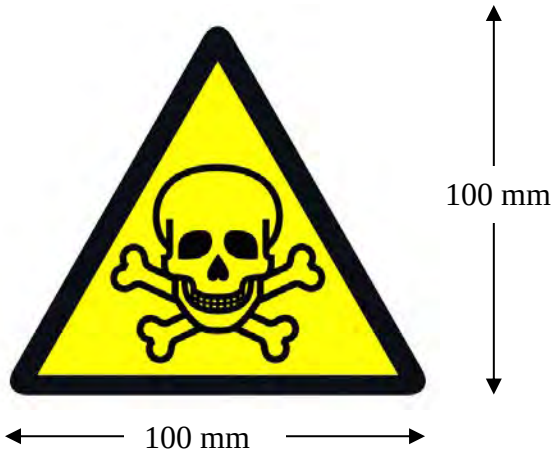

Figure 8-26: Dimensions of the HAZMAT signs used during testing [41]

8.4.3.2: Results

The images captured during the tests can be seen on the following pages. Figure 8-27 shows the Snellen chart in which the first row (the letter **E**) can be seen. However, the second row, [**F P**], can be distinguished but not clearly seen. This would suggest that the visual acuity of the produced image is 20/100. The point on the EIA resolution chart at which the lines of the wedge begin to blend, equates to a resolution of 240 lines, denoted by the red line seen in Figure 8-28. The aspect ratio of the image is distorted, as shown by the red rectangle in Figure 8-29 which should, in fact, be a square if there was no distortion of the image. The image, however, has no fish bowl effect as the proportions of the rectangles are maintained throughout the grid.

Figure 8-27: Snellen chart captured at 2.8 m

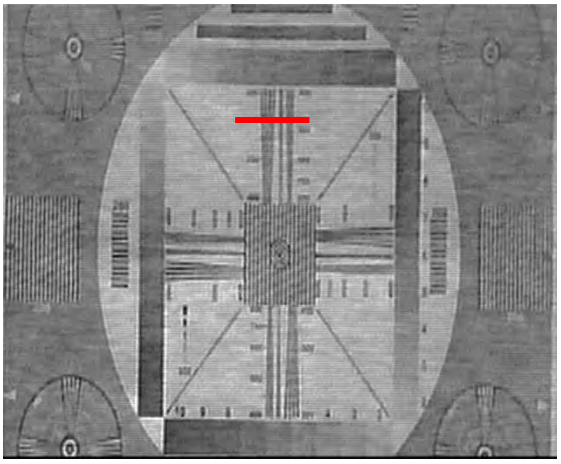

Figure 8-28: Frame captured during the EIA resolution test

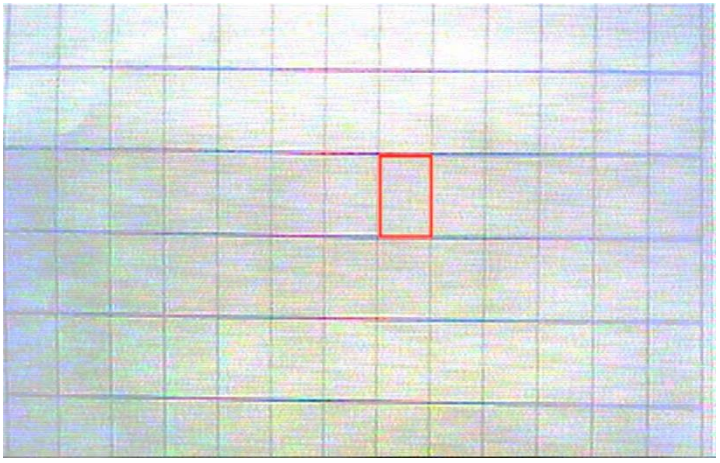

Figure 8-29: Image distortion test

The three HAZMAT warnings that were selected were poison, radiation and biohazard, going clockwise from the top left hand corner as seen in Figure 8-30. These were identifiable at 2 m. By the 3 m mark, the signs were identifiable as HAZMAT warnings, however the percise warnings were no longer identifieable – as seen in Figure 8-31.

Figure 8-30: HAZMAT charts at 2 m

Figure 8-31: HAZMAT charts at 3 m

8.4.4:

LED and camera

In the majority of cases where a USAR platform is performing a void inspection, the operation will be conducted under low or zero light conditions. LEDs were added to the system to provide an illumination source to enable operations in such conditions. The purpose of this test is, therefore, to show that the LEDs provide adequate illumination for inspection.

8.4.4.1: Procedure

The Snellen chart test was used to show that the quality of the image from the camera does not deteriorate. A LM-8000 lux metre was used to verify the lack of additional illuminations sources. The images were captured using the LabVIEW GUI.

8.4.4.2: Results

For this test the LED brightness was set to 40 %. In Figure 8-32, the **E** row can be seen, the [**F P**] in the second row can be distinguished but are not clearly identifiable. The brightness of the LEDs

was then increased (to 80 %) to identify items in the distance. This ability can be seen by the fact that a fire extinguisher sign can be seen clearly at 6 m in Figure 8-33.

Figure 8-32: Snellen chart at 2.8 m

Figure 8-33: Fire extinguisher at 6 m

8.4.5:

Orientation detection

The system has a symmetrical design and thus incorporates an orientation detection system. This enables the camera image and motor commands to be manipulated so as not to disorientate the operator. As the motors are not functional, the manipulation of the motor commands was not tested. The flipping and mirroring of the camera image was, however, verified.

8.4.5.1: Procedure

The test procedure was as follows: firstly the Scarab was rotated (by 180˚) about the X-axis (seen in Figure 8-34), this was to test the image flipping. Secondly, the Scarab was rotated about the combination of rotations seen in Table 8-11. Each combination was repeated ten times. Finally, as an accelerometer is used, the Scarab was dropped without wheels to generate a high acceleration event.

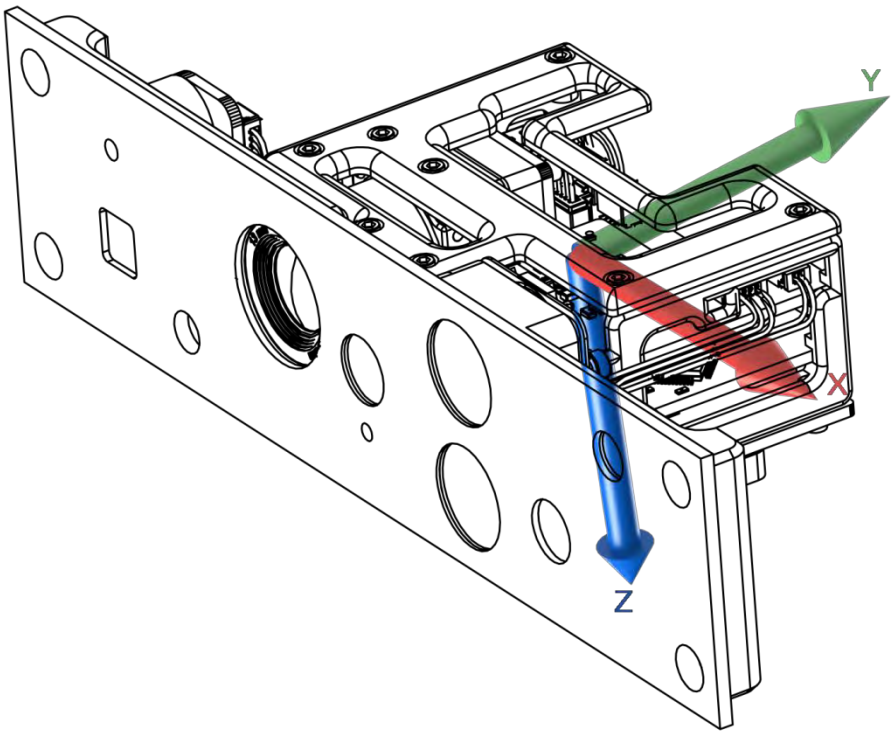

Figure 8-34: Figure showing the reference orientation of the Scarab used during testing

8.4.5.2: Results

The results from the orientation detection testing can be seen in Table 8-11. It can be noted that the rotations about the X-axis are more successful than those about the Y-axis. The extended sensor payload was far more successful in detecting the rotations about the Y-axis.

Table 8-11: Results of the orientation detection testing

Combination of Rotations about the axes	Desired Image Manipulation	Low Cost Payload Detection Rate	Extend Payload Detection Rate
180° X	Flip	100 %	100 %
180° y	Mirror Flip	80 %	100 %
90° X, 180° Y, -90° X	Mirror Flip	80 %	100 %
90° X, 360° Y -90° X	No manipulation	100 %	100 %
90° Y, 180° X, -90° Y	No manipulation	100 %	100 %
Drop	No manipulation	90 %	100 %

8.4.6. Interchangeability

While mechanically the sensor payloads are interchangeable, the time required to change the sensor payload will determine whether it is practically viable.

8.4.6.1: Procedure

As only a single payload front panel was built, it is not possible to time the changing of the payloads. In order to represent the time it would take to change the payload, a calculation was made by timing the following actions: remove the four mounting screws; remove the sensor payload; place it on a table; replace the payload and the screws.

8.4.6.2: Results

The results below (Table 8-12) show that it takes an average of 49 seconds to replace the payload using a single 3 mm Allen Key.

Table 8-12: Time taken to change the payload

Attempt	Time (hours: min: sec)
1	00:00:51
2	00:00:47
3	00:00:50

Variable packet structure

The reasoning for including a variable packet structure was explained during the design section. The test was needed to prove that the reasoning was in fact valid and the variable packet structure was not adding an unnecessary layer of complexity that should be removed in future designs.

8.4.7:

8.4.7.1: Procedure

During the testing, the number of data payload bytes received by the test GUI (Figure 8-19), was logged.

8.4.7.2: Results

The maximum possible number of bytes in a single packet is 44, which was received in the first packet. After the first packet, the majority (85 %) of the packets received were in the range of 20 to 29 bytes long, as can be seen in Figure 8-35, with a standard deviation of 4 bytes (Table 8-13).

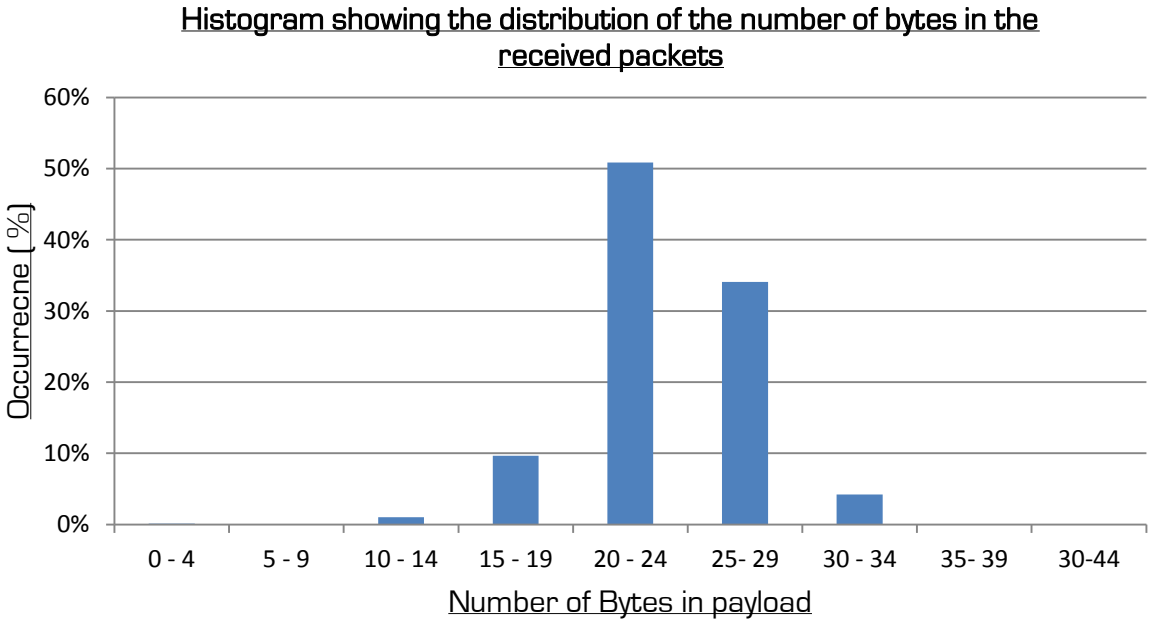

Figure 8-35: Histogram showing the distribution of the number of bytes in the received payload

Table 8-13: Summary of the number of bytes in the data payload

	Number of Bytes
minimum	4
median	24
average	23
maximum	44
standard deviation	4

Conclusions

In this chapter, conclusions based on the results of the testing and observations made during implementation and assembly of the system will be drawn. Recommendations for future work based on these conclusions will be discussed in the next chapter.

9.1: Mechanical design of the system

Chapter 9 :

System mass

Figure 9-1shows a breakdown of the subsystem masses. While the design failed to meet the required system mass specification — by 21 grams in the case of the low-cost sensor payload and 47 grams for the extended payload — the system only contributes to 26 % of the total mass of the robotic platform. There is potential for mass saving through further removal of unnecessary material on the front panel and heat sink; however, this would increase the machining costs. The implementation of mass saving techniques should be applied to the shell and motors or wheels and tail first, as there is a greater potential for reduction in those areas.

9.1.1:

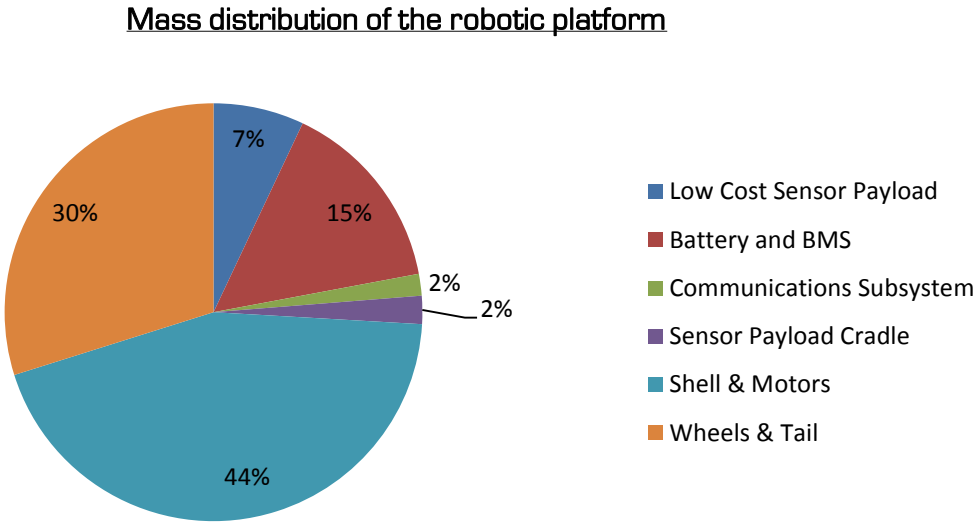

9.1.2:

Figure 9-1: Pie chart showing the mass breakdown of the robotic platform

Sensor payload and cradle design

The sensor payload was interchangeable in a short period of time. This was demonstrated by an experienced operator who was able to repeatedly change the payload within one minute using a single tool — 3 mm Allen Key. There was, however, some noticeable clearance between the cradle and the frame of the payload which at times caused a misalignment of the board edge connector. As a board edge connector was selected, the misalignment would not damage the connector. The clearance, however, reduces the support from the cradle on the payload, which could potentially lead to failure on more extreme impacts. Additionally, the dimensions of the area specified for the payload restricts the sensor selection.

9.2: Sensor payload design

The design of the payload met the specification in terms of functionality; however, the cost and mass of the system exceeded the specification, by 21 g and US$ 13.29 respectively.

Current requirements and voltage regulation system

As the composition of both sensor payloads is similar, so are the power requirements. The major difference in the current requirement is on the 3.8 V line where an additional watt is required by the FLIR quark thermal camera.

9.2.1: Testing showed the designed voltage regulation system was able to provide the required power, without overheating. The results did, however, show that there was a dramatic increase (79.7 % to 94.7 %) in the efficiency of the 3.8 V regulator between the low-cost and extended payload. This is a result of the increased current drawn by the system. This suggests that the regulator is overrated for the requirements of the low-cost sensor payload and that the theory of designing a single regulation system for all payloads, to reduce manufacturing cost, should be revised.

Camera image and LED illumination

9.2.2: The camera image produced is acceptable for inspection. Testing showed that the visual acuity is equivalent to 20/100, which can be used for inspection as demonstrated by the fact that a HAZMAT warning sign of 100 x 100 mm could be identified at 2 m. The fact that at 3 m the HAZMAT signs were identifiable, but the warning could not be identified, suggests that a zoom functionality may be required. The fact that the visual acuity remained at 20/100 during low light operations proves that the combination of a wide lens and a spot lens on the LEDs provided adequate illumination, at both short and long range with objects being identified at 6 m. The resolution was shown to be the equivalent of 240 lines which equal to that of the LCD screen on the operator controller used by the operator to control the platform.

As the motors failed during the testing of the mechanical platform, the effects of the camera's narrow FOV on the usability of the platform could not be tested.

9.2.3: Orientation detection

From the test results it can be seen that the rotations about the X-axis were more successfully detected than those about the Y-axis. The rotation about the X-axis leads to a changing of the direction of gravity relative to the Z-axis. This provides an absolute reference point and is, therefore, detected on every rotation. The rotation that requires a mirror and a flip (about the Y-axis) rely on the system's ability to detect a rotation about an axis and is, therefore, always relative to the starting orientation. Once a rotation was not detected, the error went uncorrected until a second rotation was missed or the system was reset. The increase in success in the extended payload is due to the inclusion of a gyroscope.

9.2.4:

Variable packet structure

Recording the number of bytes in the packet received by the testing LabVIEW GUI showed that, on average, the packet included 23 bytes. This is equivalent to just over half the potential number of bytes which proves the requirement for the packet structure. Data communication from the platform will, on average, occur in half the time, when compared to a communication system which uses a fixed packet length of all the data. This also reduces the potential for data corruption.

9.3: Communications design

Data communications

The communication system exceeds the required specifications. An indoor range of 45 m was reached before a complete packet loss was experienced. During the range test a worst case latency of 218.5 ms was experienced within the specified range, however, on average, the communications were executed within 15 ms. This was well within the required 50 ms required for a communication rate of 20 Hz. Potential for data loss is a concern, as the variable packet structure used by the sensor payload meant that data not communicated within the 50 ms period would be lost. However, over the communication range, an average of only 0.114 % of the communications failed to execute within 50 ms and, therefore, would only be a problem for data with infrequent data changes.

9.3.1:

Video communication

The transmitter and receiver pair was preselected for the system. The transmitter was successfully integrated into the system, however the operational temperature of the transmitter contributed significantly to a rise in the operational temperature of the system. The received image was adequate for inspection; however, significant noise was experienced in the image when the system was not at rest. A method of post processing the image should be investigated.

9.3.2:

9.4: Battery and BMS design

Battery protection

9.4.1: The primary battery protection successfully protected the battery as shown by the manner in which the MOSFETs open the circuit between the battery and the system, when a harmful state is entered. While the point at which the secondary battery protection triggers is correct, the system designed to create a permanent open circuit between the system and the battery failed. This was due to the MOSFET failing in an open state. Reconsideration is required on the selection of this MOSFET that, when closed, creates a high current path between the battery terminals, which triggers a fuse. The fuse blowing test should be repeated.

9.4.2:

Gas gauging

Gas gauging was successfully achieved through the use of a dedicated IC that implements TI's **ImpedanceTrack™** algorithm. There is an error in the estimation, however. The error was an underestimation of the time remaining, which decreased throughout the discharge of the battery. As the estimated operational time remaining would expire before the capacity of the battery is spent, the operator should be able to retrieve the system.

9.4.3:

Battery charging

9.4.4: The battery charging was implemented with a BQ24753A IC from TI. Charging is achieved safely at selectable rates of up to 6 A. An 8 A charge rate was attempted, but would require active cooling which is not practical in this system. Therefore, a charge time of 51 minutes is achievable, equal to ± 25 % of the standby operational time requirement of the system.

Battery capacity selection

The motors were damaged during the testing of the platform and therefore testing of the system with the motors was unachievable. However, from the collected data pertaining to the power

requirements of the sensor payload and communication system, the standby operational time of 5 hours was achieved, but confirmation through further testing is required.

9.5: System cost

The cost of the entire system was US$ 162.42, which is US$ 12.42 greater than the desired value specified. The battery and video transmitter account for US$ 77.63 of the total cost. This could be reduced if the standby requirements of the system are revised enabling a lower capacity and cheaper battery to be selected. This and other revisions will be discussed in the recommendations.

Recommendations based on the conclusions drawn in the previous chapter and observations made during the implementation of the design and assembly of the system will now be made. As this system formed part of the first functional prototype, there are recommendations which extend beyond the scope of this system to the electronic subsystem breakdown of the platform.

Chapter 10 :

10.1. Sensor payload

Camera

10.1.1:

The currently implemented camera has two main areas of concern: the FOV and the resolution. The resolution may be improved through the modification of the clock source and method of digitally communicating the image between the camera and the PAL encoder. Dummy pixels and rows were introduced into the image to correct a synchronization error. A RGB565 digital signal should be clocked from a 24 MHz source rather than from a 27 MHz clock source which was currently used. Alternatively, a camera with a higher resolution could replace the current camera, although this would inevitably increase the cost of an already over-budget payload.

The FOV may be corrected with stereoscopic vision, although this solution would lead to an increased cost and therefore could only be considered for the extended sensor payload. The dimensional constraints may still prove to be a limiting factor.

Orientation detection

10.1.2:

The orientation detection functioned as expected; however, it did, on occasion, not detect a rotation about the Y-axis and therefore the image was not mirrored. Alternatively, a command could be generated by the operator to mirror the image, as the motor commands would be reversed, indicating that the image was mirrored.

The cost of the sensors could be reduced, as the exact orientation is not required. A single axis gyroscope could be used to detect the rotation about Y-axis (as seen in Figure 5-20) and a mercury switch used to detect rotation about the X-axis.

10.1.3:

Data packets

Currently sensor data is communicated when the data is updated with a new value. There is a 0.114 % possibility that the data fails to communicate with the 50 ms period before another packet is prepared. A possible solution is to configure data to be transmitted, if it was not transmitted within a set period. Alternatively, rather that transmitting all the data from the payload, the operator could select the data, which is then transmitted at 20 Hz.

10.1.4:

Data communications

DMA

Both the STM32F0xx and STM32F4xx microcontrollers contain a DMA module. This DMA module can be configured to load the data from the memory to the communication peripheral. Implementing the SPI and I^2C packet communications through the DMA would improve the efficiency of the system and hence improve the processing capabilities.

Internal pull-up resistors

The system was designed with the intention of being able to power the communication and the microcontroller from the 3.3 V regulated source from the BMS when complete system functionality was not required — for example during charging. However, the SPI SCLK, MISO and MOSI communication lines for communication with the RF1101SE are shared with the motor driver on the low-cost sensor payload. These lines are internally connected through a resistor to V_{cc} in the on-board microcontroller. These hold the communications line low when the voltage regulation system is not in operation. Therefore, the microcontroller should be placed on a separate SPI channel or, alternatively, there could be a reconfiguration of the microcontrollers, as will be suggested later.

Mechanical configuration

As discussed, the dimensional constraints are a limiting factor for future sensor selection. The effect of the dimensions could be limited by removing the voltage regulation from the payload and reducing the standoff height between the PCBs in the PCB stack. The current standoff height is 8 mm. With the current components this could be reduced to 5 mm without affecting the design.

10.1.5:

The voltage regulation PCB is currently located in the PCB stack. However, it should be moved if a decision was made in favour of a single voltage regulation system. The PCB could be moved into the free space around the payload as demarcated in Figure 10-1. The lower zone is occupied by the data communication, but the upper zone is currently unused. This move would require an additional heat sink to be placed in the shell.

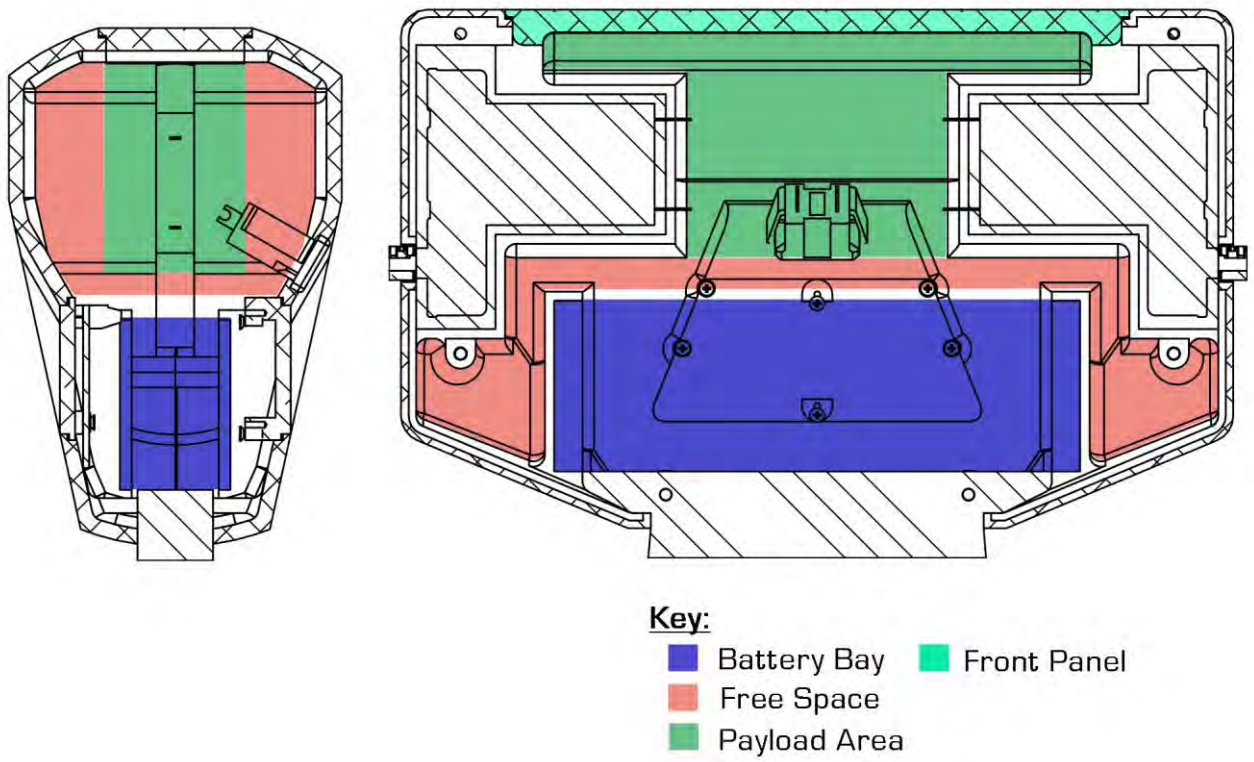

Figure 10-1: Diagram showing the areas, inside the shell, allocated to the system

10.2: Communications

The data communication system was successfully implemented; however, the communications are currently limited to a single preselected channel and power. A channel selection command could be generated, in which case EEPROM should be added to the system to store the selected channel in the event of a brownout or watchdog time-out. Both of these events would return the communication back to the original preselected channels and the communications would fail. The EEPROM could also be used to store the remaining setup values, reducing the flash overhead on the microcontroller.

The future development of the communication would require the CC110L IC to be moved off the breakout board and onto one of system PCBs. At this point it is suggested that a method of measuring the received signal strength be included. Currently, the power output is fixed, however, when the devices are in close proximity to each other the receiver becomes "swamped", causing a communication failure. Enabling the power to be measured will allow the output power to be adjusted, reducing the current draw through lowering the output power. This will prevent "swamping" and improve the efficiency of the system.

10.3: Battery management system

Battery selection and support

10.3.1: The cost of the entire system is over budget. If the specification of the standby time were to be removed, a cheaper battery with a smaller capacity could be selected. Additionally, changing the profile of the battery to four cylindrical cells, would allow volume occupied by the battery to be reduced and potentially reduce the cost of the battery.

10.3.2: ESD

During the assembly of the system, there were a number of instances where the dual N-channel MOSFET used by the charging circuit failed, potentially due to ESD. On occasion the battery charger IC failed as well. While there is ESD protection on the charge adapter port there is no ESD protection on the discharge or the signal ports. Under normal operations, the system would be assembled in a low ESD environment obviating the problem. However, removing the sensor payload exposes the board edge connector and therefore the potential for failure due to ESD should be investigated.

10.3.3:

System Present pin

The *System Present* pin is used to indicate the presence of a system. Pulling the pin low closes the circuit between the system and the battery. Currently, it also enables the power to the microcontroller and the data communications. However, there are a number of battery protection events that require the *System Present* pin to be cycled to clear the error. This disables the microcontroller. The connection should be reconsidered such that the microcontroller can be used to cycle the pin without loss of power. Therefore, the *On button* should be used to wake-up the microcontroller rather than hold the *System Present* pin low.

10.3.4:

BMS shutdown

During storage, the gas gauge should be shut down. The BQ20z45-r1 does have a shutdown command; however, it is yet to be activated. When this is done, applying power to the charge adapter port and enabling charging will wake-up the gas gauge.

10.4: Subsystem assembly

The system has been designed to be small and compact; this, however, increases the complexity and the assembly time. Currently, the subsystems are assembled and then placed into the shell and into the system. There are a number of wired connections, which, due to their location, are tedious to connect.

There are two possible recommendations. The first would be to replace the wired connections with board-to-board connectors where possible. Alternatively, a frame could be designed which supported all the internal components. The system could then be assembled outside the shell, where it could be accessed from all sides, easing the assembly and improving the ability to debug the system.

10.5: Subsystem breakdown

The subsystems were initially broken down according to projects rather than the functionality of the system. For this reason, coupled with requirement to keep costs down, the software and some of the hardware for the operation of the platform is located inside the sensor payload. The result is that the robotic platform is rendered inoperable upon removal of the sensor payload. While this is a flaw, it was done to prevent the need for a third microcontroller on board the platform, while maintaining project separation. This is because the motor drive board, which is separate to this project, required a microcontroller. A solution would be to have a single microcontroller that is responsible for the following;

- Motor control
- Data communications
- Communications with BMS
- System power management
- Platform processing

This would increase the cost of a single platform but decrease the payload cost, while increasing the volume of the payload bay, which would allow increased potential for sensor integration. It is recommended that the STM32F030 used for the low-cost sensor payload be used. This would require a complete reconfiguration of the platform.

10.6: Summary

The system design has been successfully implemented; however, there are a number of areas in which improvements can be made. The main improvement would be to reconfigure the electrical subsystems to enable platform operation without a payload. The system was over-budget, and many of the improvements suggested would further increase the cost of the system. Therefore, either the system cost should be revised, or the already limited functionality should be reduced.

.

List of References

[1] R. R. Murphy, S. Tadokoro, D. Nardi, A. Jacoff, P. Fiorini, H. Choset, and A. M. Erkmen, "Search and Rescue Robotics," in *Springer Handbook of Robotics*, vol. 15, no. 3, B. Siciliano and O. Khatib, Eds. Berlin: Springer, 2008, pp. 1151–1174.

[2] United States Fire Administration, *Technical Rescue Program Development Manual*. CreateSpace Independent Publishing Platform, 1995.

[3] S. Tadokoro, Ed., *Rescue Robotics DDT Project on Robots and Systems for Urban Search and Rescue*. London: Springer, 2009.

[4] F. Matsuno and S. Tadokoro, "Rescue Robots and Systems in Japan," *2004 IEEE Int. Conf. Robot. Biomimetics*, pp. 12–20, 2004.

[5] M. R. Blackburn, H. R. Everett, and R. T. Laird, "After action report to the joint program office: Center for the robotic assisted search and rescue (crasar) related efforts at the world trade center," *October*, no. August, 2002.

[6] M. Barnes, H. R. Everett, S. S. C, and S. L. Obispo, "ThrowBot : Design Considerations for a Man-Portable Throwable Robot."

[7] iRobot Corporation, "iRobot FirstLook Specifications," 2012.

[8] Recon Robotics, "Recon Scout XT The Throwable," 2011. [Online]. Available: http://www.reconrobotics.com/pdfs/Recon_Robotics_Throwbot_Audio_XT_10-12.pdf. [Accessed: 30-Apr-2013].

[9] D. Ciccimaro, "MPRS (URBOT) commercialization," *Proc. SPIE*, 2003.

[10] R. Murphy, J. Casper, J. Hyams, M. Micire, and B. Minten, "Mobility and sensing demands in USAR," *2000 26th Annu. Conf. IEEE Ind. Electron. Soc. IECON 2000. 2000 IEEE Int. Conf. Ind. Electron. Control Instrumentation. 21st Century Technol. Ind. Oppor. (Cat. No.00CH37141)*, vol. 1, pp. 138–142, 2000.

[11] J. Burke, "Moonlight in Miami: Field study of human-robot interaction in the context of an urban search and rescue disaster response training exercise," *... –Computer Interact.*, 2004.

[12] A. S. Sukhatme, "Distinct Human Eye." [Online]. Available: http://www.artinarch.com/vp05.html. [Accessed: 06-May-2013].

[13] "Measuring Lens Field of View (FOV) and the Entrance Pupil – PanoHelp.com." [Online]. Available: http://www.panohelp.com/lensfov.html. [Accessed: 14-May-2013].

[14] S. Burion, "Human detection for robotic urban search and rescue," *Diploma Work*, no. February, pp. 1–61, 2004.

[15] a Cavallo, a Cirillo, P. Cirillo, and G. De Maria, "Experimental Comparison of Sensor Fusion Algorithms for Attitude Estimation," *Proc. IEEE IFAC*, pp. 7585–7591, 2014.

[16] US Department of Commerce National Telecommunications and Information Administration Office of Spectrum Management, "UNITED FREQUENCY ALLOCATIONS BROADCASTING."

[17] Inscape Data, "A look into License Free Radio Spectrum World Wide," 2008.

[18] M. Bates, "Serial Communications," *Interfacing PIC Microcontrollers*, pp. 263–297, 2014.

[19] "Introduction to Serial Peripheral Interface | Embedded." [Online]. Available: http://www.embedded.com/electronics-blogs/beginner-s-corner/4023908/Introduction-to-Serial-Peripheral-Interface. [Accessed: 17-Mar-2014].

[20] "Understanding the SPI Bus with NI LabVIEW - National Instruments." [Online]. Available: http://www.ni.com/white-paper/9119/en/. [Accessed: 29-Jun-2015].

[21] "I2C - What's That? - I2C Bus." [Online]. Available: http://www.i2c-bus.org/i2c-bus/. [Accessed: 30-Jun-2015].

[22] STMicroelectronics, "STM32 Reference Manual RM0090," 2011.

[23] "Battery and Cell Chemistries. Battery primer." [Online]. Available: http://www.mpoweruk.com/chemistries.htm. [Accessed: 12-Feb-2014].

[24] "All-Battery.com: LiFePO4 Battery Category." [Online]. Available: http://www.all-battery.com/lifepo4battery.aspx. [Accessed: 30-May-2013].

[25] "Lithium Secondary - Rechargeable - Cells." [Online]. Available: http://www.mpoweruk.com/lithiumS.htm. [Accessed: 19-Feb-2014].

[26] "Battery Management and Monitoring Systems BMS." [Online]. Available: http://www.mpoweruk.com/bms.htm. [Accessed: 20-Feb-2014].

[27] K. S. Ng, C.-S. Moo, Y.-P. Chen, and Y.-C. Hsieh, "Enhanced coulomb counting method for estimating state-of-charge and state-of-health of lithium-ion batteries," *Appl. Energy*, vol. 86, no. 9, pp. 1506–1511, Sep. 2009.

[28] Y. Barsukov and J. Qian, "Battery Capacity Monitoring Accuracy and Implementation."

[29] "Types of Lithium-ion Batteries – Battery University." [Online]. Available: http://batteryuniversity.com/learn/article/types_of_lithium_ion. [Accessed: 27-May-2013].

[30] "Charging Lithium-Ion Batteries – Battery University." [Online]. Available: http://batteryuniversity.com/learn/article/charging_lithium_ion_batteries. [Accessed: 26-Jun-2015].

[31] "PCB Specs." [Online]. Available: http://www.pcb-specification.com/uk. [Accessed: 29-Jun-2015].

[32] "Kelvin Connection." [Online]. Available: http://www.electroschematics.com/6959/kelvin-connection/. [Accessed: 29-Jun-2015].

[33] "Improved Kelvin contacts boost currentsensing accuracy by an order of magnitude." [Online]. Available: http://m.eet.com/media/1130680/13254-21705di.pdf. [Accessed: 29-Jun-2015].

[34] "VGA OV7670 CMOS Camera Module 0 3 Mega Pixel Lens CMOS 640x480 Top | eBay." [Online]. Available: http://www.ebay.com/itm/VGA-OV7670-CMOS-Camera-Module-0-3-Mega-Pixel-Lens-CMOS-640X480-TOP-/281686262812?pt=LH_DefaultDomain_0&hash=item4195cf441c. [Accessed: 10-Jul-2015].

[35] Toshiba, "TCM8240MD," 2005.

[36] "ACS712ELCTR-05B-T Allegro MicroSystems, LLC | 620-1189-1-ND | DigiKey." [Online]. Available: http://www.digikey.com/product-detail/en/ACS712ELCTR-05B-T/620-1189-1-ND/1284606. [Accessed: 28-May-2013].

[37] P. Data, C. Terminals, P. Printers, M. D. Equipment, B. B. Chargers, B. B. Systems, M. Effective, D. Cycle, H. Voltage, C. Regulation, S. Two, M. Outputs, V. Threshold, B. Learn, C. Control, C. Enable, and O. B. D. Current, "Host-Controlled Li-Ion and Li-Polymer Battery Charger with Low I q and System Power Selector," *Current*, no. July, 2009.

[38] K. Keller, S. Wen, and P. M. P. Portable, "Quick-Start Guide for bq20zxx Family Gas Gauges," no. May, pp. 1–29, 2007.

[39] J. M. Evans, "Standards for Visual Acuity," *Nist.Gov*, pp. 1–18, 2006.

[40] C. G. Keith, Z. Diamond, and a Stansfield, "Visual acuity testing in young children.," *Br. J. Ophthalmol.*, vol. 56, no. 11, pp. 827–832, 1972.

[41] "Toxic Symbol Clipart - Free Clipart." [Online]. Available: http://www.cliparthut.com/toxic-symbol-clipart-mfwMWn.html. [Accessed: 31-Jul-2015].

[42] R. Products, T. Equipment, N. Computers, P. Management, B. Chargers, P. Supplies, and T. Equipment, *High or Low Side , Bi-Directional CURRENT / POWER MONITOR with Two-Wire Interface INA220*, no. June 2009. 2010.

Temperature Sensor Calibration

In order to achieve acceptably accurate temperature readings, both the ADC and the temperature sensor should be calibrated against known readings. This appendix describes the process that was used to calibrate and verify the temperature readings.

The process involved heating the entire sensor payload, in an oven, to a known temperature, and then logging the temperature as it decreased towards room temperature. In order to execute the test without the heatsinks which are integral to the structure of the payload, a test rig was constructed Figure A-1. The rig contained a thermocouple to be used as a reference temperature and an I^2C to Serial Bridge, which allows the temperatures to be transmitted to a LabVIEW GUI to be logged.

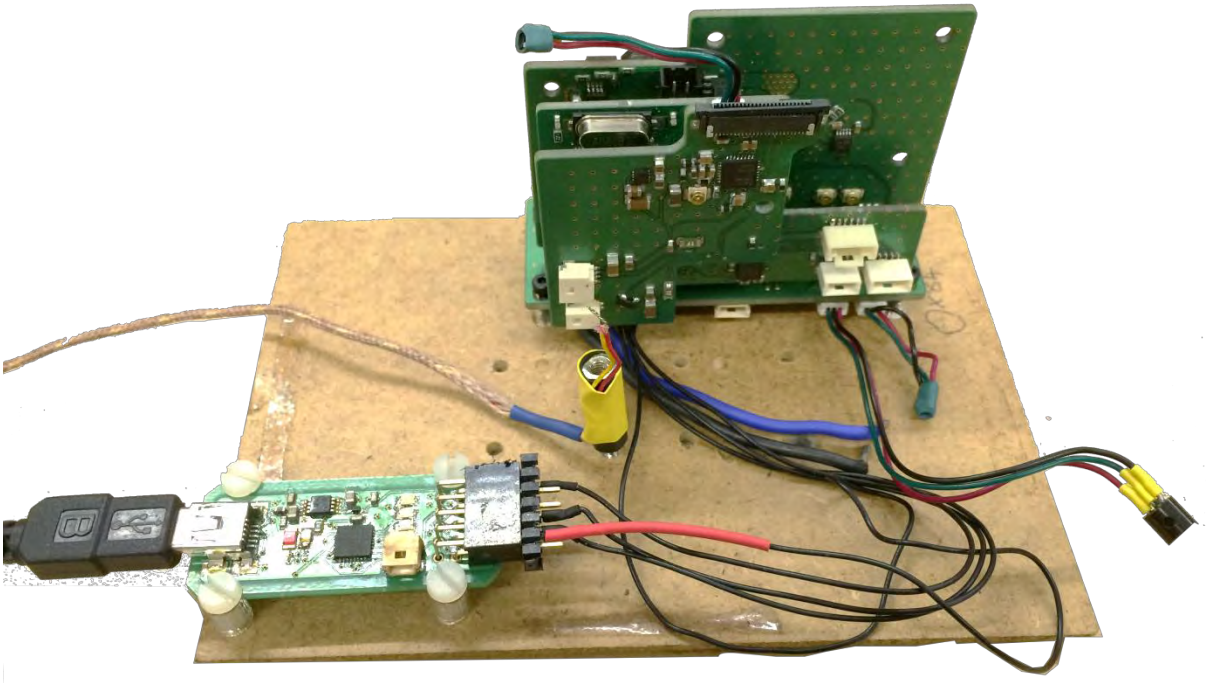

Figure A-1: The temperature calibration rig

Once the data had been logged, the method of least squares was used to determine the trend line of the data in order to establish the gain and the offset which should be applied to the ADC readings. As the ideal would be a 1:1 ratio between the actual and calculated temperature, the trend line can be used to determine the gain and offset to be applied to each temperature reading.

The gain and offset were then applied and the test was repeated in order to verify the calibration. The maximum error was found to be $\pm$ 3°C after calibration.

B.1 : USB to SPI / I²C bridge

A USB to SPI/ I²C bridge was developed to enable data to be communicated to a LabVIEW GUI for development purposes. The bridge enables the data received from the RF1101SE transceiver to be displayed via the LabVIEW GUI during testing.

A CP2102 USB to Serial Bridge was used as the interface between the computer and the microcontroller on board the PCB. The MSP430G2553 was selected, as the MISO and MOSI pins used for the SPI communications can be configured as the SDA and SCL pins for I²C. This enables the same PCB layout to be used for both communication methods. A number of LEDs were added to the PCB to indicate power and communication. To enable the pull-up resistors for I²C communication, a pair of MOSFETs are used to close the path between the pull up resistors and the communication lines. The MOSFETs are controlled programmatically from the microcontroller. The layout and pinout of the PCB can be seen in Figure B-1.

Due to code size limitations, the microcontroller is reprogrammed for either SPI or I²C or RF1101SE communications. To ensure valid Serial communications the same packet stretching and CRC check used for the wireless data transfer is used.

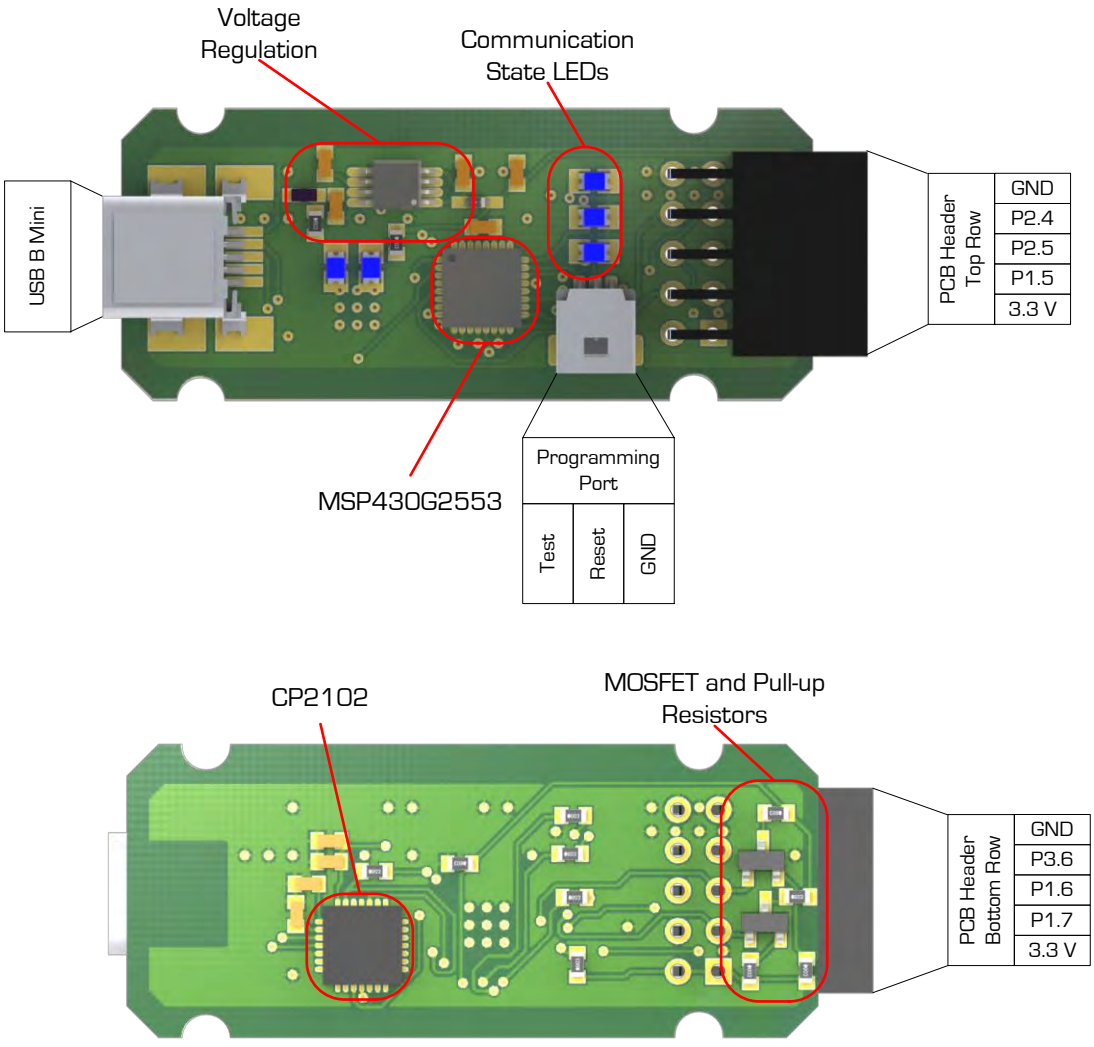

Figure B-1: USB to SPI/ I²C PCB layout

B.2 : Power sensor development PCB

In order to log the power requirements of a number of modules throughout the development process, a break-out board was developed for the INA220 Power Monitor.

The IC determines the current by measuring the voltage drop across a sense resistor in series with the power supply. The sense resistor was configured for high side current sensing. The specification of the device can be seen in Table B-1.

Table B-1: Power sensor PCB specifications

Property	Value	Unit
IC	INA220A	
Sense Resistor	10	mΩ
Maximum Voltage	32	V
Maximum Current	10	A
Current Resolution	1	mA
Voltage Resolution	4	mV

The system was designed using a 10 mΩ, 1W, resistor therefore limiting the current to 10 A. The connector pin allocations and descriptions can be seen in Figure B-2 and Table B-2 respectively. To allow for the use of different values of sense resistors, the INA220 has a calibration value that was determined to be 4096 using the method outlined in the datasheet.

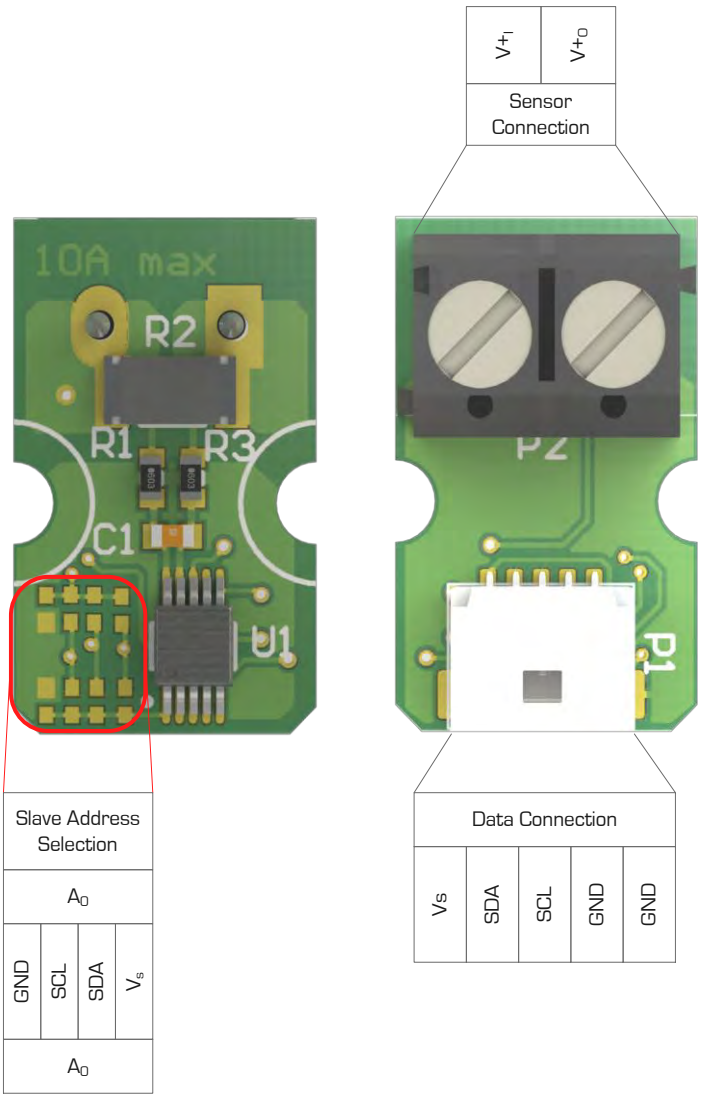

Figure B-2: Diagram showing the connection pin allocations and the slave address selection solder bridges

Table B-2: Description of the INA220 break-out PCB connection pin allocations

Sensor Connection			
Pin Name	Direction	Max Voltage	Description
$V+_I$	Input	32 V	Input from power source
$V+_O$	Output		Output connected to load
Data Connections			
V_S	IC supply	6 V	Supply for the INA220
SDA	I/O		I^2C data line
SCL	I/O		I^2C clock line
GND	IC supply	0.8 V	Supply current return path
GND	Measured GDN		Ground reference for the supply voltage reading

The advantage of using an I^2C device with selectable address is the fact that the address can be changed, to avoid duplicating slave addresses in the system. The selection of the slave address is achieved through the connection of A_1 and A_0 to GND, V_{s+}, SDA or SCL via an array of solder bridges seen in Figure B-2. The slave address resulting from the selected combination can be seen in Table B-3.

.

Table B-3: Possible INA220 slave addresses [42]

A1	A0	Slave Address
GND	GND	0x80
GND	V_{s+}	0x82
GND	SDA	0x84
GND	SCL	0x86
V_{S+}	GND	0x88
V_{S+}	V_{S+}	0x8A
V_{S+}	SDA	0x8C
V_{S+}	SCL	0x8E
SDA	GND	0x90
SDA	V_{S+}	0x92
SDA	SDA	0x94
SDA	SCL	0x96
SCL	GND	0x98
SCL	V_{S+}	0x9A
SCL	SDA	0x9C
SCL	SCL	0x9E

EBE Faculty: Assessment of Ethics in Research Projects (Rev2)

Any person planning to undertake research in the Faculty of Engineering and the Built Environment at the University of Cape Town is required to complete this form before collecting or analysing data. When completed it should be submitted to the supervisor (where applicable) and from there to the Head of Department. If any of the questions below have been answered YES, and the applicant is NOT a fourth year student, the Head should forward this form for approval by the Faculty EIR committee: submit to Ms Zulpha Geyer (Zulpha.Geyer@uct.ac.za; Chem Eng Building, Ph 021 650 4791).
NB: A copy of this signed form must be included with the thesis/dissertation/report when it is submitted for examination
This form must only be completed once the most recent revision EBE EiR Handbook has been read.

Name of Principal Researcher/Student: **Greig Knox** Department: **Mechanical Engineering**

Preferred email address of the applicant: **greigknox@gmail.com**

If a Student: Degree: **M.Sc Mechanical Eng** Supervisor: **Samuel Ginsberg**

If a Research Contract indicate source of funding/sponsorship: **NRF**

Research Project Title: **Design of a Sensor Payload for a Man-Packable, Throwable, Inspection Class Robotics System**

Overview of ethics issues in your research project:

Question 1: Is there a possibility that your research could cause harm to a third party (i.e. a person not involved in your project)?	YES	NO x
Question 2: Is your research making use of human subjects as sources of data? If your answer is YES, please complete Addendum 2.	YES	NO x
Question 3: Does your research involve the participation of or provision of services to communities? If your answer is YES, please complete Addendum 3.	YES	NO x
Question 4: If your research is sponsored, is there any potential for conflicts of interest? If your answer is YES, please complete Addendum 4.	YES	NO x

If you have answered YES to any of the above questions, please append a copy of your research proposal, as well as any interview schedules or questionnaires (Addendum 1) and please complete further addenda as appropriate. Ensure that you refer to the EiR Handbook to assist you in completing the documentation requirements for this form.

I hereby undertake to carry out my research in such a way that

- there is no apparent legal objection to the nature or the method of research; and
- the research will not compromise staff or students or the other responsibilities of the University;
- the stated objective will be achieved, and the findings will have a high degree of validity;
- limitations and alternative interpretations will be considered;
- the findings could be subject to peer review and publicly available; and
- I will comply with the conventions of copyright and avoid any practice that would constitute plagiarism.

Signed by:

	Full name and signature	Date
Principal Researcher/Student:	Greig Knox	14/06/2014
This application is approved by:		
Supervisor (if applicable):		13/11/2014
HOD (or delegated nominee): *Final authority for all assessments with NO to all questions and for all undergraduate research.*	R.D. Knuppen	17/11/2014
Chair : Faculty EIR Committee For applicants other than undergraduate students who have answered YES to any of the above questions.		

Department of Mechanical Engineering
Risk Assessment Form

- **Risk Assessments are not required for simple workshop activities covered by the Safety Declaration. However permission must be obtained from Mr Glen Newins before commencing any activity in the Workshop.**
- **A new Risk Assessment form needs to be completed for each major activity within your project.**
- **You are required to include this document (signed) in your bound project submission and mount a copy next to any rig / apparatus you are using.**

Your Name	Greig Knox
Your Supervisor	Samuel Ginsberg and Tracy Booysen
Project title and number	The Design of a Interchangeable Sensor Payload, Communication and Battery management system for a man-packable, throwable Urban Search and Rescue Robotic Platfrom
Area Safety Warden	Pierre Smith and Dillon Jacobs

This Section to be completed by the student (Must be typed and the declaration signed)			
Location where the activity will be done	Duncan Macmillan Building		
Describe the activity (use attachment with diagrams if needed)	Testing a Secondary Battery Protection System. The purpose of the test is to blow a 10 A rated fuse by using a mosfet to close a 57 A current limited path between the terminals of a Lithium Nickel Manganese Cobalt Oxide (NMC) battery. The closing of the path will cause an 18 C, where 1 C represents a full discharge in 1 hour, discharge for a period of 10 ms from a 45 C rated battery. The gate of the mosfet is controlled by an MS430G2553, with a 5 s delay between initiation and the closing of the circuit to allow the operator to clear the area.		
Names of persons involved in this activity	Greig Knox, Timothy Hope		
Describe in detail the risks you (and others) will face during this activity and the potential consequences of your activities	Should the battery overheat during the 10 ms period, it could lead to an explosive combustion.		
Does your project involve the use of any materials (chemicals, gasses, etc.) which may be hazardous to health, or the environment	No	Yes ✓	*If Yes list the chemicals / gasses to be used and attach the MSDS(s) for these materials. Lithium-Ion*
Does this activity involve any equipment / device designed or built by you which is to be plugged into mains electricity?	No ✓	Yes	*If Yes please consult with Mr Julian Mayer before connecting to the mains / switching on.*
Does your project involve any new equipment / devices designed which contain gas or volatile liquids at pressure?	No ✗	Yes ✓	*If Yes please check the relevant SANS Pressurised Equipment Regulations and consult with Dr Fuls before design, build or test.*
What precautions are required to protect against the risks detailed above?	There is a delay, of 5 s between the initiation of the gate control signal and the activation of the gate control signal. This will allow the operator to clear the area. Additionally the battery will be placed inside a charging pouch and a metal container. The charging pouch is and designed to contain the heat and flames. The test will be carried out on a non-flammable surface and the second person will remain at 10 m during the test		
Describe the personal protective equipment (PPE) required during this activity – specify in detail.	Protective Eye wear, Gloves and a CO_2 fire extinguisher		
Describe the shutdown procedure in detail.			
Describe any relevant emergency procedures, e.g. spillage response etc.	Avoid skin contact and spray with the fire extinguisher. Contain any remaining material for disposal.		

I declare that I am aware of the risks associated with this activity and will take all necessary steps to mitigate these risks.	**Student Signature**	**Date**
		9/07/15

I am aware of the student's intended activity, and have provided the necessary guidance, inputs, and oversight.	**Supervisor Signature**	**Date**
		09/07/2015

This section to be completed by the Area Safety Warden		
Level of supervision required (Please tick relevant block)	A = work may not take place without supervisor/warden present.	
	B = work may not take place without a 2nd party present.	X
	C = no specific extra supervision requirements.	
I am satisfied that the student is aware of the risks associated with this activity and grant approval for it to proceed.	**Signature** WF Fung	**Date**
	WFung	2015/7/6

Safety data sheet for product

1. PRODUCT AND COMPANY IDENTIFICATION

- Product name: Lithium ion rechargeable battery cell
- Product code: None
  (All models Sanyo manufactured and whose capacity is less than or equal to 5.4Ah, including the cell branded as Panasonic, excluding the cell whose shape is prismatic and two or more side of short / middle / long side excess 12mm/85mm/110mm.)
- Company name: Sanyo Electric Co., Ltd.
- Address: 222-1 , Kaminaizen, Sumoto City, Hyogo, Japan
- Telephone number: +81-799-24-4111
- Fax number: +81-799-23-2879
- Emergency telephone number: [Weekday] +81-799-23-3931 [Night and holiday] +81-799-24-4131

2. HAZARDS IDENTIFICATION

- GHS Classification : Not available
  (This product is outside the scope of GHS system since it's considered as an "article".)
  For the battery cell, chemical materials are stored in a hermetically sealed metal or metal laminated plastic case, designed to withstand temperatures and pressures encountered during normal use. As a result, during normal use, there is no physical danger of ignition or explosion and chemical danger of hazardous materials' leakage.
  However, if exposed to a fire, added mechanical shocks, decomposed, added electric stress by miss-use, the gas release vent will be operated. The battery cell case will be breached at the extreme, hazardous materials may be released.
  Moreover, if heated strongly by the surrounding fire, acrid gas may be emitted.

- ***Most important hazard and effects***
  Human health effects:
  Inhalation: The steam of the electrolyte has an anesthesia action and stimulates a respiratory tract.
  Skin contact: The steam of the electrolyte stimulates a skin. The electrolyte skin contact causes a sore and stimulation on the skin.
  Eye contact: The steam of the electrolyte stimulates eyes. The electrolyte eye contact causes a sore and stimulation on the eye. Especially, substance that causes a strong inflammation of the eyes is contained.
  Environmental effects: Since a battery cell remains in the environment, do not throw out it into the environment.

- Specific hazards:
  If the electrolyte contacts with water, it will generate detrimental hydrogen fluoride.
  Since the leaked electrolyte is inflammable liquid, do not bring close to fire.

3. COMPOSITION / INFORMATION ON INGREDIENTS

- Substance or preparation: Preparation
- Information about the chemical nature of product: *1

Portion	Material name	Concentration range (wt %)
Positive electrode	Lithium transition metal oxidate ($Li[M]_m[O]_n$ *2)	20~60
Positive electrode's base	Aluminum	1~10
Negative electrode	Carbon	10~30
Negative electrode's base	Copper	1~15
Electrolyte	Organic electrolyte principally involves ester carbonate	5~25
Outer case	Aluminum, iron, aluminum laminated plastic	1~30

*1 Not every product includes all of these materials.
*2 The letter M means transition metal and candidates of M are Co, Mn, Ni and Al. One compound includes one or more of these metals and one product includes one or more of the compounds. The letter m and n means the number of atoms.

4. FIRST-AID MEASURES

Spilled internal cell materials

- Inhalation:
  Make the victim blow his/her nose, gargle. Seek medical attention if necessary.
- Skin contact:
  Remove contaminated clothes and shoes immediately. Wash extraneous matter or contact region with soap and plenty of water immediately.
- Eye contact:
  Do not rub one's eyes. Immediately flush eyes with water continuously for at least 15 minutes. Seek medical attention immediately.

A battery cell and spilled internal cell materials

- Ingestion:
  Make the victim vomit. When it is impossible or the feeling is not well after vomiting, seek medical attention.

5. FIRE-FIGHTING MEASURE

- Suitable extinguishing media: Plenty of water, carbon dioxide gas, nitrogen gas, chemical powder fire extinguishing medium and fire foam.
- Specific hazards: Corrosive gas may be emitted during fire.
- Specific methods of fire-fighting: When the battery burns with other combustibles simultaneously, take fire-extinguishing method which correspond to the combustibles. Extinguish a fire from the windward as much as possible.
- Special protective equipment for firefighters:
  Respiratory protection: Respiratory equipment of a gas cylinder style or protection-against-dust mask
  Hand protection: Protective gloves
  Eye protection: Goggle or protective glasses designed to protect against liquid splashes
  Skin and body protection: Protective cloth

6. ACCIDENTAL RELEASE MEASURES

Spilled internal cell materials, such as electrolyte leaked from a battery cell, are carefully dealt with according to the followings.

- Precautions for human body:
  Remove spilled materials with protective equipment (protective glasses and protective gloves). Do not inhale the gas as much as possible. Moreover, avoid touching with as much as possible.
- Environmental precautions: Do not throw out into the environment.
- Method of cleaning up: The spilled solids are put into a container. The leaked place is wiped off with dry cloth.
- Prevention of secondary hazards: Avoid re-scattering. Do not bring the collected materials close to fire.

7. HANDLING AND STORAGE

- Handling suggestions
  - Do not connect the positive terminal to the negative terminal with electrical wire or chain.
  - Avoid polarity reverse connection when installing the battery to an instrument.
  - Do not wet the battery with water, seawater, drink or acid; or expose to strong oxidizer.
  - Do not damage or remove the external tube.
  - Keep the battery away from heat and fire.
  - Do not disassemble or reconstruct the battery; or solder the battery directly.
  - Do not give a mechanical shock or deform.
  - Do not use unauthorized charger or other charging method. Terminate charging when the charging process doesn't end within specified time.
- Storage
  - Do not store the battery with metalware, water, seawater, strong acid or strong oxidizer.
  - Make the charge amount 30~50% then store at room temperature or less (temperature= -20~35 degree C) in a dry (humidity: 45~85%) place. Avoid direct sunlight, high temperature, and high humidity.
  - Use insulative and adequately strong packaging material to prevent short circuit between positive and negative terminal when the packaging breaks during normal handling. Do not use conductive or easy to break packaging material.

8. EXPOSURE CONTROLS / PERSONAL PROTECTION (WHEN THE ELECTROLYTE LEAKS)

- Control parameters
  ACGIH has not been mentioned control parameter of electrolyte.
- Personal protective equipment
  Respiratory protection: Respirator with air cylinder, dust mask
  Hand protection: Protective gloves
  Eye protection: Goggle or protective glasses designed to protect against liquid splashes
  Skin and body protection: Working clothes with long sleeve and long trousers

9. PHYSICAL AND CHEMICAL PROPERTIES

- Appearance
  Physical state: Solid
  Form: Cylindrical or Prismatic or Pouch (laminated)
  Color: Metallic color or black(without tube if it has tube)
  Odor: No odor

10. STABILITY AND REACTIVITY

- Stability: Stable under normal use
- Hazardous reactions occurring under specific conditions
  - Conditions to avoid: When a battery cell is exposed to an external short-circuit, crushes, deformation, high temperature above 100 degree C, it will be the cause of heat generation and ignition. Direct sunlight and high humidity.
  - Materials to avoid: Conductive materials, water, seawater, strong oxidizers and strong acids.
  - Hazardous decomposition products: Acrid or harmful gas is emitted during fire.

11. TOXICOLOGICAL INFORMATION

Organic Electrolyte

- Acute toxicity:
  LD_{50}, oral - Rat 2,000mg/kg or more
- Irritating nature: Irritative to skin and eye

12. ECOLOGICAL INFORMATION

- Persistence/degradability:
  Since a battery cell and the internal materials remain in the environment, do not bury or throw out into the environment.

13. DISPOSAL CONSIDERATIONS

- Recommended methods for safe and environmentally preferred disposal:

Product (waste from residues)

Specified collection or disposal of lithium ion battery is required by the law like as "battery control law" in several nations. Collection or recycle of the battery is mainly imposed on battery's manufacturer or importer in the nations recycle is required.

Contaminated packaging

Neither a container nor packing is contaminated during normal use. When internal materials leaked from a battery cell contaminates, dispose as industrial wastes subject to special control.

14. TRANSPORT INFORMATION

In the case of transportation, avoid exposure to high temperature and prevent the formation of any condensation. Take in a cargo of them without falling, dropping and breakage. Prevent collapse of cargo piles and wet by rain. The container must be handled carefully. Do not give shocks that result in a mark of hitting on a cell. Please refer to Section 7-HANDLING AND STORAGE also.

UN regulation

- ***UN number: 3480 (3481 when the battery is contained in equipment or packed with equipment)***
- Proper shipping name:
  Lithium ion batteries ("lithium ion batteries contained in equipment" or "lithium ion batteries packed with equipment")
- Class: 9 *
- Packing group: II *

** However this product is defined as above, it is **not** recognized as "DANGEROUS GOODS" or is treated as almost non-DANGEROUS GOODS when its transport condition accords with instructions or provisions depend on region and transportation mode.*

About the instructions or provisions, please see descriptions in box brackets of following regulations.

Regulation depends on region and transportation mode

- Worldwide, air transportation:
  IATA-DGR [As non-DANGEROUS GOODS: "packing instruction 965 section II" /
  Almost as above however displayed as DANGEROUS GOODS: "packing instruction 965 section IB"]
  (When batteries are packaged with equipments or contained in equipments, refer packing instruction 966 or 967 instead of 965.)
- Worldwide, sea transportation:
  IMO-IMDG Code [special provision 188]
- Europe, road transportation:
  ADR [special provision 188]

15. REGULATORY INFORMATION

- Regulations specifically applicable to the product:
  Wastes Disposal and Public Cleaning Law [Japan]
  Law for Promotion of Effective Utilization of resources [Japan]
  US Department of Transportation 49 Code of Federal Regulations [USA]

** About overlapping regulations, please refer to Section 14-TRANSPORT INFOMATION.*

16. OTHER INFORMATION

- ***This safety data sheet is offered an agency who handles this product to handle it safely.***
- The agency should utilize this safety data sheet effectively (put it up, educate person in charge) and take proper measures.
- ***The information contained in this Safety data sheet is based on the present state of knowledge and current legislation.***
- This safety data sheet provides guidance on health, safety and environmental aspects of the product and should not be construed as any guarantee of technical performance or suitability for particular applications

Reference

Dangerous Goods Regulations – 56th Edition Effective 1 January 2015: International Air Transport Association (IATA)
IMDG Code – 2014 Edition: International Maritime Organization (IMO)
The European Agreement concerning the International Carriage of Dangerous Goods by Road – 2015: The United Nations Economic Commission for Europe (UNECE)

First edition: Apr. 28, 2010
Prepared and approved by
Technical Administration Group
Portable Rechargeable Battery Business Division
Sanyo Electric Co., Ltd.

Appendix E:

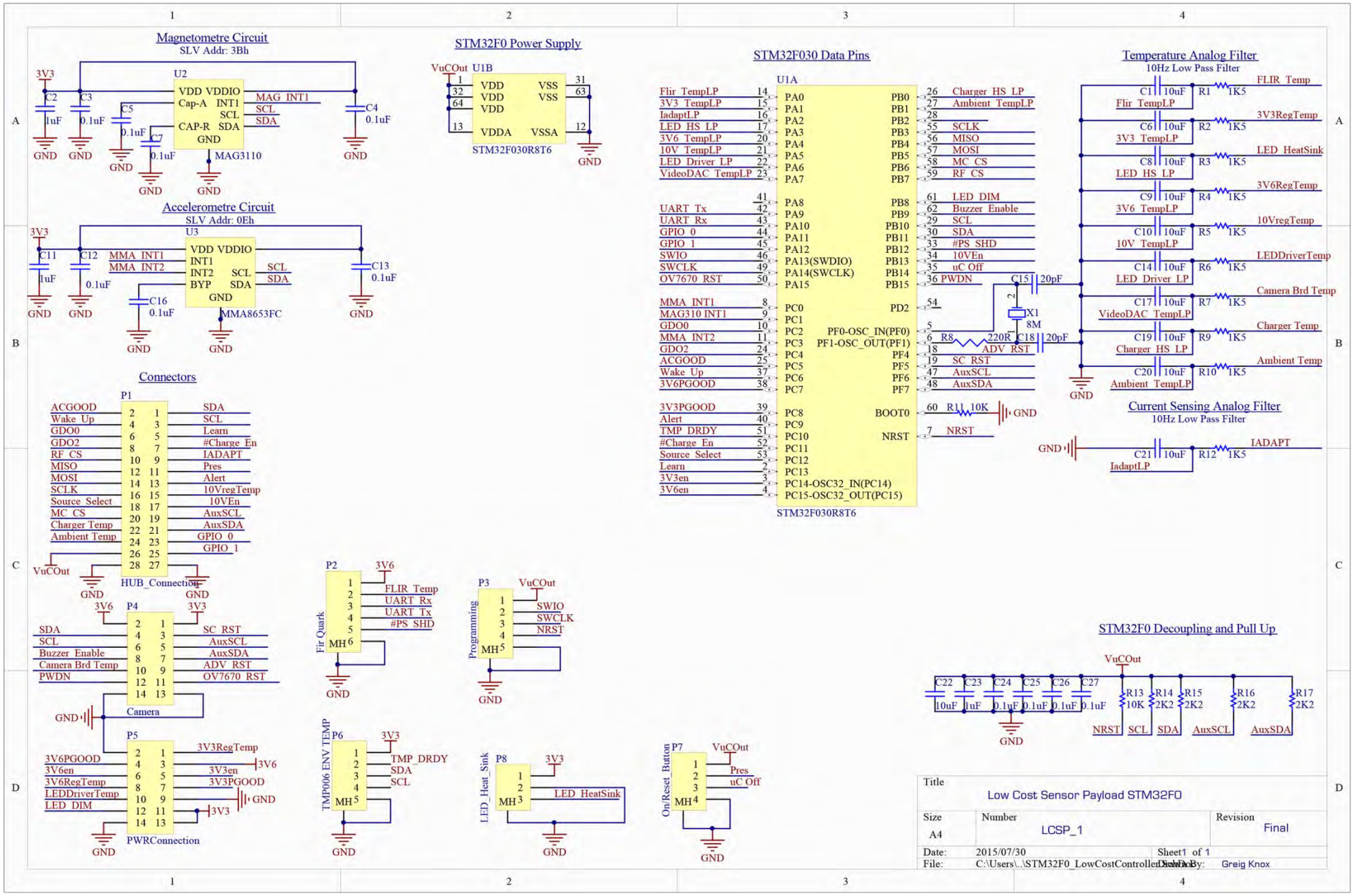
Magnetometre Circuit
SLV Addr: 3Bh
U2
MAG3110
Accelerometre Circuit
SLV Addr: 0Eh
U3
MMA8653FC
STM32F0 Power Supply
U1B
STM32F030R8T6
STM32F030 Data Pins
U1A
STM32F030R8T6
Temperature Analog Filter
10Hz Low Pass Filter
Current Sensing Analog Filter
10Hz Low Pass Filter
Connectors
P1
HUB_Connection
P2
Fir Quark
P3
Programming
P4
Camera
P5
PWRConnection
P6
TMP006 ENV TEMP
P7
On/Reset Button
P8
LED_Heat_Sink
STM32F0 Decoupling and Pull Up
Title
Low Cost Sensor Payload STM32F0
Size
A4
Number
LCSP_1
Revision
Final
Date:
2015/07/30
Sheet1 of 1
File:
C:\Users\..\STM32F0_LowCostControllerBoard.SchDoc
Drawn By:
Greig Knox

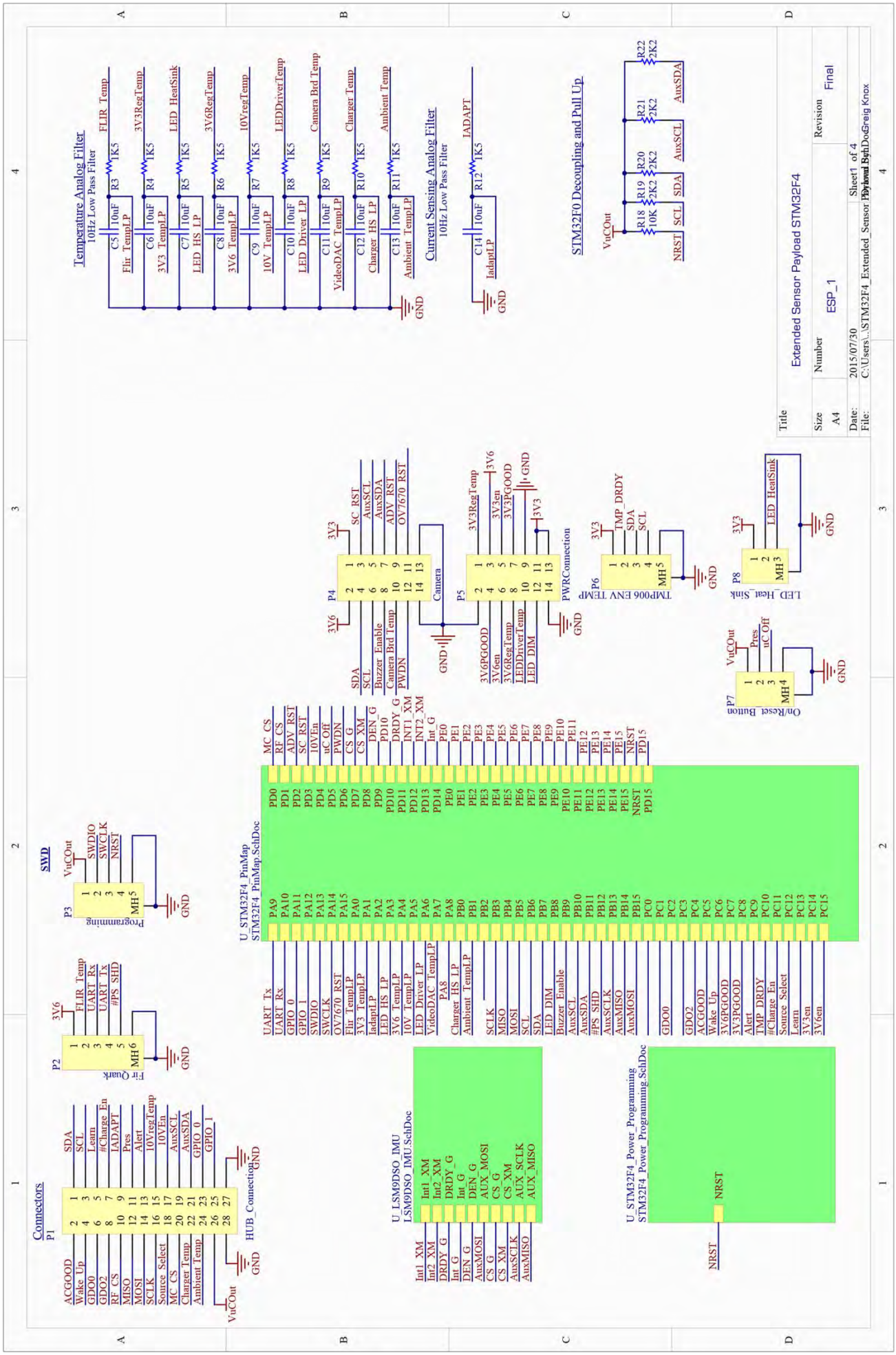
Temperature Analog Filter
10Hz Low Pass Filter
Current Sensing Analog Filter
10Hz Low Pass Filter
STM32F0 Decoupling and Pull Up
Connectors
SWD
U_STM32F4_PinMap
STM32F4_PinMap.SchDoc
U_LSM9DSO_IMU
LSM9DSO_IMU.SchDoc
U_STM32F4_Power_Programming
STM32F4_Power_Programming.SchDoc
Camera
PWRConnection
TMP006 ENV TEMP
LED_Heat_Sink
On/Reset_Button
Fir Quark
Programming
HUB_Connection
Title
Extended Sensor Payload STM32F4
Size
A4
Number
ESP_1
Revision
Final
Date:
2015/07/30
Sheet 1 of 4
File:
C:\Users\...\STM32F4_Extended_Sensor_Payload.SchDoc
Drawn By:
Greig Knox

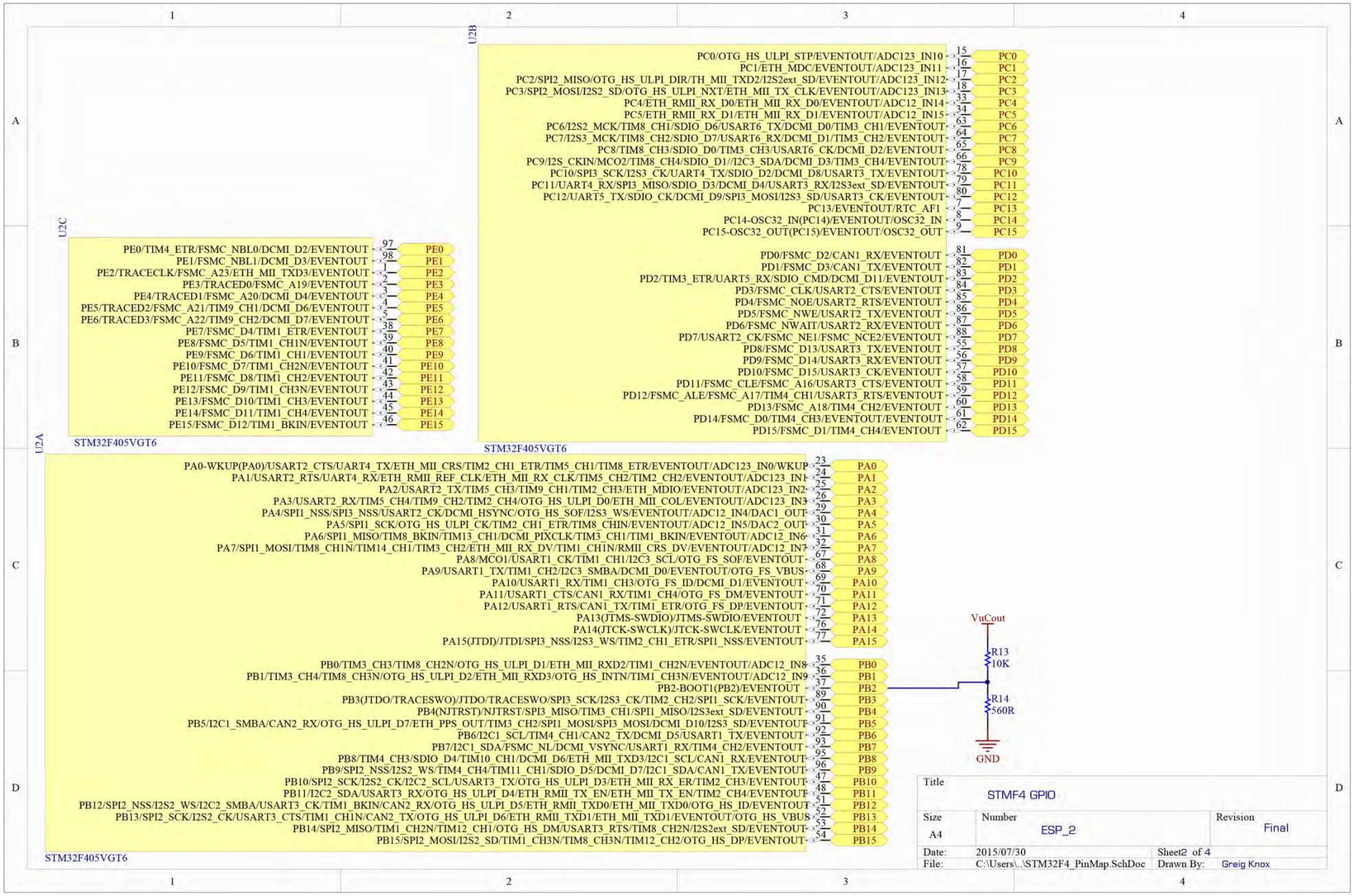
U2C
PE0/TIM4_ETR/FSMC_NBL0/DCMI_D2/EVENTOUT
PE1/FSMC_NBL1/DCMI_D3/EVENTOUT
PE2/TRACECLK/FSMC_A23/ETH_MII_TXD3/EVENTOUT
PE3/TRACED0/FSMC_A19/EVENTOUT
PE4/TRACED1/FSMC_A20/DCMI_D4/EVENTOUT
PE5/TRACED2/FSMC_A21/TIM9_CH1/DCMI_D6/EVENTOUT
PE6/TRACED3/FSMC_A22/TIM9_CH2/DCMI_D7/EVENTOUT
PE7/FSMC_D4/TIM1_ETR/EVENTOUT
PE8/FSMC_D5/TIM1_CH1N/EVENTOUT
PE9/FSMC_D6/TIM1_CH1/EVENTOUT
PE10/FSMC_D7/TIM1_CH2N/EVENTOUT
PE11/FSMC_D8/TIM1_CH2/EVENTOUT
PE12/FSMC_D9/TIM1_CH3N/EVENTOUT
PE13/FSMC_D10/TIM1_CH3/EVENTOUT
PE14/FSMC_D11/TIM1_CH4/EVENTOUT
PE15/FSMC_D12/TIM1_BKIN/EVENTOUT
97 98 1 2 3 4 5 38 39 40 41 42 43 44 45 46
PE0 PE1 PE2 PE3 PE4 PE5 PE6 PE7 PE8 PE9 PE10 PE11 PE12 PE13 PE14 PE15
STM32F405VGT6
U2B
PC0/OTG_HS_ULPI_STP/EVENTOUT/ADC123_IN10
PC1/ETH_MDC/EVENTOUT/ADC123_IN11
PC2/SPI2_MISO/OTG_HS_ULPI_DIR/TH_MII_TXD2/I2S2ext_SD/EVENTOUT/ADC123_IN12
PC3/SPI2_MOSI/I2S2_SD/OTG_HS_ULPI_NXT/ETH_MII_TX_CLK/EVENTOUT/ADC123_IN13
PC4/ETH_RMII_RX_D0/ETH_MII_RX_D0/EVENTOUT/ADC12_IN14
PC5/ETH_RMII_RX_D1/ETH_MII_RX_D1/EVENTOUT/ADC12_IN15
PC6/I2S2_MCK/TIM8_CH1/SDIO_D6/USART6_TX/DCMI_D0/TIM3_CH1/EVENTOUT
PC7/I2S3_MCK/TIM8_CH2/SDIO_D7/USART6_RX/DCMI_D1/TIM3_CH2/EVENTOUT
PC8/TIM8_CH3/SDIO_D0/TIM3_CH3/USART6_CK/DCMI_D2/EVENTOUT
PC9/I2S_CKIN/MCO2/TIM8_CH4/SDIO_D1//I2C3_SDA/DCMI_D3/TIM3_CH4/EVENTOUT
PC10/SPI3_SCK/I2S3_CK/UART4_TX/SDIO_D2/DCMI_D8/USART3_TX/EVENTOUT
PC11/UART4_RX/SPI3_MISO/SDIO_D3/DCMI_D4/USART3_RX/I2S3ext_SD/EVENTOUT
PC12/UART5_TX/SDIO_CK/DCMI_D9/SPI3_MOSI/I2S3_SD/USART3_CK/EVENTOUT
PC13/EVENTOUT/RTC_AF1
PC14-OSC32_IN(PC14)/EVENTOUT/OSC32_IN
PC15-OSC32_OUT(PC15)/EVENTOUT/OSC32_OUT
PD0/FSMC_D2/CAN1_RX/EVENTOUT
PD1/FSMC_D3/CAN1_TX/EVENTOUT
PD2/TIM3_ETR/UART5_RX/SDIO_CMD/DCMI_D11/EVENTOUT
PD3/FSMC_CLK/USART2_CTS/EVENTOUT
PD4/FSMC_NOE/USART2_RTS/EVENTOUT
PD5/FSMC_NWE/USART2_TX/EVENTOUT
PD6/FSMC_NWAIT/USART2_RX/EVENTOUT
PD7/USART2_CK/FSMC_NE1/FSMC_NCE2/EVENTOUT
PD8/FSMC_D13/USART3_TX/EVENTOUT
PD9/FSMC_D14/USART3_RX/EVENTOUT
PD10/FSMC_D15/USART3_CK/EVENTOUT
PD11/FSMC_CLE/FSMC_A16/USART3_CTS/EVENTOUT
PD12/FSMC_ALE/FSMC_A17/TIM4_CH1/USART3_RTS/EVENTOUT
PD13/FSMC_A18/TIM4_CH2/EVENTOUT
PD14/FSMC_D0/TIM4_CH3/EVENTOUT/EVENTOUT
PD15/FSMC_D1/TIM4_CH4/EVENTOUT
15 16 17 18 33 34 63 64 65 66 78 79 80 7 8 9 81 82 83 84 85 86 87 88 55 56 57 58 59 60 61 62
PC0 PC1 PC2 PC3 PC4 PC5 PC6 PC7 PC8 PC9 PC10 PC11 PC12 PC13 PC14 PC15 PD0 PD1 PD2 PD3 PD4 PD5 PD6 PD7 PD8 PD9 PD10 PD11 PD12 PD13 PD14 PD15
STM32F405VGT6
U2A
PA0-WKUP(PA0)/USART2_CTS/UART4_TX/ETH_MII_CRS/TIM2_CH1_ETR/TIM5_CH1/TIM8_ETR/EVENTOUT/ADC123_IN0/WKUP
PA1/USART2_RTS/UART4_RX/ETH_RMII_REF_CLK/ETH_MII_RX_CLK/TIM5_CH2/TIM2_CH2/EVENTOUT/ADC123_IN1
PA2/USART2_TX/TIM5_CH3/TIM9_CH1/TIM2_CH3/ETH_MDIO/EVENTOUT/ADC123_IN2
PA3/USART2_RX/TIM5_CH4/TIM9_CH2/TIM2_CH4/OTG_HS_ULPI_D0/ETH_MII_COL/EVENTOUT/ADC123_IN3
PA4/SPI1_NSS/SPI3_NSS/USART2_CK/DCMI_HSYNC/OTG_HS_SOF/I2S3_WS/EVENTOUT/ADC12_IN4/DAC1_OUT
PA5/SPI1_SCK/OTG_HS_ULPI_CK/TIM2_CH1_ETR/TIM8_CHIN/EVENTOUT/ADC12_IN5/DAC2_OUT
PA6/SPI1_MISO/TIM8_BKIN/TIM13_CH1/DCMI_PIXCLK/TIM3_CH1/TIM1_BKIN/EVENTOUT/ADC12_IN6
PA7/SPI1_MOSI/TIM8_CH1N/TIM14_CH1/TIM3_CH2/ETH_MII_RX_DV/TIM1_CH1N/RMII_CRS_DV/EVENTOUT/ADC12_IN7
PA8/MCO1/USART1_CK/TIM1_CH1/I2C3_SCL/OTG_FS_SOF/EVENTOUT
PA9/USART1_TX/TIM1_CH2/I2C3_SMBA/DCMI_D0/EVENTOUT/OTG_FS_VBUS
PA10/USART1_RX/TIM1_CH3/OTG_FS_ID/DCMI_D1/EVENTOUT
PA11/USART1_CTS/CAN1_RX/TIM1_CH4/OTG_FS_DM/EVENTOUT
PA12/USART1_RTS/CAN1_TX/TIM1_ETR/OTG_FS_DP/EVENTOUT
PA13(JTMS-SWDIO)/JTMS-SWDIO/EVENTOUT
PA14(JTCK-SWCLK)/JTCK-SWCLK/EVENTOUT
PA15(JTDI)/JTDI/SPI3_NSS/I2S3_WS/TIM2_CH1_ETR/SPI1_NSS/EVENTOUT
PB0/TIM3_CH3/TIM8_CH2N/OTG_HS_ULPI_D1/ETH_MII_RXD2/TIM1_CH2N/EVENTOUT/ADC12_IN8
PB1/TIM3_CH4/TIM8_CH3N/OTG_HS_ULPI_D2/ETH_MII_RXD3/OTG_HS_INTN/TIM1_CH3N/EVENTOUT/ADC12_IN9
PB2-BOOT1(PB2)/EVENTOUT
PB3(JTDO/TRACESWO)/JTDO/TRACESWO/SPI3_SCK/I2S3_CK/TIM2_CH2/SPI1_SCK/EVENTOUT
PB4(NJTRST)/NJTRST/SPI3_MISO/TIM3_CH1/SPI1_MISO/I2S3ext_SD/EVENTOUT
PB5/I2C1_SMBA/CAN2_RX/OTG_HS_ULPI_D7/ETH_PPS_OUT/TIM3_CH2/SPI1_MOSI/SPI3_MOSI/DCMI_D10/I2S3_SD/EVENTOUT
PB6/I2C1_SCL/TIM4_CH1/CAN2_TX/DCMI_D5/USART1_TX/EVENTOUT
PB7/I2C1_SDA/FSMC_NL/DCMI_VSYNC/USART1_RX/TIM4_CH2/EVENTOUT
PB8/TIM4_CH3/SDIO_D4/TIM10_CH1/DCMI_D6/ETH_MII_TXD3/I2C1_SCL/CAN1_RX/EVENTOUT
PB9/SPI2_NSS/I2S2_WS/TIM4_CH4/TIM11_CH1/SDIO_D5/DCMI_D7/I2C1_SDA/CAN1_TX/EVENTOUT
PB10/SPI2_SCK/I2S2_CK/I2C2_SCL/USART3_TX/OTG_HS_ULPI_D3/ETH_MII_RX_ER/TIM2_CH3/EVENTOUT
PB11/I2C2_SDA/USART3_RX/OTG_HS_ULPI_D4/ETH_RMII_TX_EN/ETH_MII_TX_EN/TIM2_CH4/EVENTOUT
PB12/SPI2_NSS/I2S2_WS/I2C2_SMBA/USART3_CK/TIM1_BKIN/CAN2_RX/OTG_HS_ULPI_D5/ETH_RMII_TXD0/ETH_MII_TXD0/OTG_HS_ID/EVENTOUT
PB13/SPI2_SCK/I2S2_CK/USART3_CTS/TIM1_CH1N/CAN2_TX/OTG_HS_ULPI_D6/ETH_RMII_TXD1/ETH_MII_TXD1/EVENTOUT/OTG_HS_VBUS
PB14/SPI2_MISO/TIM1_CH2N/TIM12_CH1/OTG_HS_DM/USART3_RTS/TIM8_CH2N/I2S2ext_SD/EVENTOUT
PB15/SPI2_MOSI/I2S2_SD/TIM1_CH3N/TIM8_CH3N/TIM12_CH2/OTG_HS_DP/EVENTOUT
35 36 37 89 90 91 92 95 96 47 48 51 52 53 54 23 24 25 26 29 30 31 32 67 68 69 70 71 72 76 77
PB0 PB1 PB2 PB3 PB4 PB5 PB6 PB7 PB8 PB9 PB10 PB11 PB12 PB13 PB14 PB15 PA0 PA1 PA2 PA3 PA4 PA5 PA6 PA7 PA8 PA9 PA10 PA11 PA12 PA13 PA14 PA15
STM32F405VGT6
VuCout
R13
10K
R14
560R
GND
Title
STMF4 GPIO
Size
A4
Number
ESP_2
Revision
Final
Date:
2015/07/30
Sheet2 of 4
File:
C:\Users\...\STM32F4_PinMap.SchDoc
Drawn By:
Greig Knox

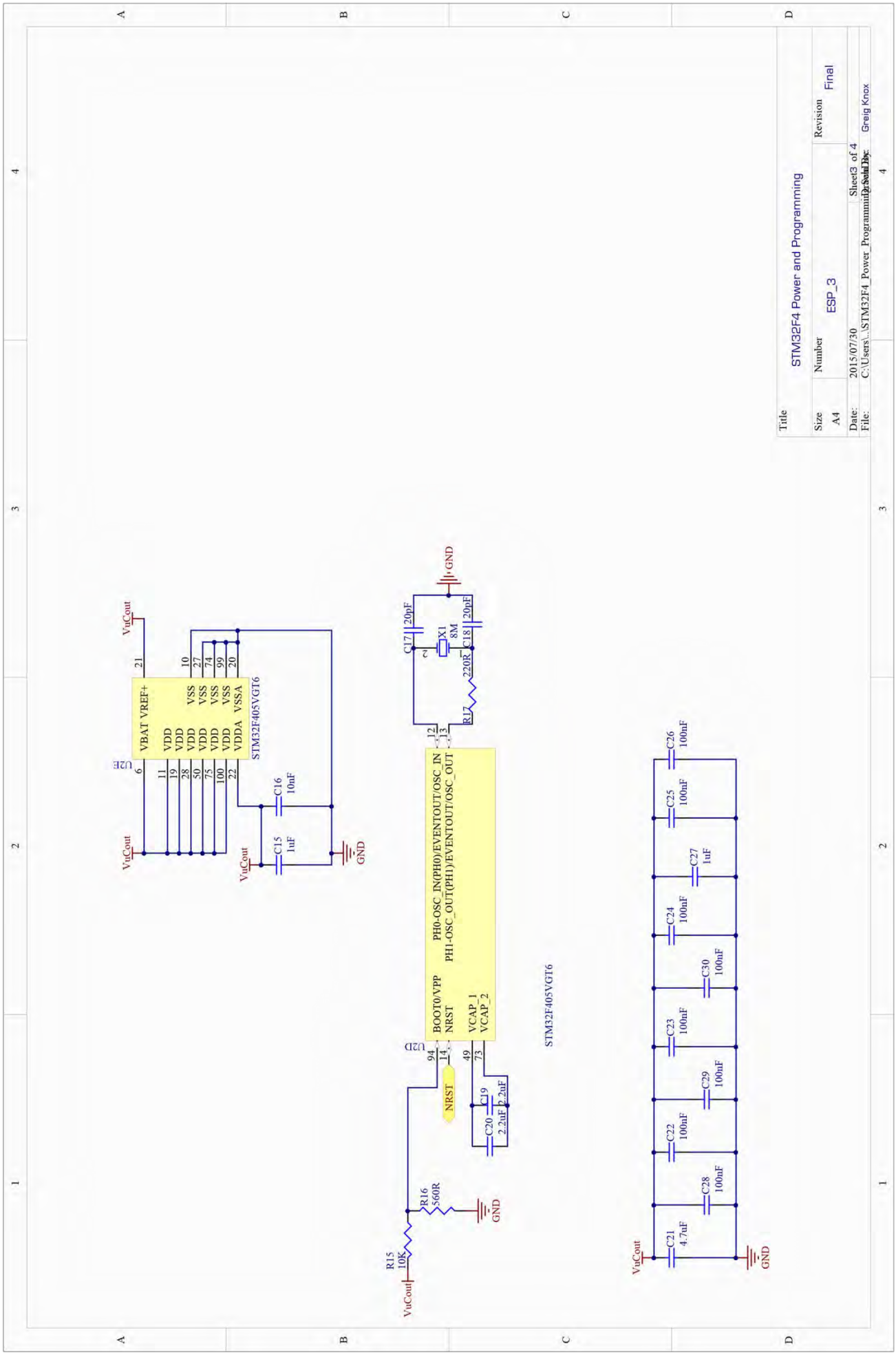
Title
STM32F4 Power and Programming
Size
A4
Number
ESP_3
Revision
Final
Date:
2015/07/30
Sheet3 of 4
File:
C:\Users\...\STM32F4_Power_Programming.SchDoc
Greig Knox
STM32F405VGT6
VBAT VREF+
VDD VDD VDD VDD VDD VDD VDDA
VSS VSS VSS VSS VSS VSSA
PH0-OSC_IN(PH0)/EVENTOUT/OSC_IN
PH1-OSC_OUT(PH1)/EVENTOUT/OSC_OUT
BOOT0/VPP
NRST
VCAP_1
VCAP_2
VuCout
GND
C15 1uF
C16 10nF
C17 20pF
C18 20pF
X1 8M
R15 10K
R16 560R
R17 220R
C19 2.2uF
C20 2.2uF
C21 4.7uF
C22 100nF
C23 100nF
C24 100nF
C25 100nF
C26 100nF
C27 1uF
C28 100nF
C29 100nF
C30 100nF

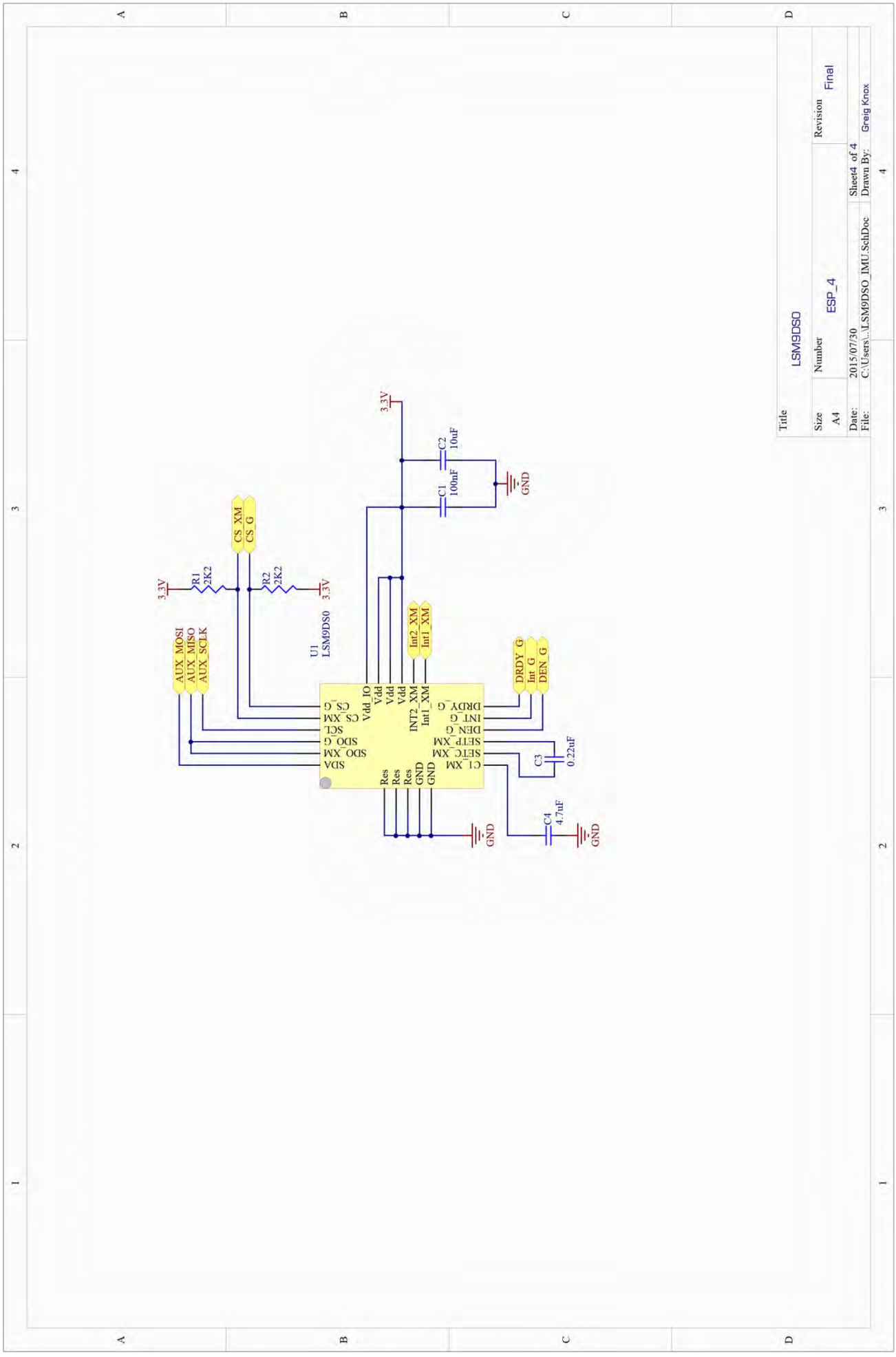
Title
LSM9DS0
Size
A4
Number
ESP_4
Revision
Final
Date:
2015/07/30
Sheet4 of 4
File:
C:\Users\...\LSM9DS0_IMU.SchDoc
Drawn By:
Greig Knox
3.3V
C2
10uF
C1
100nF
GND
CS_XM
CS_G
R1
2K2
R2
2K2
3.3V
3.3V
U1
LSM9DS0
AUX_MOSI
AUX_MISO
AUX_SCLK
Int2_XM
Int1_XM
DRDY_G
Int_G
DEN_G
SDA
SDO_XM
SDO_G
SCL
CS_XM
CS_G
Vdd_IO
Vdd
Vdd
Vdd
INT2_XM
Int1_XM
DRDY_G
INT_G
DEN_G
SETP_XM
SETC_XM
C1_XM
Res
Res
Res
GND
GND
C3
0.22uF
C4
4.7uF
GND
GND

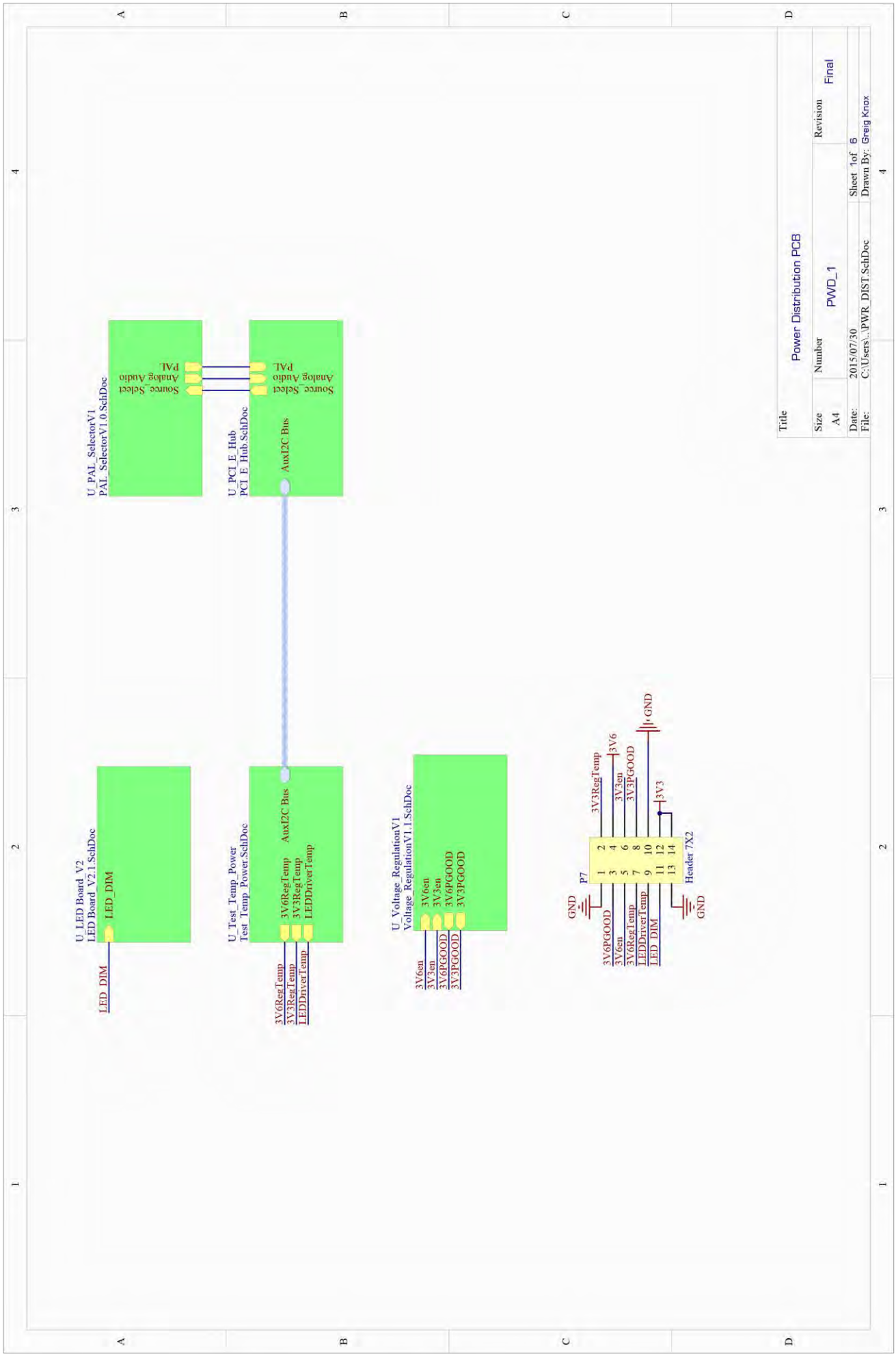
U_PAL_SelectorV1
PAL_SelectorV1.0.SchDoc
Source_Select
Analog Audio
PAL
U_PCI_E_Hub
PCI_E_Hub.SchDoc
AuxI2C Bus
U_LED Board_V2
LED Board_V2.1.SchDoc
LED_DIM
U_Test_Temp_Power
Test_Temp_Power.SchDoc
3V6RegTemp
3V3RegTemp
LEDDriverTemp
U_Voltage_RegulationV1
Voltage_RegulationV1.1.SchDoc
3V6en
3V3en
3V6PGOOD
3V3PGOOD
P7
Header 7X2
GND
3V6
3V3
Title
Power Distribution PCB
Size
A4
Number
PWD_1
Revision
Final
Date:
2015/07/30
Sheet 1of 6
File:
C:\Users\...\PWR_DIST.SchDoc
Drawn By:
Greig Knox

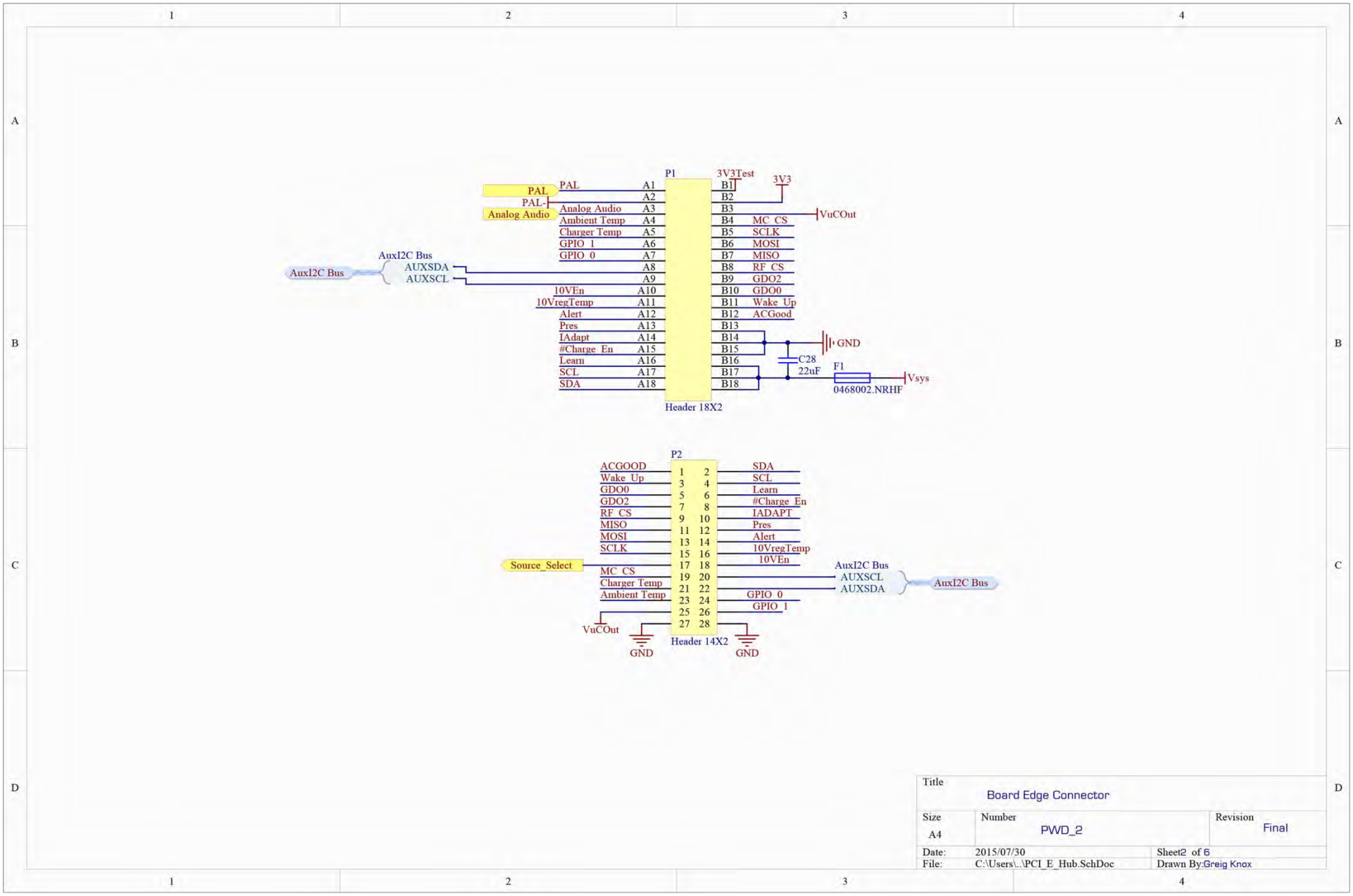

Title	Board Edge Connector	
Size: A4	Number: PWD_2	Revision: Final
Date: 2015/07/30		Sheet2 of 6
File: C:\Users\..\PCI_E_Hub.SchDoc		Drawn By:Greig Knox

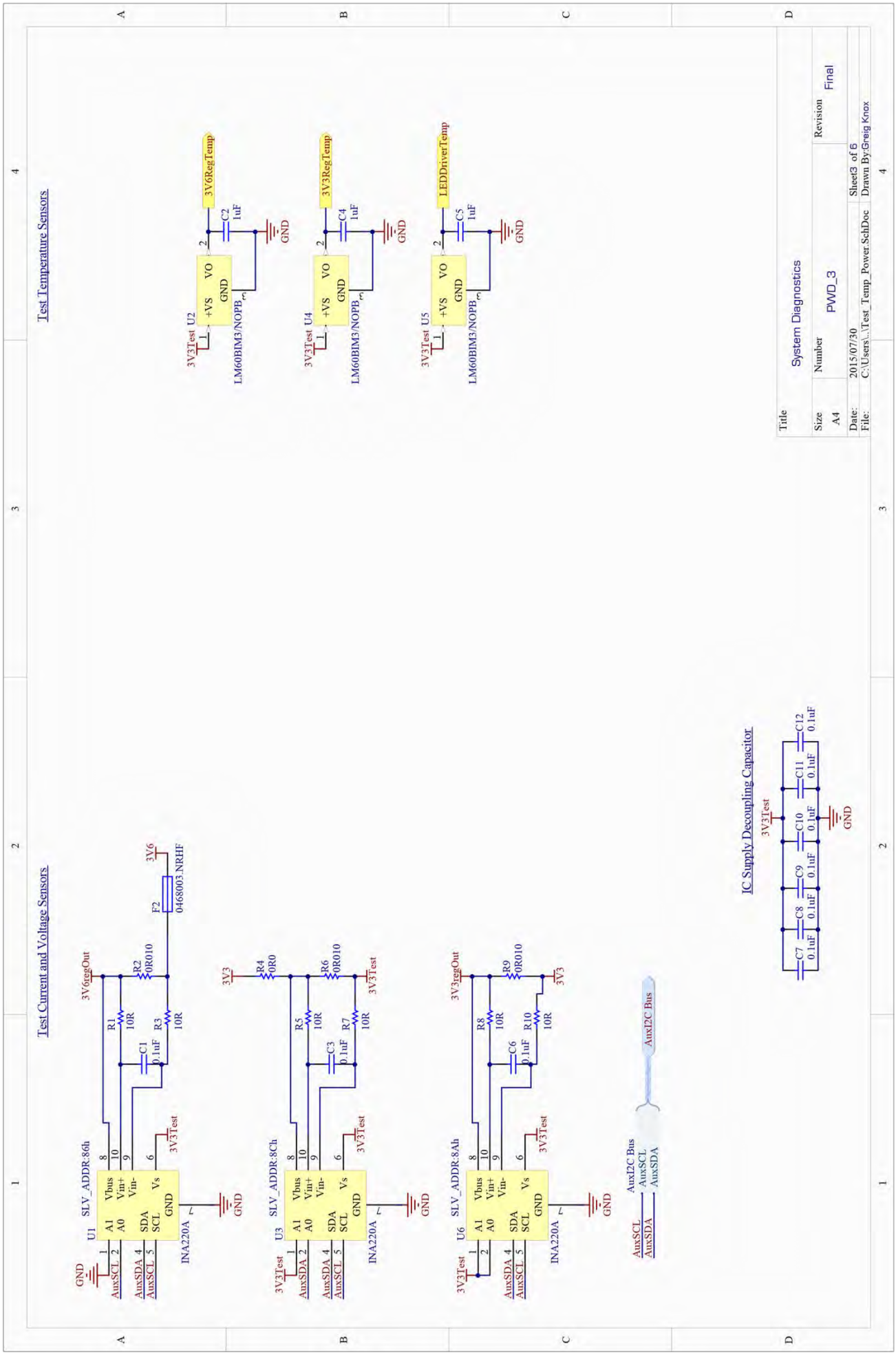
Test Temperature Sensors
Test Current and Voltage Sensors
IC Supply Decoupling Capacitor
System Diagnostics
PWD_3
Final
Sheet3 of 6
2015/07/30
C:\Users\...\Test_Temp_Power.SchDoc
Drawn By:Greig Knox
3V6RegTemp
3V3RegTemp
LEDDriverTemp
LM60BIM3/NOPB
SLV_ADDR:86h
SLV_ADDR:8Ch
SLV_ADDR:8Ah
INA220A
0468003.NRHF
AuxI2C Bus
AuxSCL
AuxSDA
3V3Test
3V6regOut
3V3regOut
3V3
3V6
GND

Switch Mode Regulation

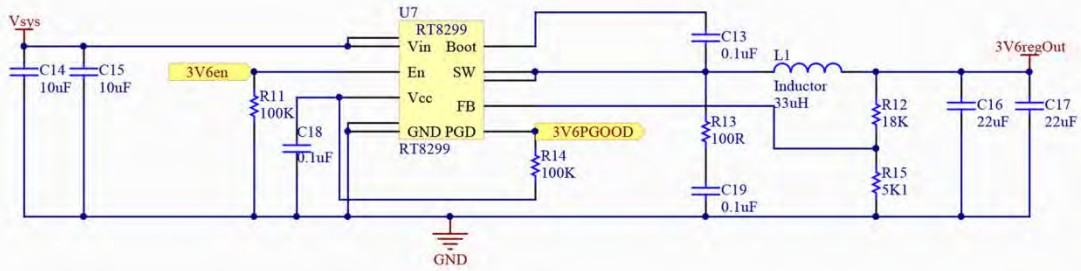

3V3 LDO Regulator

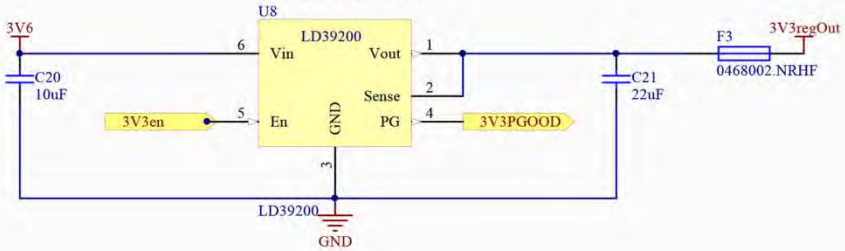

Title	Voltage Regulators		
Size: A4	Number: PWD_4	Revision: Final	
Date: 2015/07/30		Sheet 4 of 6	
File: C:\Users\..\Voltage_RegulationV1.1.SchDoc		Drawn By: Greig Knox	

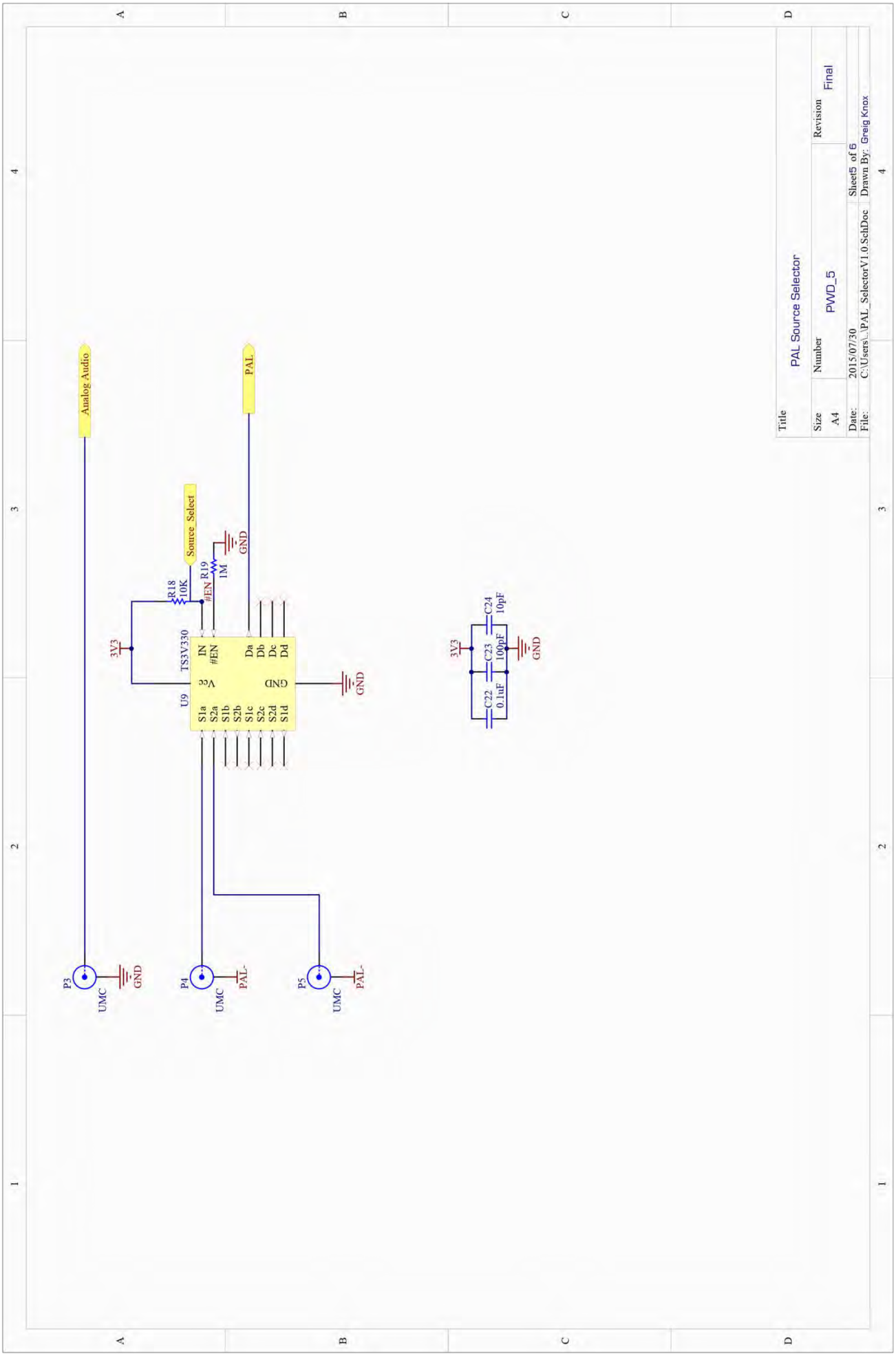
Analog Audio
PAL
Source Select
R18
10K
R19
1M
#EN
3V3
GND
U9
TS3V330
IN
#EN
Da
Db
Dc
Dd
S1a
S2a
S1b
S2b
S1c
S2c
S2d
S1d
C24
10pF
C23
100pF
C22
0.1uF
P3
P4
P5
UMC
PAL-
Title
PAL Source Selector
Size
A4
Number
PWD_5
Revision
Final
Date:
2015/07/30
Sheet5 of 6
File:
C:\Users\...\PAL_SelectorV1.0.SchDoc
Drawn By:
Greig Knox

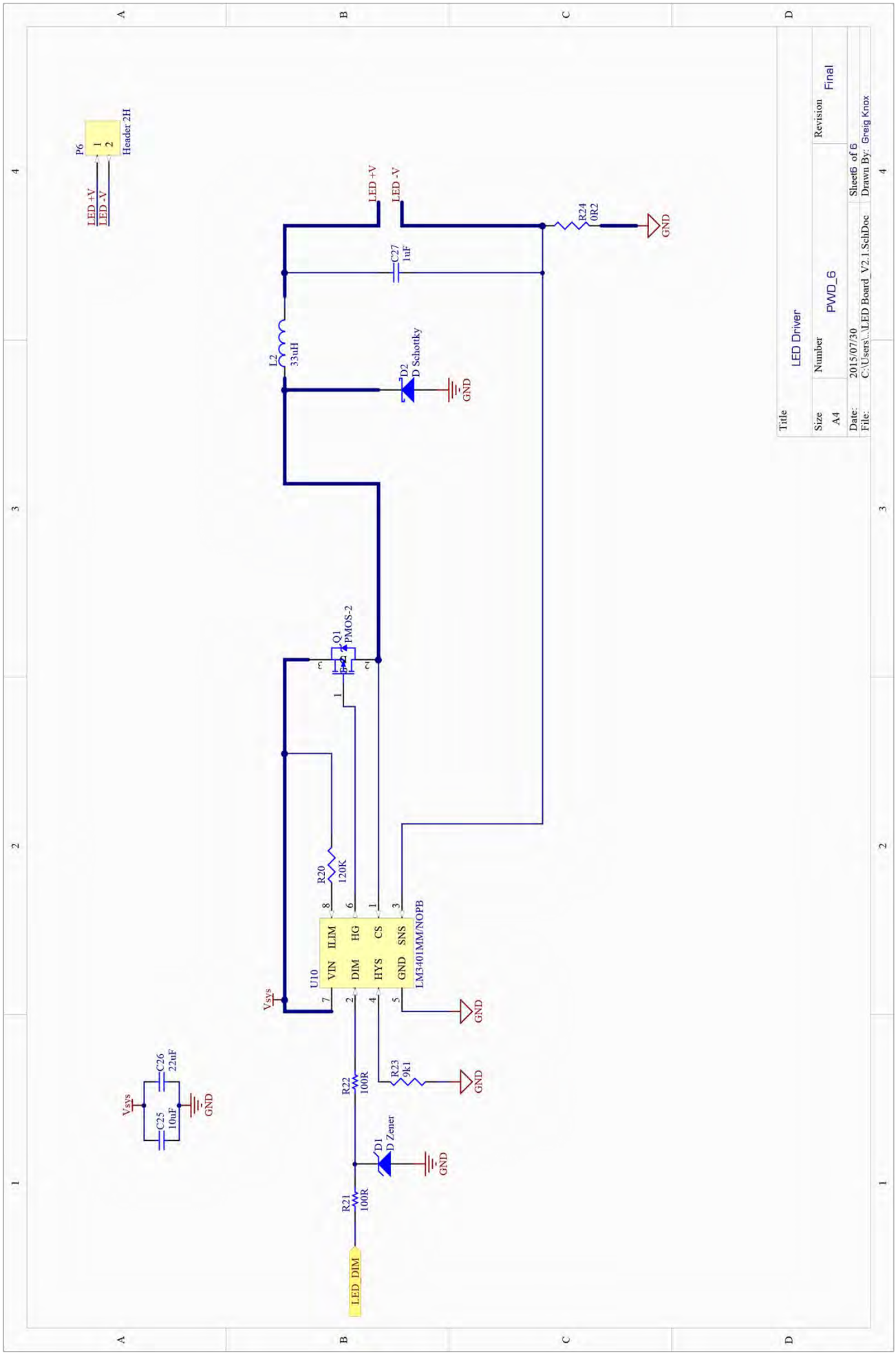
P6
Header 2H
LED +V
LED -V
L2
33uH
D2
D Schottky
GND
C27
1uF
R24
0R2
Q1
PMOS-2
R20
120K
U10
VIN
ILIM
HG
CS
SNS
DIM
HYS
GND
LM3401MM/NOPB
Vsys
C26
22uF
C25
10uF
R22
100R
R23
9k1
D1
D Zener
R21
100R
LED_DIM
Title
LED Driver
Size
A4
Number
PWD_6
Revision
Final
Date:
2015/07/30
Sheet6 of 6
File:
C:\Users\...\LED Board_V2.1.SchDoc
Drawn By:
Greig Knox

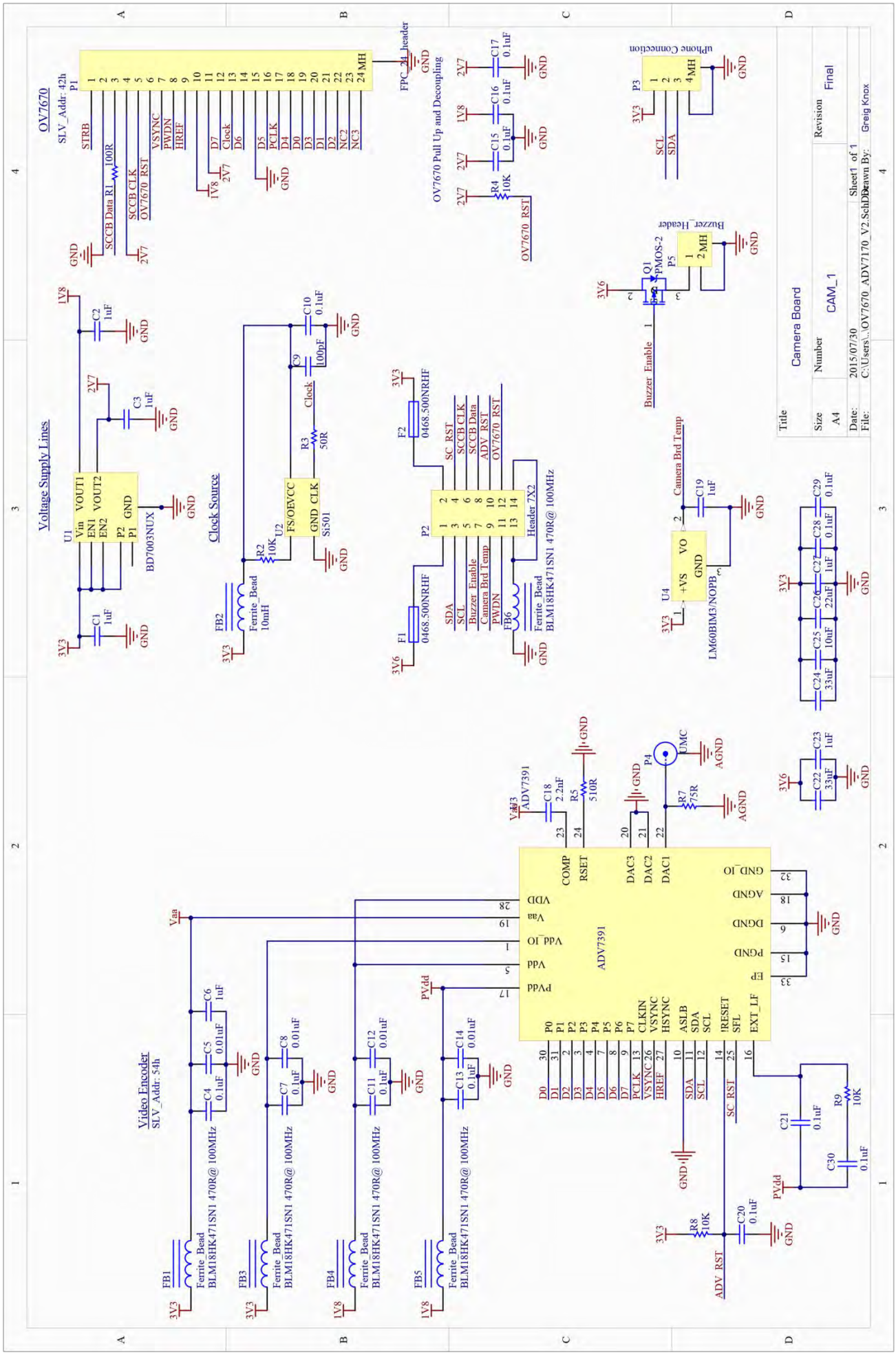
OV7670
SLV_Addr: 42h
Voltage Supply Lines
Clock Source
OV7670 Pull Up and Decoupling
uPhone Connection
Buzzer_Header
Video Encoder
SLV_Addr: 54h
ADV7391
Camera Board
Size
A4
Number
CAM_1
Revision
Final
Date:
2015/07/30
File:
C:\Users\...\OV7670_ADV7170_V2.SchDoc
Sheet1 of 1
Drawn By:
Greig Knox

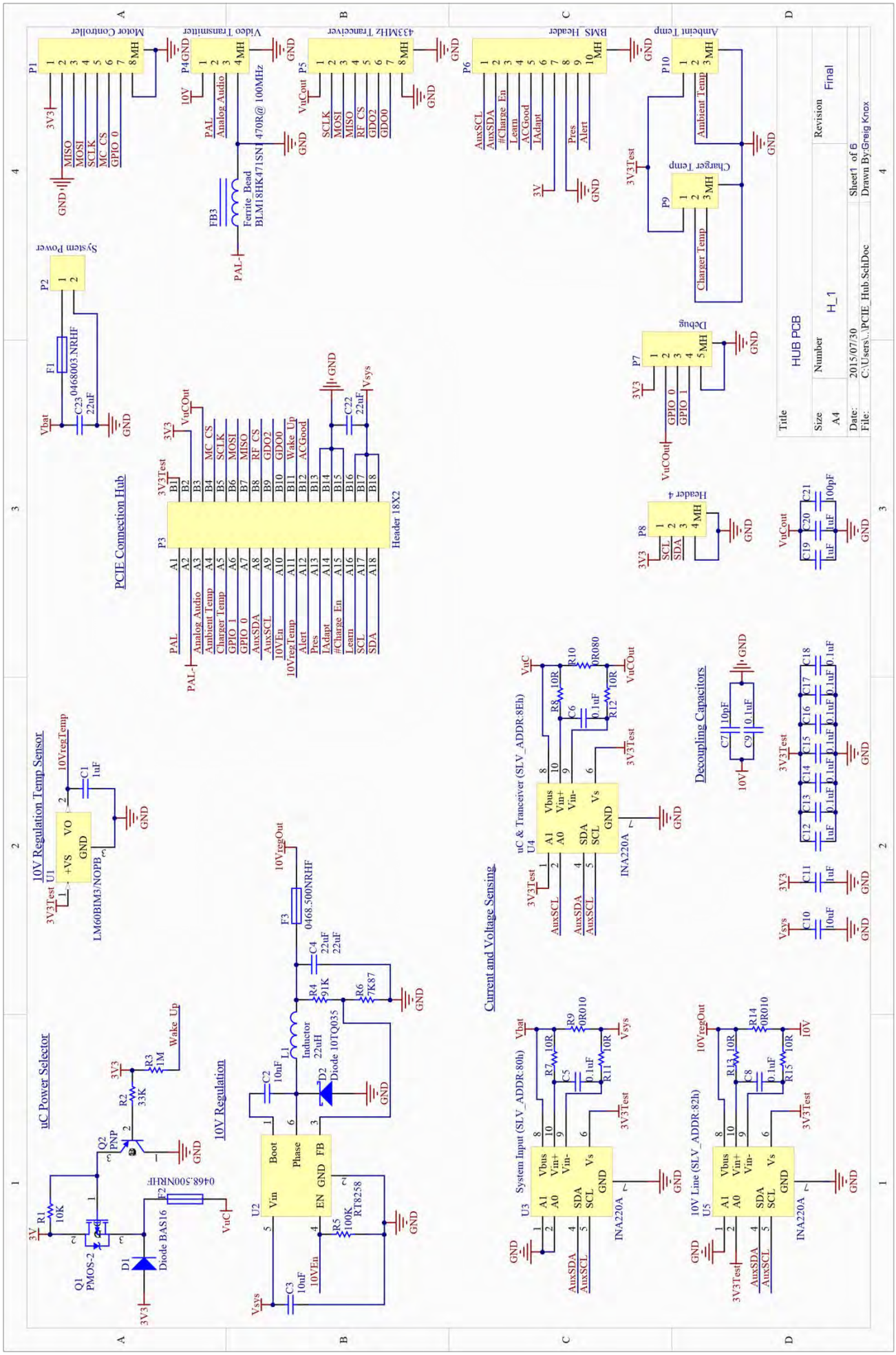
Motor Controller
Video Transmitter
433MHz Transceiver
BMS Header
Ambient Temp
System Power
PCIE Connection Hub
Header 18X2
Debug
Header 4
Charger Temp
10V Regulation Temp Sensor
LM60BIM3/NOPB
uC Power Selector
10V Regulation
RT8258
Current and Voltage Sensing
uC & Tranceiver (SLV_ADDR:8Eh)
System Input (SLV_ADDR:80h)
10V Line (SLV_ADDR:82h)
INA220A
Decoupling Capacitors
Title
HUB PCB
Size
A4
Number
H_1
Revision
Final
Date:
2015/07/30
Sheet1 of 6
File:
C:\Users\..\PCIE_Hub.SchDoc
Drawn By:Greig Knox

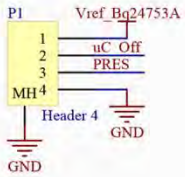

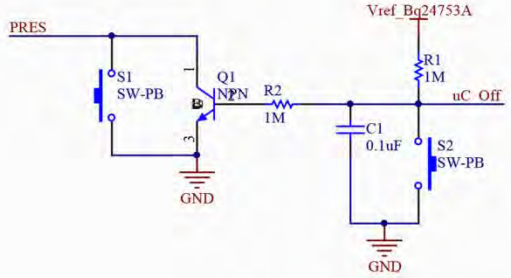

Title	On / Reset Button	
Size: A4	Number: ORB_1	Revision: Final
Date: 2015/07/30	Sheet1 of 1	
File: C:\Users\...\On_Buttonvf.SchDoc	Drawn By: Greig Knox	

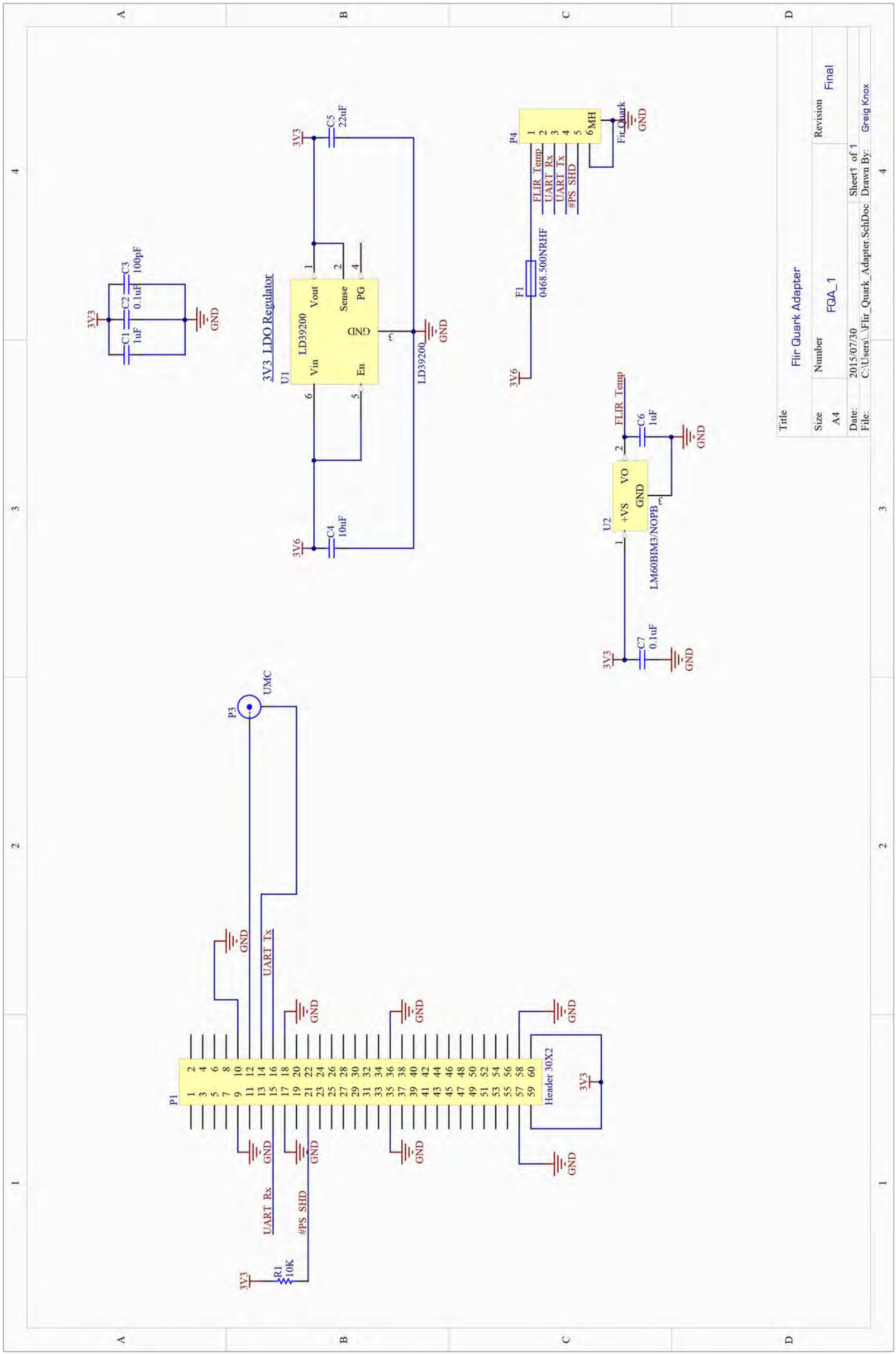
Title
Flir Quark Adapter
Size
A4
Number
FQA_1
Revision
Final
Date:
2015/07/30
Sheet1 of 1
File:
C:\Users\...\Flir_Quark_Adapter.SchDoc
Drawn By:
Greig Knox
3V3_LDO Regulator
U1
LD39200
Vin
Vout
En
Sense
PG
GND
C1
1uF
C2
0.1uF
C3
100pF
C4
10uF
C5
22uF
F1
0468.500NRHF
P1
Header 30X2
P3
UMC
P4
FLIR_Temp
UART_Rx
UART_Tx
#PS_SHD
Flir_Quark
R1
10K
U2
LM60BIM3/NOPB
+VS
VO
GND
C6
1uF
C7
0.1uF
3V3
3V6
GND

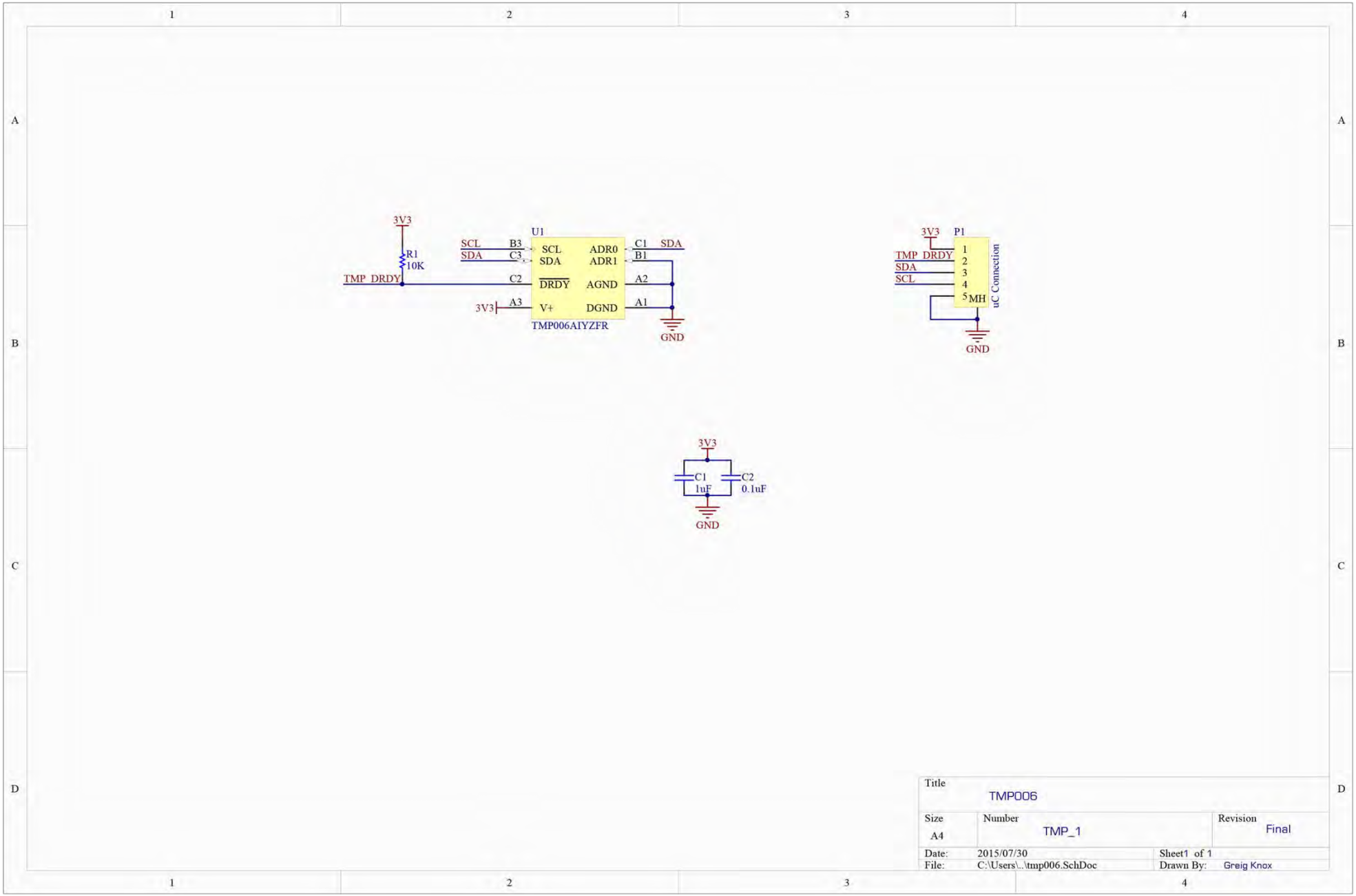
1
2
3
4
A
B
C
D
3V3
R1
10K
TMP_DRDY
U1
SCL
SDA
B3
C3
C2
A3
3V3
SCL
SDA
DRDY
V+
ADR0
ADR1
AGND
DGND
C1
B1
A2
A1
SDA
GND
TMP006AIYZFR
3V3
P1
TMP_DRDY
SDA
SCL
1
2
3
4
5
MH
uC Connection
GND
3V3
C1
1uF
C2
0.1uF
GND
Title
TMP006
Size
A4
Number
TMP_1
Revision
Final
Date:
2015/07/30
Sheet1 of 1
File:
C:\Users\...\tmp006.SchDoc
Drawn By:
Greig Knox

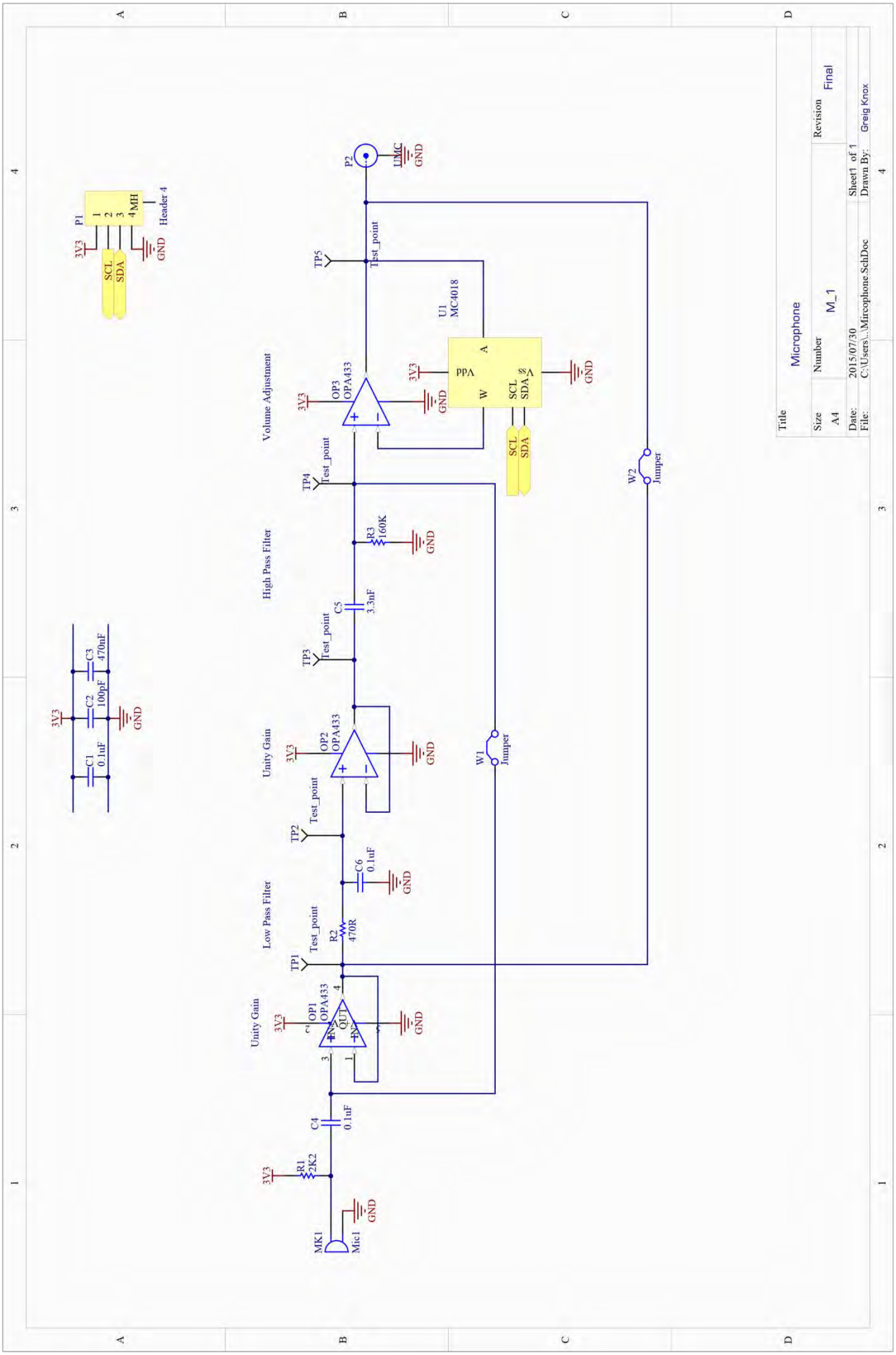
Microphone
Title
Size
A4
Number
M_1
Revision
Final
Date:
2015/07/30
Sheet1 of 1
File:
C:\Users\...\Mircophone.SchDoc
Drawn By:
Greig Knox
Header 4
Volume Adjustment
High Pass Filter
Unity Gain
Low Pass Filter
Unity Gain
Test_point
Jumper
OPA433
MC4018
100pF
470nF
0.1uF
3.3nF
160K
470R
2K2
Mic1
LMIC
GND
3V3
SCL
SDA

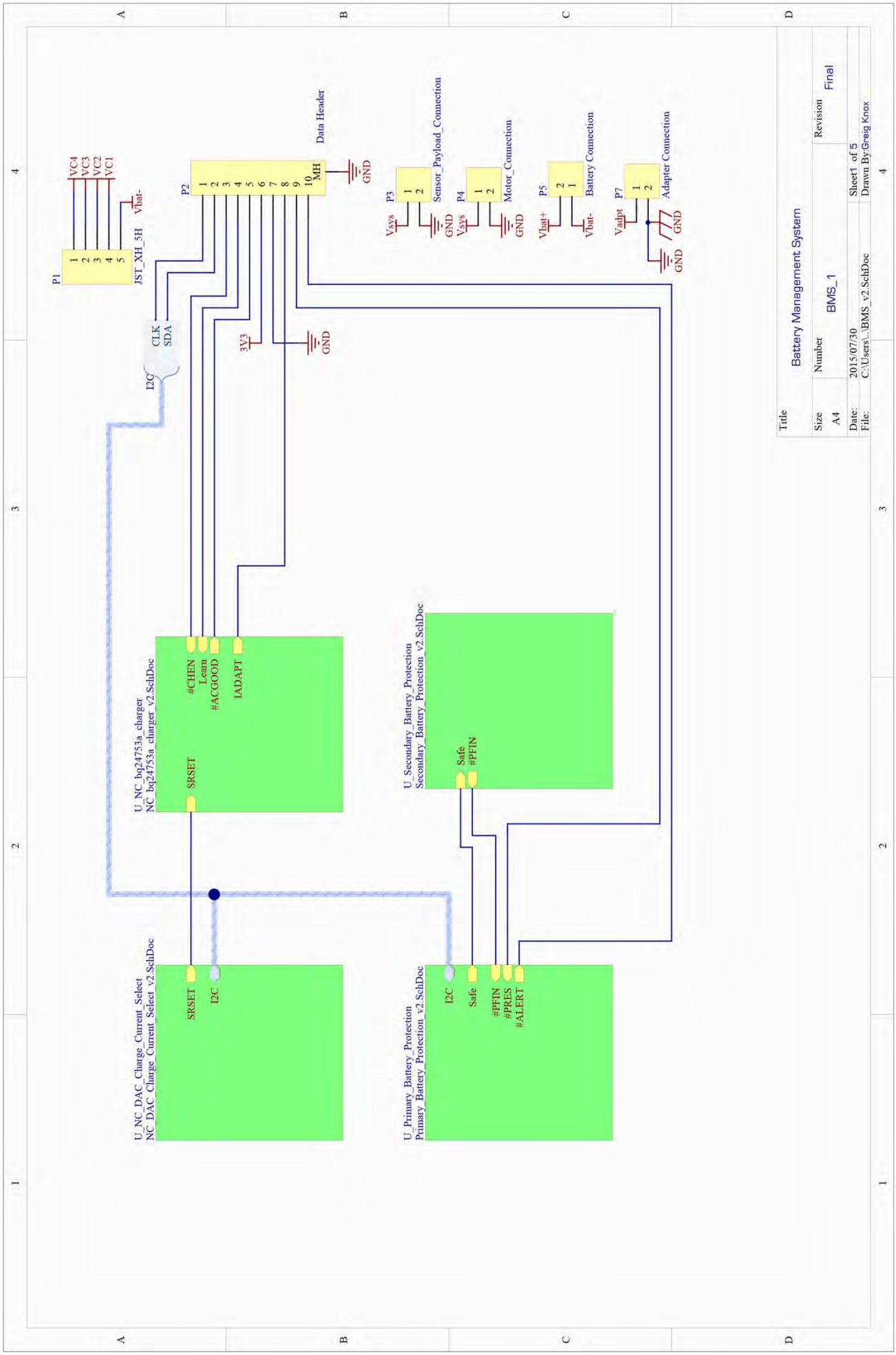
Title
Battery Management System
Size
A4
Number
BMS_1
Revision
Final
Date:
2015/07/30
Sheet1 of 5
File:
C:\Users\...\BMS_v2.SchDoc
Drawn By:Greig Knox
P1
JST_XH_5H
VC4
VC3
VC2
VC1
Vbat-
P2
Data Header
MH
GND
P3
Sensor_Payload_Connection
Vsys
GND
P4
Motor_Connection
Vsys
GND
P5
Battery Connection
Vbat+
Vbat-
P7
Adapter Connection
Vadpt
GND
I2C
CLK
SDA
3V3
GND
U_NC_bq24753a_charger
NC_bq24753a_charger_v2.SchDoc
#CHEN
Learn
#ACGOOD
IADAPT
SRSET
U_Secondary_Battery_Protection
Secondary_Battery_Protection_v2.SchDoc
Safe
#PFIN
U_NC_DAC_Charge_Current_Select
NC_DAC_Charge_Current_Select_v2.SchDoc
SRSET
I2C
U_Primary_Battery_Protection
Primary_Battery_Protection_v2.SchDoc
I2C
Safe
#PFIN
#PRES
#ALERT

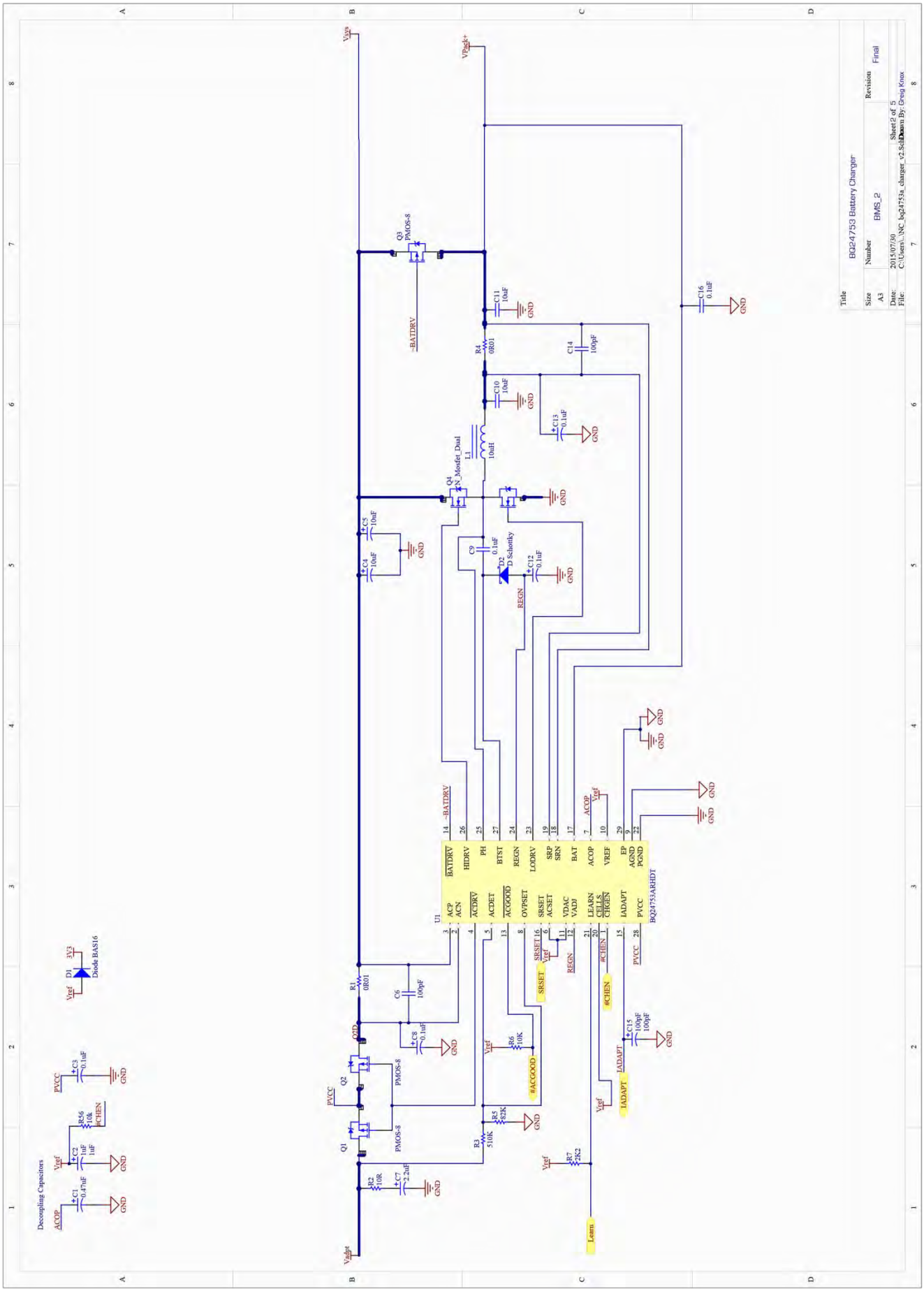
Title
BQ24753 Battery Charger
Size
A3
Number
BMS_2
Revision
Final
Date:
2015/07/30
Sheet 2 of 5
File:
C:\Users\...\NC_bq24753a_charger_v2.SchDoc
Drawn By: Greig Knox
Vsys
VPack+
Vadpt
BQ24753ARHDT
Decoupling Capacitors
Learn

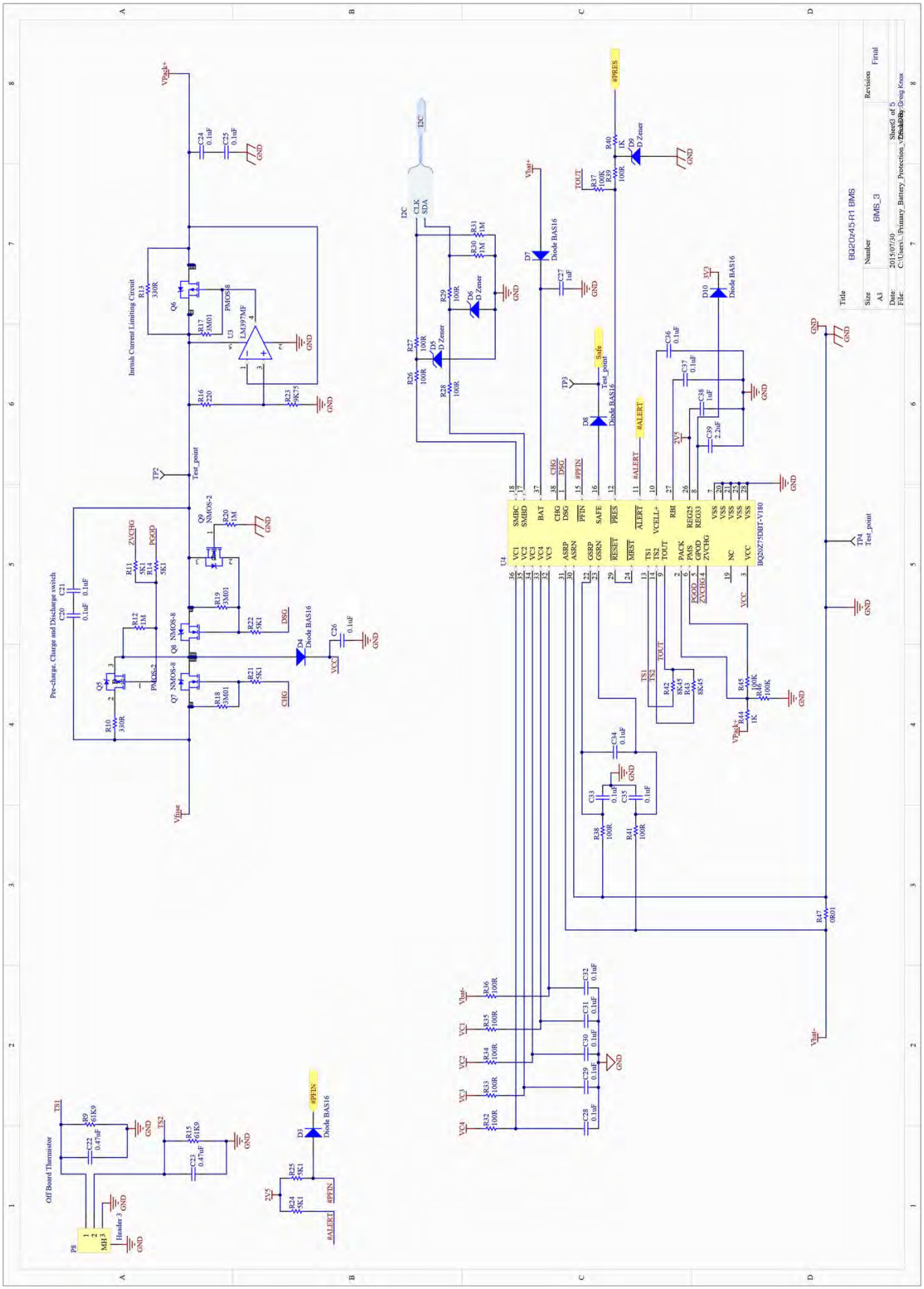
BQ20z45-R1 BMS
BMS_3
Final
Sheet6 of 5
Pre-charge, Charge and Discharge switch
Inrush Current Limiting Circuit
Off Board Thermistor
BQ20Z75DBT-V180
Diode BAS16
PMOS-2
NMOS-8
LM397MF
Test_point
D Zener

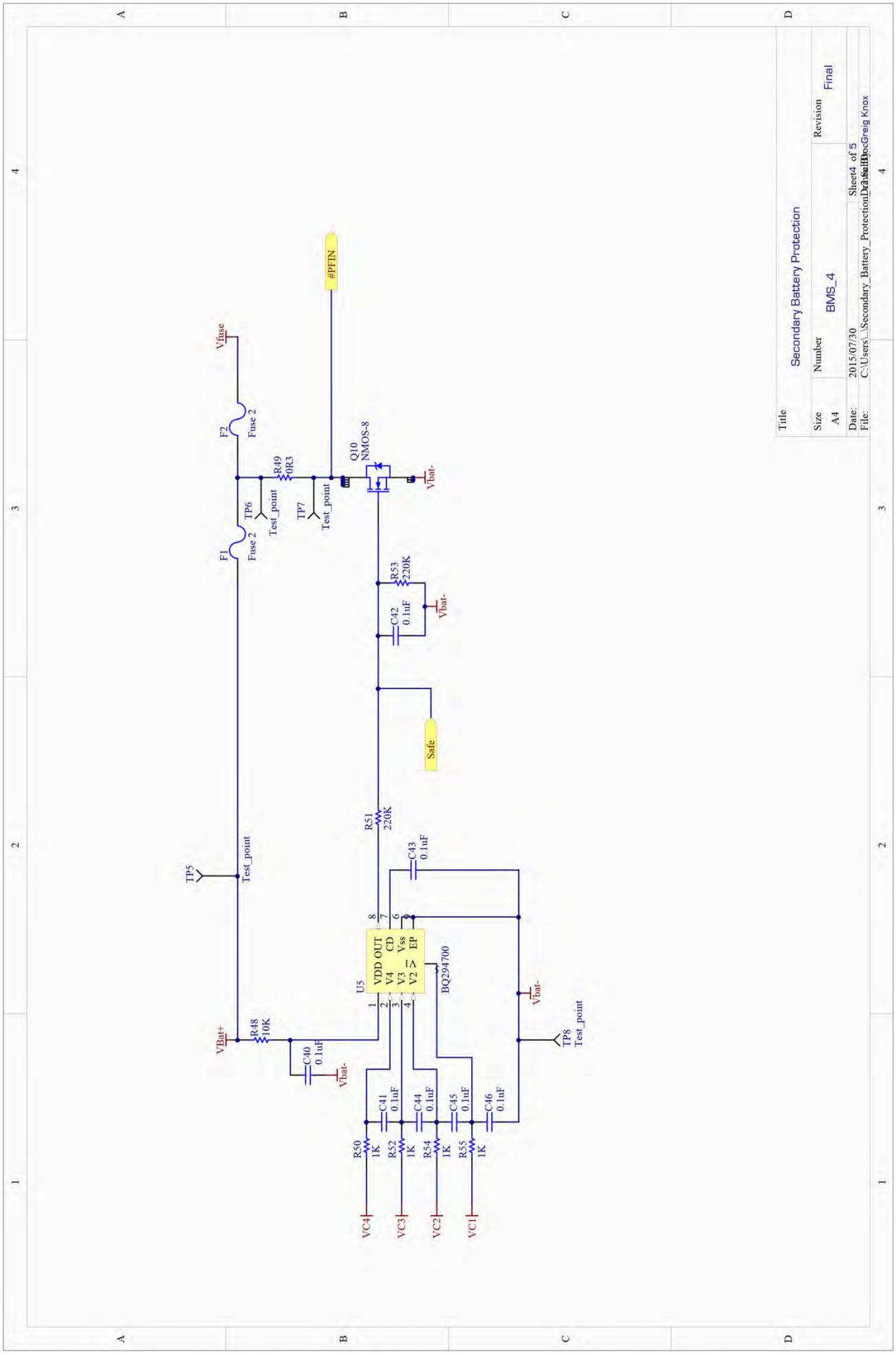
Secondary Battery Protection
Number
BMS_4
Revision
Final
Size
A4
Date:
2015/07/30
Sheet4 of 5
File:
C:\Users\...\Secondary_Battery_Protection.DocGreig Knox
#PFIN
Vfuse
F2
Fuse 2
R49
0R3
Q10
NMOS-8
Vbat-
TP6
Test_point
TP7
Test_point
F1
Fuse 2
R53
220K
C42
0.1uF
Safe
R51
220K
C43
0.1uF
TP5
Test_point
U5
VDD
OUT
CD
Vss
EP
V4
V3
V2
BQ294700
VBat+
R48
10K
C40
0.1uF
TP8
Test_point
C41
0.1uF
C44
0.1uF
C45
0.1uF
C46
0.1uF
R50
1K
R52
1K
R54
1K
R55
1K
VC4
VC3
VC2
VC1

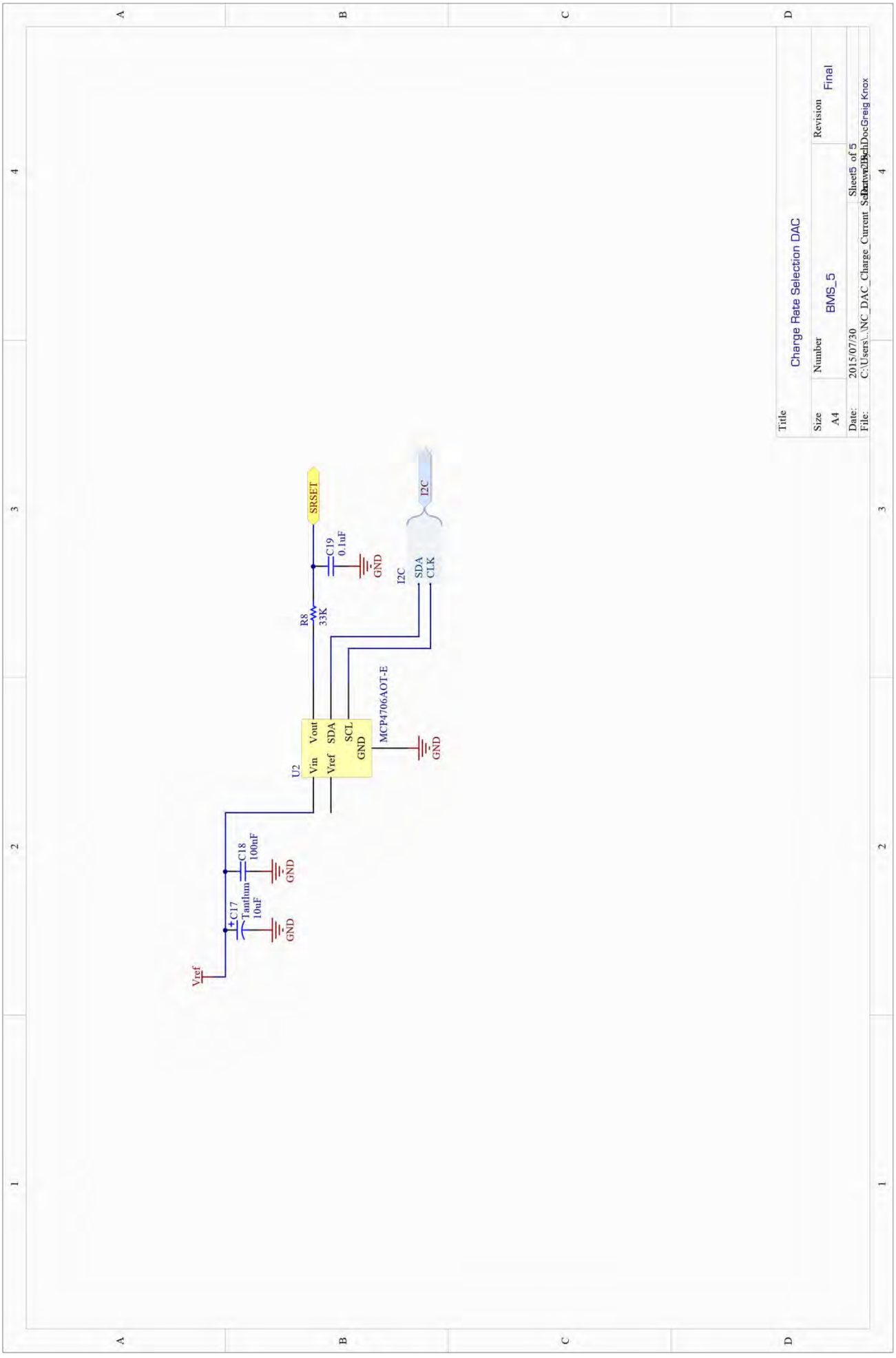
Title
Charge Rate Selection DAC
Size
A4
Number
BMS_5
Revision
Final
Date:
2015/07/30
Sheet5 of 5
File:
C:\Users\...\NC_DAC_Charge_Current_Selection.SchDoc
Drawn By:
Greig Knox
SRSET
C19
0.1uF
GND
R8
33K
I2C
SDA
CLK
I2C
U2
Vin
Vout
Vref
SDA
SCL
GND
MCP4706AOT-E
GND
Vref
C17
Tantlum
10uF
C18
100nF
GND
GND

Appendix F:

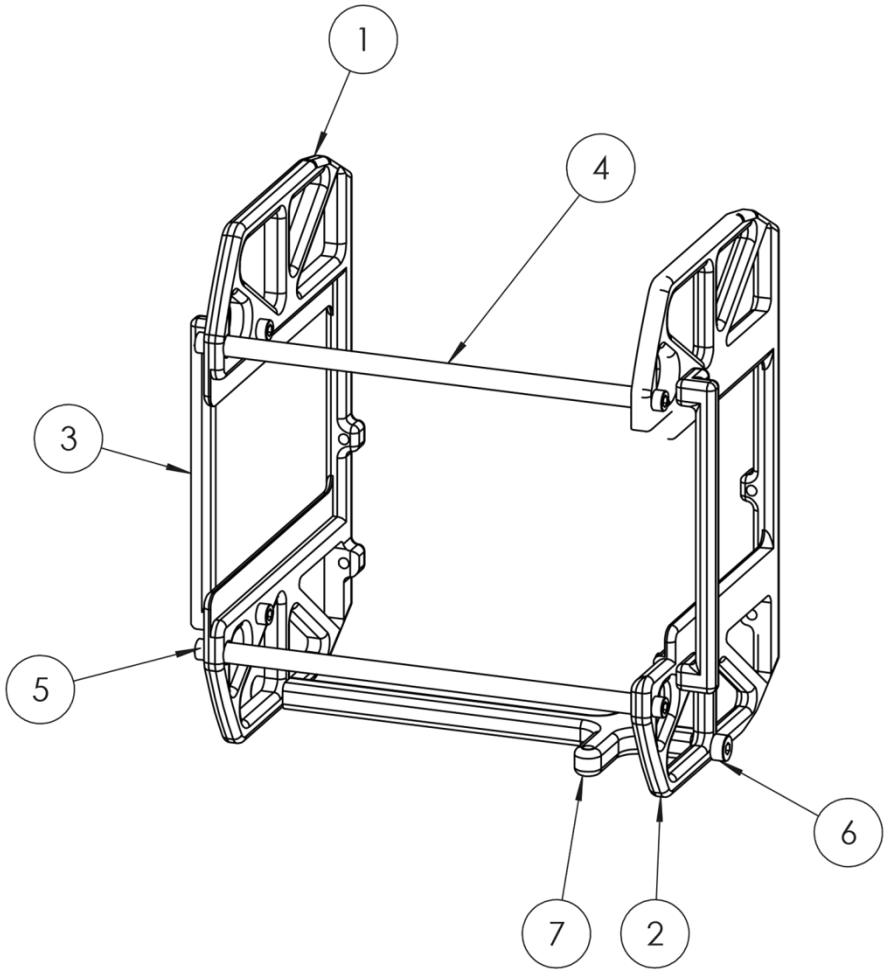

ITEM NO.	PART NUMBER	QTY.
1	SP_Rail_Right	1
2	SP_Rail_left	1
3	Rail_Support	2
4	3mm_Spacer_Rod	2
5	socket head cap screw_iso	8
6	ISO 4762 M2 x 6 --- 6N	2
7	Tranciever_Mounting	1

A4 Landscape	University of Cape Town Department of Mechanical Engineering			
	Title: Cradle			
Assembly Drawing	Scale: 1:1	Date: 2015/08/14	Sheet1	of 5
	Drawn By: Greig Knox		Drawing Number SCAR_CRAD_01	

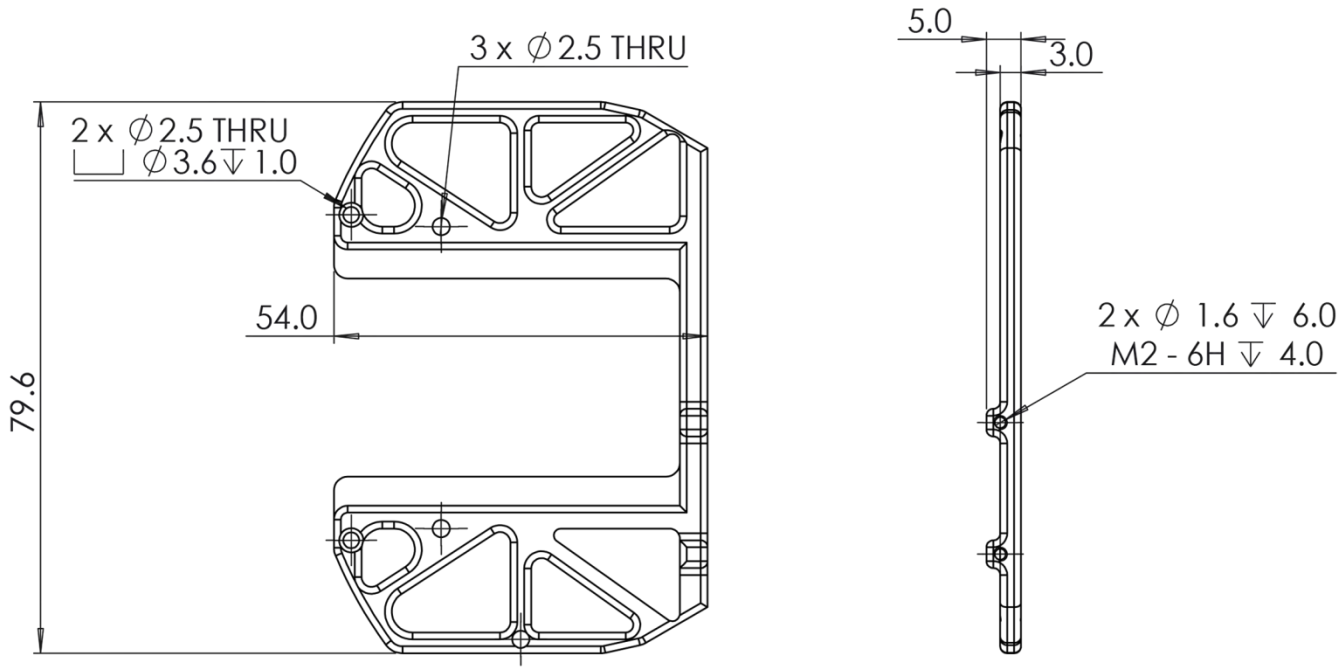

Part to be 3D Printed use Gcode file: RR.gcode

A4 Landscape	University of Cape Town Department of Mechanical Engineering			
	Title: SP_Rail_Right			
Assembly Drawing	Scale: 1:1	Date: 2015/08/14	Sheet2	of 5
	Drawn By: Greig Knox		Drawing Number SCAR_RR_01	

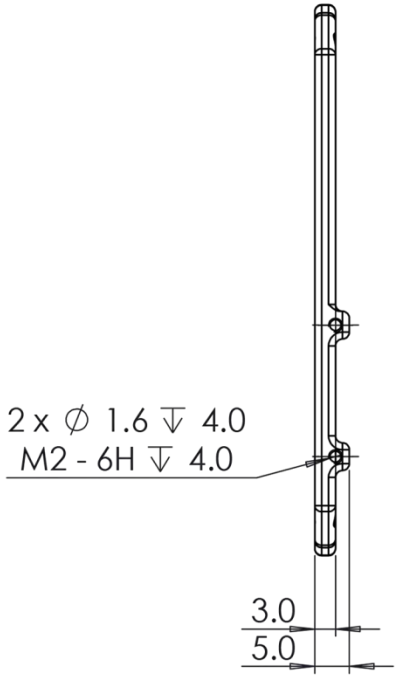

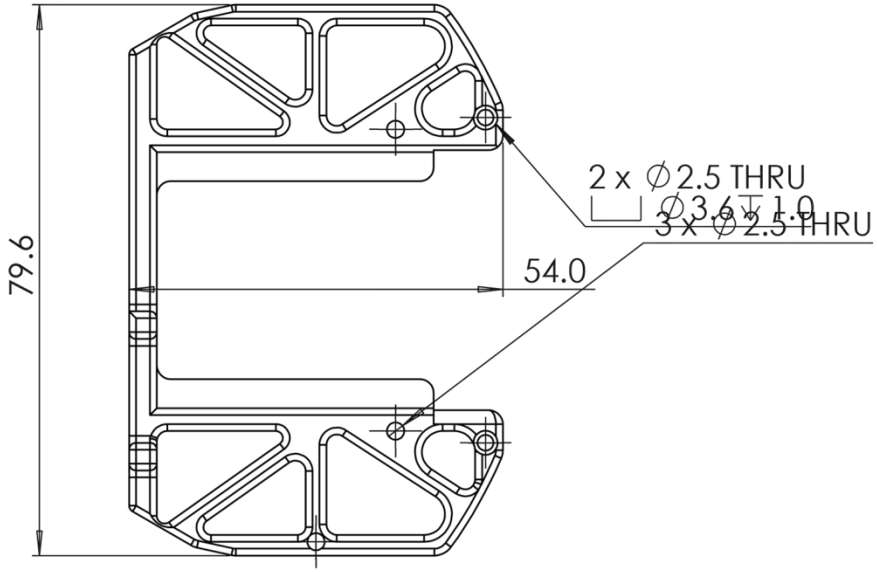

Part to be 3D Printed use Gcode file: RL.gcode

A4 Landscape	University of Cape Town Department of Mechanical Engineering			
	Title: SP_Rail_left			
Part Finish	Scale: 1:1	Date: 2015/08/14	Sheet3	of 5
Material:	Drawn By: Greig Knox		Drawing Number SCAR_RL_01	

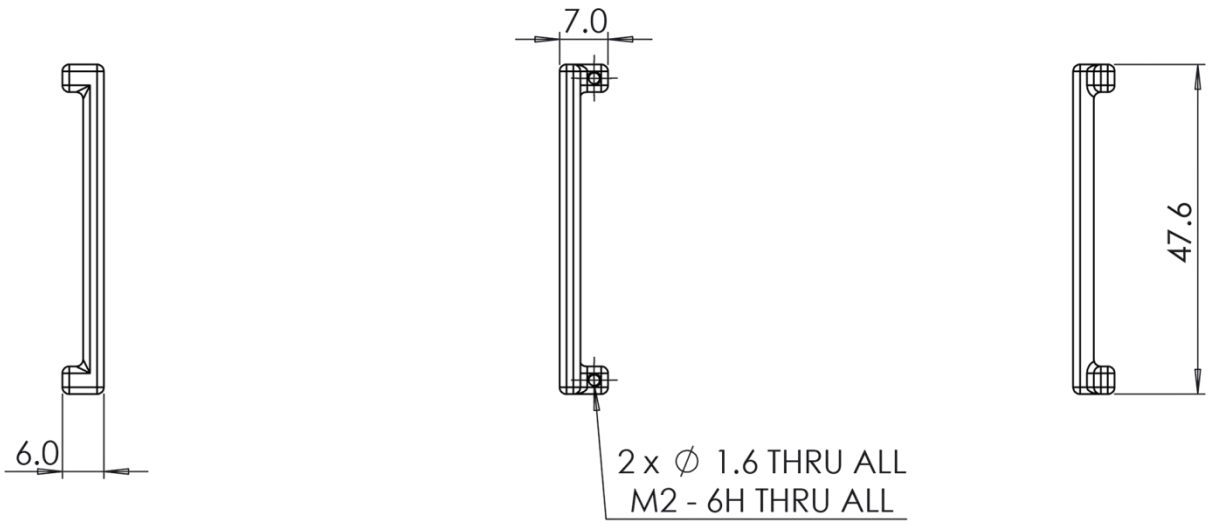

Part to be 3D Printed use Gcode file: RS3.gcode

A4 Landscape	University of Cape Town Department of Mechanical Engineering			
	Title: Rail_Support			
Part Finish	Scale: 1:1	Date: 2015/08/14	Sheet4	of 5
Material: PLA	Drawn By: Greig Knox		Drawing Number SCAR_RS_01	

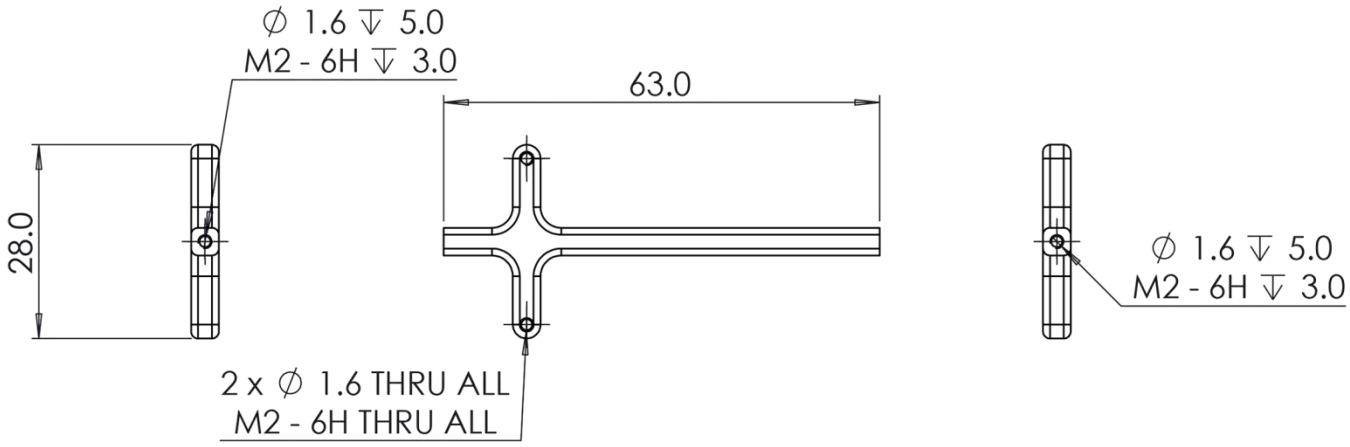

Part to be 3D Printed use Gcode file: TM.gcode

A4 Landscape	University of Cape Town Department of Mechanical Engineering			
	Title: Tranciever_Mounting			
Part Finish	Scale: 1:1	Date: 2015/08/14	Sheet5	of 5
Material: PLA	Drawn By: Greig Knox		Drawing Number SCAR_TRM_01	

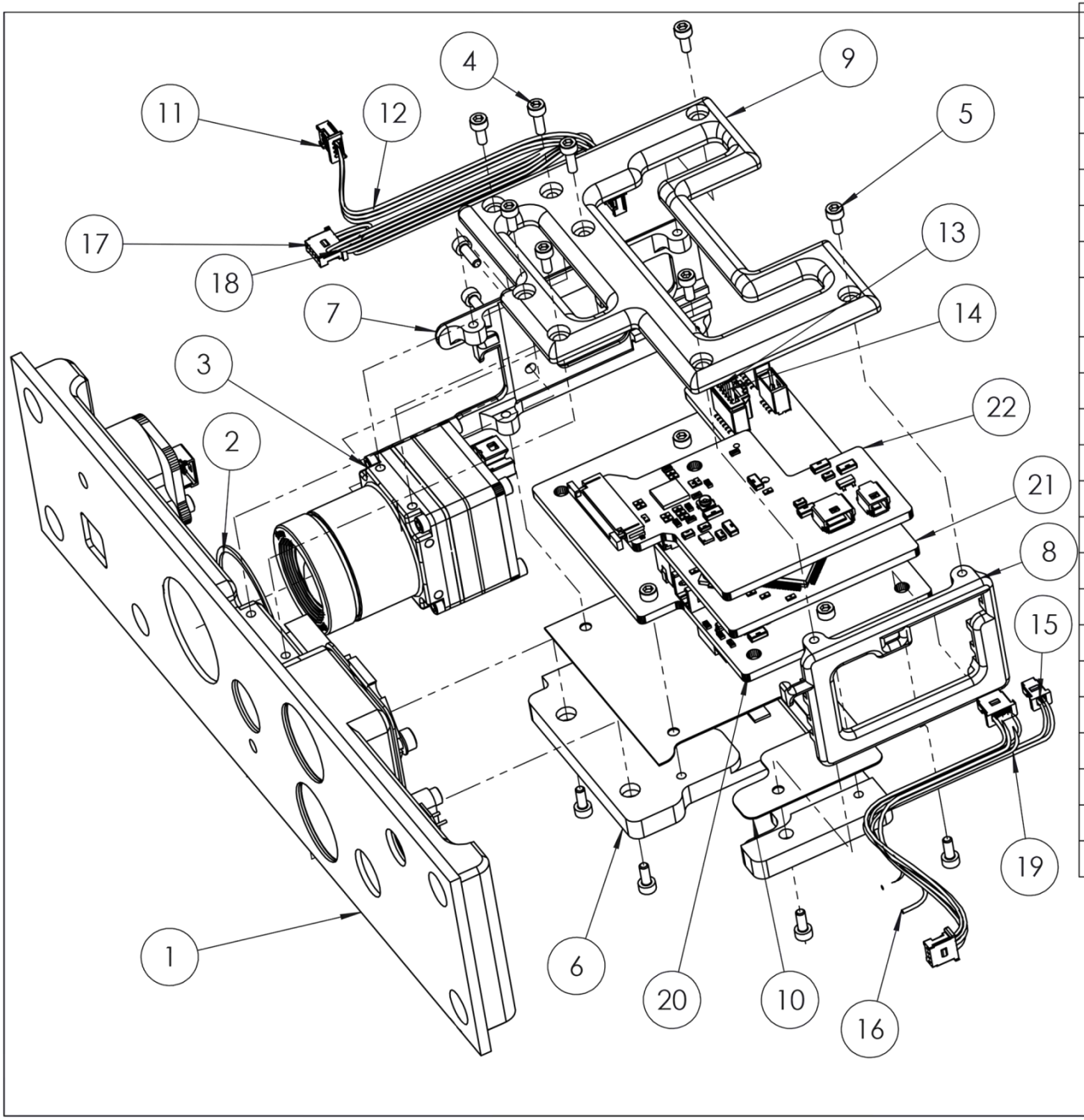

ITEM NO.	PART NUMBER	QTY.
1	Front_Panel_and_Sensors^Sensor_Payload_V1.6	1
2	FLir_quark_seal	1
3	FLIR_Quark_WTH_ADAPTER	1
4	ISO 4762 M1.6 x 5 --- 5N	4
5	socket head cap screw_iso	15
6	Heat_SinkV1	1
7	Right_terminal_protection_frame	1
8	Left_terminal_protection	1
9	Top_Pannel_V2	1
10	Heat_Pad	1
11	Pico_4W_wthcrimp	4
12	Cable_ResetButton	1
13	Pico_6W_wthcrimp	2
14	FlirConnection	1
15	Pico_2W_wthcrimp	1
16	BuzzerPower	1
17	Pico_5W_wthcrimp	2
18	TMP006Connection	1
19	MircoPhoneConnection	1
20	PWR_DIST_V1.3	1
21	STM32F0_boardV1	1
22	Camera_Boardv1	1

A4 Landscape	University of Cape Town Department of Mechanical Engineering			
	Title: Sensor_Payload_V1.6			
Assembly Drawing	Scale: 1:1	Date: 2015/08/16	Sheet1	of 1
	Drawn By: Greig Knox		Drawing Number SCAR_SP_01	

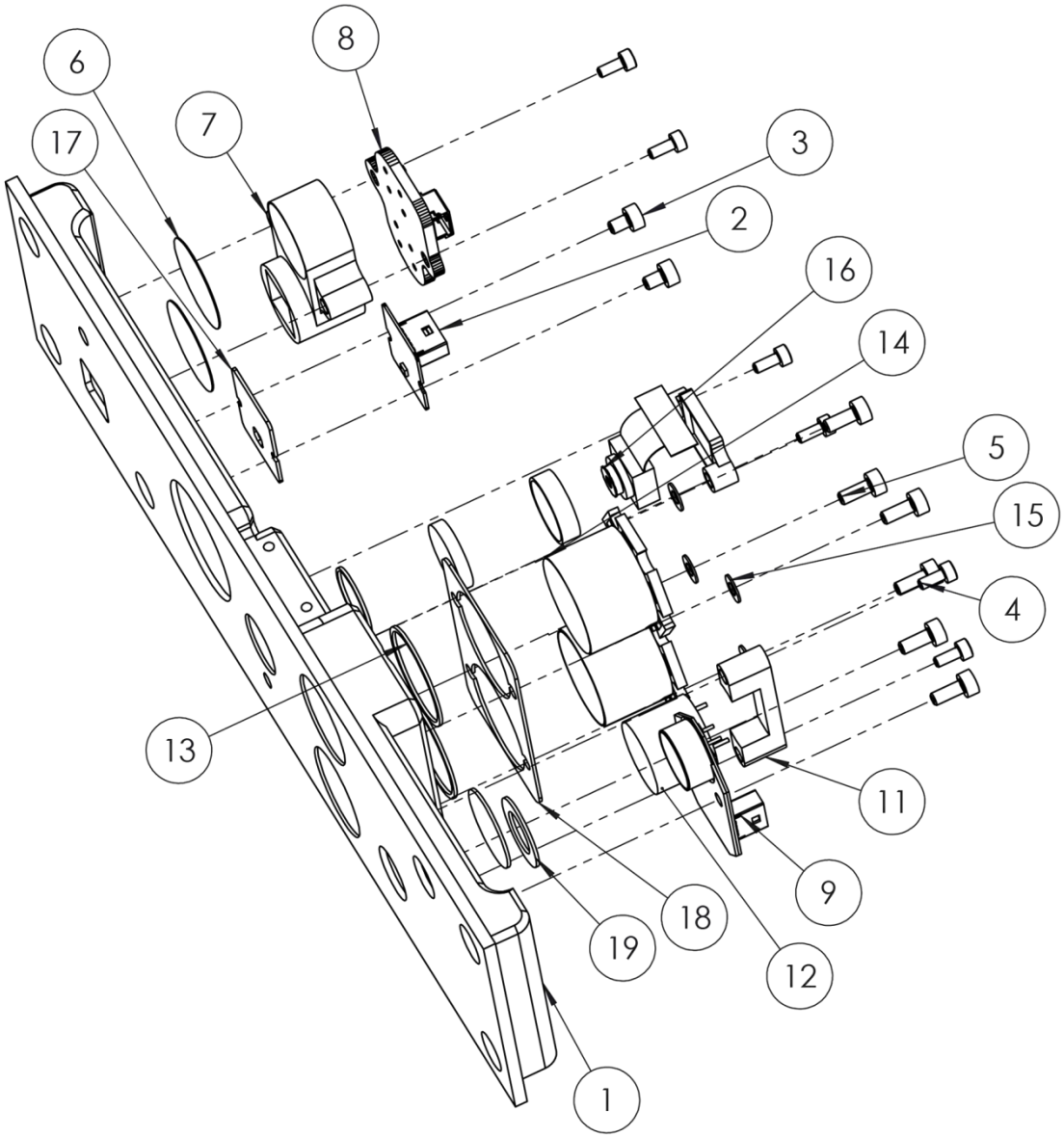

ITEM NO.	PART NUMBER	QTY.
1	Front_Panel_V1.7	1
2	tmp006v1	1
3	ISO 4762 M2 x 3 --- 3N	2
4	socket head cap screw_iso	6
5	ISO 4762 M2 x 5 --- 5N	6
6	Button_seal	2
7	ON_Reset_Button_Support	1
8	On_Reset_Button_vf	1
9	microphone	1
10	Buzzer_Diaphrame	1
11	Buzzer_Mount	1
12	Buzzer_TDB05	1
13	LED_Seal	2
14	LED	2
15	Washer ISO 7092 - 2	4
16	camera_and_mounting	1
17	TMP006_HeatPad	1
18	LED_HeatPad	1
19	uPhone_seal	1

A4 Landscape	University of Cape Town Department of Mechanical Engineering			
	Title: Front_Panel_and_Sensors			
Assembly Drawing	Scale: 1:1	Date: 2015/08/16	Sheet1	of 1
	Drawn By: Greig Knox		Drawing Number SCAR_FPS_01	

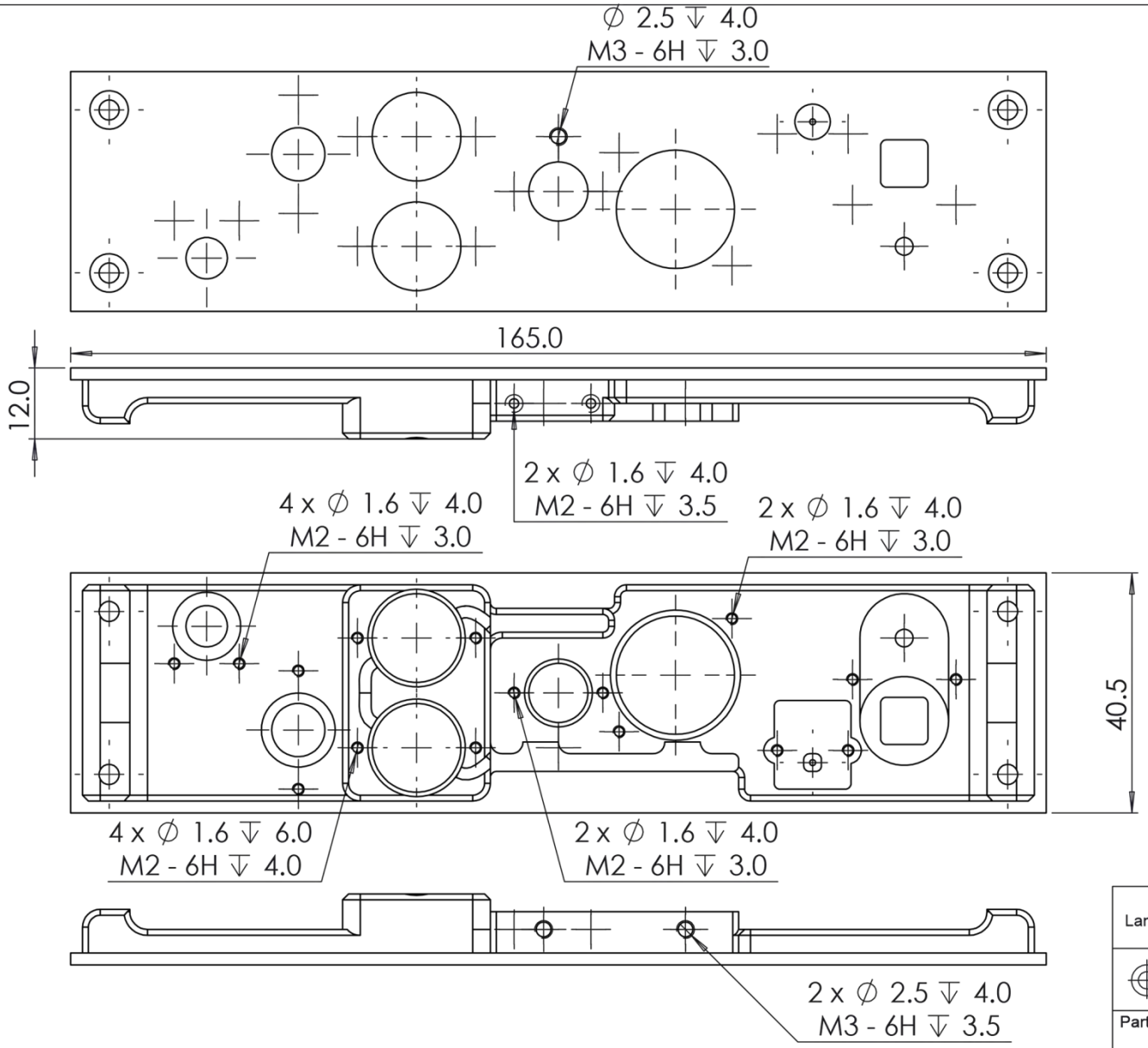

Part to be CNC Machined

A4 Landscape	University of Cape Town Department of Mechanical Engineering			
	Title: Front_Panel_V1.7			
Part Finish	Scale: 1:1	Date: 2015/08/14	Sheet1	of 1
Material: 6061 Alloy	Drawn By: Greig Knox		Drawing Number SCAR_FP_01	

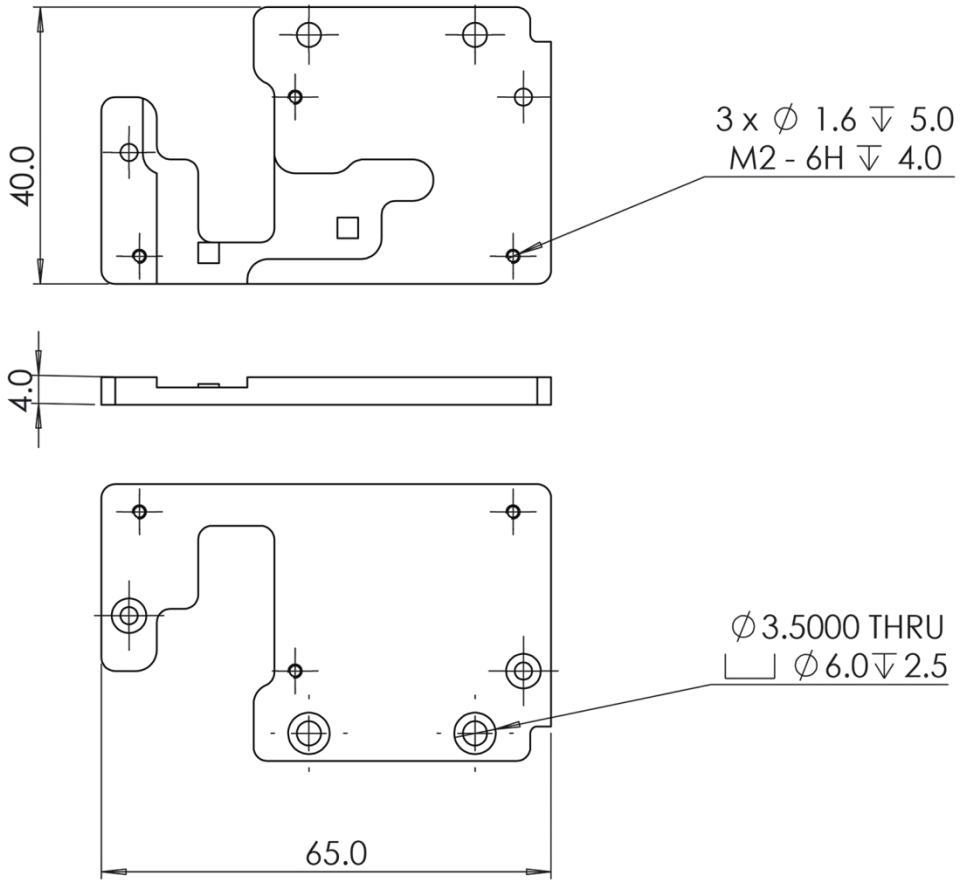

Part to be CNC Machined

A4 Landscape	University of Cape Town Department of Mechanical Engineering			
	Title: Heat_SinkV1			
Part Finish	Scale: 1:1	Date: 2015/08/14	Sheet1	of 1
Material: 6061 Alloy	Drawn By: Greig Knox		Drawing Number SCAR_SPHS_01	

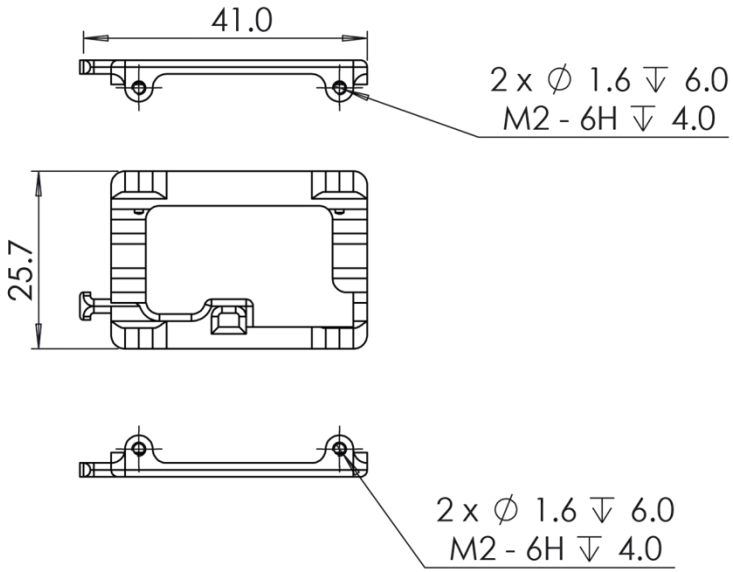

Part to be 3D Printed use Gcode file: LT4.gcode

A4 Landscape	University of Cape Town Department of Mechanical Engineering			
	Title: Left_terminal_protection			
Part Finish	Scale: 1:1	Date: 2015/08/14	Sheet1	of 1
Material: PLA	Drawn By: Greig Knox		Drawing Number SCAR_LTP_01	

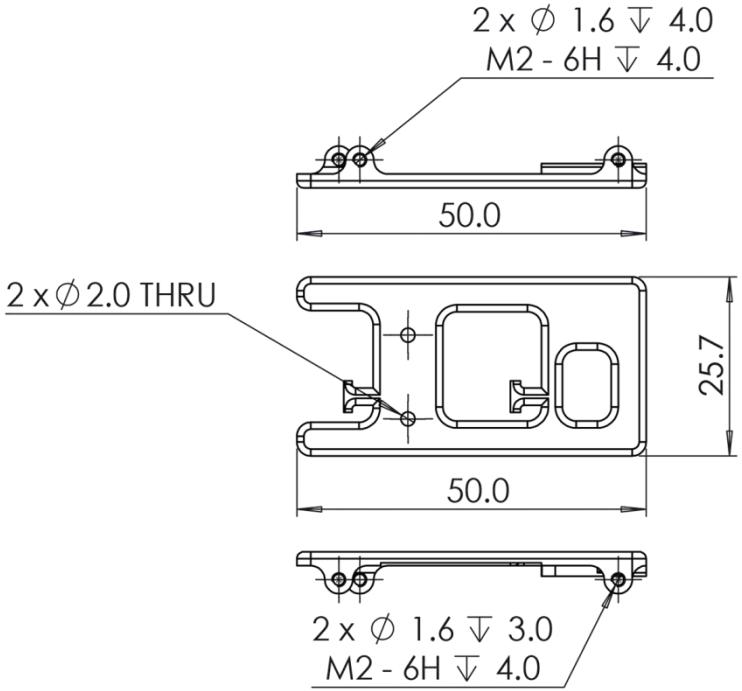

Part to be 3D Printed use Gcode file: RT5.gcode

A4 Landscape	University of Cape Town Department of Mechanical Engineering			
	Title: Right_terminal_protection_frame			
Part Finish	Scale: 1:1	Date: 2015/08/14	Sheet1	of 1
Material: PLA	Drawn By: Greig Knox		Drawing Number SCAR_RTP_01	

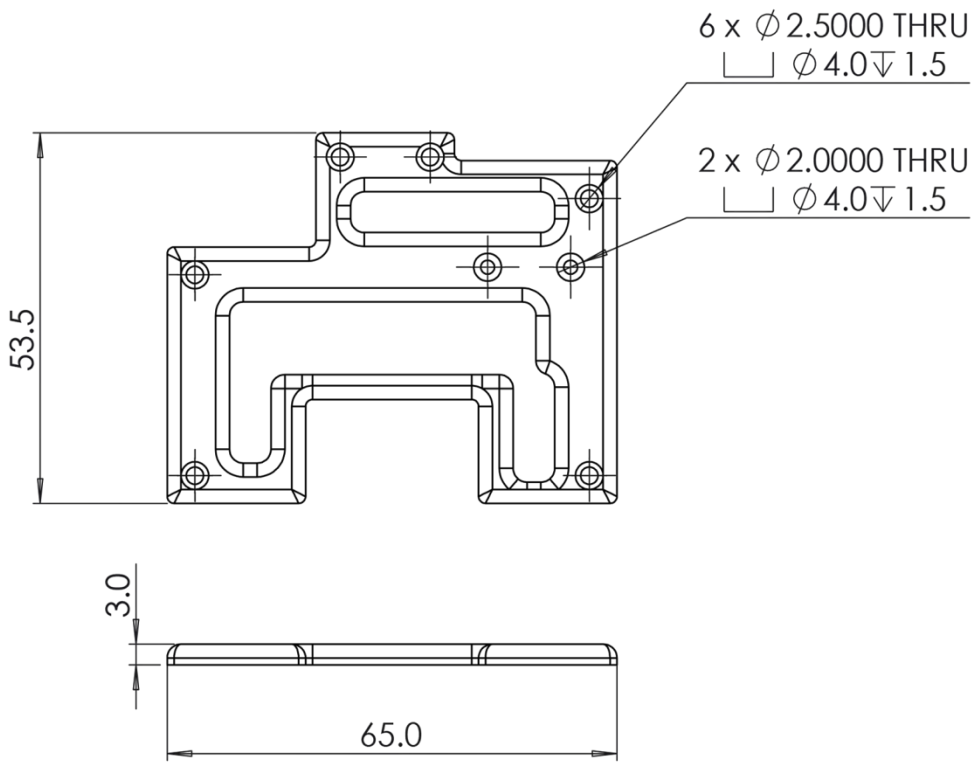

Part to be 3D Printed use Gcode file: Top_P.gcode

A4 Landscape	University of Cape Town Department of Mechanical Engineering			
	Title: Top_Pannel_V2			
Part Finish	Scale: 1:1	Date: 2015/08/14	Sheet1	of 1
Material: PLA	Drawn By:		Drawing Number SCAR_TP_01	